AIRBUS

2, Rond point Dewoitine
31703 Blagnac Cedex
France

FROM: Airport Operations
DATE: 25th October, 2001
ISSUE: Issue 1.0

Subject: A380 Pavement Experimental Programme (PEP) – Flexible brochure

Objective:

The A380 PEP, including flexible and rigid phases, was launched in June 1998 with the aim of studying the impact on pavements using aircraft of large capacity such as the A380. Both phases consist in simulating aircraft coverages on an airport runway using a vehicle simulator able to reproduce various types of aircraft bogies such as A340, A380, B747, B777 or MD11. The variable parameters were mainly the load applied (individual wheel loads, tires pressure), the geometrical configuration of the landing gears (track, base, type of bogie) under a given thermal load (for rigid pavement). Up to 22 wheels could be individually loaded up to 32 t.
The present phase, dedicated to flexible tests, consisted in designing and testing a pavement with varying instrumented surfaces of bituminous materials. Results are enclosed in the present brochure (October 2001). Two targets were assigned:
− Provide comparative experimental data sustaining Airbus Industrie A380 Main Landing Gear configuration selection process.
− Provide fundamental full-scale data to provide a better understanding of flexible pavement structures behavior against wide bodies loading cases for comparison with LEA predictions and/or to support development of other models.
Ultimately, the A380 Pavement Experimental Program will have participated in the development of a new pavement design method. A multi-layered linear model addressing flexible pavement design shall be proposed, which will be more rational than the current CBR design procedure.
The second phase involves with rigid pavements. The aims of the rigid phase are, first, to obtain a set of data to improve pavements knowledge and secondly to correlate mathematical models using finite element method. See A380 Pavement Experimental Programme (PEP) – Rigid brochure
These models would supersede the ACN / PCN method and obtain a much more reliable classification of aircrafts and pavements which would be aligned with the latest pavement design procedures.

For any question, please contact airport operations department
airport.compatibility@airbus.com

Related documents: A380 Pavement Experimental Programme (PEP) – Rigid brochure

LCPC / AIRBUS / STBA

A380 PAVEMENT EXPERIMENTAL PROGRAMME

AIRBUS INDUSTRIE, A380 Programme, Toulouse, France

25th October 2001

Table of contents

I- THE PROGRAM 1

I-1 THE OBJECTIVES 1
I-1-1 A380 – Landing gear definition philosophy 2
I-1-2 Pavement Design method 3

I-2 PARTNERSHIP 4

I-3 THE Phase and the TIMETABLE 5

II- FLEXIBLE PHASE 7

II-1 TESTING FACILITIES AND MEANS 7

II-1-0 "ALIZÉ" Software 7
II-1-0-1 Presentation 7
II-1-0-2 Comparison with Circly / APSDS 8
II-1-0-3 Preliminary studies 12

II-1-1 The Runway 13
II-1-1-1 SITE Selection 13
II-1-1-2 SPECIFICATION 14
II-1-1-2-1 Pavements structure 14
II-1-1-2-2 Experimentation Area 18
II-1-1-2-3 Pavements construction 19

II-1-2 The instrumentation 31
II-1-2-1 OBJECTIVES 31
II-1-2-2 Description of the instrumentation used 31
II-1-2-2-1 Resilient strain measurements 31
II-1-2-2-2 Transverse profiles of measurement 33
II-1-2-2-3 Deflection bowl measurement 35
II-1-2-2-4 Temperature measurement 35
II-1-2-2-5 Instrumentation during fatigue test 36
II-1-2-3 Installation of the instrumentation 36

II-1-3 Data acquisition unit 37

II-1-4 The Simulation Vehicle "Turtle" 38
II-1-4-1 OBJECTIVES 38
II-1-4-2 DESCRIPTION 39
II-1-4-2-1 Modularity 39
II-1-4-2-2 Load on the subgrade 44
II-1-4-2-3 Vehicle power train 44
II-1-4-2-4 Direction – Trajectory 45
II-1-4-2-5 Acclivity 46
II-1-4-2-6 Control panel 46
II-1-4-2-7 Configuration modification 47
II-1-4-2-8 Vehicle design 48
II-1-4-2-9 recycling materials 48
II-1-4-2-10 Safety – Ergonomic 48
II-1-4-3 STATIC TESTS PROCEDURE 48
II-1-4-4 FATIGUE TESTS STEPS 49
II-1-4-5 USE 49
II-1-4-6 SAFETY EQUIPMENT 50
II-1-4-7 Maintenance 50
II-1-4-8 CONFIGURATION SAMPLES 50

II-2 The Static Tests *59*

II-2-1 Objectives 59

II-2-2 Configuration selection 60
II-2-2-1 TIMETABLE 60
II-2-2-2 List of configurations & issues 60

II-2-3 Test procedures 63
II-2-3-1 REFERENCE load 63
II-2-3-1-1 why the reference load is necessary 63
II-2-3-1-2 Reference load procedures 63
II-2-3-2 TYPICAL configuration test sequence 64
II-2-3-3 SIGNAL ACQUISITION 65

II-2-4 Data analysis 65
II-2-4-1 STEP for analysis of strain measurement 65
II-2-4-2 CONFIGURATIONS selected for the exploitation and interpretation 66
II-2-4-3 Spatial and temporal harmonization 66
II-2-4-4 Running of the instrumentation 73
II-2-4-4-1 Standard signals 73
II-2-4-4-2 Strains kinematics 76
II-2-4-5 Results of strain measurement after double harmonization 78
II-2-4-6 SYNTHESIS for numerical modeling 83
II-2-4-6-1 Synthesis procedure 83
II-2-4-6-2 Analyze and comments 85
II-2-4-7 SOFTWARE Alizé calibration 87
II-2-4-7-1 Hypothesis 87
II-2-4-7-2 Step of adjustment of the model 88
II-2-4-7-3 Results of the adjustments with the L.E.M model 89
II-2-4-7-3 Conclusions on the capacities of the elastic model multi-layer 92
II-2-4-7-4 First elementary visco-elastic simulation of PEP test 93

II-3 The fatigue tests *99*

II-3-1 Objectives 99

II-3-2 Preliminary 99
II-3-2-1 Repair of transition areas and section A 99
II-3-2-2 Simulator configuration for the fatigue campaign 101
II-3-2-3 Pavement status before the fatigue campaign 104
II-3-2-4 Additional sensors 104

II-3-3 Tests procedures 106
II-3-3-1 Phase 1 of the fatigue campaign 106
II-3-3-2 Phase 2 of the fatigue campaign 107
II-3-3-3 Pavement Condition Follow-up 108
II-3-3-4 Materials samplings 109
II-3-3-5 Materials testing 110
II-3-3-5-1 Planned tests for unbound materials 110
II-3-3-5-2 Planned tests for bituminous materials 111

II-3-4 Data analysis (preliminary) 112
II-3-4-1 Evolution of the service Index after 5000 movements 112
II-3-4-1-1 The « Service Index » Method 112
II-3-4-1-2 Topographical survey 118
II-3-4-1-3 Synthesis of the results 121
II-3-4-2 Radar auscultation 124

APPENDIX 130

BACKGROUND

In the context of the NLA development, Airbus Industrie proposed the A380 program, an aircraft whose mission is to transport 555 Pax over 7920nm (A380-800).

The aircraft sets the standard for new Code F airports (80m wing span, Landing Gear (L/G) Outer Wheel Span >14m) and will feature 20 or 22 Main Landing Gear wheels for MTOW ranging from 560t to 600t with development potential beyond 640t.

The issue of pavement compatibility was considered to be fundamental to the programme, especially as the current ACN/PCN method, was shown to have reached its limit of reability with the unpredicted failures of pavements subject to 6 wheel bogie loads. The pavement designers from Airport and Airforce Bases Engineering Dept. (Direction Générale de l'Aviation Civile - Service Technique des Bases Aériennes DGAC-STBA), ICAO ACNSG European voting member, the pavement structure and materials experts (French Laboratory for Civil Engineering – Laboratoire Central des Ponts et Chaussées LCPC) and the European aircraft manufacturer AIRBUS INDUSTRIE felt the need for an ambitious research program aiming at defining more accurate pavement design methods.

AIRBUS INDUSTRIE set up in partnership with STBA and LCPC the experimental part of this research via the A380 Pavement Experimental Program to be able to bring in the pavement compatibility issue into the Landing gear (L/G) configuration selection decision process.

I- THE PROGRAM

I-1 THE OBJECTIVES

Airbus Industrie, the STBA (Service Technique des Bases Aériennes) and the LCPC (Laboratoire Central des Ponts et Chaussées) launched the A380 Pavement Experimental Program to provide full-scale data to be compared to theoretical simulations carried out with Multi-Layered Elastic Models by STBA and LCPC.

The pavement test facility built in Toulouse was representative of the four internationally recognized subgrade categories A, B, C and D for flexible structures. The pavement structures consist of three layers above the subgrade: subbase, base courses and asphalt surfacing. Only the subbase had a variable thickness depending on the subgrade category and for comparison purposes.
Each layer of pavement structures was instrumented with sensors, especially to measure deflections and elongation.
The simulation vehicle was able to represent full-scale Main Landing Gear configurations of various wide bodies: A380, A340, B747, B777, MD11.Up to 22 wheels could be individually loaded up to 32 tons. The vehicle features variable dimensions for bogie position, wheels and axle spacing.
The program focused in 1998 and early 1999 on quasi-static comparisons of Landing Gear configurations. These tests provided data on effects of interference when wheels or legs spacing changed, comparisons between various A380, A340, A320 L/G configurations and with their main competitors. In 1999 another fatigue test campaign was launched to study structure rupture modes.

I-1-1 A380 – Landing gear definition philosophy

The A380 Pavement Experimental Program (A380 PEP) was launched in June 1998. Two targets were assigned:

- Provide comparative experimental data sustaining Airbus Industrie A380 Landing Gear configuration selection process. (6-6-6-6, 6-4-4-6, 4-6-6-4 etc.)

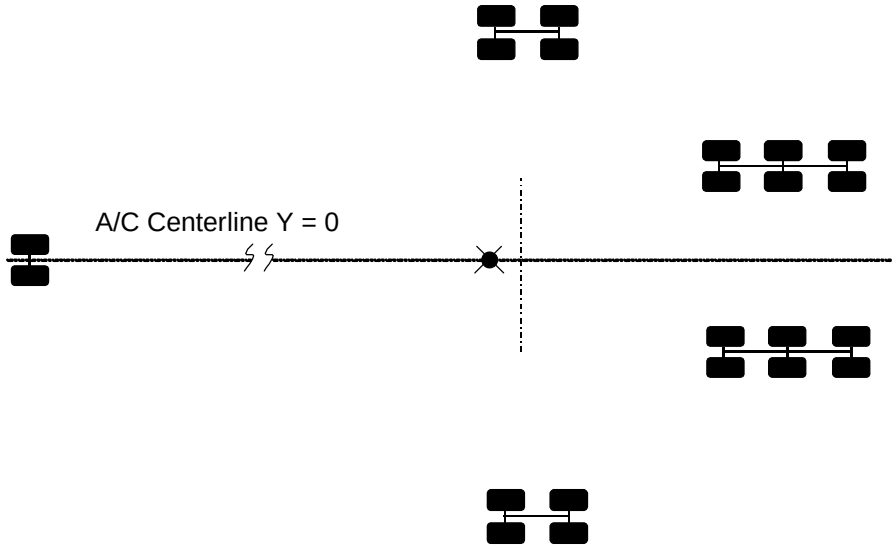

Example: 4 6 6 4

- Provide fundamental full-scale information to provide a better understanding of flexible pavement structures behavior against wide bodies loading cases for comparison with Linear Elastic Model predictions and/or to support development of other models.

Ultimately, the A380 Pavement Experimental Program will have participated in the development of a new pavement design method. A multi-layered linear model addressing flexible pavement design shall be proposed, which will be more rational than the current CBR method.

The initial aim was to provide a design method for flexible pavement structures based on quasi static (low speed taxiing) and fatigue (cumulative damage) factors.

Subsequently (2001-2003) the project (today available) will be extended to rigid pavement structures (see timetable).

I-1-2 Pavement Design method

ALIZE PRELIMINARY STUDIES

ALIZE is a multi-layered elastic model dedicated to flexible pavement design based on Burmister's mathematical model (similar to Julea and Circly). The model was used to predict surface deflection, strain, and elongation predictions for the various quasi-static tests that were intended during the experimental phase.

From these simulations, STBA was able to validate the chosen flexible specimen pavement structures, the depth of subgrade reconstitution. The LCPC deduced from the predicted elongation profiles, appropriate sensor interval for each individual instrumentation layer.

Instrumented Pavement:

The site selected for building the specimen pavement was on Toulouse Blagnac airport as extension of an existing taxiway. The test pavement was 165m long, 30m wide. Each test section was 35m long separated from the next one by a 5m long "neutral zone".

Four sections of flexible pavement structures were designed according to the CBR method for four different subgrade categories: CBR 4, 6, 10, 15.The test taxiway was built to the current design standard for a B747-400. Structures made of the same materials and the same thickness for bituminous layers (Bituminous Concrete 8cm, Bituminous Gravel 2*12cm), the subbase layer had a variable thickness depending on the Subgrade and made of Recombined Humidified Gravel. Three out of four subgrades were found on site (CBR 15, 10, and 6). The weakest subgrade, CBR 4, was reconstituted with imported material.

Material properties (CBR, humidity, Proctor, etc) were continuously controlled by the civil works company's laboratory and by the Regional Laboratory "des Ponts et Chaussées" acting as an exterior independent third party.

Static Testing Instrumentation Philosophy:

Each specimen pavement section was instrumented on one side only due to symmetry. Four main strain sensors layers were installed, namely: the Top of the Subgrade, the Bottom of the Subbase (GRH), the Top of the Subbase (GRH), and the Bottom of the Bituminous Gravel (GB).

This aimed at studying the resilient behavior of the various materials during the passage of a L/G in relation with their most probable failure or deformation mode in the long term (tensile fatigue at the base of the Bituminous Gravel, permanent strength in unbound layers).

Vertical strain gauges were installed in the Subgrade and in the Subbase whereas horizontal strain gauges were used for the Bituminous Gravel. A total of some 250 sensors were installed into the four sections to provide redundancy.

The separation interval between sensors was larger for the deepest layers where the wheel grouping effect was expected to induce a larger area of loading influence (Subgrade and Bottom Subbase interval was 60cm)

In the upper layers, the stress diffusion pattern is sharper and restricted to a smaller area around the wheel, therefore there was a need for closer sensors (Top Subbase and Bituminous Gravel interval is 30cm).

Fatigue Testing Instrumentation Philosophy:

In addition to the existing resilient strain gauging, specific permanent deformation sensors were installed in 1999 for the specific fatigue testing campaign.

These sensors locating at the GB/GRH interface and GRH/subgrade interface are anchored at 6 m depth, in the subgrade, and are intended to provide individual layer permanent deformation in the two weakest test sections (CBR 6 and 4).

Real aircraft were towed on the specimen pavement during static testing to simulate and evaluate A320 and A330 for MTOW development.

The opportunity to manoeuvre real aircraft on specimen pavement enabled validation both the vehicle mechanical concept and the tire pressure setting procedure. Especially by comparing aircraft and test vehicle B747 configurations, resilient deformations correlated very well (with some 5% difference piling up measuring error, temperature effect, and speed effect). Thereby proving the concept.

Real Aircraft on Test Site **Picture 1**

I-2 PARTNERSHIP

Due to the short-term target of A380 Landing Gear Configuration selection scheduled for early 1999, Airbus Industrie was directly involved in the sponsoring and set up of this program. Its contribution consisted at supporting pavement designers and scientists with aircraft Landing Gear system and structure features as well as facilitating the organization and logistics of the program.

Airport and Airforce Bases Engineering Dept. (Direction Générale de l'Aviation Civile - Service Technique des Bases Aériennes DGAC-STBA), contributes in the specification of the specimen pavements, definition of test programs and test procedures.

French Laboratory for Civil Engineering (Laboratoire Central des Ponts et Chaussées), expert in civil engineering provides expertise for pavement instrumentation, data acquisition and analysis. LCPC intends to develop with STBA a rational airfield pavement design method.

Aéroports de Paris joined the Program in 1999 for the fatigue test campaign.
It had supplied a cabling/instrumentation service and provided radar consulting.

BOGEST Enterprise (Toulouse based Design Office**)** was subcontracted for the manufacturing of the simulation vehicle as they developed a specialized skill over the past years with STBA for several other airports' infrastructure test prototypes.

MICHELIN, MESSIER BUGATTI.

I-3 THE Phase and the TIMETABLE

The "Flexible" phase of the A380 Pavement Experimental Program took place in 1998 and 1999.

1998: A380 Pavement Experimental Program's Go Ahead was given at June's A380 Subgrade Handling Workshop in Amsterdam to which airlines and airports representatives involved in the A380 development participated.

Starting in June 1998, the Specimen Pavement was built in a short time without major technical difficulties and inaugurated for the A380 PEP Kick-Off Meeting September the 10th, 1998 with major European Airports representatives as well as European and Japanese Airport Authorities.

The simulation vehicle was produced and assembled in a similar short period and made its first roll on October the 2nd 1998.

Some minor technical modifications were made over October 1998 to the vehicle, especially improve directional control.

During the same period the instrumentation data acquisition chain was tested and validated. STBA performed a first specimen pavement strength measurement campaign.

The actual go ahead to the 1998 so-called "Static Test Campaign" was given early November 1998, only two weeks beyond official schedule with the aim to provide valuable comparative indications between A380, B747 and B777 by early 1999 and thereby supporting A380 L/G design freeze.

Each static test (one L/G configuration) provides more than 1000 sensors signals to be analyzed.

1999: Some more static tests went on until March 1999 to deal with other Airbus products subject to MTOW increases such as A340-500/-600, A321, A330. The critical MD11 configuration was also tested.

A transition period (April to June 1999) was used to check again specimen pavement structure strength and install new sensors dedicated to the measurement of permanent deformations. In June 1999, a so-called "Fatigue" campaign will be launched with the aim to study the failure modes of the various test sections.

Three failure criteria will be particularly surveyed:

- Subgrade failure,
- Top Subbase rutting,
- Bituminous Concrete rutting and cracking.

The parameter of vehicle wandering has been accounted for in the test procedure.

At the end of the fatigue testing, some pavement structure samples will be extracted from the test site to be used for laboratory fatigue testing.

Aéroports de Paris Laboratory is becoming an important contributor to the A380 Pavement Experimental Program in 1999 for the fatigue exercise.

2000: FATIGUE TEST

Starting in September 1999, this campaign target was to classify flexible pavement failure criteria (subgrade rutting, top layer rutting/cracking, vertical strain in lower layers…) and assessing cumulative damage.

Landing gear comparison:

- Comparison with same climatic conditions
- Wandering simulation (Gaussian)
- Regular stops: step by step failure process evaluation
- Pavement condition visual checks
- Permanent strain measurements
- Transversal profiles measurements
- Topography controls

Test vehicle

One configuration was used in the fatigue tests (1/2 A380-900 + 1/4 B777-300 + 1/4 B747-400)
Self-powered 5 Km/h
Full scale Landing gear: Can accommodate existing & future aircraft main gear configuration

SYNTHESIS

The A380 Pavement Experimental Program is the first and sole full-scale experimental program conducted in Western Europe aiming at supporting both the L/G configuration freeze of a new generation aircraft and assembling the basic data for a new pavement design method.

The co-operations set up were agreed in a record time because of convergent interests and provided the reactivity necessary to meet the very tough targets. The program's 1998 phase is about to meet the industrial objectives as STBA and LCPC experts start analyzing initial data.

Both the civil aviation and the airport partners have a lot to learn from that experiment. Undoubtedly that the better scientific knowledge was acquired in terms of pavement mechanics, materials behavior and landing gear loading cases which will benefit to the future enhanced compatibility between aircraft design and airport infrastructure at an optimized overall costs.

Keenly convinced by the importance of the issue, AIRBUS INDUSTRIE decided to include pavement compatibility parameters at the early stage of the A380 L/G definition.

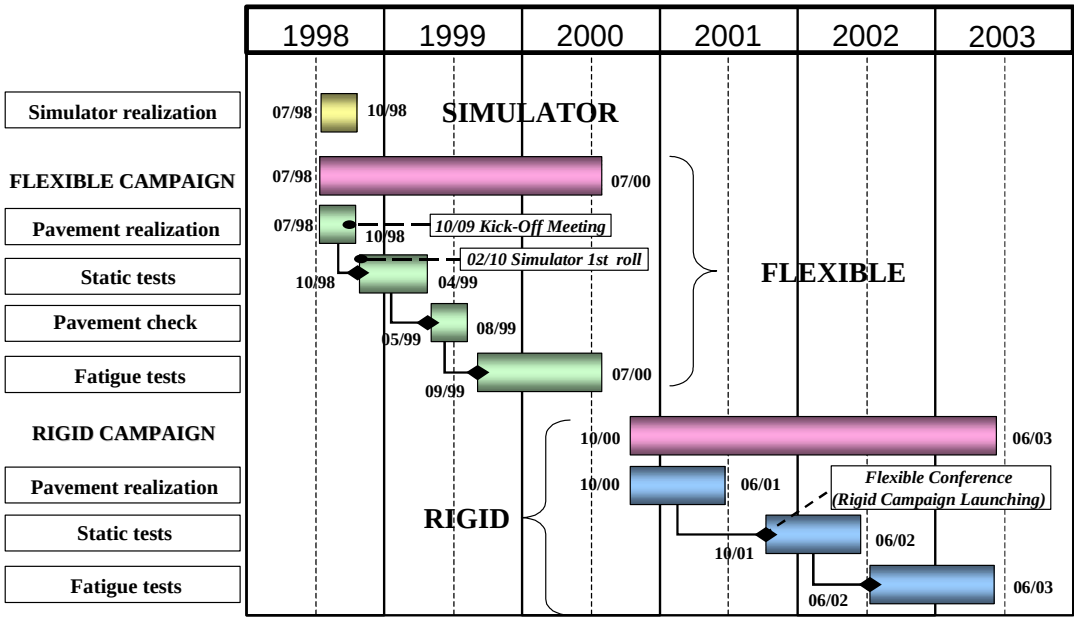

II- FLEXIBLE PHASE

II-1 TESTING FACILITIES AND MEANS

II-1-0 "ALIZÉ" Software

II-1-0-1 Presentation

The theoretical model used to analyze the results of the experimentation is ALIZÉ, the French basic computer program for the design of roads and pavements. It is based on the well known Burmister's semi-analytical solution for elastic multi-layered media submitted to uniform circular loads (for infinite horizontal extent and considering only isotropic elasticity for each later).

The French roads design method is based on the comparison between the strains calculated by ALIZÉ and the allowable levels of strain for one million coverages of the reference load determined by laboratory tests.
The calibration of the method is possible thanks to LCPC circular test track, which is able to simulate a real traffic on a pavement in order to compare theoretical and real duration of life.

LCPC circular test track, at Nantes

The « road » software has been adapted to aeronautical specifications: instead of point to point calculations, grid calculations are necessary because of the complex landing gear footprint (up to 20 wheels). Procedures of iteration and the adding of each gear contributions have been modified to speed the calculation.

The version of the software allows so calculating deflections, strains and stresses tensors generated by a full aircraft landing gear, in each point of a grid (with variable step), for a multi-layered pavement. The calculation duration is acceptable: about twenty seconds for ten thousands points, with a six layers structure, loaded with a twenty gears footprint. The software allows 2D or 3D visualization of calculated parameters.

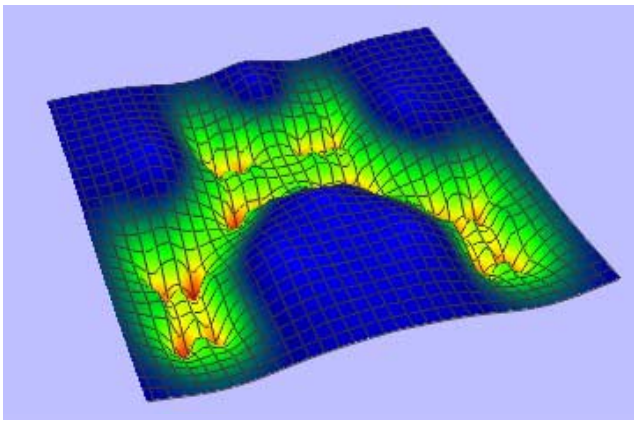

II-1-0-2 Comparison with Circly / APSDS

APSDS is well-known Australian software developed by Mincad Systems, to calculate damage in airfield pavement. It is based on a linear elastic multi-layered model Circly. A comparison has been done between ALIZÉ and Circly.

Data:

The aircraft considered is the C1 Seri, with the following footprint:

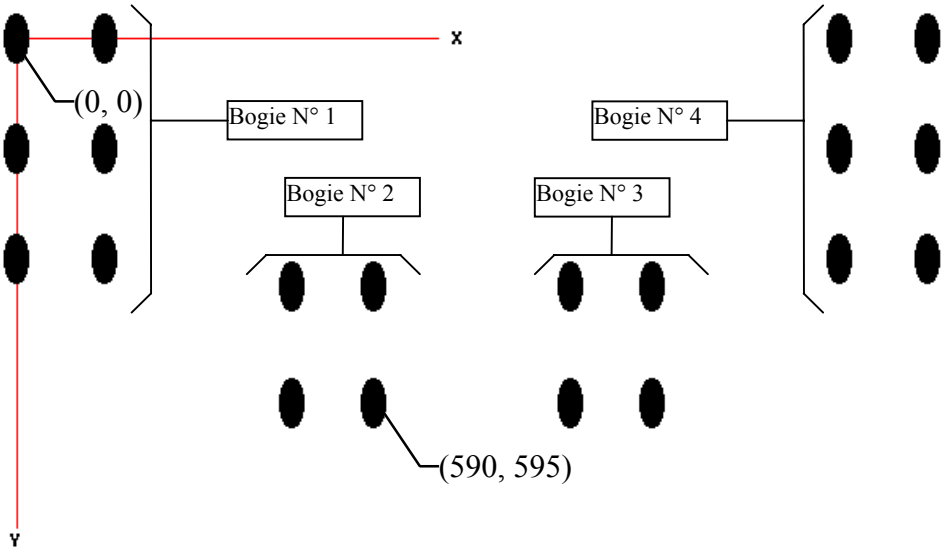

Bogie	X	Y
1	0	0
1	145	0
1	0	180
1	145	180
1	0	360
1	145	360
2	455	405
2	590	405
2	455	595
2	590	595
3	915	405
3	1050	405
3	915	595
3	1050	595
4	1360	0
4	1505	0
4	1360	180
4	1505	180
4	1360	360
4	1505	360

(dimensions in cm)

Weight: 520 tons on 20 wheels (26 tons per wheel)
Contact Pressure: 1,7 MPa
Contact area radius: 21,85 cm

For symmetric reason, the grid calculation is limited between [-100 cm; 800 cm] both for X and Y (with a step of 10 cm).

Three subgrade, corresponding to category B, C and D of the ACN / PCN method are considered. The pavement model (based on road experience in France) used in the simulation are the following:

Type D CBR 3:

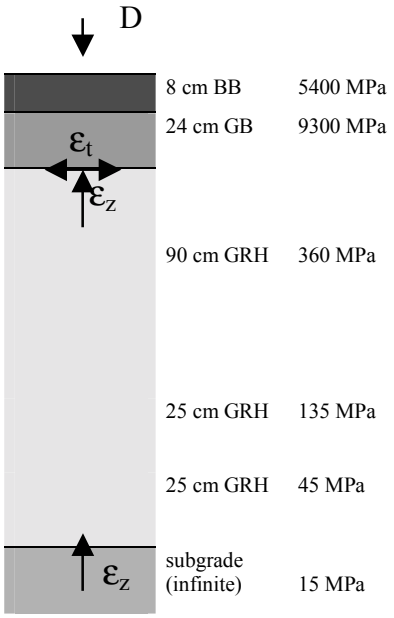

Type C CBR 6:

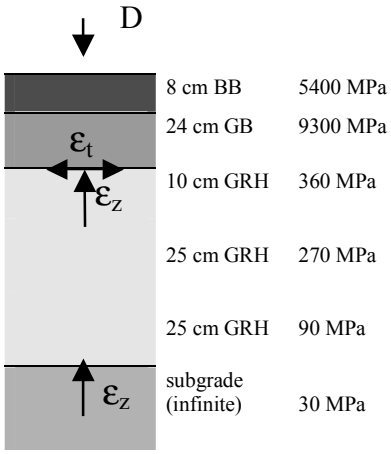

Type B CBR 10:

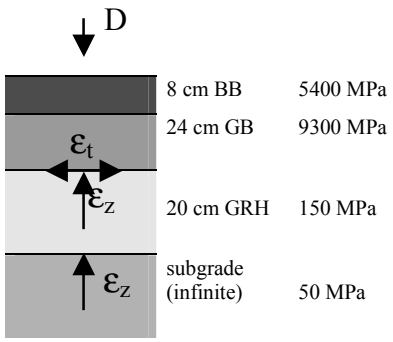

BB : asphalt concrete
GB : asphalt gravel
GRH : humidify reconstituted crushed gravel

D : deflection surface

ε_t : tensile strain

ε_z : vertical strain

Results:

Maximum values:
In both simulations, maximum values are close: the maximum relative error is less than 1%. Furthermore, the location of this maximum values are the same, excepted for two case (surface deflection for CBR 6 and CBR10, and subgrade vertical strain for CBR3) for which the location is only very close.

Circly 4.0		Surface: D (1/100e mm)	GB: ε_t (µstrain)	GRH: ε_z (µstrain)	Subgrade : ε_z (µstrain)
Sub. type D CBR 3	Max	**1980**	**202**	**526**	**1730**
	Location (X , Y)	*(590 , 410)*	*(450 , 400)*	*(0 , 180)*	*(80 , 180)*
Sub. Type C CBR 6	Max	**1240**	**267**	**519**	**1734**
	Location (X , Y)	*(580 , 420)*	*(450 , 400)*	*(0 , 180)*	*(100 , 180)*
Sub. Type D CBR 10	Max	**819**	**275**	**726**	**1378**
	Location (X , Y)	*(130 , 190)*	*(450 , 400)*	*(0 , 180)*	*(10 , 180)*

ALIZÉ		Surface: D (1/100e mm)	GB: ε_t (µstrain)	GRH: ε_z (µstrain)	Subgrade: ε_z (µstrain)
Sub. type D CBR 3	Max	**1974**	**202**	**526**	**1729**
	Location (X , Y)	*(590 , 410)*	*(450 , 400)*	*(0 , 180)*	*(100 , 200)*
Sub. Type C CBR 6	Max	**1236**	**266**	**519**	**1733**
	Location (X , Y)	*(540 , 440)*	*(450 , 400)*	*(0 , 180)*	*(100 ,180)*
Sub. Type D CBR 10	Max	**818**	**275**	**726**	**1377**
	Location (X , Y)	*(130 , 180)*	*(450 , 400)*	*(0 , 180)*	*(10 , 180)*

Global values:
The following charts show the difference between ALIZÉ and Circly for all the points of the grid (for CBR3 only; the results are the same for the two other subgrade type).
NB: X = vertical axis; Y = horizontal axis

Deflection

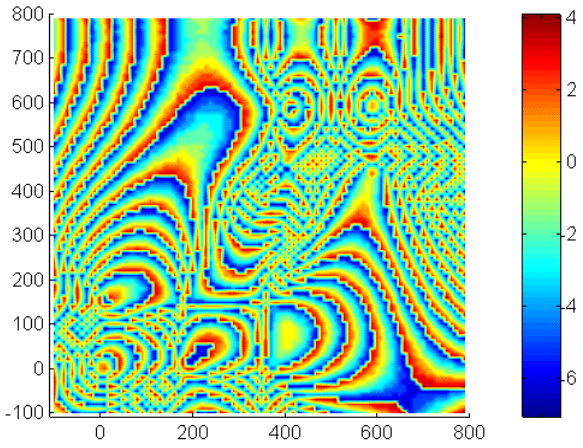

Error from -6 to 4 (1/100e mm). Deflection values are up to 10 mm.
For more than 80% of the points, the error is less than 41/100e de mm.
Error is not located.

EpsZ (GRH)

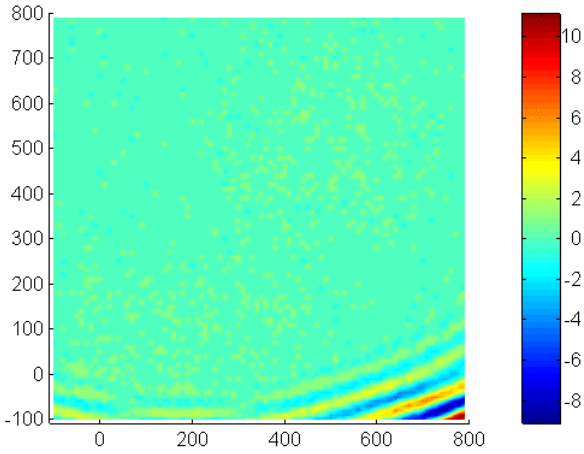

Error from -8 to 10 µstrain Maximum value is about 500 µstrain
For more than 96% of the points, the error is less than 1 µstrain
Error is located substantially in the zone defined by : -100<X<100 et 400<Y<800.

EpsT (GB)

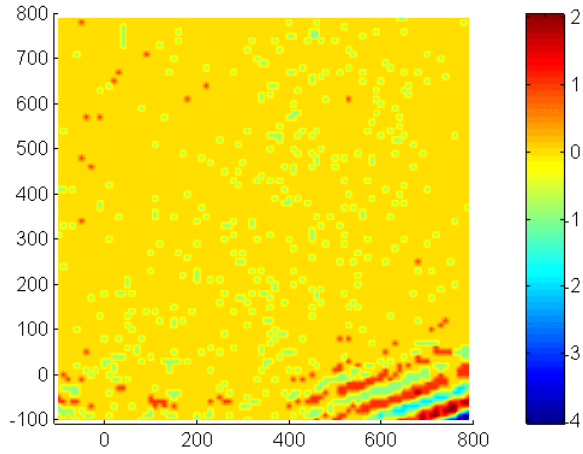

Error from -4 to 2 µstrain Maximum value is about 200 µstrain
For more than 98% of the points, the error is less than 1 µstrain
Error is located mainly in the zone defined by : -100<X<100 et 400<Y<800.

EpsZ (Top Subgrade)

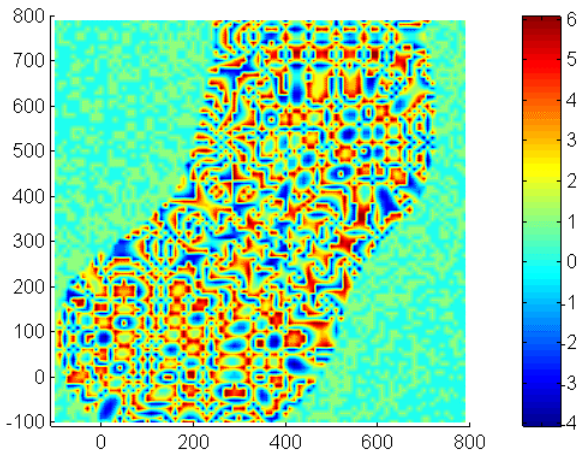

Error from -4 to 6 µstrain Maximum value is about 1750 µstrain.
For more than 90% of the points, the error is less than 4 µstrain
Error is located mainly under the area of the footprint

Conclusions:

In most of cases, the correlation between the results of ALIZÉ and Circly is very good:

- For more than 95% of the points, the relative error is less than 5%
- For more than 85% of the points, the relative error is less than 0,5%

Furthermore, the location of the maximum difference between the results of the software are far from the influence area of the gears; so, the difference are all the less significant as the values in these area are very small.

II-1-0-3 Preliminary studies

At the beginning of the program, several preliminary simulations have been made with ALIZÉ (Before calibration). The airport pavement have been then modeling as the same way as road pavement (especially in term of modulus for subgrade and for sub-layering of the unbound granular course):

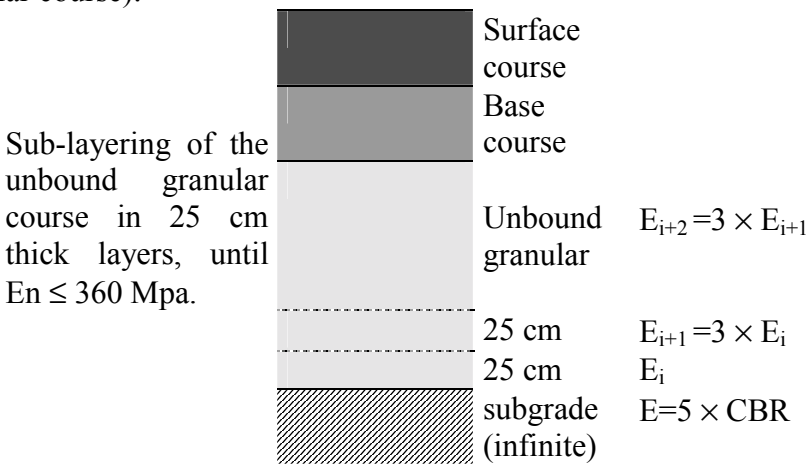

The models used for this preliminary calculation are exactly the same used for the comparison between Circly and ALIZE. On these structures, we have tested the first A380 data pack and other configurations (B747, B777...).
Here are some results for the B747:

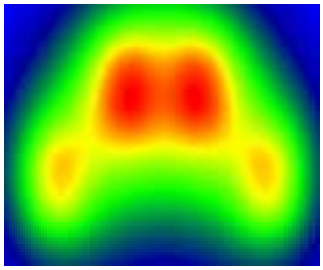

Vertical strain at the top of subgrade D

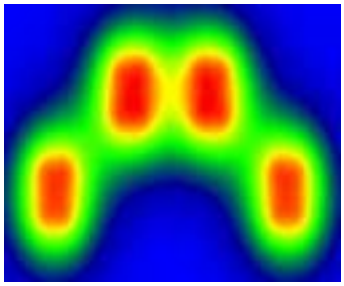

Vertical strain at the top of subgrade C

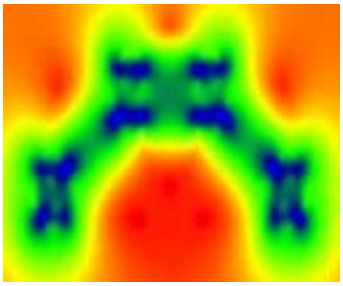

Tensile (horizontal) strain at the bottom of bituminous gravel (Struc C)

This example illustrates that we expected interactions between the bogie, especially for vertical strain at the top of subgrade, and very low strength subgrades.
This is why we have decided a full-scale experimentation, with the entire footprint of the aircraft (and not only isolated bogies).

The second observation of these preliminary calculations is the very high level of tensile strain at the bottom of subbase and very high vertical compressive strain on the top of subgrade, comparatively with usual “road” values. This observation has influenced the design of experimental pavement as described later.

II-1-1 The Runway

II-1-1-1 SITE Selection

All participants agreed that a full-scale experiment, as soon as practical, was required.
The site had to be in "open air" conditions, because of significant influence of external meteorological conditions on pavement, and the requirement to subject the pavement to real aircraft loads.
Because of the location of Airbus Industrie, the site was chosen in the area of Toulouse-Blagnac airport.
It is composed of 2 independent runways operated in a mixed mode (arriving and departing traffic mixed on the same runway). The runway 15R/33L was built for Concorde and is now mainly used by the manufacturers.

EADS site

At the Pavement Experimental Program (PEP) beginning, the development program of the maneuvering areas of Toulouse-Blagnac airport, included the lengthening of Taxiway B10 and B20 to improve taxiing time to the runway thresholds.
The experimentation site (measuring 164m × 30m) had to be integrated in the development program of the airport, with minimal impact on the runway operations (radioelectrical interference caused by the simulator; air traffic procedure affected by the erection of a 26m high telescopic crane used to load the simulator, especially in LVP procedure i.e. visibility less than 1000m or ceiling less than 200 ft…).

Finally, the experimental site was chosen at the southern end of the taxiway B20.

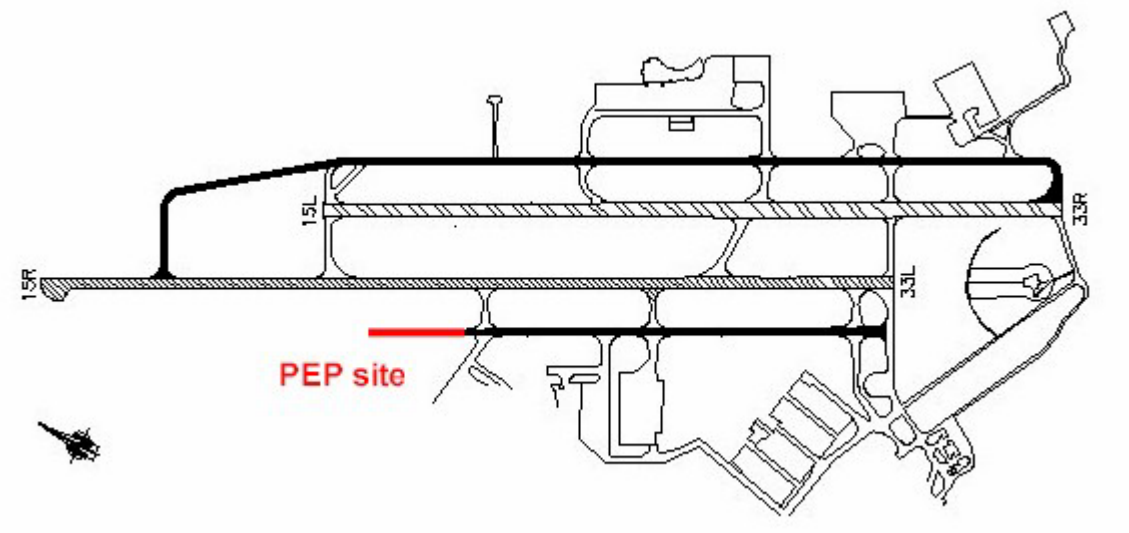

II-1-1-2 SPECIFICATION

It was decided that the tests would be representative of all types of subgrade considered by the ACN / PCN method, from very low strength to very high strength. This subgrade are characterized by:

- Subgrade A: CBR = 15
- Subgrade B: CBR = 10
- Subgrade C: CBR = 6
- Subgrade D: CBR = 3

II-1-1-2-1 Pavements structure

General Design Calculation

The French method for airfield pavement design uses the CBR method, based on "Equivalent Single Wheel" concept.
The complex landing gear is first converted in an Equivalent Single Wheel thanks to the Boyd and Foster simplified method :

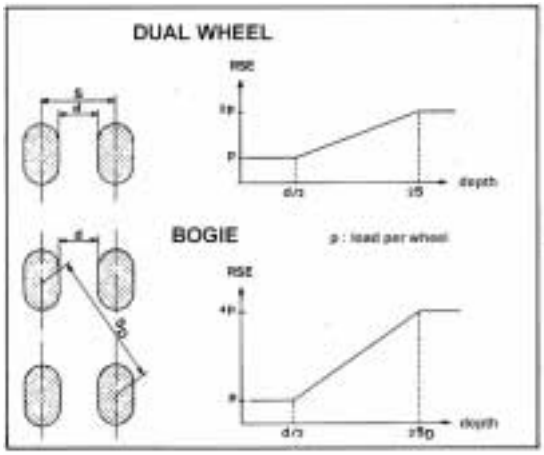

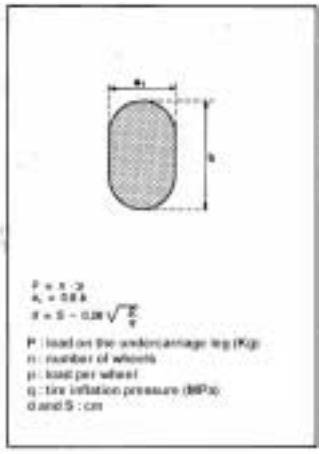

The CBR formula, determined by the US Corps of Engineers, allows the calculation of an equivalent thickness of pavement for which the vertical stress produced at the top of the pavement by a single load P at a pressure q applied 10.000 times produces acceptable stress at the subgrade level; this formula, combined with Boyd and Foster transformation allows to draw design charts for each aircraft:

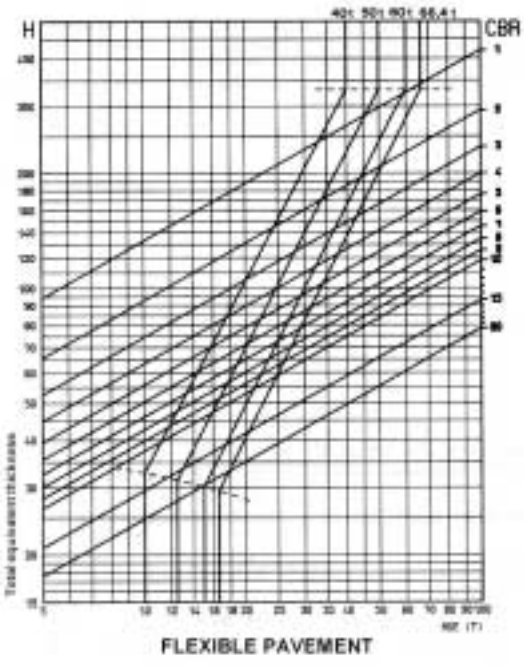

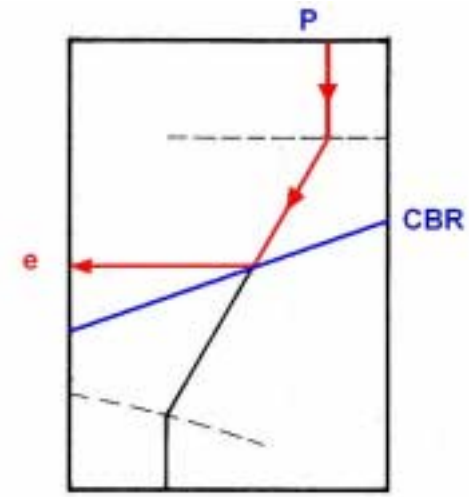

The CBR formula outputs an effective thickness for an homogeneous body constituted by a reference material (unbound gravel, crushed and well graded, with an elastic modulus E = 500 MPa). In reality, the pavement is composed of several courses each having different mechanical quality. Equivalent thickness is transformed in real thickness thanks to the concept of coefficient of equivalence, which is different for each type of materials :

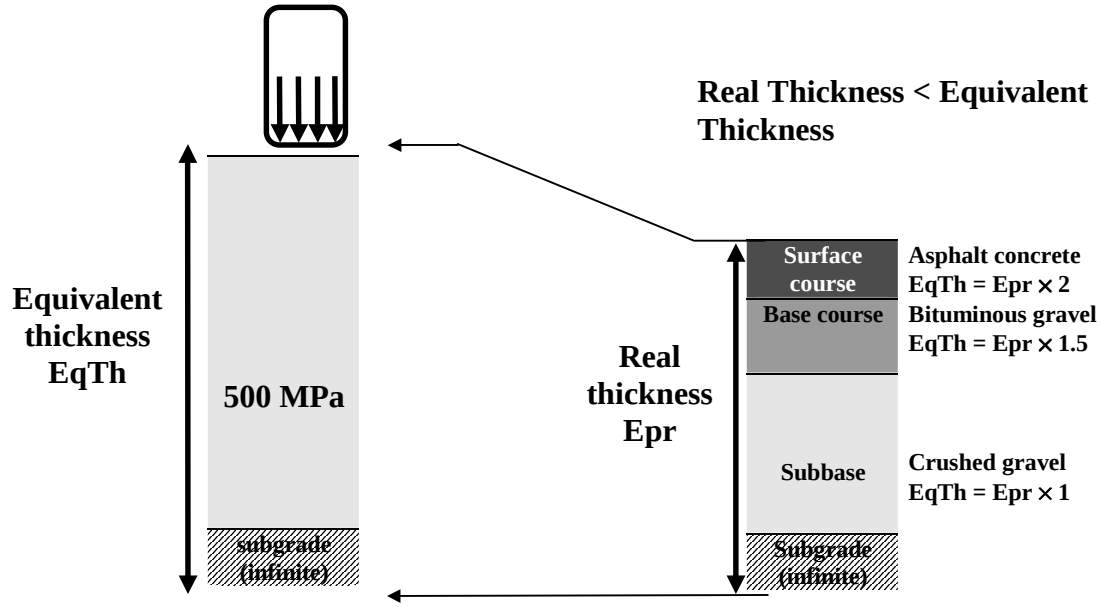

Bounded materials have to have a minimal thickness, deduced from the following chart.

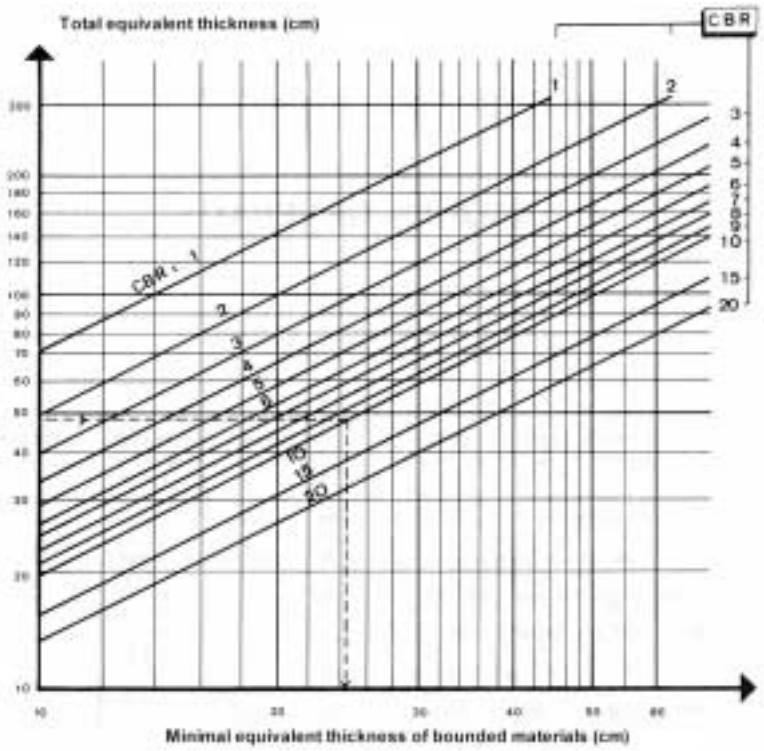

Choice of pavement structure

The reference aircraft chosen to design the experimental pavement is the B747 – 400 with the following characteristics:

- MTOW: 398 tons
- Load per wheel: 23.2 tons
  - Tire pressure: 1.38 Mpa
  (Contact pressure: 1.6 Mpa)

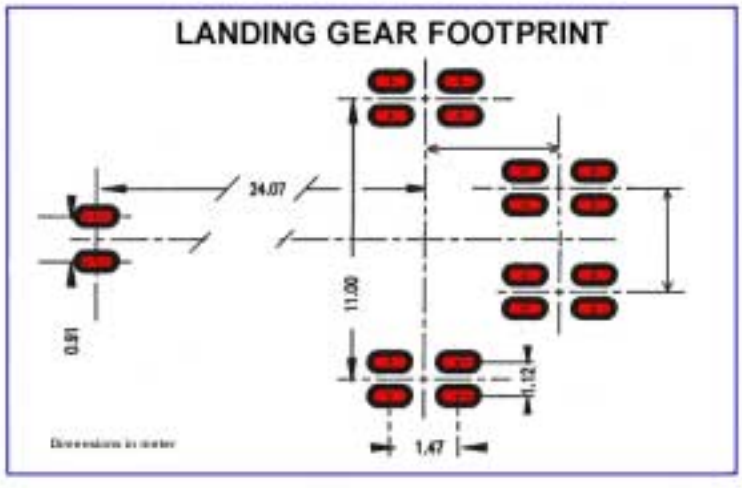

The design has been made for the effective load of the B747, traffic of 10 movements per day and a time life of 10 years for the pavement.

The results are the following:

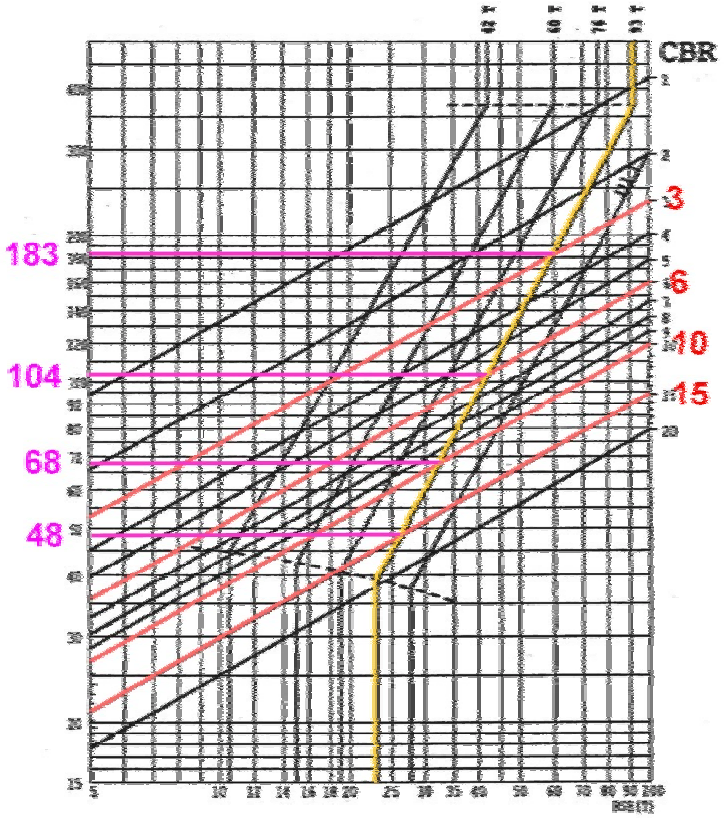

CBR = 3 Eq = 183 cm
Et = 46 cm
CBR = 6 Eq = 104 cm
Et = 41 cm
CBR = 10 Eq = 68 cm
Et = 35 cm
CBR = 15 Eq = 48 cm
Et = 31 cm

In order to simplify the pavement construction, we have decided to choose the same equivalent thickness of bounded materials for all the structures (46-cm).

The equivalent thickness is then transformed as following:

	Equivalent thickness
Surface course : 8 cm of Asphalt concrete	$2 \times 8 =$ **16 cm**
Base course : 20 cm of bituminous crushed gravel	$1.5 \times 20 =$ **30 cm**
Subbase course Recombined - wetted crushed gravel	
Type D (CBR = 3) 137 cm	Round to **140 cm**
Type C (CBR = 6) 56 cm	Round to **60 cm**
Type B (CBR = 10) 22 cm	Round to **20 cm**
Type A (CBR = 15) 2 cm	-

A few simulations have been made, based on these parameters, with ALIZÉ software to control the level of strain for each structure loaded in accordance with the first A380 data pack and other configurations (B747, B777)… At this stage, the model of the pavement is typically based on a "road" model (values of the modulus…).

We found high level of tensile strain at the bottom of subbase and very high vertical compressive strain on the top of subgrade, compared to "road" values.

The thickness of the base course was modified and fixed at **24 cm**. The levels of deformations calculated by new ALIZÉ simulations then appeared in better adequacies with the estimated performances of materials.
Finally, the four experimental structures are:

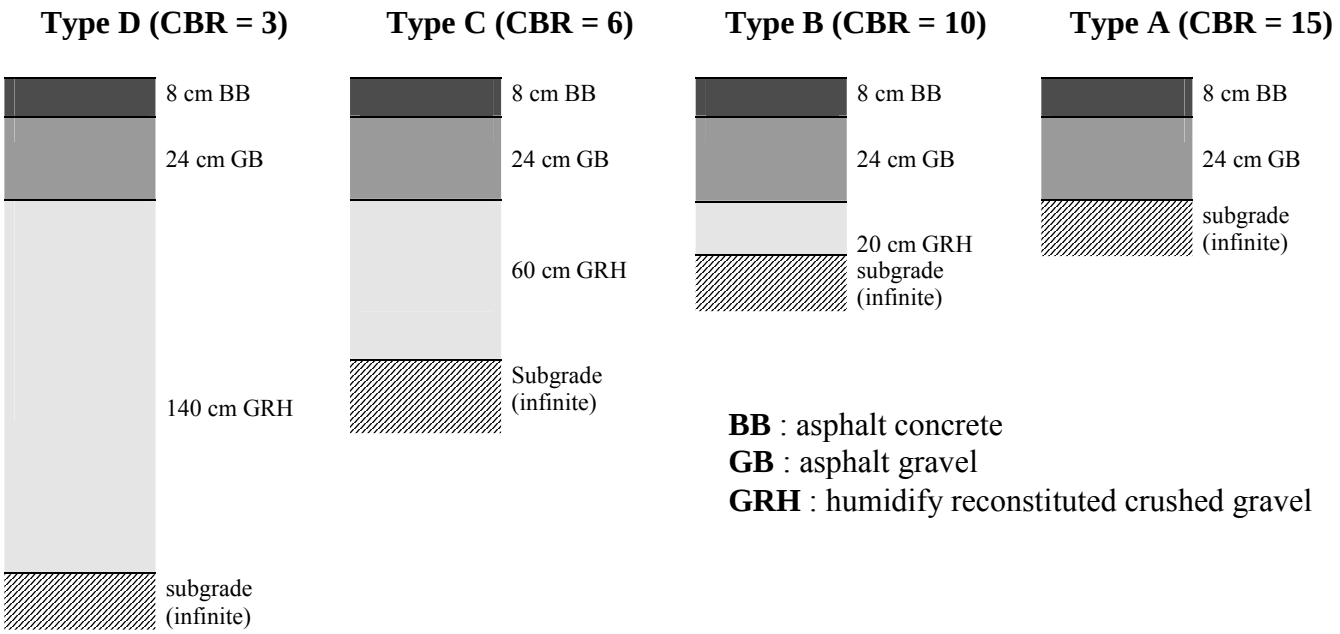

II-1-1-2-2 Experimentation Area

The test area was a combination of four sections (one for each subgrade type) separated by transition sections.

Simulations made with ALIZÉ on predefined structures loaded with single and multiple gear legs, have shown theoretical interference at the subgrade level between multiple gear , especially on low CBR subgrade.
Consequently, it was decided that the experiments would be carried out with full-scale landing gear (no use of isolated bogies for example).

The outer wheel track varied from 16 m for the A380, to a minimum of 12 m (for such as B747, B777, MD11, A340).
To minimize border effect and to allow lateral wander of the landing gear simulator, the width of each test section was fixed to 30 m.

Each experimental section was 30 m long, and the transition section was 5 m. long.

A section of pavement at the end of the test pavement was built to allow the parking of the simulator for maintenance and loading.

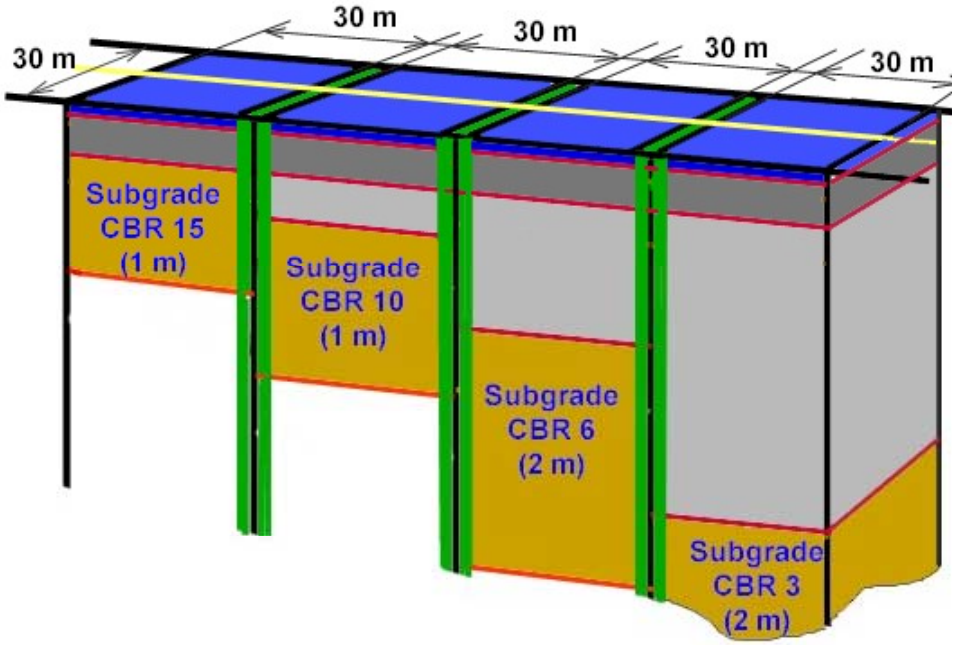

The open field test site gave early results in realistic environmental conditions (temperature, sun, wind and rain) and allowed possibility with real aircraft maneuvering.
Conversely, these open field conditions could be a problem for the pavement building (moisture control during subgrade construction) and even for the analysis of the test results (temperature corrections...). The results of the experimentation cannot be generalized automatically to every kind of climatic condition.

II-1-1-2-3 Pavements construction

- ***General Specifications***

The typical cross section and the longitudinal profile section conformed with ICAO standards. The transverse slope on the runway is 1.5 % and the longitudinal mean pavement slope is 0% in order to facilitate the simulator tracking.

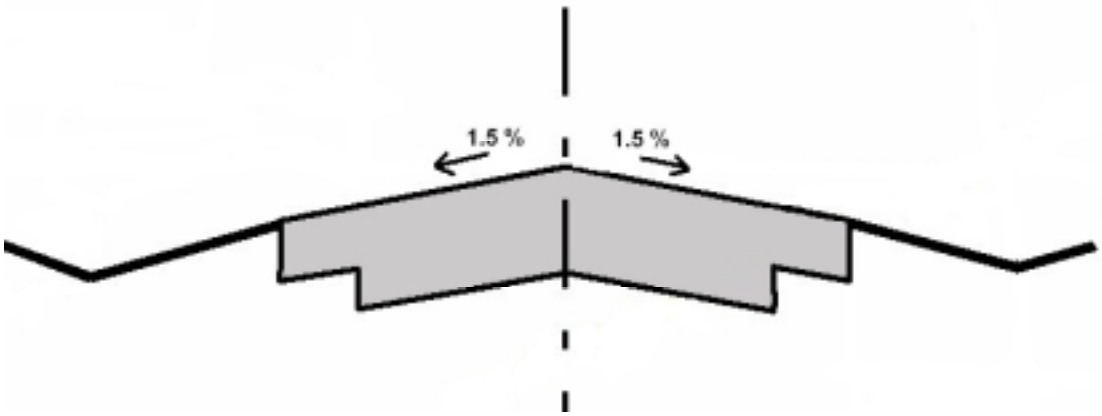

Typical cross section

- ***Pavement Materials Specifications***

All the works done for the construction of the experimental pavements were made in compliance with specifications based on general regulations used in French public works domain.

This specific prescriptions include rules for the definitions of work modalities, choices, specifications and controls of all the materials used in the construction.

Details are in a document (called "Pavement Specifications") which is a kind of conditions of contract, given to firms during the invitation to tender.

Surface course materials :

The course is 8 cm thick of aeronautic asphalt concrete (BB), which is a standardized material (standard NF P 98 131).
The specifications required a 0/10 continuous grading with the following characteristics:

- **Grading**: sand 0/2: about 37%
  Aggregate 2/6.3: about 19%
  Aggregate 6.3/10: about 42%
  Fines: about 2%
- **Aggregate classification**: B III a (standard NF XP P 18 540)
- **Bitumen 50/70**: about 6.2% ([1])
- **Reference density**: 2.40
- **Gyratory shear compacting press test:** (standard NF P 98 252)
  % Of voids for 10 gyrations: > 10%
  % Of voids for 60 gyrations: between 4% and 6%
- **Duriez test**: (standard NF P 98 251-1) water sensitivity measurement
  Resistance to compression (dry): > 6 MPa
  Ratio (wet / dry): > 0.8

The mean value of the in situ compaction had to be between 94% and 97%.

[1] The bitumen content is defined by French definition : $\frac{\text{bitumen mass}}{\text{aggregate mass}}$

Base course materials :

The course is divided in two layers of 12 cm thick each of bituminous gravel class2 (GB2). GB2 is a standardized material (standard NF P 98 138)
The specifications required a 0/14 continuous grading with the following characteristics:

- **Grading**: sand 0/2: about 35%
  Aggregate 2/6.3: about 13%
  Aggregate 6.3/10: about 50%
  Fines: about 2%
- **Aggregate classification**: C III a (standard NF XP P 18 540)
- **Bitumen 35/50**: about 4.5% ([1])
- **Reference density**: 2.30
- **Gyratory shear compacting press test:** (standard NF P 98 252)
  % Of voids for 10 gyrations: > 11%
  % Of voids for 60 gyrations: between 5% and 7%
- **Duriez test**: (standard NF P 98 251-1) water sensitivity measurement
  Resistance to compression (dry): > 7 MPa
  Ratio (wet / dry): > 0.75

Subbase course materials :

A number of successive layers, depending of the final thickness constitute the course. The material used is high quality crushed gravel (GRH).
A graded recombined humidified aggregate 0/20 instead of a coarse gravel had to be used because this material is made in a stabilization plant from elementary gradation cut off (0/2, 2/6, 6/10 and 10/20) which avoids segregation and moisture content is controlled.
The specifications required a 0/20 graded GRH with the following characteristics :

- **Aggregate classification** : C III a (standard NF XP P 18 540)
- **Crushed index** : > 60%
- **Moisture** : 6%

Subgrade materials :

The construction of the subgrades was the most critical work.

Trial boring has been taken in the area of the experimental pavements in order to analyze.
Three types of subgrades were found, classified by the GTR (French subgrade classification) as following:

- C1B5, clay material with gravel
- C1B6, clay material with gravel
- A2, pure clay.

Geotechnical studies have shown that these materials can be used to construct the subgrades; laboratory tests have then been done to determine the appropriate moisture to obtain the wished CBR value.

The specifications are then the following:

Type of pavement	Subgrade classification	Moisture targeted	EV2 Modulus ([2])
A CBR 15	C1B5	8.2 %	120 MPa *+/- 8 MPa*
B CBR 10	C1B6	10.5 %	70 MPa *+/- 5 MPa*
C CBR 6	A2	18 %	35 MPa *+/- 4 MPa*
D CBR 3	A3 (to be found by the contractor	26 %	20 MPa *+/- 3 MPa*

- ***Construction***

Contractors:

The Earthworks have been achieved by **ESBA** (specialized team of STBA).

The contractor for building was Enterprise **MALET** (French firm of public works).

Methods and machines:

To be as representative as possible of real pavement, we had use usual construction methods and roadbuilding machines. No special machines were developed for this experimentation, especially for the installation of sensors

Subgrade achievement

During the Earthworks, there were one Motorscapers team, two tracked excavator and dumper teams and one bulldozer team. Works lasted for one week. 12000 cubic meters have been extracted. The return seems little, but all materials have been selected according their GTR classification (C1B5, C1B6 and A2).

The first work of the contractor was to find A3 materials in a site outside from the airport area. The borrow pit has been scoured, clay A3 has been scraped and sprayed with water. 4000 cubic meters of A3 have been used, and 7% of water has to be added to obtain the lowest CBR. That is to say 600 cubic meter.

Every day, there was a loading team at the borrow pit and an other one on the airport site. Two other formations set the materials: the first one constituted with a bulldozer on platforms C and D, and the second one constituted by a grader and one mixed compactor for platforms A and B. A geometer checked all layers and the laboratory of the contractor took materials to check CBR and water susceptibility.

[2] the CBR test is no more used in France for roadworks controls. The usual control is a plate bearing test given the EV2 modulus (approaching Young Modulus) ; the targeted values correspond to the wished CBR.

Continuous EV2 tests allowed to build homogeneous layer: for example, when theoretical water susceptibility was too low, resistance to deformation (measured by EV2 test) was too high, the subgrade was scraped and sprayed with water until obtaining the specified values. Inversely, the subgrade was scraped when weather was sunny to dry the subgrade.

The EV2 measurement principle is based on Boussinesq's theory:

Under an uniform pressure applied on a circular plate (radius a), the surface deflection W is given by :

$$W = 1.5 \times \frac{q}{E} a\left(1 - \upsilon^2\right)$$

The characteristics of the test are: q = 0.2 Mpa; a = 0.3 m

With usual value of ν = 0.25, the EV2 modulus is given by $EV2 = \frac{90}{W_2}$, where W_2 is the surface measured deflection after two loads.

Once the layers were finished, the contractor laboratory made final plate test: one every 25 m (120 units).
In order to maintain the water susceptibly of each material, the contractor sprayed a bituminous slurry seal all platforms and used a "geotextile" on platform D.

After this phase, a first work stop allowed to set vertical strain gauges at the top of subgrade (see a forward section).

Foundation course achievement

Trucks were covered on to avoid evaporation during GRH transportation, in order to control GRH moisture.
A trax, a laser grader, a pneumatic tired roller and a compactor insured compliance with specifications. Layers were 30 cm deep so as not to damage instrumentation below (for such depth, compaction energy is not high).

On each intermediate layer, the contractor laboratory controlled moisture content and density.
On the final layer, the geometer took the level of the whole platforms and density tests with gammadensimeter (one every 25 m²) and plate tests (6 per platform) have been done.

After this phase, a second work stop allowed to set horizontal and vertical strain gauges in the GRH course and at the base of the base course (see a forward section).

Base and surface course achievement

These courses were used by two teams each constituted by one finisher, one pneumatic tire roller and one compactor, for two reasons: quality (hot longitudinal joint, best compaction) and full capacity.
The base course was achieved in two layers.
All the layers were adhered to one other with cationic emulsion.
Density tests with gammadensimeter have been done for each layer (every 25 m²), and the final level has been taken by the geometer. Transversal and longitudinal profiles have been checked.

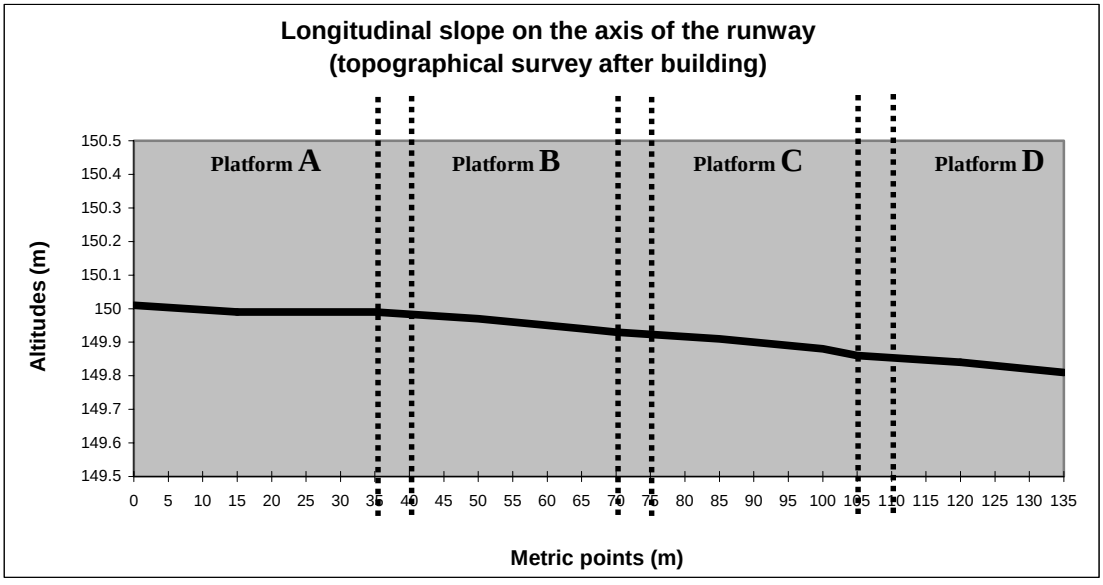

Mean slope: 0.14 % (0% targeted)

- ***Results of controls - Building drawbacks***

One of the keys points for the experimentation was the subgrade construction.

Type of pavement	Subgrade classification	Moisture targeted	EV2 Modulus	Moisture in situ	EV2 Modulus (mean) ([3])
A CBR 15	C1B5	8.2 %	120 MPa *+/- 8 MPa*	7.3 % to 9.4%	124.2 MPa
B CBR 10	C1B6	10.5 %	70 MPa *+/- 5 MPa*	8.0 % to 11.0%	74.6 MPa
C CBR 6	A2	18 %	35 MPa *+/- 4 MPa*	17.0 % to 19.0%	33.4 MPa
D CBR 3	A3	26 %	20 MPa *+/- 3 MPa*	25.6 % to 30.9%	20.3 MPa

The mean value respect the prescriptions and the results are quite homogenous over the whole platforms (see following chart).

Working conditions were very hard for the subgrade D construction, because the targeted value (20 MPa) means that this subgrade has very low bearing capacity. That was not a problem for the bulldozer that used materials, but the water sprayer has to be pulled with a cable because it has sunk! Plate test have been made with PSP bearings for allowing the test truck trafficability (it explains the only one half plate bearing test section for platforms C and D ; the test section is under sensors location)
For real aeronautic pavement building, a subgrade of CBR 3 is always treated with lime to increase its bearing capacity to avoid the problems we have voluntarily encountered for this experimentation.

[3] the CBR test is no more used in France for roadworks controls. The usual control is a plate bearing test given the EV2 modulus (approaching Young Modulus); the targeted values correspond to the wished CBR.

Values of EV2 Modulus (MPa)

Pavement B

104.6	70.3	81.8	76.3	75	72.6	75
76.3	76.3	72.6	62.1	73.6	75	83.3
72.6	75	81.8	76.3	67.2	76.3	80.3
70.3	72.6	81.8	90	75	71.4	72.6
72.0	69.2	75	76.3	75	66.2	73.8
75.0	78.9	75	72.6	112.5	77.6	81.8
109.7	75.0	66.2	65.2	75	56.2	112.5

Mean : 74.6 MPa
Standard deviation : 5.2 MPa

Pavement A

125.0	121.6	128.6	125	121.6	128.6	128.6
121.6	115.4	118.4	121.6	118.4	128.6	118.4
118.4	118.4	136.4	136.4	118.4	128.6	115.4
118.4	145.2	118.4	160.7	109.8	118.4	140.6
132.4	128.6	132.4	121.6	115.4	128.6	118.4
128.6	115.4	112.5	118.4	125.0	115.4	118.4
128.6	128.6	140.6	125.0	128.6	109.8	109.8

Mean : 124.2 MPa
Standard deviation : 9.72 MPa

13 m	
10 m	
5 m	
Axis	
5 m	
10 m	
13 m	

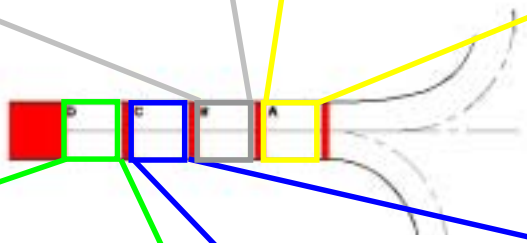

Pavement D

19.8	22.4	22.3	16.8	20.0	16.2	21.6
22.4	21.4	21.9	21.9	17.6	17.4	17.7
22.6	17.6	19.6	30.0	14.5	13.4	20.9
21.0	23.7	25.0	20.4		19.6	21.4

Mean : 20.3 MPa
Standard deviation : 3.38 MPa

Pavement C

28.7	37.5	30.5	31.2	30.0	31.7	31.2
37.5	32.2	31.4	33.2	30.0	30.0	37.5
33.1	31.0	32.1	36.9	32.2	31.2	32.1
39.4	39.1	37.5	30.4	33.8	40.9	33.1

Mean : 33.4 MPa
Standard deviation : 3.4 MPa

The above values (EV2 modulus on platforms) were measured just after the achievement of layers.
Because of the open field conditions (and despite of the different curing layers), the structures were still « vulnerable » to water until the first bituminous layer has been set.
Unfortunately, when the weather was very fine for earthworks, subgrade construction and GRH use, a rainstorm has suddenly fallen on the site just before the implementation of GB.
Reconstructed subgrades B, C and D have been "protected" by the gravel layer and their moisture had not significantly changed. Conversely, platform A has no gravel layer and the rain fell directly on the subgrade. This type of subgrade (C1B5, clay with gravel) is water susceptible and so, its bearing capacity decreased (heterogeneously along a cross section). After only few coverage of the simulator on platform A, surface ruts and depressions appeared and all the vertical sensors set in GB were destroyed because of the high level of strain in the pavement. Platform A area has been partially rebuilt to set new sensors.
This water pollution of the platform A is important to explain all the drawbacks encountered on this section during the tests.

- ***Bearing capacity controls***

After the end of building, the experimental pavement bearing capacity has been checked by plate bearing tests, with the method developed by STBA for airfield pavement evaluation. It is important to say that this method is usual for **old** pavement. Plate bearing test on new pavement can be altered because the global ultimate settlement is not yet reached for example.

Each plate bearing tests are operated with the « Bearing strength evaluation trailer » developed by STBA.
This apparatus consists in :

- a road size tractor,
- a laboratory cabin equipped with micro-computer controlling the tests automatically, together with acquisition, remote processing and recording the measurements,
- a 40 m3 container providing a 60 t mass
-A hydraulic jack and a plate placed just under the trailer's center of gravity,
-Measurement devices (reference beam, compressive stress gauge, vertical deformation and horizontal elongation gauges).

- ***Test principle for flexible pavement***

The plate bearing test on flexible pavement consist in applying a repeated loading fatigue test on the subgrade pavement complex, in order to determine the pavement working load which after 10,000 applications induces an allowable settlements.
The pavement is loaded and unloaded with growing load levels, chosen to bracket the assumed working load. Several tests showed that the residual settlements after loading increased linearly with the logarithm of the number of load application. This law is used to calculate for each loading level the residual settlement after 10,000 cycles with the one

measured after the first ten. Then, the curve residual settlement = f(10,000 cycles repeated loads) is drawn.
The pavement-working load is given by this curve and the value of the allowable residual settlement selected in function of the pavement type and the shape of the curve.

- ***Test methodology***

The plate diameter is selected so that the mean pressure applied to the pavement is representative of usual tire pressure of aircraft taxiing on the pavement.
So, a diameter of 42 cm is generally chosen for loads less than 20 metric tons and a diameter of 65 cm for the ones between 20 and 50 metric tons.

Vertical deformations are measured by gauges (one through the plate, and the others at regular distances from the edge of the plate) in order to define the shape of the deflection curve.

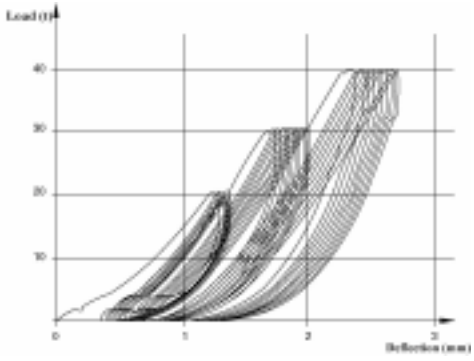

Ten loading-unloading cycles are applied for the pavement for each loading level.
The first one is low (less than the supposed working load) and the next ones increases in function of the settlements obtained with the previous load.
In most of cases, three or four loading levels are used to determine the pavement-working load.

- ***How the measurement are used***

The residual settlement at the end of the ten cycles measured for each load is extrapolated to 10,000 cycles along the experimental logarithmic law.
Then, the curve residual settlement = f(10,000 cycles repeated loads) is drawn (with three or four point, depending on the number of loading levels).
The working load of the point tested is deduced from an allowable residual settlement, usually chosen between 2.5 and 5 mm for flexible pavement. This value depends on parameters such as the age and visual aspect of pavement, and the R3d value (Product of R, curve radius of the deflection curve under the first gauge, into d, deflection under the load).
The working load Ps of a homogeneous area is the mean P of the working load for each tested point in the area, reduced of the standard deviation δ of all the measurements on the area. ($P_s = \overline{P} - \delta$).
Laboratory or in situ tests give the geotechnical characteristics of:

- subgrade, and especially CBR
- Materials of each layer

The values of the equivalence coefficient for each layer are then estimated as a function of the age of the pavement.

The characteristic of each homogeneous area is obtained by comparing the working load given by the "reverse design method" which estimates an equivalent coefficient and C.B.R of the subgrade.
When the values are close, the homogeneous area is characterized by:

- C.B.R. value of subgrade,
- Equivalent thickness of pavement,
- Pavement working loads Pa (single isolated wheel (R.S.I.), dual wheels (J) and dual tandem wheels (B)) deduced from the graphical design for a typical undercarriage (based on the two previous sets of data).

- ***Results for experimental pavements***

Three series of test were conducted on the test pavements:

The first series were made two months after the completion of the pavement construction, the second at the end of static tests and the last one after the fatigue tests. The pavement temperature conditions were similar for the three period of testing and ranged between 15°C and 20°C. All the tests has been conducted in accordance with the procedure described here above.
The last two series are presented in a following part.

The first series tests were made very close to the end of construction (2 months). Normally the evaluation of bearing capacity of new aeronautical pavements is made at minimum of two year after the building works to allow the stabilization of the structures. For that reason the results given hereafter must be considered in a relative way.

The bearing capacity for each platform is ranged from:

- 20T to 34T for the platform A
- 22T to 32T for the platform B
- 18T to 24T for the platform C
- 18T to 36T for the platform D

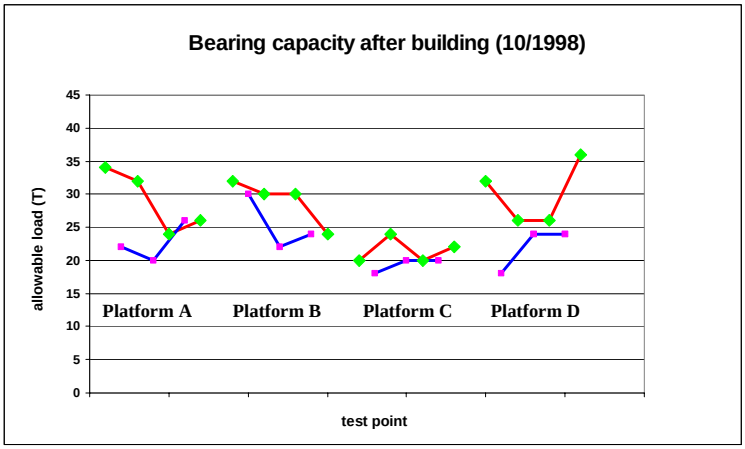

These results are not very homogeneous. First, the age of the tested pavement was not really adapted for the method. Moreover, this plate-bearing test is very sensitive to variations into the Subgrade. The modulus heterogeneity observed during controls (even if the values respect the prescriptions) can explain this difference of bearing capacity (because of differential settlements, accentuated by the age of the pavement).

II-1-2 The instrumentation

II-1-2-1 OBJECTIVES

The main objective of the instrumentation is to get a comprehensive description of the pavement behavior during the static and fatigue campaigns.

This included:
- the resilient deflection under the simulator (static test)
- the resilient strains in the different layers of the structures (static and fatigue tests)
- the permanent component of the vertical displacement of the different layers (fatigue test)
- the temperature profile in the structures (static and fatigue tests).

The aim was to provide:
- comparative data between the different configurations tested during the static campaign
- information about the damage process at stake during the fatigue campaign
- Absolute data for the assessment of theoretical models and the elaboration of a new design method for airfield pavements in the longer term.

II-1-2-2 Description of the instrumentation used

II-1-2-2-1 Resilient strain measurements

The instrumentation of the pavements includes primarily strain gauges allowing the measurements of the reversible strains caused by moving load in various materials. Each specimen pavement section was instrumented on one side only due to symmetry. It must be underlined that this whole set of equipment is similar to that used by LCPC for in situ experimentation on roads, and on the experimental pavements tested with Nantes Accelerated Load Test (ALT) facility **[ref°1]** and is fully validated.
These strain gauges are positioned:
- At the base of asphalt concrete (GB) on the 4 sections.

Horizontal strain sensors on GB base.

These gauges are placed at approximately 1 cm above the top of the interface with the subgrade (structure A) or with the GRH untreated graded material (structure B, C and D). They are laid out horizontally, some of them in the longitudinal direction parallel with the axis of displacement. These gauges aim at quantifying the traction developed by the loads at the base of GB, where these effects are maximum.

- At the top and the base of the GRH (structures C and D) and in the medium of the GRH (structure B). These second type of gauges are placed vertically. They ensure the measurement of the vertical resilient strains created by the loads, at a distance of

approximately 10 cm from the top and the bottom of the GRH layer (structures C and D), or at the middle of the layer (structure B). These measurements are used to quantify the effects of reversible compression supported by the GRH. Rutting of untreated graded material is depending to this resilient compression according to usual dimensioning models.

- At the top of the subgrade on the 4 sections. These last gauges are positioned vertically. They allow the measurement of the resilient vertical strains at 10 cm of depth in the subgrade. As for the GRH, the current dimensioning models connect the rutting of the subgrade, to the vertical compression created by the traffic to its top.

Vertical strain sensors on top subgrade and their cabling.

In this way, a total of some 250 resilient strain sensors is installed into the four sections and is able to provide redundancy.

II-1-2-2-2 Transverse profiles of measurement

The possibilities of lateral displacement of the simulator are limited. In practice, its movement during the static test will be carried out by aligning the interior of the right wheel of wing bogie on a fixed and single axis for all the configurations (the "yellow line"). Consequently, it was necessary to lay out the strain sensors of the various types according to transverse profiles, in order to make sure that the maximum strain related to each configuration of load tested could be recorded by the system.

Figures 1 to 4 specify the transverse distributions retained, according to the level of the group of strain sensors considered. It will be observed that two strategies were adopted.

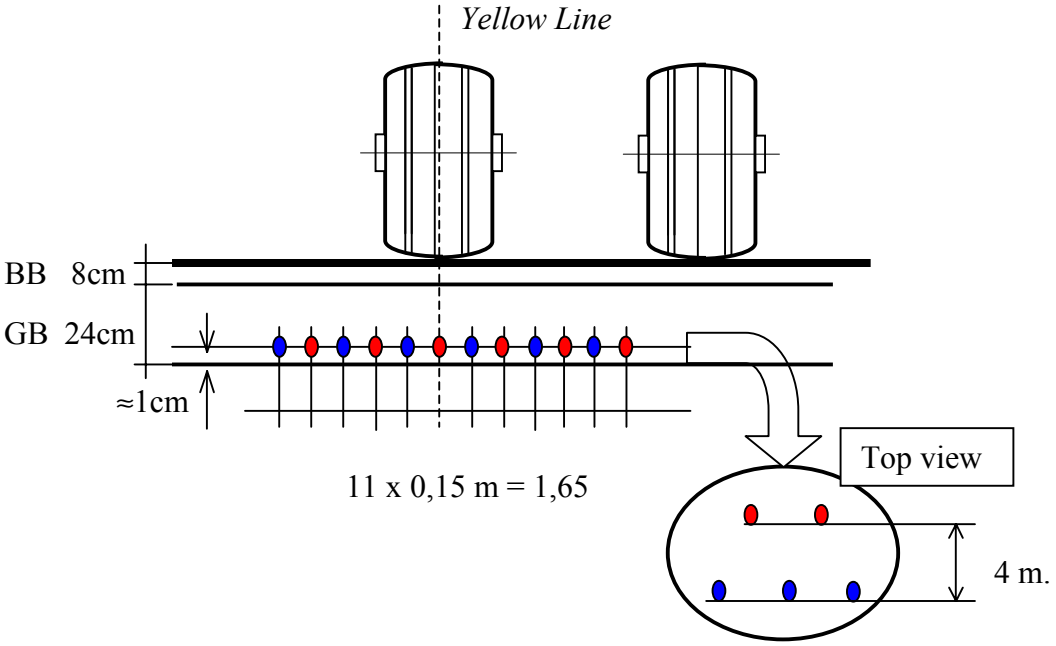

Figure 1: Alternated gauges location transversal profile on GB base.

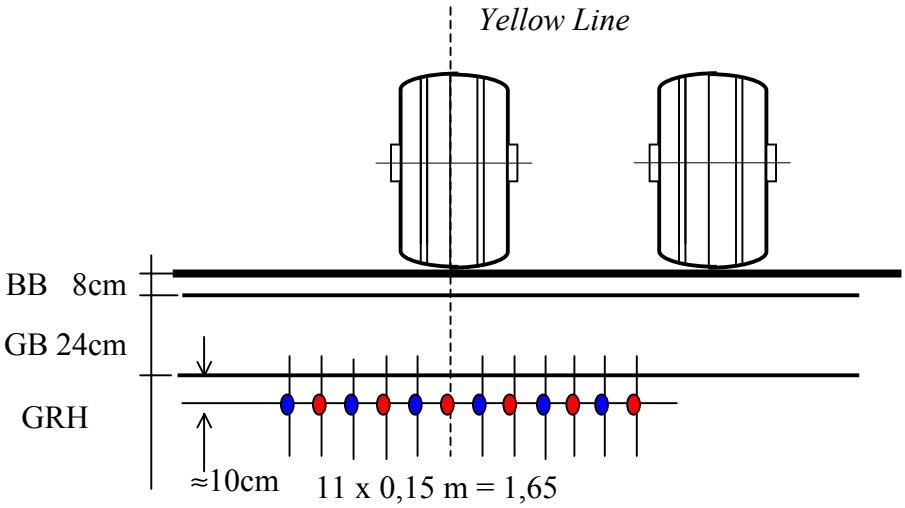

Figure 2: Alternated gauges location transversal profile on top GRH (Structures B, C & D) and subgrade (structure A).

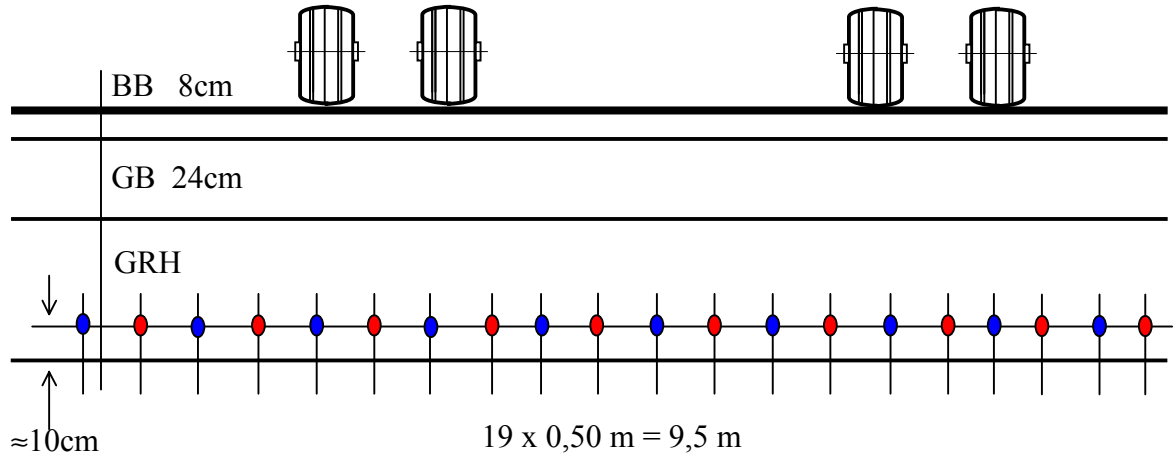

Figure 3: Alternated gauges location transversal profiles on GRH base (structures C & D).

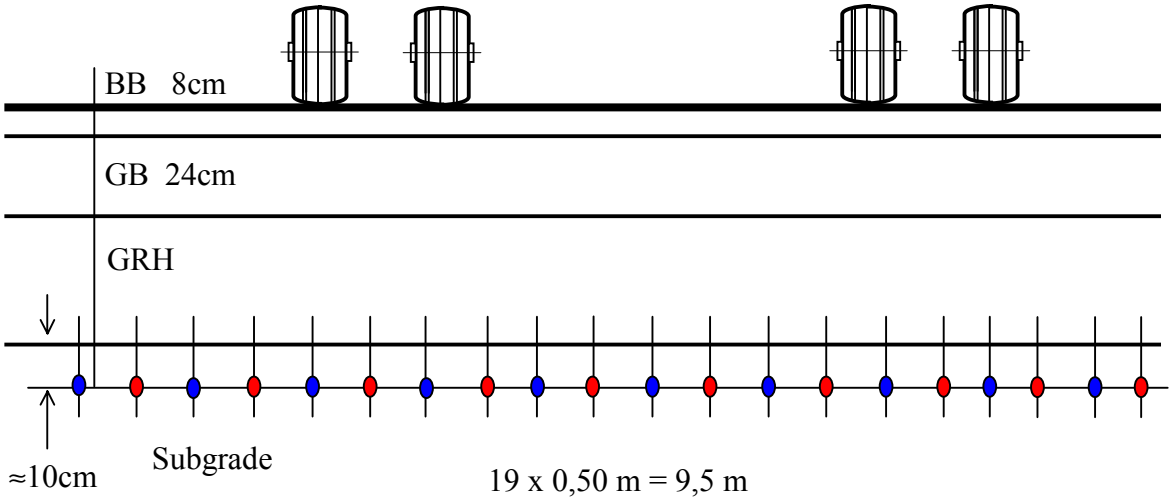

Figure 4: Alternated gauges location transversal profile on top subgrade (structures C & D).

First strategy: sensors of group B

The first strategy is applied to the gauges located at low depth:

- gauges at the base of GB,
- gauges at the top of the structures C and D and at the middle of the GRH of the structure B,
- gauges at the top of the subgrade of the structures A and B.

The depth of strain measurement ensured by these sensors lie between approximately 31 cm (bases GB) and 62 cm (top of the subgrade structure B). The first strategy was dictated by the general shape of the strain field in flexible pavement, such as it comes out from experimental study or numerical simulations. Indeed, at these low depths, the horizontal gradients of the strains created by the wheel are strong, and strong peaks located below the wheels are visible on the horizontal strain profiles. The interaction between close bogies is quasi-non-existent.

The experimental determination of the maximum strains generated by the load in the structure thus requires, with these low depths, a good transverse resolution of the measurement device.

This is obtained by a limited transverse spacing between sensors, which has been fixed at 15 cm. The 12 sensors thus laid out will allow a good definition of the strain profiles over a width of 1,65 m. Only the effects of the right external bogie of the tested configurations will thus be recorded by this first group of gauges. These gauges are gathered under the term of the group B.

Second strategy: sensors of group A

The second strategy is applied to the gauges located at more important depths:
- gauges at the base of GRH of the structures C and D,
- gauges at the top of the subgrade of these two structures.

The depths of strain measurement ensured by these sensors lie between approximately 82 cm (base of GRH structure C) and 182 cm (top of the subgrade structure D).

With these depths, the horizontal gradients of the strains created by the loads on the contrary are attenuated, because of the diffusion in the thickness of the higher layers, of the vertical stresses applied to the road surface. There is covering of the elementary effects of the wheels of the same bogie, and the covering of the effects of adjacent bogies is possible. The weak horizontal gradients of strains to be measured authorizes a less transverse resolution of the measurement device. Thus transverse spacing between sensors can be increased. On the other hand, the localization of the maximum strains concerns a priori a width of pavement much wider than for the preceding strategy. Its possible localization is at the vertical of the wheel center, or bogie center and eventually at the vertical of the median of two adjacent bogies, according to geometrical characteristics of the complete load configuration and the rigidity of the structure.

For this second group of gauges, called group A, transverse spacing running is thus fixed at 50 cm. The total width covered by the system of measurement is 9.50 meters.

12 horizontal strain gauges were added according to the diagonal direction in structure A, at the base of GB base asphalt concrete. These sensors aim at determining strain rotations in the horizontal plane. On the whole, one thus counts 280 horizontal and vertical strain gauges set up in the 4 structures.

II-1-2-2-3 Deflection bowl measurement

Removable inclinometers are positioned temporarily transversally at the surface of the pavement during the fatigue campaign.
They are used to determine the deflection bowl resulting from the various load configuration tests. The deflection itself is obtained from integration with time of the inclinometer signals.
(See **Picture 1** on § I-1-2)

II-1-2-2-4 Temperature measurement

It is well known that temperature strongly influences the behavior of the bituminous pavement. This requires a continuous temperature monitoring during the tests. It is ensured by a vertical profile of 5 thermocouples, placed in the structure C at depths of 1cm, 8 cm, 20 cm 32 cm and 52 cm. The temperature of the ambient air is also recorded.

II-1-2-2-5 Instrumentation during fatigue test

The instrumentation described below mainly concerns the static test campaign. For the fatigue test, only a limited number of these strain gauges were kept in operation. Because of the change of data acquisition system between static test and fatigue test, available channels during fatigue campaign were in fact less numerous.

Moreover, from our experiment the evolution of resilient strains in material over on site fatigue test can not be reliably connected with the damage process of the pavement.

In the opposite, permanent strains and displacements in pavement material and subgrade are interesting data, directly depending on the rutting development of the material.

Therefore, in addition to the existing resilient strain gauges, 12 specific sensors were installed in 1999 to measure the permanent vertical displacement of the 2 structures with the weakest subgrade (CBR 6 and 4), during the fatigue testing campaign. These sensors are anchored at 6m depth and sealed at different levels:

- GB/GRH interface (structure B and C),
- bottom of GRH for structure C,
- as well as mid-depth of GRH for structure D

II-1-2-3 Installation of the instrumentation

The putting into place of resilient strain gauges was done during the construction of the pavement. The greatest care was exercised in the placing and the protection of the sensors and of the wiring, which is laid in narrow trenches.
Sensors intended for the instrumentation of the subgrades and of the untreated materials are placed in holes, which are filled in again with materials having the same density than the surrounding material.

The sensors placed at the base of the bituminous layer were glued on the surface and covered by some asphalt taken from the feed hopper of the finisher. Then they were foot-compacted before the finisher was allowed through. Precautions were taken, in order to prevent the finisher from running over the sensors. Roller was used without vibration for smoothing during surface finishing.

II-1-3 Data acquisition unit

In order to maintain a reasonable inquiry time for the strain measurement, the LCPC's ALT facility acquisition system was used for the whole static campaign.

Gauges signals were filtered, amplified and digitized by remote stations placed as close as possible to the sensors along the experimental runway. The signals were transferred in the digitized form towards the main computer by one single cable. This system makes it possible to process signals of approximately 5 µstrain.

All the signals were recorded in binary files, which were transmitted for a first examination to LCPC’s center.

The measurement of temperatures was carried out by another data acquisition system, which performed automatic inquiries every hour throughout the test, simultaneously with the strain gauges measurement.

During the fatigue test, The LCPC's data acquisition system for strain gauges was not available. HBM spider devices replaced it.

II-1-4 The Simulation Vehicle "Turtle"

II-1-4-1 OBJECTIVES

The simulation vehicle is able to represent full-scale Main Landing Gear configuration of various wide bodies.
The simulation vehicle is able to represent same coercion when wide bodies are on the subgrade.
It is self-powered and the speed for a static test is 2 km/h., up to 5 km/h during fatigue test.
The direction control of the simulation vehicle is able to maintain a straight trajectory during 160 meters +/- 5 cm. (lateral deviation)
The translation can maintain the speed on a 1% uphill slope.
The configuration change has to be done very quickly.
The development of the simulation vehicle is done with a less cost.
The components of the vehicle can be recycled.
The simulation vehicle is in accordance with the safety and ergonomic norms.

II-1-4-2 DESCRIPTION

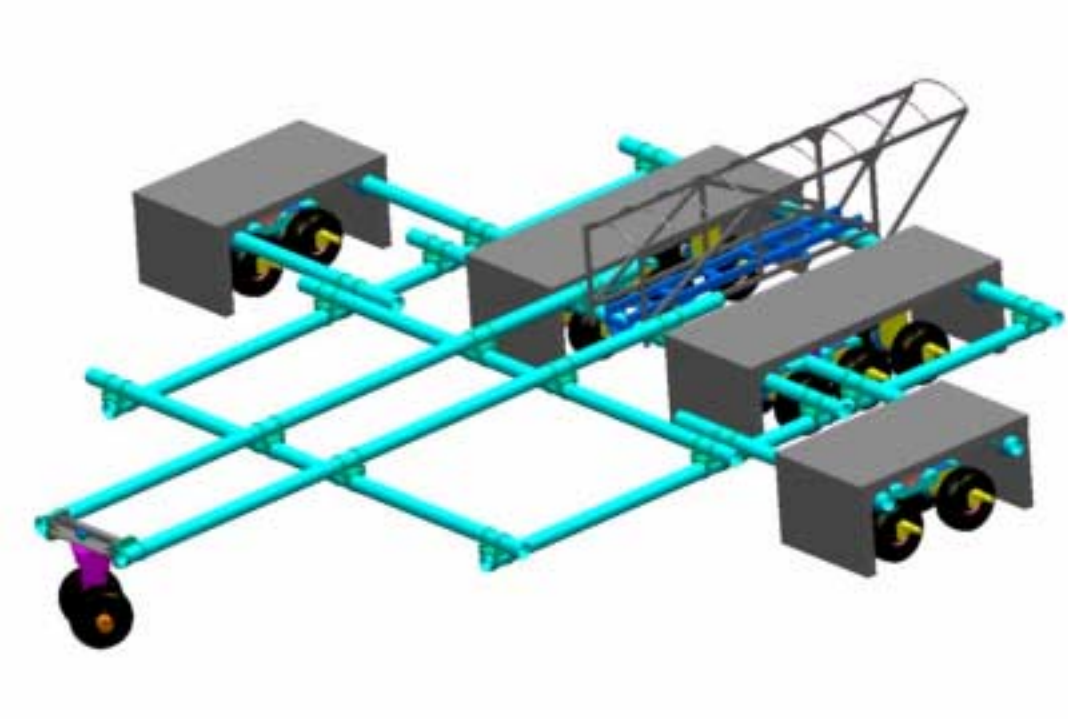

II-1-4-2-1 Modularity

The maximum mass of the simulation vehicle was 631T.
The different configurations with an identical load through each wheel are the followings:

- being 22 wheels with 2 steering wheels
- being 20 wheels with 2 steering wheels
- being 16 wheels with 2 steering wheels
- being 12 wheels with 2 steering wheels

The steering axle installed in front of the vehicle with a low load has not effect on the measure (13T).

Configurations with different loads by wheel are possible:
4 (114T) – 6 (143T) – 6 (172T) – 4 (93T) for example

Moreover, 2 modules are used to calibrate the measure equipment:
One with 2 or 6 wheels capability
One with 2 wheels capability only

These modules for calibration are not motorized (it must be towed).

II-1-4-2-1.1 Modules

The modules were made with 3 steel plates 220mm thickness. One of these plates constituted the horizontal tray, and the two other are assembled to the extremities of the tray.
The bearing subassembly was fixed under the tray. The axles were articulated one time in case of 4 wheels module, or two times in case of 6 wheels module.
Each axle was cross-articulated.
This mounting was used to ensure that the system was isostatic and the load distribution by wheel for a module was identical.

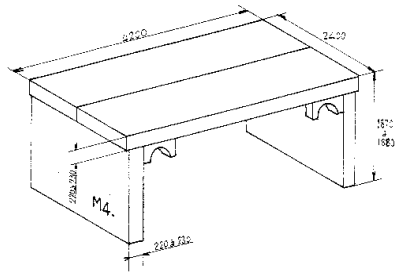

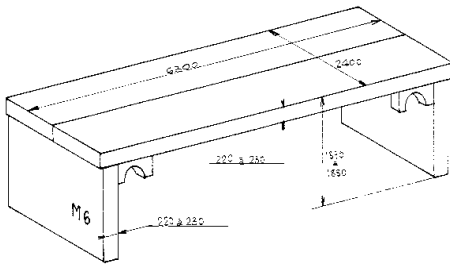

All modules can be configured :
Width between bogies
Width of the axles

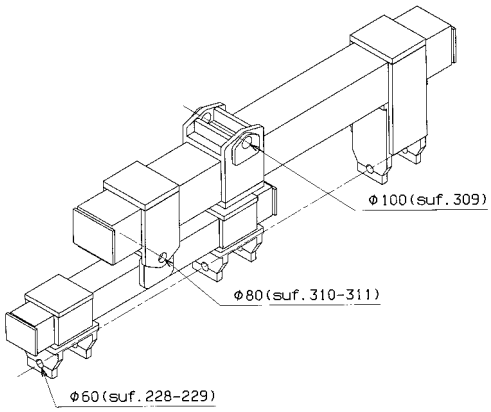

A reference module(as twin) had to be passed on flexible pavement before every simulator configuration, for the instrumentation calibration.(cf. § II-2-3)

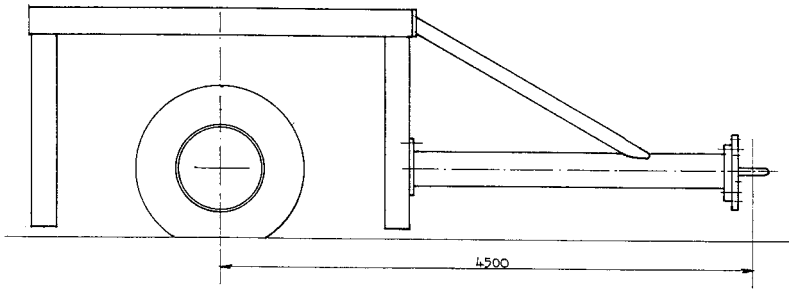

II-1-4-2-1.2 Wheels

The wheels were the same of the A340. The external sizes of the wheels are 1400mm for the diameter, and 530mm wide.
The rims were standards, but no nuts were used for fixing bolts. The screws fixed a crown with internal gears for the driving.

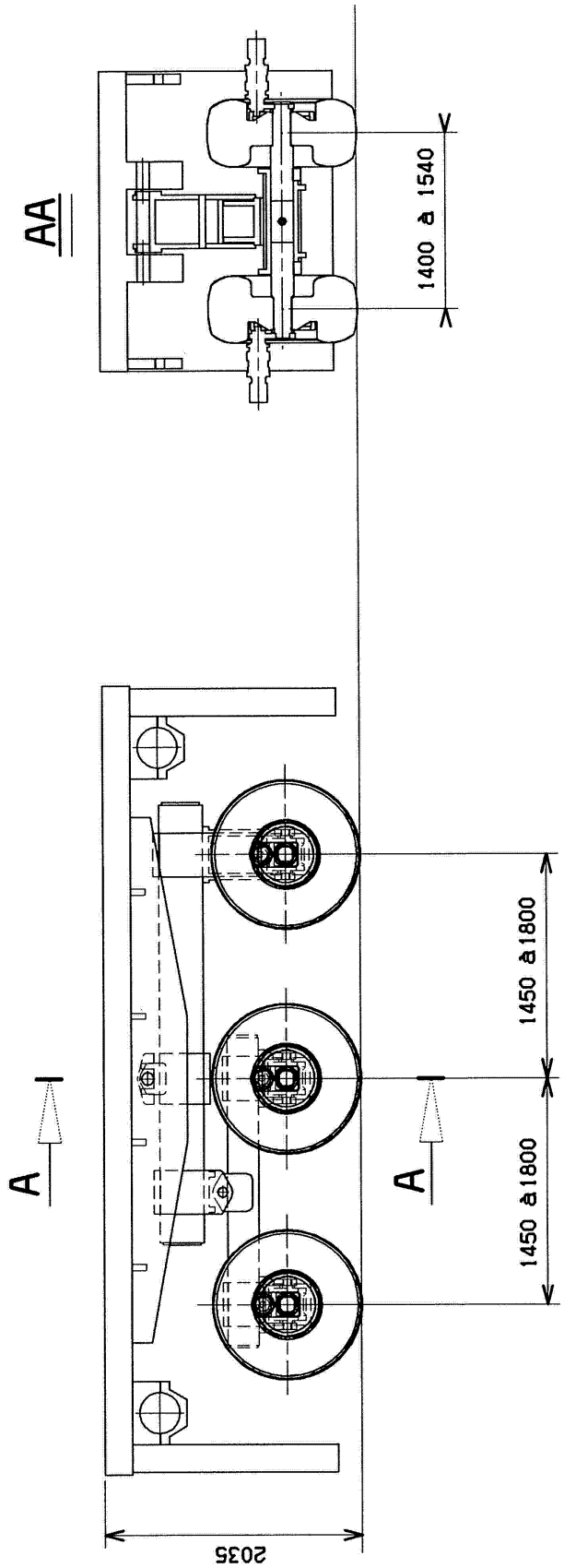

6 WHEEL BOGIE

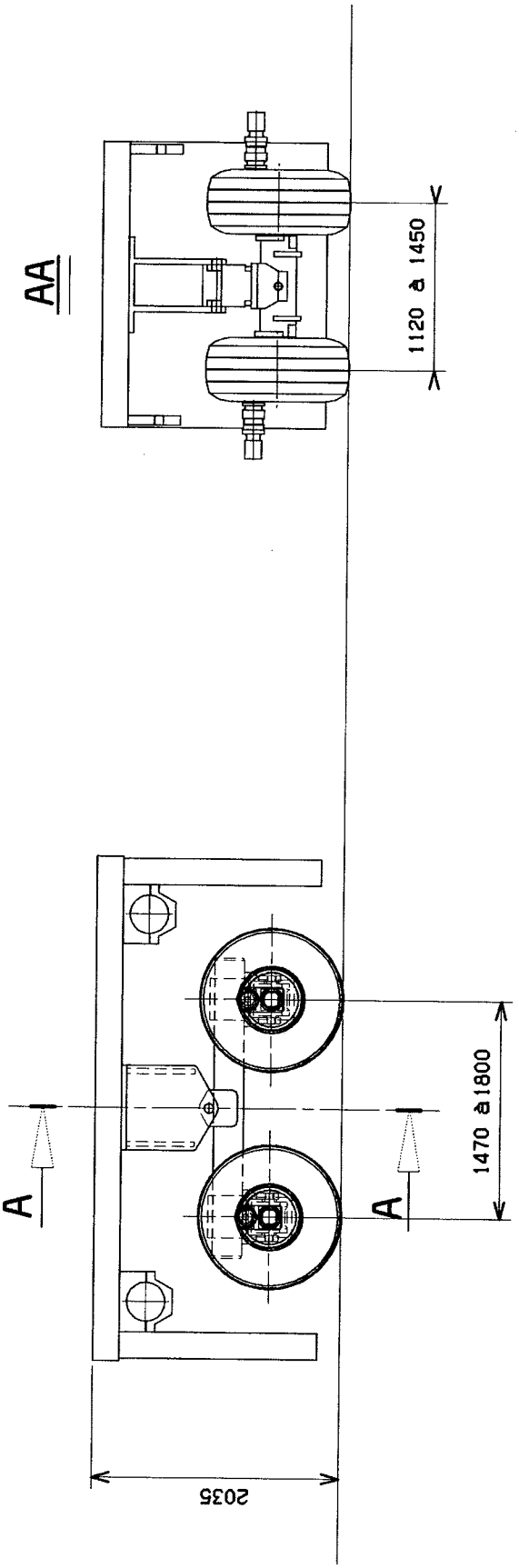

4 WHEEL BOGIE

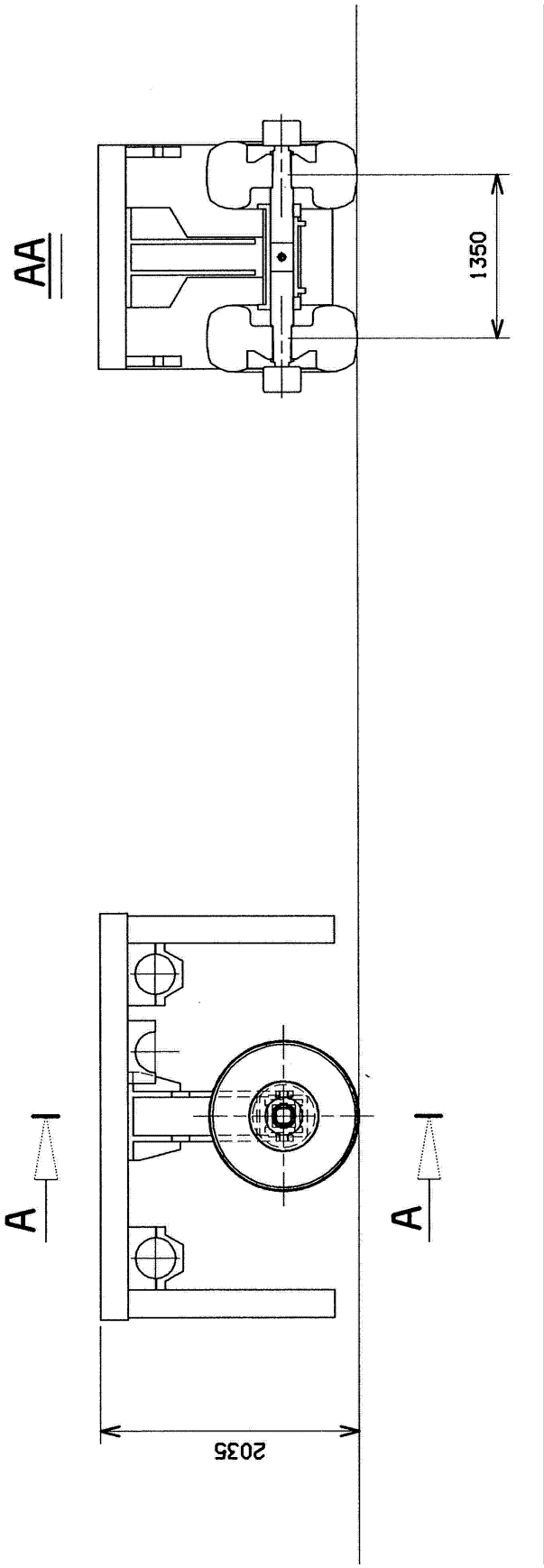

TANDEM

II-1-4-2-1.3 Load variation

On the top of the tray, there are 4 indexes to assure the positioning and to keep the pigs.
These pigs are made with steel (E24) plates 220mm thickness, and the dimensions are the same of the module tray.

II-1-4-2-1.4 Loads

6 wheels module	57.5T empty	16 pigs 13T each
4 wheels module	38.5T empty	16 pigs 8.7T each
2 wheels module	23T empty	12 pigs 5T each
Hydraulic generation	2.5T	10 pigs 2T each
		10 pigs 1T each

II-1-4-2-1.5 Vehicle assembly

The modules are assembled by a tubular structure. This structure has a low rigidity in the vertical plan in order to avoid interaction between modules.
These tubes are 232mm internal diameter. They are fixed with simple collars under the tray of the modules.
Collars with orthogonal axis do the tube links. This disposal can position the modules, from the hydraulic generation and the steering axle.
For example, the simulation vehicle can have 21m length, 20m large and 3.4m height.

II-1-4-2-2 Load on the subgrade

The simulation vehicle have only one type of tire, consequently the load on the subgrade for different tires is based on the tire sprocket.
Consequently, the inflation pressure was varied to change the equivalent surface for a load.

II-1-4-2-3 Vehicle power train

II-1-4-2-3.1 Gas oil motor RVI250KW at 2300t/mn

In the front of the vehicle: A constant flow pump 20cm3/T tarred 220 bars for directional control.
At the back of the vehicle: a distribution box to drive the motive pumps.

II-1-4-2-3.2 Hydraulic circuit

Direction:
The pump is equipped with a filter on the aspiring circuit, and a filter on the pressure circuit. The pump discharges into a manual distributor on the control board; this distributor controls the hydraulic jack of which the 2 chambers have the same section.
A back filter completes the installation.

Translation:
2 adjustable flow pumps with manual control installed on the control board; they were open circuit mounted.
These pumps discharged through a pressure filter in the bored blocs. They 22-gear motor with brake for the wheels.

Filters:
Aspiring pressure and backs.

Cooling:
Electric drive for each pump.

Specifications:

Feed tank	600 liters
Pump	89cm3 – 350b pressure
Motor	25cm3 – 350b pressure
Pinion-Crown ratio	1/8, 61
Drive ratio	1/5, 77

Speed variation:
Two possibilities can be used:
Action on the speed of the heat motor (the maximum torque is about 1250T/mm)
Action on the flow of the pumps with the manual control
With 20 driving wheels, the theoretical speed is 2,9km/h (drag 26T)
With 12 driving wheels, the theoretical speed is 4,9km/h (drag 15T)

Speed control:
An encoder, fixed on a referential wheel, transmits the speed on a dial on the control panel.

II-1-4-2-4 Direction – Trajectory

The steering axle is installed at 19m forward the rear module.
The jack is applying 15T pressure.
The axle is assembled on a directing crown with external gears. This gear controls the angular position of the axle by means of an encoder with display on the control panel.

The trajectory is ensure like followed:
On the subgrade a continuous line is plotted on all the length of the runway; the large of this line is 3 to 5 cm.
2 cameras are installed on 2 graduated gauges.
One of the gauges is in the front of the vehicle, the other is at the back. The operator has 2 screens on the control panel; he steers the vehicle following the line in the axis of the screen.

The gradation of the gauges is used to change the trajectory with regard to the axis of the runway.

II-1-4-2-5 Acclivity

The vehicle has not enough power to standing start on an acclivity more than 1%. On the other hand, when moving, the vehicle can step over the runway deformations.

II-1-4-2-6 Control panel

The whole commands and control systems of the vehicle are available on the control panel.
The functions are followings:
Power source operating
Translation
Direction
Safety equipment.

II-1-4-2-6.1 engine operating

Revolution
Timer
Gas oil gauge
Oil temperature of the engine indicator
Water temperature light
Oil pressure of the engine light
Battery load light
Ignition key
Starter button

II-1-4-2-6.2 Translation

Speed indicator (km/h)
Digital display for the HP pressure circuit left pump
Digital display for the HP pressure circuit right pump
Two controls levers for the pumps dipping
One button to power on the aero-cooling
One button to power on the flashes
A digital display for the oil temperature circuit.

II-1-5-2-6.3 Direction

Left and right control lever
Screen display of the front camera
Screen display of the back camera
Digital display for the angular position

II-1-4-2-6.4 Safety and control equipment

11 clogging indicators (hydraulic filters)
1 emergency stop with key and bracelet for the operator
1 emergency stop
1 disconnecting switch
1 power on light
1 green light “power on permit”
1 red light “hydraulic oil level circuit”
1 light “emergency stop is on”
1 push button to power on the electrical box.

II-1-4-2-7 Configuration modification

II-1-4-2-7.1 General case

Use jacks to put the module horizontally on its skirts (First one side then clamp, then the second side).
When all modules are clamped at the same height, lock the crossbar.
The lock system is composed:
1 fixed part with 2% allowance on the 2 sides
1 mobile part with only one allowance (4 to 5mm) on one side.
The module always on the slips installed the pigs in accordance with the configuration.
With jacks, side by side, remove a part of wedges. Be careful, the module does not sloped.
When the module is on the wheels, keep the wedges on the 4 angles
Link by tubes the vehicle
With jacks, wheel by wheel, axle by axle, remove the mobile part of the crossbar locked system.
The vehicle can now move.

II-1-4-2-7.2 axle Width modification

A lifting jack is used under the axle and the width can be chosen.
For this operation it is not necessary to lift the module. The axles are articulated and only one jack is enough.

II-1-4-2-7.3 Width between bogie modification

For this operation, the pigs must be removed and the module lifted.
During the fatigue testing, we have continuous modifications. A crane is installed near the runway.

II-1-4-2-7.4 Landing gears position modification

For this operation a crane is also required, and the overhaul of the link tubes is necessary.

II-1-4-2-8 Vehicle design

The design is very simple because the vehicle is very rustic.
Only one design modification was made: a platform was added with seat driving capability. It is necessary during the fatigue tests (5000 continuous ways are required).
The welded structure of the vehicle is less machining.
The components of the translation and the direction come from the trade and very used for the earth working vehicles.

II-1-4-2-9 recycling materials

The vehicle can be recycling up to 95%.

II-1-4-2-10 Safety – Ergonomic

During the post-project, the development office and the safety office are worked together.
The staff has being informed about the safety because the trial runway is situated in an airport.
The access is continuously guarded.
The static test is done with an operator seated on board.

II-1-4-3 STATIC TESTS PROCEDURE

The static test includes 20 different configurations from 12 wheels (load 287T) to 22 wheels (load 575T).

This static test has been done without steering axle. The trajectory has been respect by the flow difference between the 2 pumps.

Temperature check	:	continuously
Tire pressure check	:	before every tests, morning and midday
Vehicle check	:	every morning
Tightening of the wheel bearing	:	every 1000 moving
Tightening of the link bolts of the rim	:	every 1000 moving

The tests are done zone by zone (A-B-C-D) :
3 moving by zone with check of the first sensor line
3 moving by zone with check of the second sensor line
Before each 3 moving series, the sensors are calibrated with the towed module.

The measures are collected in the same direction.
These measures are written down in a checking form.

II-1-4-4 FATIGUE TESTS STEPS

The vehicle is equipped with the steering axle and with a covered platform on a level of the driving place.
The trajectories can change in position and way quantity.
A board is followed by the operator to do 5000 ways.
The modification of the trajectory is done by moving cameras on the graduated gauges.

Temperature check	:	continuously
Tire pressure check	:	before every tests, morning and midday
Vehicle check	:	every morning
Tightening of the wheel bearing	:	every 1000 moving
Tightening of the link bolts of the rim	:	every 1000 moving

II-1-4-5 USE

1° - Engine on
Check the control acceleration is minimum
Check the control pump flow variation is neutral position
Check the oil level in the tank
Set the ignition key in the 1 position: check all lights put out on the control panel and check the fuel gauge.
Push the starter button and simultaneously the command button of the starter electrovalve.
The engine must run low rate during 5mn.
Post an operator near emergency button placed on the 4 angles of the vehicle.
The operators must stayed behind of the modules, always protected by the skirt and never in the lateral continuation of the wheels. Clear the lateral pavement.
Check the fill pressure between 25 to 35 bars. If this pressure goes down 20 bars: stop the engine. If this pressure goes over 45 bars: check the control pump flow variation and eventually move the control to the neutral position.
With the control acceleration adjust the speed engine to 2000t/mn.
At this time, the vehicle is ready to move by simple action on the control pump flow variation. Before moving the vehicle, use the klaxon to prevent.

2° - Module loading
Use jacks to put the module in horizontal position on the skirts
First one side then clamped then does same for the other side. After that follow to the next module.
When all modules are clamped at the same level, lock the crossbar.
The lock system is composed:
1 fixed part with 2% allowance on the 2 sides
1 mobile part with only one allowance (4 to 5mm) on one side.
The module always on the slips, installed the pigs in accordance with the configuration.
With jacks, side by side, remove a part of wedges. Be careful, the module does not sloped.
When the module is on the wheels, keep the wedges on the 4 angles
Link by tubes the vehicle
With jacks, wheel by wheel, axle by axle, remove the mobile part of the crossbar locked system.
The vehicle can move now.

II-1-4-6 SAFETY EQUIPMENT

On the control panel: one emergency stop button
On the 4 angles of the vehicle: emergency stop and orange flash
Translation: automatic break when lost pressure on the 22 wheels.
Klaxon to signal the vehicle goes to move.
Hydraulic pumps equipped pressure limiter
Hydraulic circuit: the tank has a level/temperature and an engine stop in case of short oil.
Filters: 2 H.P. filters running in the 2 ways with clogging indicator displayed on the control panel.
1 filter on the inlet with clogging indicator displayed on the control panel (red light)
1 filter on the return with clogging indicator displayed on the control panel (red light)

II-1-4-7 Maintenance

1° - Before tests
Fuel check: visual
Hydraulic tank oil level: visual
Tire pressure check: AIRBUS notice 12879-318 tool
Check light of the control board
Check the availability of the extinguishers
Clean the runway if necessary
Check hydraulic leaks, same for engine oil and fuel: visual
Check the lubrication of the driver crown: visual

2° - Recurrent verifications
The maintenance operations are done on the subgrade, hydraulic plant removed.

If an operation is necessary on the hydraulic plant not removed, a stepladder is available (used for to fill fuel and oil also).

3° - Annual checks
The lift rings have identification and must be check by a competent organization.

II-1-4-8 CONFIGURATION SAMPLES

See drawings next:

Configuration C17	4-4-4	A340
Configurations CB2 & C22	6-6	B777
Configuration CB1	4-4-4-4	B747
Configuration C1	6-4-4-6	A380
Configurations C5H & C7	4-6-6-4	A380
Configuration C8	4-6-2-6-4	A380
Configuration	4-6-6-4	with different loads on the wheels, and additional modules (fatigue tests).

CONFIGURATION 4-4-4 (C17)

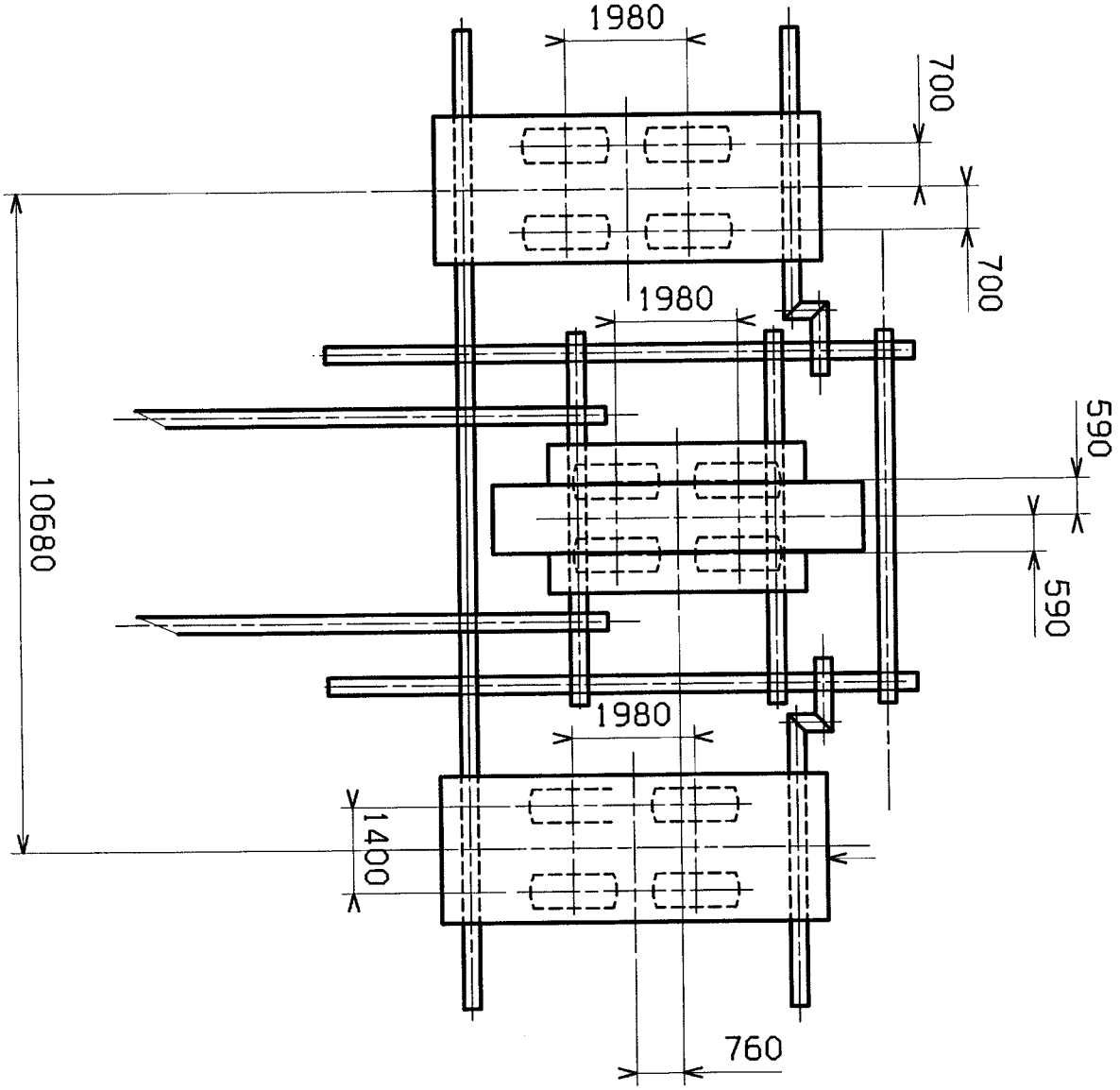

CONFIGURATION 6-6 (CB2)

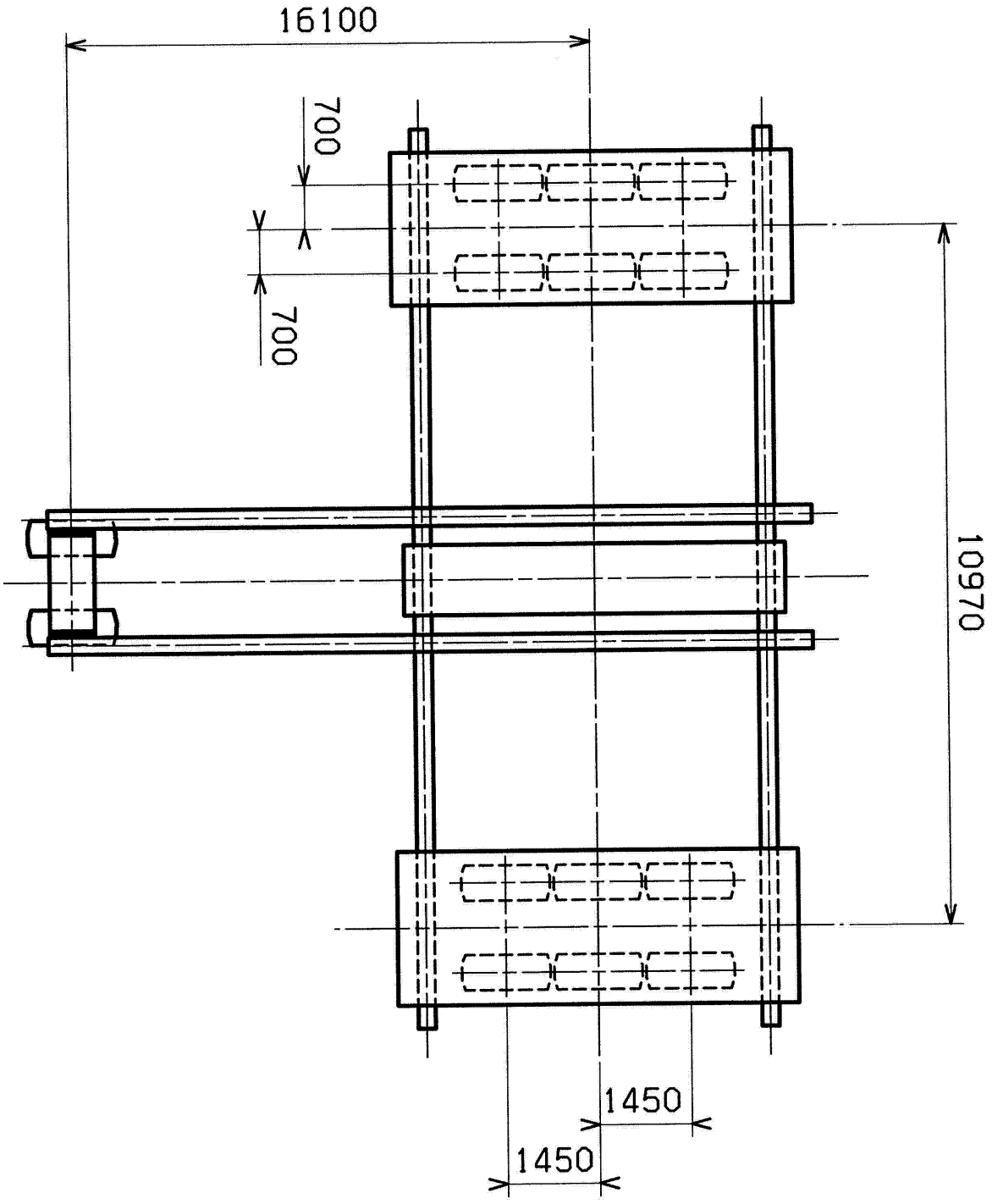

CONFIGURATION 6-6 (C22)

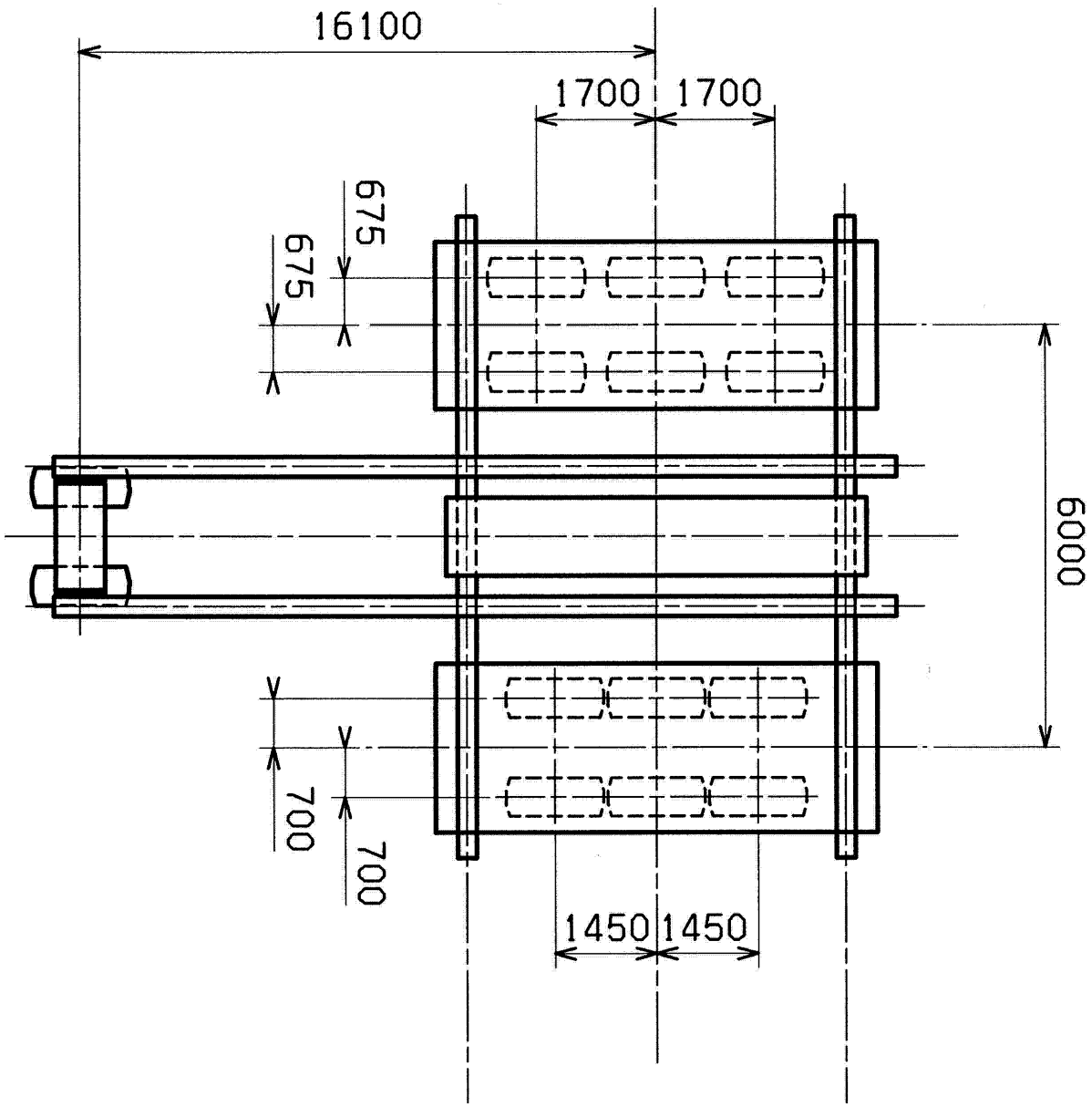

CONFIGURATION 4-4-4-4 (CB1)

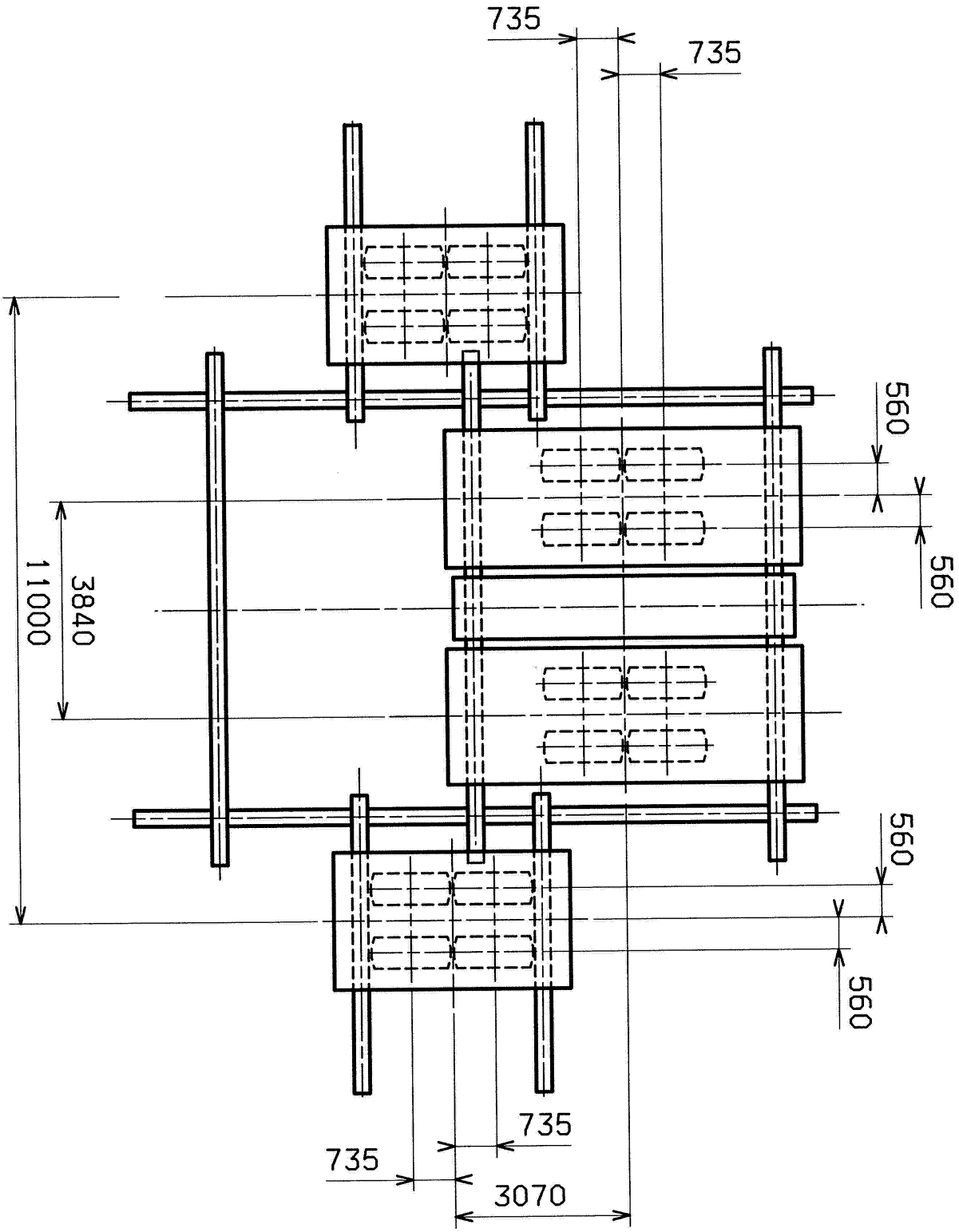

CONFIGURATION 6-4-4-6 (C1)

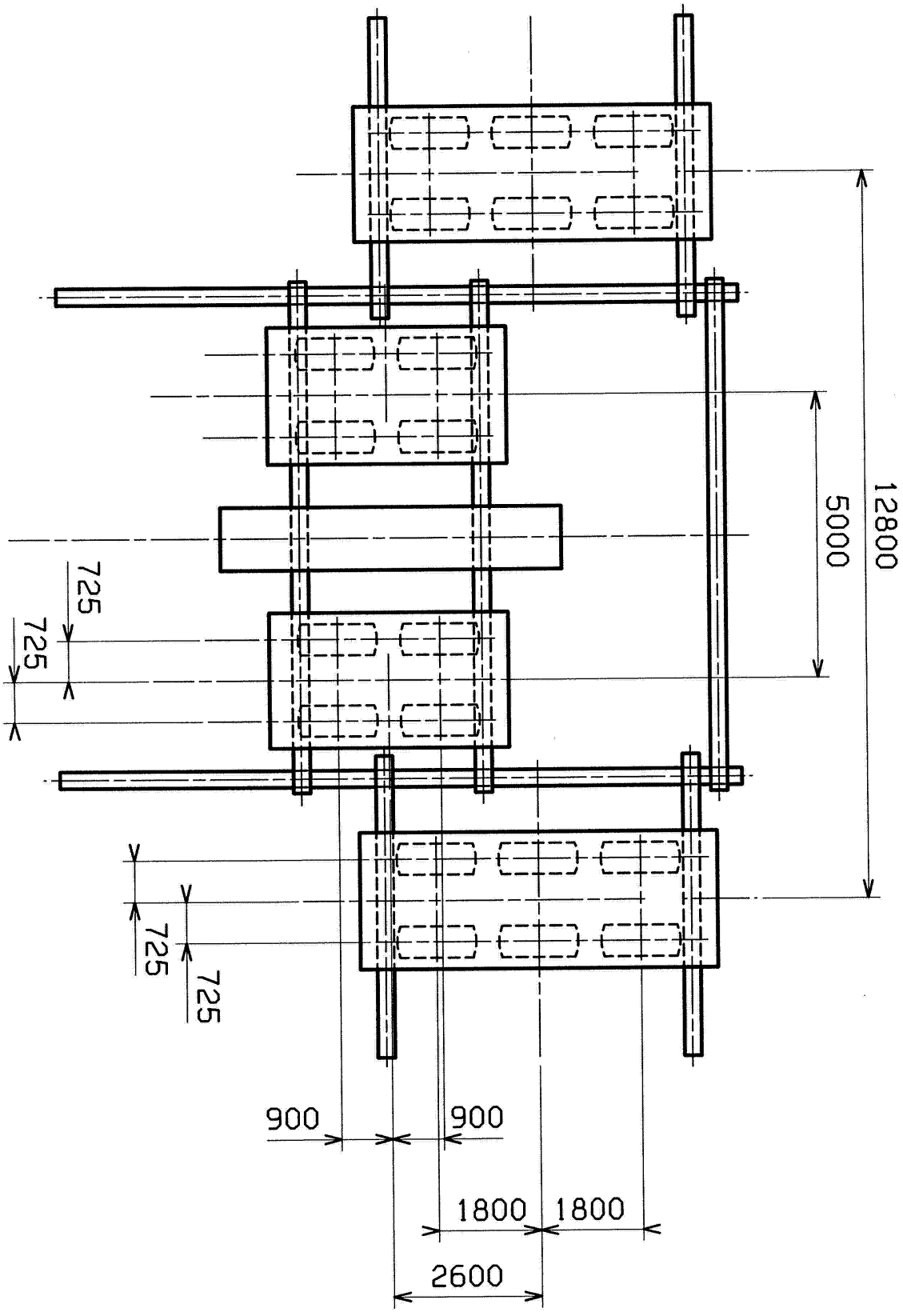

CONFIGURATION 4-6-6-4 (C5H)

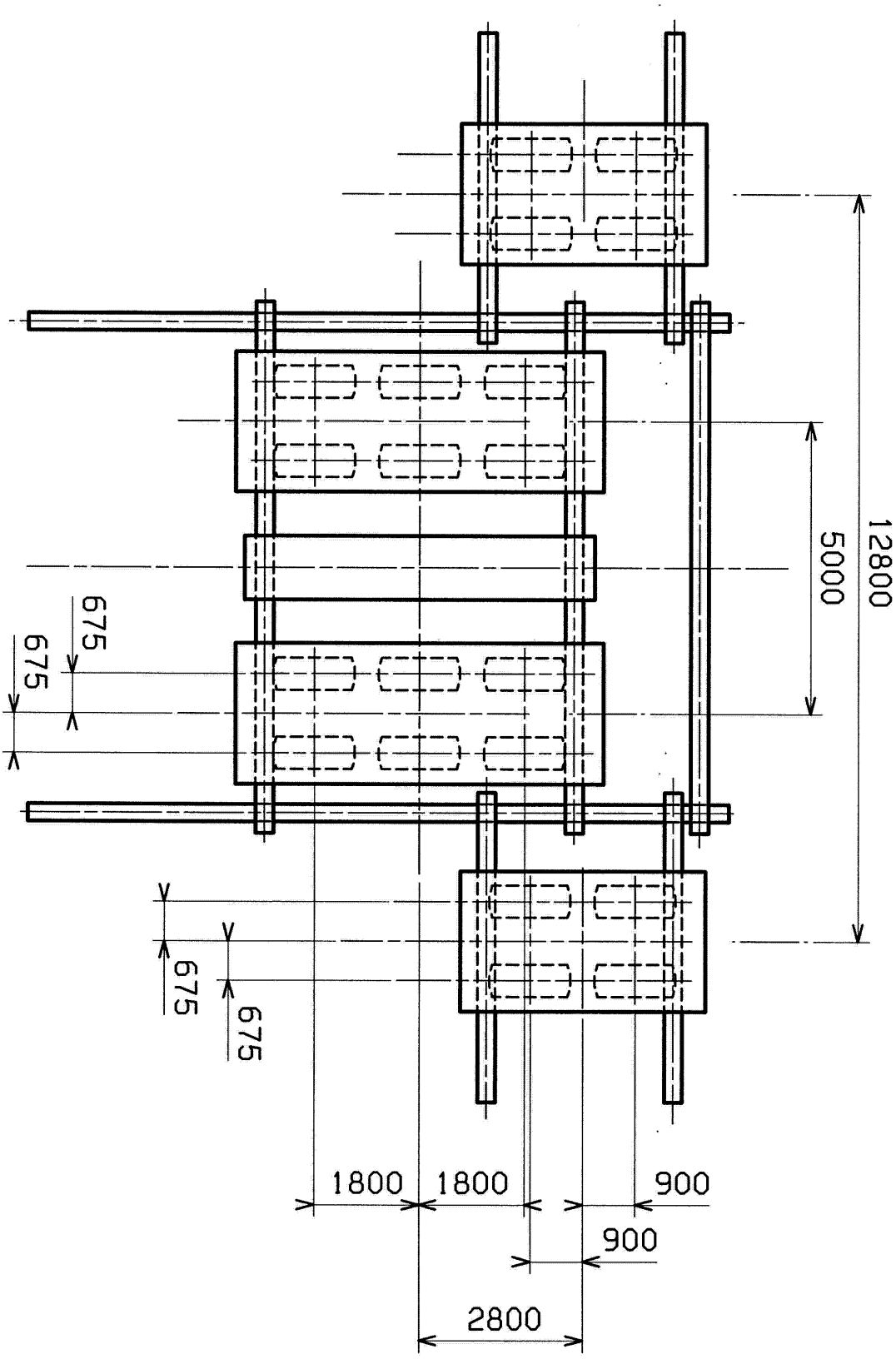

CONFIGURATION 4-6-6-4 (C7)

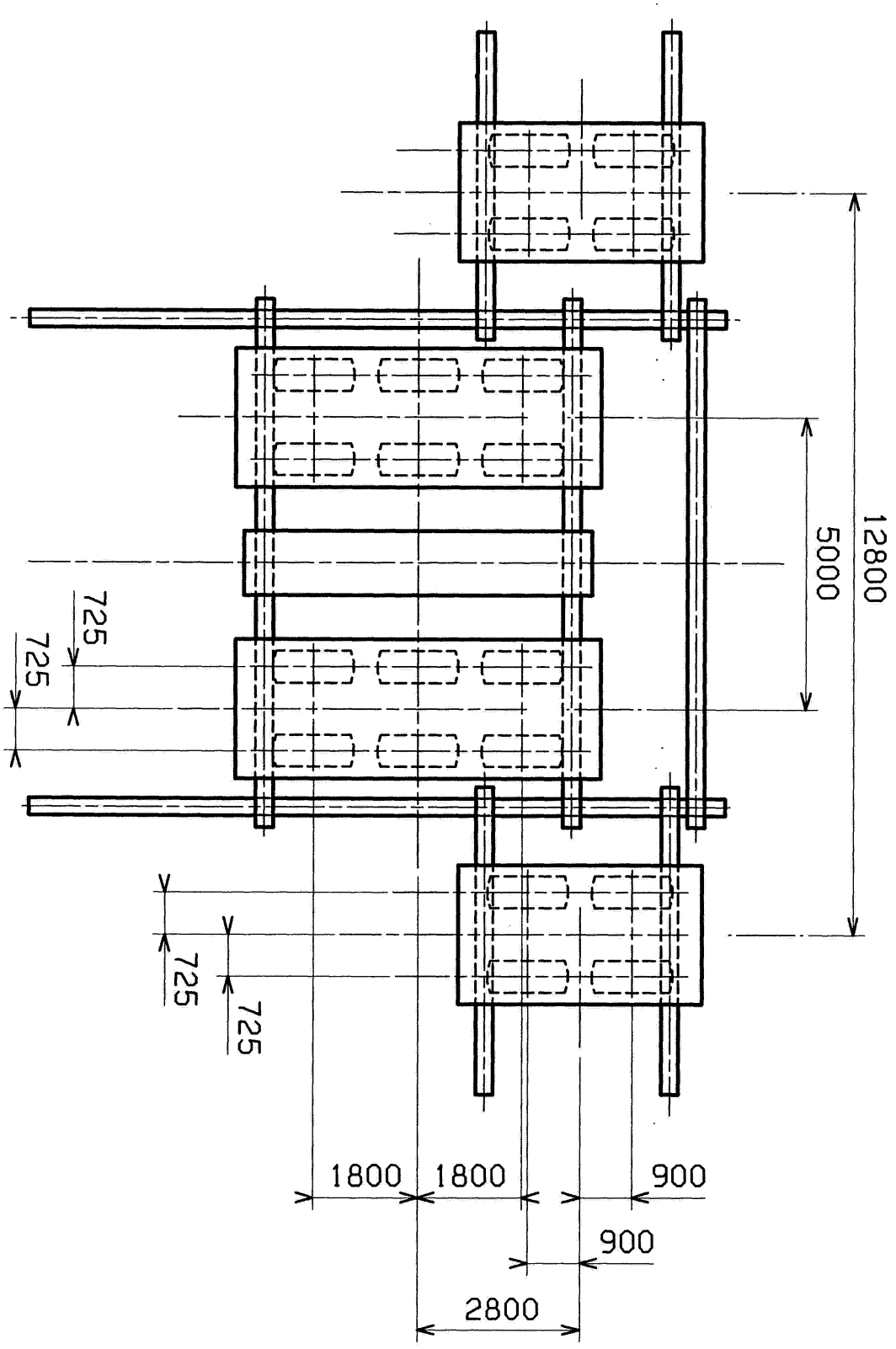

CONFIGURATION 4-6-2-6-4 (C8)

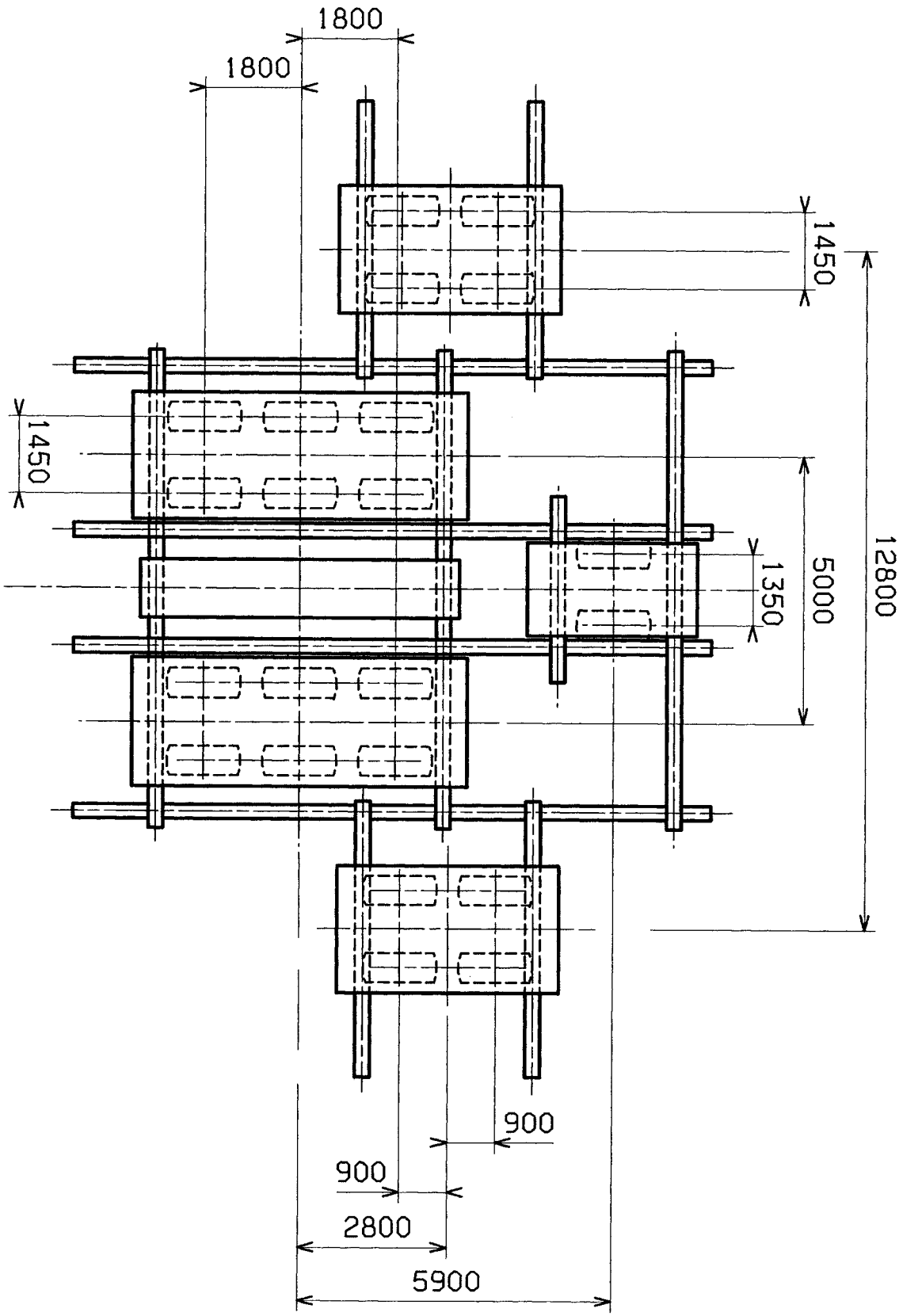

II-2 The Static Tests

II-2-1 Objectives

Pavement Experimental Program objectives are to optimize the A380 L/G configuration and minimize airport modification cost. In this relation, we were looking for characterized his MLG from experimental flexible pavement build as already existing ones, and instrumented for a comportment data analysis.

The process for the A380 L/G configuration selection was issued.

The technical objective has been to choose between the 6446 and the 4664 MLG concept in relation with the wheel well bulk of each MLG leg, as well as Aircraft Classification Numbers, more over to assess the different interference from geometry to optimize this last for lowest impact on pavement.

The effect of slight geometrical changes (10 to 25 cm.) in a given aircraft L/G configuration can not be easily extracted from pure experimental data as this effect is there combined with other effects like temperature, speed which may have a greater order of magnitude.

The subject has been therefore covered by a software calibration (ALIZE) for those static parameters.
Nether the less, it has been necessary to compare the A380 with competitors, as the B747 and B777, on flexible pavement, for a concrete positioning.

At the same time of all test configuration execution, it has been necessary to validate the simulator concept.
In this relation, we have defined realism of simulator contact strength thanks to his comparison with real aircraft ones (Corsair B747, A320, A330), and to instrumented pavement.
The test philosophy set by AI/LE consists in varying one parameter at a time for one-to-one comparison. Modified parameters were principally the load (MTOW, Loaded Tire Pressure) and the L/G geometry (track, wheel-base, X spacing: see **Figure 5**).
To reach those objectives, it was necessary to perform test procedures before realize it, and be able to select the good static configuration thanks to data analysis.

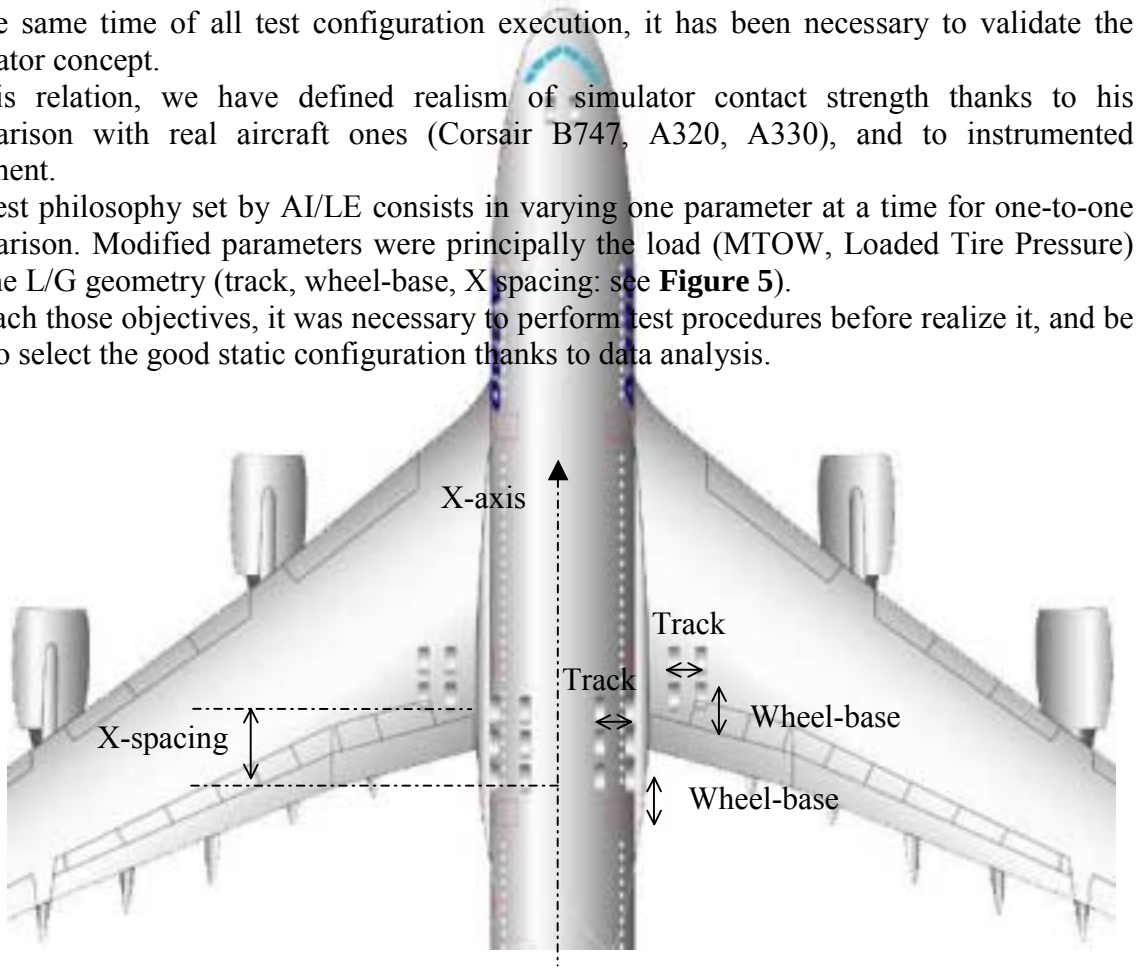

Figure 5

II-2-2 Configuration selection

II-2-2-1 TIMETABLE

The static test campaign began the 3rd November 1998 to finish the 28th April 1999, and have tested 15 simulator configurations, as 3 real aircrafts.

Date	*03&04/11/98*	*09,10 & 11/11/98*	*17,18 & 19/11/98*	*23 & 24/11/98*
Configuration	CB1	CB2	C1b	C7

Date	*26 & 27/11/98*	*02 & 03/12/98*	*07 & 08/12/98*	*14 & 15/12/98*
Configuration	C10	C5 hybrid	C5	C6

Date	*06 & 07/01/99*	*13 & 14/01/99*	*20 & 21/01/99*	*27 & 28/01/99*
Configuration	C8	C15	C16	C17

Date	*03 & 04/02/99*	*09 & 10/02/99*	*11/02/99*	*02/03/99*
Configuration	C18	A 320	A 330	C22

Date	*10/03/99*	*16 & 17/03/99*	*27 & 28/04/99*
Configuration	B 747-100	C20	C 24

II-2-2-2 List of configurations & issues

All configurations were chosen for Pavement Experimental Program and from six criteria:

1. *Gears configuration effect*
2. *Bogie dimension effect*
3. *Gears proximity effect*
4. *Center gear effect*
5. *M.T.O.W. effect*
6. *A.C.N. effect*

A380 Config.	*L/G footprint*	*MTOW (tons)*	*Wing Gear Geometry (mm.)*	*Body Gear Geometry (mm.)*	*Center Gear Track*	*X Spacing (mm.)*	*Overall Track (mm.)*	*Loaded Tire Pressure (bars)*	*Pneumatic Caract.*	*Config. Directly Comparable*	*Researched point*
C1	6446	540	1450x1800	1450x1800	N/A	2600	14780	13.4	1400x530 R23	**Reference**	*(see config. 3 page n°57)*
C1b	6446	540	1450x1800	1450x1800	N/A	2600	14780	13.4	1400x530 R23		C1 real application
C7	4664	540	1450x1800	1450x1800	N/A	2800	14780	13.4	1400x530 R23	C1	Gears footprint effect
C10	4664	540	1450x1800	1450x1800	N/A	3600	15980	13.4-14.8	1400x530 R23	C7	Gears proximity effect
C5 Hybrid	4664	540	1350x1800	1350x1800	N/A	2800	14680	13.4	1400x530 R23	C7	Track effect
C5	4664	540	1350x1900	1350x1900	N/A	2800	14680	13.4	1400x530 R23	C5 Hybrid.	Wheel base effect
C6	4664	590	1450x1800	1450x1800	N/A	2800	14780	14.8	1400x530 R23	C7	MTOW effect
C8	46264	590	1450x1800	1450x1800	1350	2800	14780	13.4	1400x530 R23	C6	Center Gear effect
C15	4664	540	1450x1700	1450x1700	N/A	2800	14780	13.4	1400x530 R23	C7	Wheel Base effect
C16	4664	540	1350x1650	1350x1650	N/A	2800	14680	13.4	1400x530 R23	C15	Smaller bogies effect

Shading cells show values that change with regard to comparable configuration.

Config.	*L/G foot-print*	*MTOW (tons)*	*Wing Gear Geometry (mm.)*	*Body Gear Geometry (mm.)*	*Center Gear Track*	*X Spacing (mm.)*	*Overall Track (mm.)*	*Loaded Tire Pressure (bars)*	*Pneumatic Caract.*	*Config. Directly Comparable*	*Researched point*
C17	444	385	1397x1981	1176x1981	N/A	760	12611	16.8	1400x530 R23		A340-600 equivalence
C18	424	284.3	1370x1630	950	N/A	760	12570	14.4/12.7	1400x530 R23		MD 11 equivalence
B 747	4444	278.1	1120x1470	1120x1470	N/A	3070	12552	12.7 (11.4)	49x17 28PR		Calibration (Corsair B 747-100 A/C)
C20	4444	278.1	1120x1470	1120x1470	N/A	3070	12650	11.1	1400x530 R23	B 747	B 747-100 equivalence
CB1	4444	373.3	1120x1470	1120x1470	N/A	3070	12650	8.8	1400x530 R23	C20	B 747-200 equivalence
A 320	22	73.5	N/A	927	N/A	N/A	8949	16 (13.8)	46x17 R20		Calibration
A 330	44	230	N/A	1397x1981	N/A	N/A	12611	14.45 (14.2)	1400x530 R23		Calibration (modified A340)
CB2	66	305	N/A	1400x1450	N/A	N/A	12900	15.3	1400x530 R23		B 777 equivalence
C22	6 6	365 305	N/A	1350x1700 1400x1450	N/A	N/A	7905	14.8 15.3	1400x530 R23	CB2	A380 MLG on center line; 6 wheels space (> 3.5 m.) no-interference effect
C24	66	179.2	N/A	1400x1450	N/A	N/A	12900	9.6	1400x530 R23	CB2	B 777 equivalence

Underline configurations are real aircrafts

II-2-3-1 REFERENCE load

II-2-3-1-1 why the reference load is necessary

A more or less long space of time separates necessarily the strain gauge recordings relative to two load configurations. During this time, the parameters of structural behavior of the pavement in general change under the effects of the variations of the environmental conditions. It can be a temperatures or hygrometry fluctuation that influence the rigidity of the materials. It may also result from the evolution of the structural rigidity due to the effects of the materials post-compaction caused by the circulation of the heavy loads. The establishment of objective comparisons between the various configurations of load will thus require a first harmonization called the “temporal harmonization”. It is intended to correct measurements from the effects of the variations of environmental conditions of the pavements during all the duration of the test. The temporal harmonization is based on the analysis of the strains measured by the whole gauges, for a load that is kept unchanged all over the static campaign. This particular load is called the "reference load"(cf. § II-1-4-2).

A second type of harmonization is necessary as explained now. For a layer of a given structure, the localization of the maximum strain varies with the load configuration. The strain gauge revealing the maximum value could thus be different from one configuration to another. But the response to a given load of several gauges of a given type is not single: its is sensitive to meteorological conditions, to the characteristics of its insertion in material, and also to the natural heterogeneity of instrumented material. The establishment of objective comparisons between configurations will also require a second harmonization called the “space harmonization”. It is intended to correct measurements from the dispersion effects, which affect the specific responses of the different gauges. The space harmonization is based too on the analysis of the maximum strains measured by the whole gauges of a given type, for the same reference load

The expressions of temporal harmonization factors and spatial harmonization factors are detailed in part II-2-4-1.

The load of reference is made up until mid-February 1999 of the rear axle of a STBA's truck (single axle with double wheels, load with the axle 191 kN). After mid-February 1999, the load of reference consists of a module of two wheels charged each one with 30 tons, towed by the same truck.

II-2-3-1-2 Reference load procedures

Spatial harmonization data

- Group A instrumentation: just before the test of each plane configuration, the strains measured by group A sensors under reference load are recorded. For these measures, the reference load moves transversally to the axis of the pavement, with the centerline of one of its rear wheel twinning exactly centered on the axis of the group A gauges.

- Group B instrumentation: the spatial harmonization will use the data from particular passages of the reference load, which have been realized once and for all at the beginning of the static test in September 1998, and not repeated after for each configuration test. They consist in 15 longitudinal passing of the reference load on both sides of the main longitudinal axis (yellow line), with an offset of 15cm between each passing.

Temporal harmonization data

- Group A instrumentation: the transversal crossing of the reference load which precedes the configuration test (see above spatial harmonization data) areas also used for the temporal harmonization.

- Group B instrumentation: before each new configuration test, a single longitudinal passage of the reference load along the yellow line is applied. The temporal harmonization thus requires for each structure and each type of sensor, the choice of a particular gauge: the one giving the maximum strain value under the referenced load, this particular gauge being kept unchanged all over the whole static test.

II-2-3-2 TYPICAL configuration test sequence

Each new plane configuration gives place to a complete measurement campaign, declined in three phases:

1. Recording of configuration A sensors (structures C and D), for the five following passages:
   - 2 transverse passages of the reference load, gauges of the group A being in fact distributed into 2 transversal profiles, 4 meters distant each from the other. These 2 passages are dictated by the temporal and spatial harmonization.
   - 3 longitudinal passages of the simulator (or the real plane), with the interior wheels of the right bogie centered on the principal axis of measurements (yellow line).

2. Recording of the configuration B sensors (all structures), for the four following passages:
   - 1 longitudinal passage of the reference load centered on the yellow line. This passage is dictated by the temporal harmonization.
   - 3 longitudinal passages of the simulator, interior wheels of the right bogie centered on the yellow line.

3. Inclinometric (all structures) with the 6 inclinometers, for the four following passages:
   - 1 longitudinal passage of the reference load centered on the yellow line.
   - 3 longitudinal passages of the simulator, interior wheels of the right bogie centered on the yellow line.

II-2-3-3 SIGNAL ACQUISITION

Precision concerning the acquisition of gauges signal have been given before, see §II-1-3. Description of signal will be given below, see § II-2-4-2.

II-2-4 Data analysis

II-2-4-1 STEP for analysis of strain measurement

The general step retained with the partners of the project to carry out the exploitation and the interpretation of static measurements was articulated in the following way:

1. **Selection of the most interesting configurations for the analysis**

The various sequences of the experimentation do not present obviously all the same interest with respect to the aims in view, as it the case of any experiment research project of this type. On the totality of the configurations tested, 8 configurations are selected, taking into account the two following criteria:

The selected configurations must be representative of the whole situations tested. In particular, the values of the characteristic bogie parameters (wheel base, wheel track, number wheels and load per wheel) of these 8 configurations must correctly frame the values of these same parameters on the 20 configurations tested on the whole;

Quality of measurements: the gauges recording of the selected configurations must not raise any interrogation, and the whole test parameters during measurement have to be correctly controlled.

2. **Exploitation and harmonization of measurements for the 8 selected configurations**

For each configuration, the exploitation of the strain gauge measurements will primarily aim to identify the maximum strains created in the various layers of materials.

Only the structures B (CBR 10), C (CBR 6) and D (CBR 4) will be concerned with this treatment. Structure A (CBR 15) was not examined. This structure cannot be indeed regarded as representative of a pavement structure in a normal state of operation, because of the problems encountered with its initial construction. From the start of the test, its defective structural state required various stages of repair.

The research of the maximum strain values requires the double harmonization of the raw measurements.

3. **Assessment of the elastic linear multi-layer model (LCPC's Alizé software)**

The experimental results are used to evaluate the numerical possibilities of simulation of the flexible pavements of the PEP, with this classical elastic linear multi-layers model used for the dimensioning of road pavement.

II-2-4-2 CONFIGURATIONS selected for the exploitation and interpretation

The choice of the configurations retained for the detailed analysis and theoretical interpretation is guided by the criteria specified before. These height configurations and their main characteristics are indicated in **table 1.**

Tested Configuration		Load /wheel (kN)	Tire Press. Load (MPa)	Track (cm)	Wheel base (cm)	L1 (cm)	L2 (cm)	L3 (cm)
CB1	4-4-4-4	232	0.88	112	147	1100	384	307
CB2	6-6	239	1.53	140	145	1097	/	/
C1	6-4-4-6	260	1.34	145	180	1280	500	260
C7	4-6-6-4	260	1.34	145	180	1280	500	280
C10	4-6-6-4	260	1.34	145	180	1400	500	360
C5H	4-6-6-4	260	1.34	135	180	1280	500	280
C5	4-6-6-4	260	1.34	135	190	1280	500	280
C8	4-6-2-6-4	261	1.34	145	180	1280	500	280
C17	4-4-4	311	1.65	140-118-140	198	1068	/	76
C22	6-6	286 239	1.48 1.53	135 - 140	170 - 145	600	/	/

L1: spacing between WLG axes
L2: spacing between CLG axes
L3: X spacing between WLG and CLG axes

Table 1: 10 configurations selection for detailed exploitation.

Configurations C7 and C5H are only different by the wheel base values of the bogie: 1.45 meter for the C7 configuration, 1.35 meter for C5H configuration.

II-2-4-3 Spatial and temporal harmonization

The reference load procedure for the acquisition of data necessary to spatial and temporal harmonization has been described before, see section II-2-2.
The determination of measure harmonization coefficients is presented now.

Spatial harmonization coefficient for group A instrumentation

S(réf,k)j refers to the maximum strain value measured by the sensor n°j of a given type in a given structure, under the reference load passage preceding the test of configuration n°k.

S(réf,k)m refers to the average value of the maximum strains S(réf,k)j given by the operational sensors of group A.

The expression of the space harmonization coefficient $Chs_{k,j}$ of the sensor n°j for the test of the configuration n°k is the following :

$$Chs_{k,j} = \frac{S(réf,k)_m}{S(réf,k)_j}$$

It will appear thereafter that $Chs_{k,j}$ coefficients present a very good stability in the time, i.e. $Chs_{k,j}$ values are practically not dependent on the configuration n°k tested. This will lead to consider as spatial harmonization coefficient the mean value of the $Chs_{k,j}$ relative to the configurations selected for the analysis.

Spatial harmonization coefficient for group B instrumentation

Data for the spatial harmonization of group B sensors have been collected once and for all in September 1998.

S(réf,0)j refers to the maximum strain value measured by the sensor n°j of a given type in a given structure, under the passage of the reference load, during measurements of September 1998.

S(réf,0)m is the average value of the strains S(réf,0)j measured by the operational sensors of the group.

The expression of the space harmonization coefficient Chs_j of the sensor n°j is the following:

Temporal harmonization coefficient for group A instrumentation

S(réf,tréf)m indicates the average strain value of the various sensors of a given type in a given structure, under the reference load passage which precedes the test carried out at the date tréf. tref is the date of the test of the configuration chosen like reference configuration.

S(réf,t)m indicates the average strain value measured by the operational sensors of the group, under the reference load that precedes the test of a given configuration (at the date t).

The temporal harmonization coefficient Cht is identical for the whole sensors of the type and structure considered. Its expression is:

$$Cht = \frac{S(réf,tréf)_m}{S(réf,t)_m}$$

Temporal harmonization coefficient for group B instrumentation

The temporal harmonization cannot be carried out in the same manner for the strain gauges of the instrumentation B. For these gauges indeed, the reference load circulates on a single longitudinal axis.

Temporal harmonization thus requires, for each structure B, C and D, the choice of a particular gauge, the number of which is jref. This reference gauge is unchanged all over the

different tests. It generally is the sensor for which the measured strain under the reference load passage along the longitudinal axis is the maximum.

S(réf,tref)jref refers to the strain value measured by the reference gauge n°jref under the reference load that precedes the test carried out at the date tref.

S(ref,t)jref refers to the strain value measured by this reference gauge, under the passage of the reference load which precede the test carried out at the date t.

The temporal harmonization coefficient is obtained by the relation:

$$Cht = \frac{S(réf, tréf)jref}{S(réf, t)jréf}$$

Final expression of the harmonization of measurements

S(cfk,t)j indicates the maximum rough strain value, i.e. before any harmonization, measured by the gauge n°j under the passage of the configuration n°k (at time t).

S(cfk,tréf)j-hst is the value of this same measure after double spatial and temporal harmonization, where tref is the reference date.

The double space and temporal harmonization of a strain measure is expressed by the same relation for group A gauges as for group B gauges. Only differs the expression of the temporal harmonization coefficient Cht.

Temporal harmonization coefficients for the 8 selected configurations

Table 2 presents the value of the coefficients of temporal harmonization obtained for the three structures B, C and D and for the four types of gauges analyzed in this study:

- horizontal strains (longitudinal and transversal) at the base of the GB
- Vertical strains at the top of the GRH and at the top of the subgrade.

Configura--tion	Structure	ε_l & ε_t GB base	ε_z on top GRH	ε_z on top Subgrade
CB1	B	0.673	0.714	0.781
	C	0.783	0.721	0.860
	D	1.025	0.900	0.806
CB2	B	0.729	0.823	0.731
	C	0.793	0.978	1.089
	D	0.911	0.946	1.000
C1	B	1.000	1.000	1.000
	C	1.000	1.000	1.000
	D	1.000	1.000	1.000
C7	B	1.000	1.038	0.995
	C	1.585	1.278	1.153
	D	1.281	1.164	0.882
C5H	B	1.094	1.185	1.126
	C	1.300	1.255	1.153
	D	1.577	1.256	1.000
C8	B	0.729	0.913	0.839
	C	0.970	1.122	1.167
	D	1.242	1.099	0.962
C17	B	1.129	1.241	1.110
	C	1.327	1.112	1.111
	D	1.025	1.205	1.087
C22	B	0.700	0.969	0.963
	C	1.083	0.983	1.065
	D	0.932	0.855	1.042

Table 2: Temporary harmonization coefficient – reference to configuration C1

The vertical strains at the base of the GRH are not analyzed. One could observe that for the majority of the measurement, the values of these vertical strains and those measured at the top of the subgrade are in fact very close.

The determination of the temporal harmonization coefficients for the transversal strain gauges at the base of the bituminous layer GB raises in fact some difficulties. Because of their low depth in the structure, these strains are indeed extremely sensitive to the exact transversal positioning of reference load on the pavement surface (strong strain gradient in the transverse direction: cf. experimental and numerical results).

For this reason, the temporal harmonization coefficients Cht calculated according the standard procedure appear not very reliable. Therefore the calculation of the Cht coefficients for these transverse gauges has been abandoned. We decided then to allot to them the Cht coefficients calculated for the longitudinal gauges, which seems an acceptable approximation taking into account the nature of the corrections aimed through these coefficients.

The reference configuration adopted for the establishment of the temporal harmonization is the C1 configuration (bogie 6 wheels). The average temperatures in the bituminous layer (BB

+ GB) during the test of the C1 configuration are approximately 16°C (structure B and C) and approximately 12°C (structure D).

The coefficients of temporal harmonization obtained vary according to following range:

- strains at the base of asphalt concrete (GB) : between 0.67 and 1.58
- strains at the top of the GRH: between 0.71 and 1.28
- strains at the top of the Subgrade: between 0.3 and 1.17

The lowest values are mainly those observed for the first configurations tested, and the values close to the unit or higher are rather those observed for the configurations tested in second part of the program.

The sensitivity of the Cht coefficients to the temperature in bituminous materials has been examined. This is the subject of **figures 6, 7 and 8**, which represent the variations of Cht coefficients with the average temperature in the bituminous materials, respectively for the Cht coefficients relative to the GB, the GNT and the subgrade.

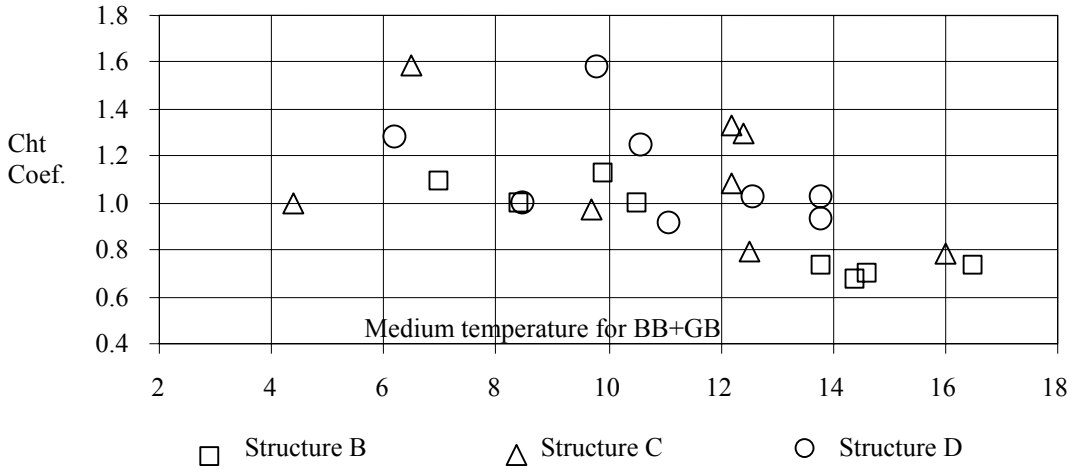

Figure 6: Temporal harmonization coefficients Cht for GB base gauges. Variations with medium temperature in bituminous materials (BB and GB).

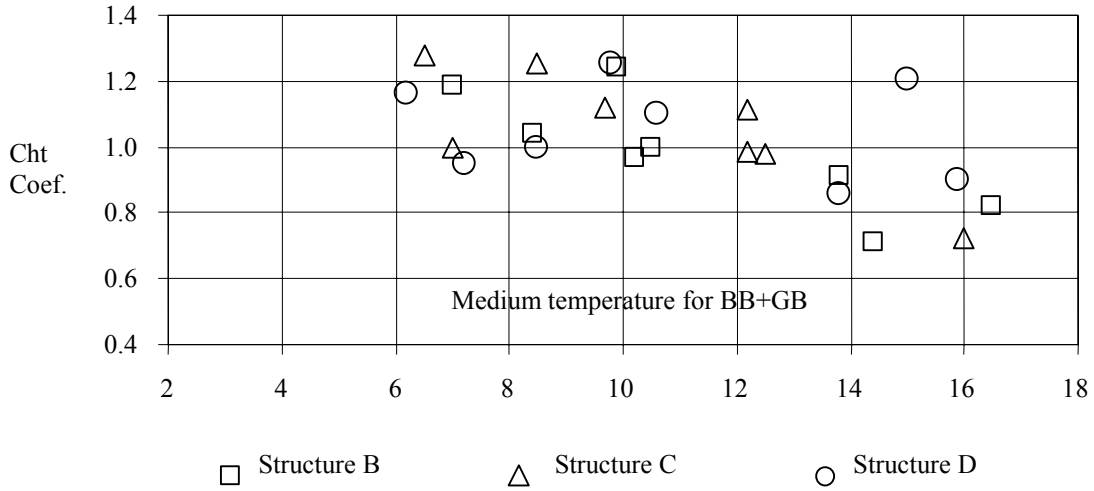

Figure 7: Temporal harmonization coefficients Cht for top GNT gauges. Variations with medium temperature in bituminous materials (BB and GB)

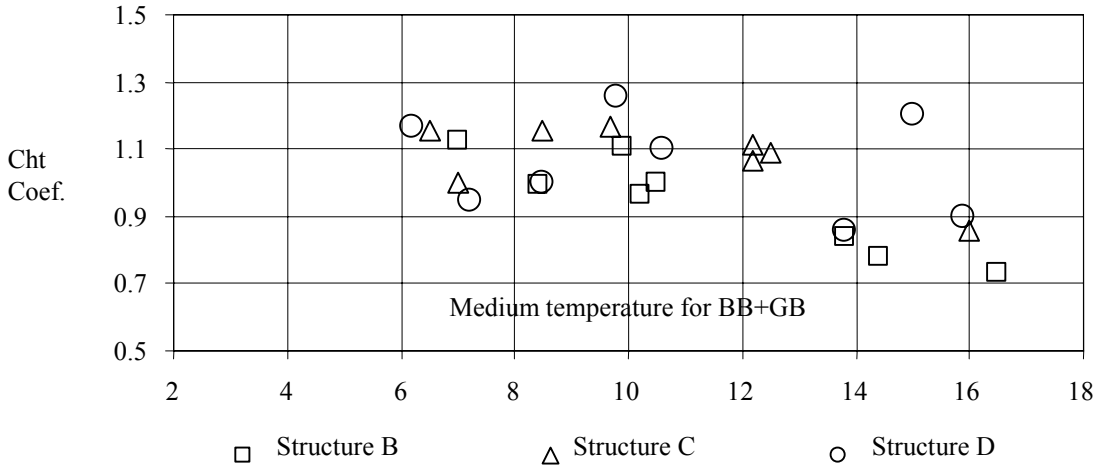

Figure 8: Temporal harmonization coefficients Cht for top subgrade gauges. Variations with medium temperature in bituminous materials (BB and GB)

The general tendency coming out from these graphs, like awaited, is the global decrease of the Cht coefficients with the temperature. But it appears clearly that the Cht coefficients are far from varying in a monotonous way, nor in a bi-univocal way, with the temperature in the bituminous layer. This last parameter is not thus enough alone to explain the variations in gauges measurement for the reference load, that are aimed by the temporal harmonization.

This confirms that other factors of environmental nature also influence the evolution in the time of measurements under constant loading. Who more is, the influence of these other factors is apparently of an order of magnitude very comparable with the individual influence exerted by the temperature in the bituminous materials.

Spatial harmonization coefficients for the 8 selected configurations

The temporal harmonization leads to Chs coefficients common to all the gauges of a given type, that for each structure and each analyzed configuration

Space harmonization leads on the contrary, to an individual Cht coefficient for each gauge, common to the whole analyzed configurations. The values of the Chs coefficients of spatial harmonization, for the whole of the gauges, are provided in **appendix A1**. **Table 3** presents a synthesis, expressed in the form of the standard deviations of these coefficients per type of gauge and structure.

gauge type	Structure		
	B	C	D
ε_l GB base	16.4%	12.3%	17%
ε_t GB base	12.2%	19.1%	24%
ε_z on top GRH	27.6%	22.3%	33%
ε_z on top subgrade	33.9%	12.4%	12%

Table 3: Spatial correction coefficients – deviation by sensor group and structure

Dispersions appear slightly less for the horizontal strain gauges placed in the GB, than for the vertical gauges in the GNT and the subgrade. This is in agreement with our experience in pavement instrumentation. It is explained above all by the natural heterogeneity of the not treated materials, which is in general much higher than that presented by bounded materials.

Some comments on the harmonization coefficients

For the spatial as for the temporal harmonization, it is observed that the coefficients Chs and Cht obtained express corrections to be applied to the rough strains, which are often higher than several tens of percent. These corrections are necessary to establish objective and quantified comparisons between the various configurations tested. Their high order of magnitude:

- justifies the place which is given in our analysis, to the operations of harmonization of the strain measurement

- Invites right now to consider with prudence the comparisons between the tested configurations, which should be based exclusively on the corrected extensometric measurements. Keeping constant the tire load, it is clear that geometrical changes of the bogie of a few centimeters exert variations on the internal strains in the pavement, which are quite lower than the corrections of harmonization of the measurements attached to each configuration.

II-2-4-4 Running of the instrumentation

II-2-4-4-1 Standard signals

The twenty configurations tested during the static tests made it possible to constitute a very complete database. It gathers the whole of the signals of the strain gauges, measured with the passage of the simulator and of the reference load, for each static configuration,
In its various configurations, the simulator circulates on the experimental pavement with the interior wheel of the external bogie centered on the yellow line.
The speed of the machine is always close to 0.5 meter per second (1,8 km/h). The exploitation of gauge measurements thus does not require any additional harmonization relative to the effects of the speed, which would have been the case if speed had varied significantly during the static campaign.
The strain signal acquisition of the various gauges corresponding with one passage of the simulator or of the reference load is carried out over one total duration of approximately 90 seconds. It is started approximately 20 seconds before the passage of the first axle of the load, above the line of sensors concerned. The scanning frequency is approximately 50 Hz: this corresponds to the acquisition of a point of measurement every 10 mm of advance of the simulator.
The whole of the strain signals is numerically filtered at 10 Hz before exploitation. The maximum values of strain extracted from these signals correspond to the maximum values at peaks, after centering with zero of the signal filtered by total translation of amplitude equal to the average value of the signal calculated on its the first 300 points (except very particular case).
On the whole of acquisitions carried out, it can be observed that the general shape of the strain signal is characteristic of the type of gauge considered: longitudinal GB, transversal GB, vertical high GRH, low GRH, or top of the subgrade. This is in agreement with our experiment in the road pavement field.
On the other hand, for a type of sensor given, the signals are obviously sensitive to the test parameters attached to the structure, to the load tested, and of course to the temperature conditions. These parameters exert influence mainly on the amplitude of the signal, and on the number of local extremis that it comprises (in general equal to the number of single axles composing the tested bogie: two and three peaks respectively for the four wheels bogie and for the six wheels bogie).

Figures 9 provide as an example the standard signals, characteristic of the five types of sensors. It concerns the strain gauges placed in the structure D, and the C22 configuration (6x6). The temperature at the top of BB is then of +15,8°C, and the average temperature on thickness BB+GB is 11,7°C (03-03-1999, 13h56 min).

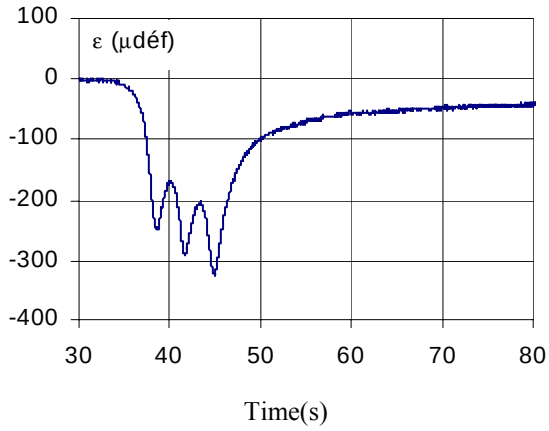

Fig. 9a: Transversal Strain (gauge 1T03)

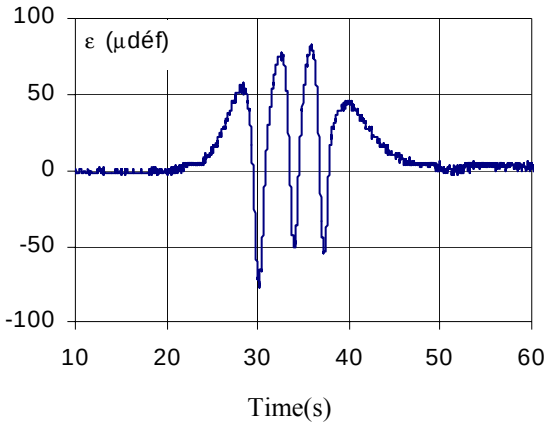

Fig. 9b: Longitudinal Strain(gauge 1L03)

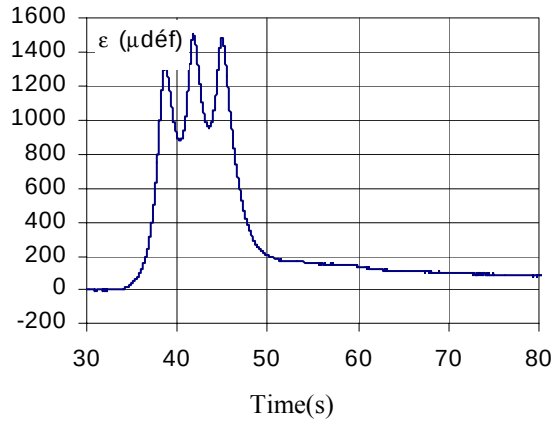

Fig. 9c: Vertical Strain on top of GRH (gauge 1H09)

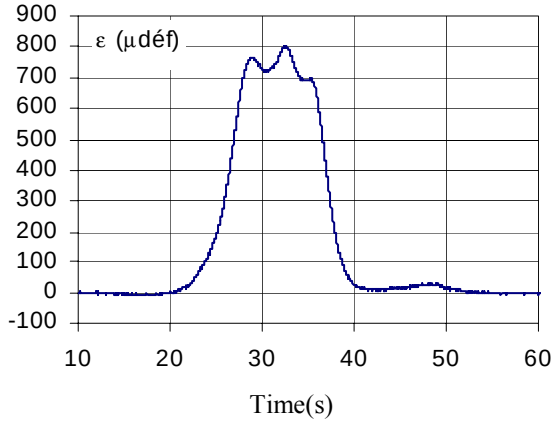

Fig. 9d: Vertical Strain on base of GRH (gauge 1B06)

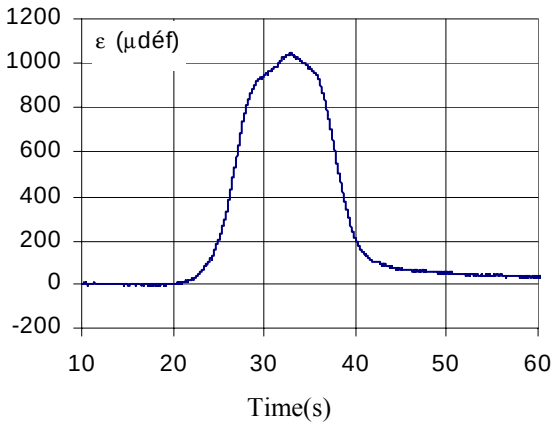

Fig. 9e: Vertical Strain on top of subgrade (gauge 1S07)

Figures 9: Extensometric measures, standard signals (before double harmonization). Example for C22 configuration (6x6), structure D (03-03-1999)

At the base of GB

The signal of transverse and longitudinal gauges is very clearly different.

In the transverse direction, the base of GB is always in extension. The signal presents three peaks corresponding to the successive passages of the three axles composing the 6-wheel bogie. The inequality between the peak values is well marked. The strain corresponding to the passage of the third wheel is in almost cases appreciably higher than those corresponding to the passage of the preceding wheels. This effect, all the more important since the temperature in bituminous materials is high, is directly connected with the viscoelastic behavior of these materials. A perfectly elastic behavior of materials would lead involve indeed, a symmetry of the signal about the axis of the load (equality of the strains relative to the first and the third load).

In the longitudinal direction, the base of GB presents on the contrary successive periods of extension and compression: extension at the passage of the wheels and compression during the time which precedes these passages directly and which succeed to them. The viscoelasticity of bituminous materials always results in inequality between peak values, but this time the maximum value of extension of GB can correspond to one or the other of the three axles of the bogie.

The transversal strain signal is characterized by the persistence of a residual strain, also in connection with the viscoelasticity of materials. It varies approximately between 10 μstrain and 20 μstrain; and it persists until the end of the signal or is erased more or less quickly. On the contrary, the return to zero of the longitudinal signals is done quickly after the passage of the load. One can explain this difference in behavior between the transverse and longitudinal gauges, by considering the average value of strains over the total duration of the passage of the load. This average value is about null for the longitudinal strain, and it is strongly negative (in extension) for the transversal one.

At the top of the GRH:

The signal relative to the top of the GRH presents compression strains comprising two (4 wheels) or three separated peaks (6 wheels). In the case of the 6 wheels bogie, the central peak, or the third peak, has the greatest amplitude in general. The return to zero of the signal is always differed in time, due to the viscoelastic behavior of the bituminous mix. It can be also explained by a possible plasticization of the untreated materials at the passage of the load.

At the base of the GRH and the top of the subgrade

The signals of the vertical gauges at bottom of the GRH and at the top of the subgrade have similar forms. They show a general compression with the passage of the load, with peaks under the wheels all the less marked as much than the layer of GRH is thick (case of the D structure). After application of the space corrections, which is not the case of signals presented on **figures 9**, it will be observed that the maximum strain measured at the base of the GRH and those measured at the top of the subgrade are in fact very close. The variation between the two values exceeding only exceptionally 13%.

II-2-4-4-2 Strains kinematics

The complete signals of the gauges bring information on the kinematics of the strain fields in the structures. These information, if they are not directly exploited in the continuation of this study, are however useful, at the same time, for checking of the correct working of the instrumentation, and for a better comprehension of the mechanical functioning of the structures tested.

Figures 10 and 11 illustrate the possibilities of visualization, by the gauge signals, of the internal strain fields in the structure. The simulator is here in C5H configuration (4x6x6x4). One considers the transversal profiles of strains at the top of the subgrade of the structures C and D, at two moments:

- Time t1 where the central axis of the two 6 wheel bogies passes above the transversal line of A instrumentation. The transversal profiles of strains measured at the top of the subgrade are presented on **figures 10a and 11a** respectively for the structures C and D
- Time t2 following the moment t1, several seconds later. At time t2, the central axis of the two bogies 4 wheels passes above the transversal line of A instrumentation. The transversal profiles of strains measured at the top of the subgrade are presented on the **figures 10b and 11b** respectively for the structures C and D.

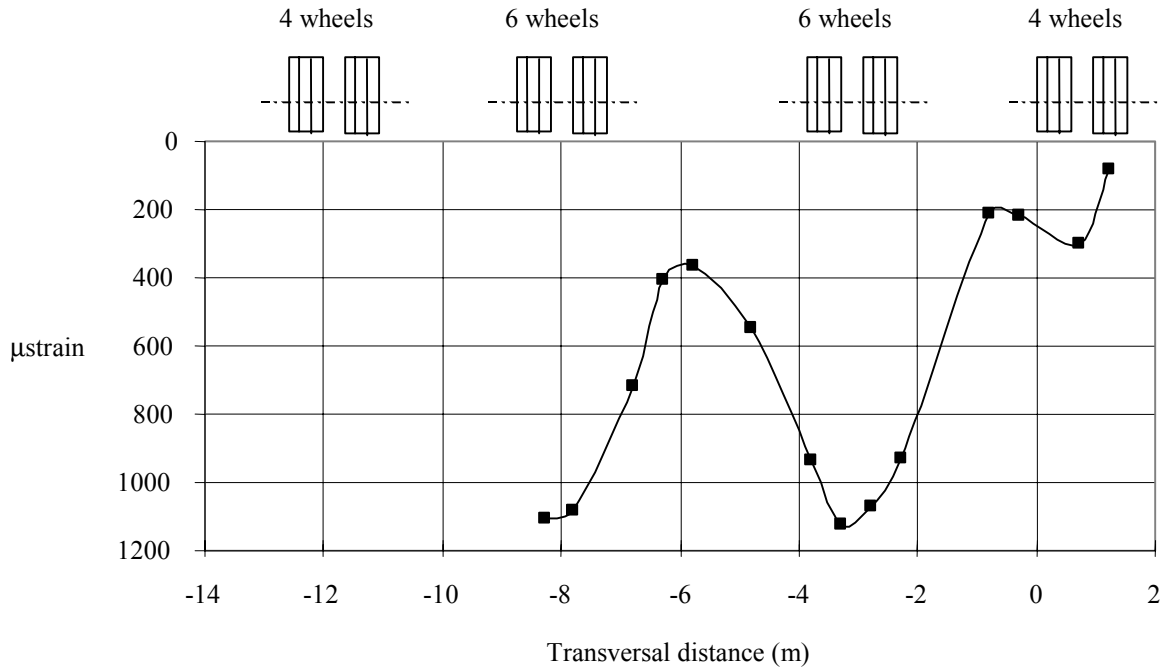

Fig. 10a: Transversal strain profile during 6 wheels bogie central axle pass.

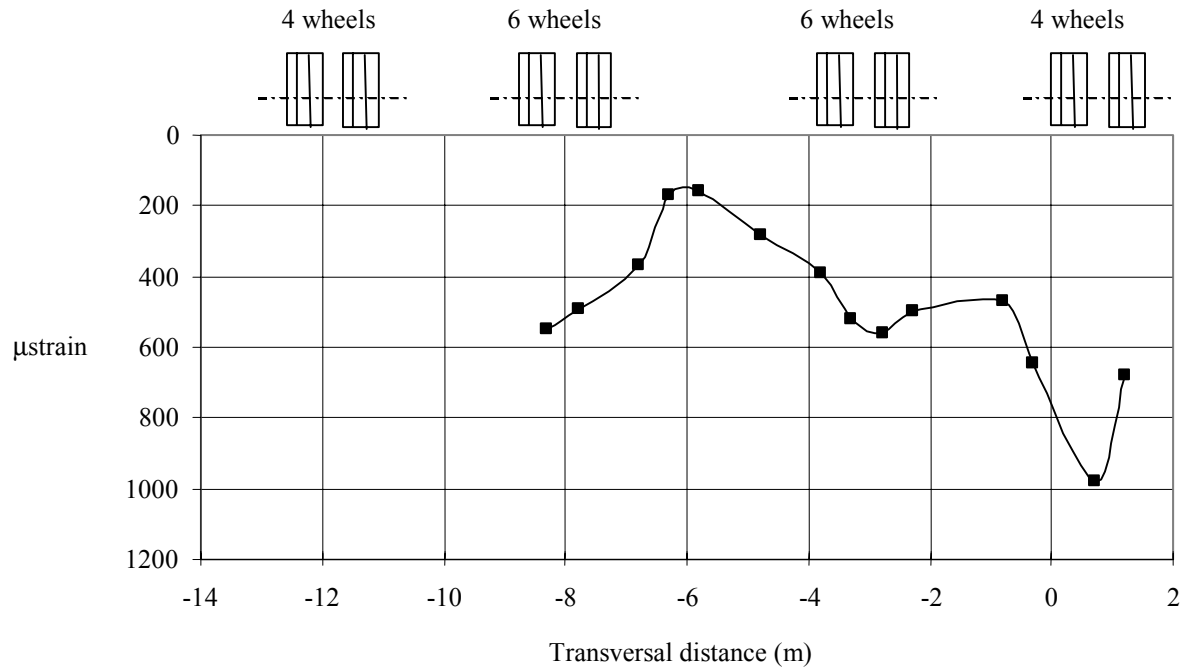

Fig. 10b: Transversal strain profile during 4 wheels bogies median axle pass.

Figures 10: Structure C, configuration C5H - global cinematic of vertical distortions on top subgrade.

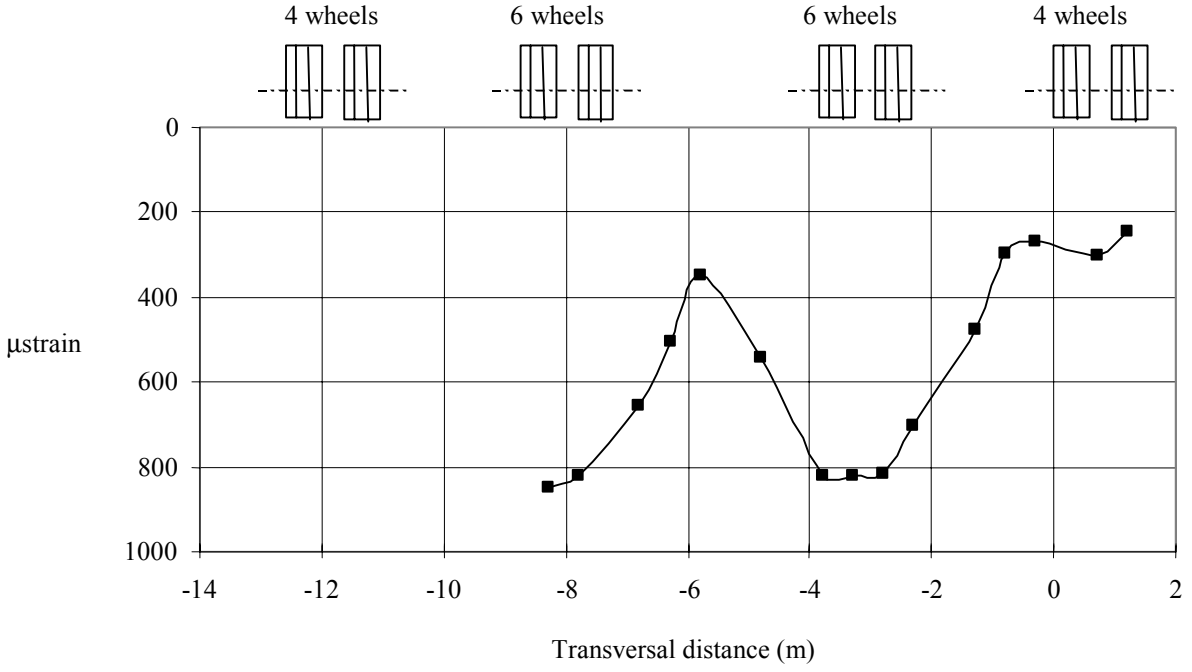

Fig. 11a: Transversal strain profile during 6 wheels bogie central axle pass.

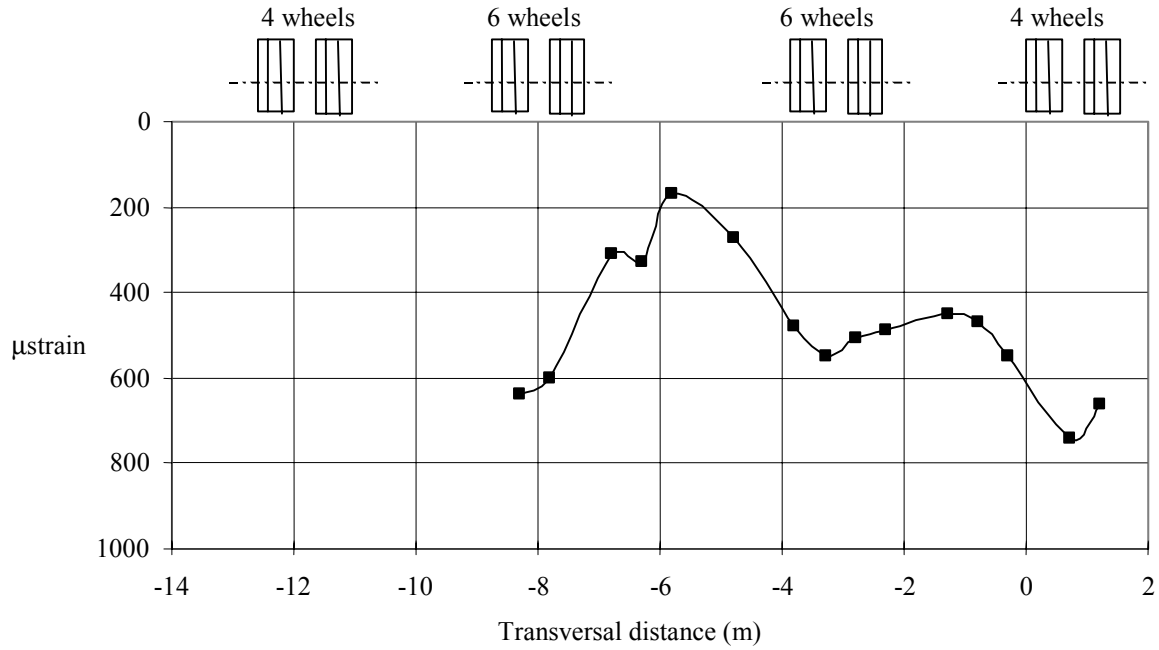

Fig. 11b: Transversal strain profile during 4 wheels bogies median axle pass.

Figures 11: Structure D, configuration C5H - global cinematic of vertical strains on top subgrade.

The strains presented here are the strains after spatial harmonization. This example shows that the implemented instrumentation permits a very satisfactory definition of the strain fields in the structures. It can be observed, in particular, a good symmetry of the transversal profiles about longitudinal axis of the loading. In addition the levels of strain measured at the passage of the 6 wheels bogies are appreciably higher than those measured with the passage of the 4 wheels bogie.

One also observes on these various profiles that the strains at the top of the subgrade in the median zones between the bogies are not negligible. In this area, interaction between nearby bogies is present. The transversal profiles suggest any time that this interaction is especially sensitive in the median zones between bogies. On the other hand, the maximum strains located below the 4 wheel bogies and the 6-wheel bogie do not seem affected, with the first order, by the effects of the close bogies.

II-2-4-5 Results of strain measurement after double harmonization

For each of the 8 selected configurations and the three structures B, C and D, the exploitation of the strain measurements takes into account the parameters of harmonization specified above.

The values of the maximum strains obtained after double harmonization at the base of the

bituminous layer, at the top of the GRH and at the top of the subgrade have been extracted from the signals.

These three maximum strains are consigned in **tables 4, 5 and 6** respectively for the strains at the base of the GB, at the top of the GRH and at the top of the subgrade. In these tables, the bogies are classified in the strain ascending order.

For the gauges of the group B (strains at the base of GB and at the top of the GRH for all structures, and at the top of the subgrade for structure B), the strain values obtained correspond to the effects of the external bogie of the simulator (in general a wing bogie), which only influences this group of sensors. For example, for a configuration 4x6x6x4, we have only access to the maximum strain created by the 4-wheel bogie of the left wing. The instrumentation does not inform about the strain created by the central 6-wheel bogies. A priori, for the sensors of the group B, in particular for 4x6x6x4 configurations, one remains in the ignorance of the specific maximum values to each configuration tested.

On the opposite, the instrumentation implemented indeed makes it possible to measure, for the gauges of the A instrumentation (top of subgrade structures C and D), as well the vertical strains in the subgrade under the bogie of wing as under the fuselage bogie.

The whole of the results of **tables 4, 5 and 6** are also presented on the graphs of **figures 12, 13 and 14**. On these graphs, the configurations are classified in two groups (4 wheels and 6 wheels), and by ascending order for of weight applied to the wheel inside each group.

Deformation base GB - Structure B

Tested configuration		Bogie type	weight/ wheel (kN)	Tire press. load (MPa)	Track (m)	Wheel base (m)	ε_{max} (µm/m)	Δ(%)
C5H	4x6x6x4	4wheels	260	1.34	1.35	1.80	187	79%
C8	4x6x2x6x4	4wheels	261	1.34	1.45	1.80	192	81%
C7	4x6x6x4	4wheels	260	1.34	1.45	1.80	210	89%
CB1	4x4x4x4	4wheels	232	0.88	1.12	1.47	224	95%
C1	6x4x4x6	6wheels	260	1.34	1.45	1.80	236	100%
C17	4x4x4x4	4wheels	316	1.34	1.40/1.18/1.40	1.98	266	113%
C22	6x6	6wheels A380	286	1.48	1.35/1.45/1.35	1.70	267	113%
CB2	6x6	6wheels	239	1.53	1.40	1.45	303	128%
Deformation base GB - Structure C								
CB1	4x4x4x4	4wheels	232	0.88	1.12	1.47	224	86%
C1	6x4x4x6	6wheels	260	1.34	1.45	1.80	261	100%
C7	4x6x6x4	4wheels	260	1.34	1.45	1.80	272	104%
C5H	4x6x6x4	4wheels	260	1.34	1.35	1.80	281	108%
CB2	6x6	6wheels	239	1.53	1.40	1.45	291	112%
C8	4x6x2x6x4	4wheels	261	1.34	1.45	1.80	348	134%
C17	4x4x4x4	4wheels	316	1.34	1.40/1.18/1.40	1.98	441	169%
C22	6x6	6wheels A380	286	1.48	1.35/1.45/1.35	1.70	475	182%

Deformation base GB - Structure D								
C17	4x4x4x4	4wheels	316	1.34	1.40/1.18/1.40	1.98	240	73%
C5H	4x6x6x4	4wheels	260	1.34	1.35	1.80	265	81%
C7	4x6x6x4	4wheels	260	1.34	1.45	1.80	277	85%
C22	6x6	6wheels A380	286	1.48	1.35/1.45/1.35	1.70	285	87%
C8	4x6x2x6x4	4wheels	261	1.34	1.45	1.80	294	90%
CB1	4x4x4x4	4wheels	232	0.88	1.12	1.47	320	97%
C1	6x4x4x6	6wheels	260	1.34	1.45	1.80	328	100%
CB2	6x6	6wheels	239	1.53	1.40	1.45	329	100%

Table 4: Max. Values of measured horizontal distortions on Asphalt-Gravel (GB) base, for 8 selected configurations (transversal deformations in all cases).

Tested configuration		Bogie type	weight/ wheel (kN)	Tire press. load (MPa)	Track (m)	Wheel base (m)	ε_{max} (µm/m)	Δ(%)
Deformation on top GRH - Structure B								
C7	4x6x6x4	4wheels	260	1.34	1.45	1.80	1229	90%
C8	4x6x2x6x4	4wheels	261	1.34	1.45	1.80	1300	95%
CB1	4x4x4x4	4wheels	232	0.88	1.12	1.47	1301	95%
C1	6x4x4x6	6wheels	260	1.34	1.45	1.80	1365	100%
C5H	4x6x6x4	4wheels	260	1.34	1.35	1.80	1388	102%
C22	6x6	6wheels A380	286	1.48	1.35/1.45/1.35	1.70	1565	115%
CB2	6x6	6wheels	239	1.53	1.4	1.45	1596	117%
C17	4x4x4x4	4wheels	316	1.34	1.40/1.18/1.40	1.98	1799	132%
Deformation on top GRH - Structure C								
CB1	4x4x4x4	4wheels	232	0.88	1.12	1.47	1024	97%
C1	6x4x4x6	6wheels	260	1.34	1.45	1.80	1055	100%
C22	6x6	6wheels A380	286	1.48	1.35/1.45/1.35	1.70	1094	104%
C8	4x6x2x6x4	4wheels	261	1.34	1.45	1.80	1122	106%
C5H	4x6x6x4	4wheels	260	1.34	1.35	1.80	1160	110%
CB2	6x6	6wheels	239	1.53	1.4	1.45	1161	110%
C7	4x6x6x4	4wheels	260	1.34	1.45	1.80	1187	113%
C17	4x4x4x4	4wheels	316	1.34	1.40/1.18/1.40	1.98	1393	132%
Deformation on top GRH - Structure D								
CB2	6x6	6wheels	239	1.53	1.40	1.45	835	93%
CB1	4x4x4x4	4wheels	232	0.88	1.12	1.47	868	97%
C1	6x4x4x6	6wheels	260	1.34	1.45	1.80	900	100%
C5H	4x6x6x4	4wheels	260	1.34	1.35	1.80	928	103%
C7	4x6x6x4	4wheels	260	1.34	1.45	1.80	1063	118%
C8	4x6x2x6x4	4wheels	261	1.34	1.45	1.80	1094	122%
C17	4x4x4x4	4wheels	316	1.34	1.40/1.18/1.40	1.98	1117	124%
C22	6x6	6wheels A380	286	1.48	1.35/1.45/1.35	1.70	1132	126%

Table 5: Max. Values of measured vertical distortions on Humidified Reconstituted Crushed Gravel (GRH) top, for 8 selected configurations.

Tested configuration		Bogie type	weight/ wheel (kN)	Tire press. load (MPa)	Track (m)	Wheel base (m)	ε_{max} (µm/m)	Δ(%)
Deformation on top Subgrade - Structure B								
C7	4x6x6x4	4wheels	260	1.34	1.45	1.80	1115	92%
C8	4x6x2x6x4	4wheels	261	1.34	1.45	1.80	1132	93%
C5H	4x6x6x4	4wheels	260	1.34	1.35	1.80	1144	94%
CB2	6x6	6wheels	239	1.53	1.4	1.45	1162	95%
CB1	4x4x4x4	4wheels	232	0.88	1.12	1.47	1202	99%
C1	6x4x4x6	6wheels	260	1.34	1.45	1.80	1217	100%
C22	6x6	6wheels A380	286	1.48	1.35/1.45/1.35	1.70	1444	119%
C17	4x4x4x4	4wheels	316	1.34	1.40/1.18/1.40	1.98	1509	124%
Deformation on top Subgrade - Structure C								
C7	4x6x6x4	4wheels	260	1.34	1.45	1.80	1172	89%
C5H	4x6x6x4	4wheels	260	1.34	1.35	1.80	1224	93%
C1	6x4x4x6	4wheels	260	1.34	1.45	1.80	1232	94%
C8	4x6x2x6x4	4wheels	261	1.34	1.45	1.80	1311	100%
C1	6x4x4x6	6wheels	260	1.34	1.45	1.80	1313	100%
CB1	4x4x4x4	4wheels	232	0.88	1.12	1.47	1327	101%
C7	4x6x6x4	6wheels	260	1.34	1.45	1.80	1416	108%
C5H	4x6x6x4	6wheels	260	1.34	1.35	1.80	1466	112%
C8	4x6x2x6x4	6wheels	261	1.34	1.45	1.80	1496	114%
CB2	6x6	6wheels	239	1.53	1.40	1.45	1590	121%
C22	6x6	6wheels B777	239	1.53	1.40	1.45	1633	124%
C17	4x4x4x4	4wheels	316	1.34	1.40/1.18/1.40	1.98	1709	130%
C22	6x6	6wheels A380	286	1.48	1.35/1.45/1.35	1.70	1714	131%
Deformation on top Subgrade - Structure D								
C7	4x6x6x4	4wheels	260	1.34	1.45	1.80	773	79%
C5H	4x6x6x4	4wheels	260	1.34	1.35	1.80	806	82%
C8	4x6x2x6x4	4wheels	261	1.34	1.45	1.80	806	82%
CB1	4x4x4x4	4wheels	232	0.88	1.12	1.47	844	86%
C7	4x6x6x4	6wheels	260	1.34	1.45	1.80	845	87%
C1	6x4x4x6	4wheels	260	1.34	1.45	1.80	883	90%
C8	4x6x2x6x4	6wheels	261	1.34	1.45	1.80	919	94%
C5H	4x6x6x4	6wheels	260	1.34	1.35	1.80	961	98%
C17	4x4x4x4	4wheels	316	1.34	1.40/1.18/1.40	1.98	976	100%
C1	6x4x4x6	6wheels	260	1.34	1.45	1.80	977	100%
C22	6x6	6wheels B777	239	1.53	1.40	1.45	1051	108%
CB2	6x6	6wheels	239	1.53	1.40	1.45	1071	110%
C22	6x6	6wheels A380	286	1.48	1.35/1.45/1.35	1.70	1263	129%

Table 6: Max. Values of measured vertical distortions on top subgrade, for 8 selected configurations.

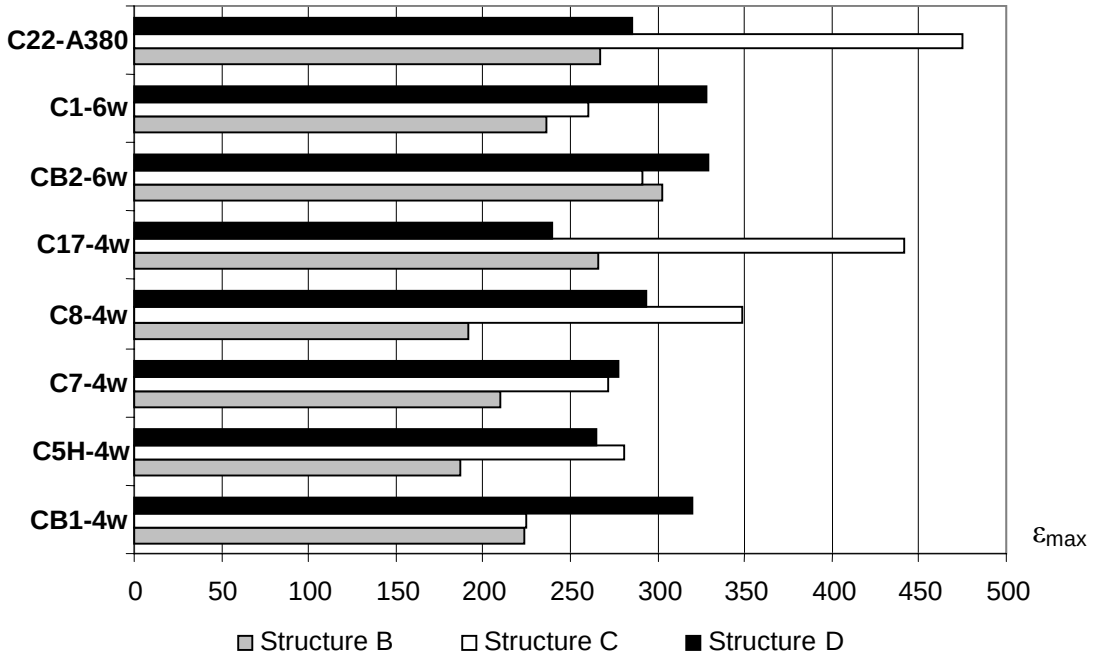

Figure 12: Max. Values of measured horizontal strains on GB base, for 8 selected configurations, and after spatial and temporal harmonization (transversal strain in all cases)

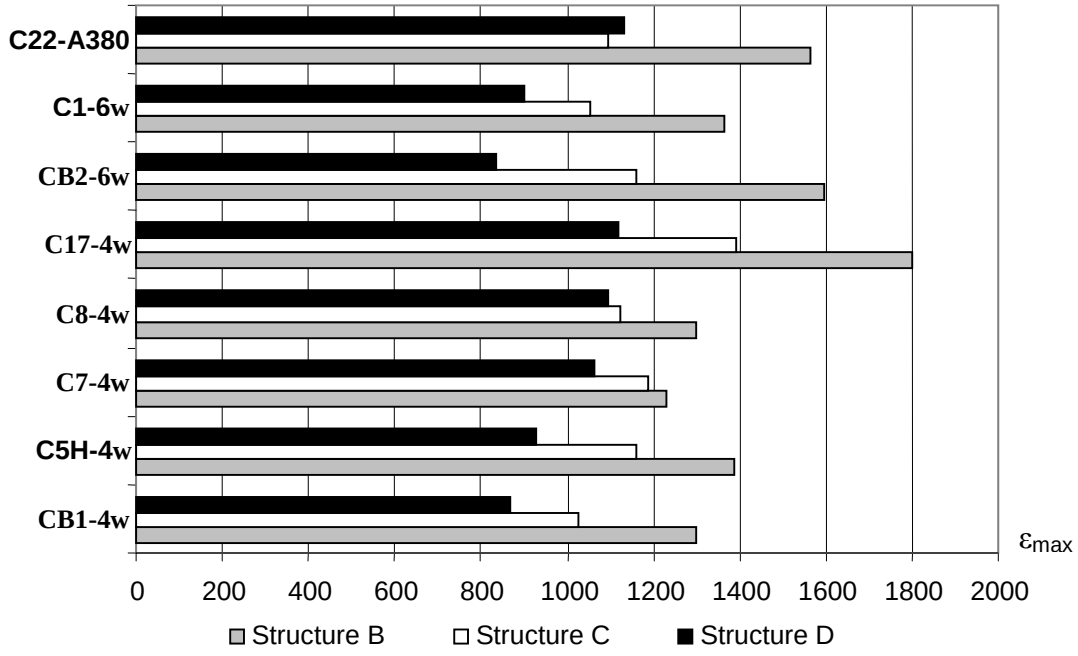

Figure 13: Max. Values of measured vertical strains on top GRH, for 8 selected configurations, and after spatial and temporal harmonization.

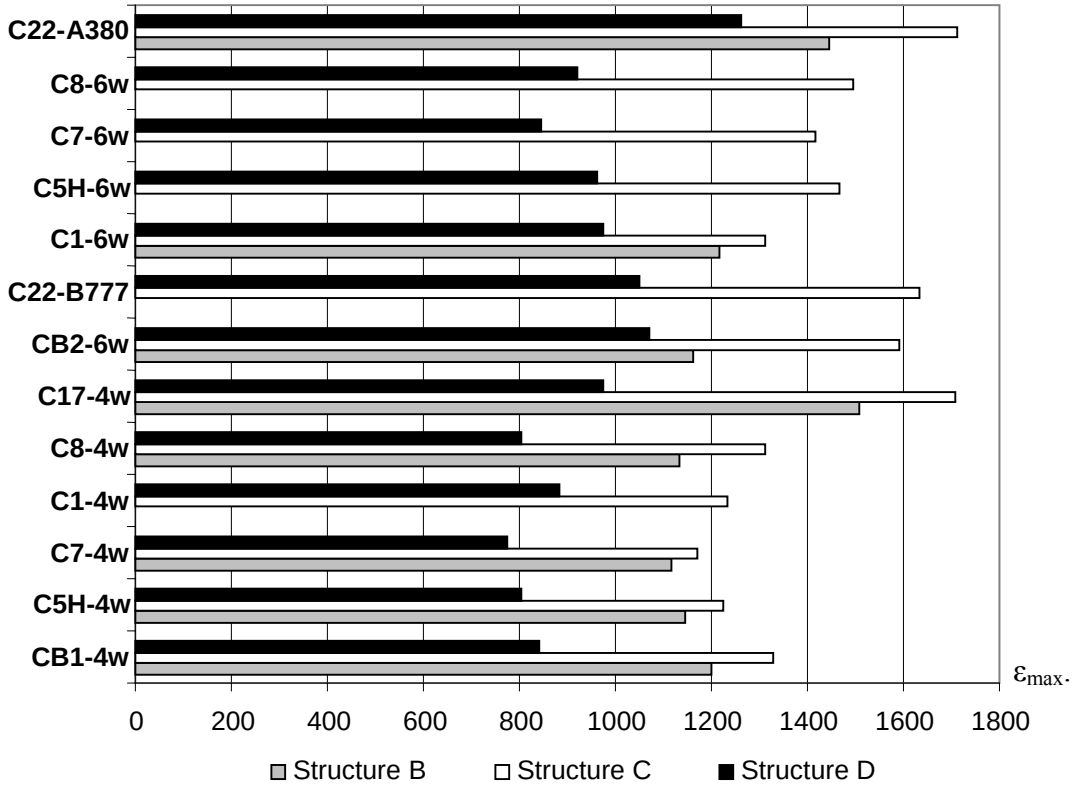

Figure 14: Max. Values of measured vertical strains on top subgrade, for 8 selected configurations, and after spatial and temporal harmonization.

II-2-4-6 SYNTHESIS for numerical modeling

II-2-4-6-1 Synthesis procedure

The results of the strains measurements presented before are the subject of a final synthesis intended to facilitate work of numerical simulation that will follow. This synthesis is established while considering the not-interaction between them of the various bogies composing a given configuration, like that is exposed before.

We shall retain, for a bogie of characteristics given (number of wheels, geometry, weight per wheel and inflation pressure), a single value of the maximum strain created by these bogie in a structure and a given layer of material, independently of the global geometry of the configuration to which it belongs. One admitted to consider as the same bogie, several bogies whose wheel-base varies from a value lower or equal to 10 cm, all other characteristics unchanged.

For example, the bogie whose characteristics follow is common to configurations C5H, C7 and C8:

- type : 4 wheel
- weight per wheel : 260 kN
- inflate pressure : 1,34 MPa
- wheel base : 1,35 à 1,45 m
- wheel track : 1,80 m

To a bogie such as the bogie that precedes, common to several configurations, we associate in a structure and a given layer of material, the average value of the maximum strains measured for a given configuration. A checking of the coherence of this average is however carried out, it relates to the variations with the average presented by various measurements intervening in it calculation. This examination lead to exclude from the final synthesis certain measurement, judged not very coherent with the overall results, without it being possible besides, sometimes, to identify the reasons of these reject.

The precision of measurements, relative at the same time to the adjustment of the loading by the simulator (weight, trajectory, speed), and, to the operations of double harmonization, result in admitting that the complete experimental system does not make it possible to distinguish the effects of a variation of ten cm in the geometry of the bogie. This thus leads us to assimilate, in this synthesis, the bogies of wheel base 1,35 m and 1,45 m.

The present synthesis finally results in identifying 6 bogies of different characteristics, 3 bogies with 4 wheels noted in the continuation bogie 4a, 4b and 4c, and 3 bogies with 6 wheels noted bogie 6a, 6b and 6c. The synthesis is presented in **table 7**. **Table 8** clarifies the plane configurations taken into account to establish the synthesis suitable for each of the 6 bogies.

Bogie n°	bogie type	weight/ wheel (kN)	Tire press. load (MPa)	Track (m)	Wheel base (m)	ε_t max base GB	ε_z max on top GRH	ε_z max on top subgrade
Structure B								
4a	4 wheels	260	1.34	1,35/1.45	1.80	196	1306	1131
4b	4 wheels	232	0.88	1.12	1.47	224	1301	1202
4c	4 wheels	316	1.34	1.4/1.18/1.4	1.98	266	1799	1509
6a	6 wheels	239	1.53	1.40	1.45	303	1596	1162
6b	6 wheels	260	1.34	1.45	1.80	236	1365	1217
6c	6 wheels	286	1.48	1.35/1.45/1.35	1.70	267	1565	1444
Structure C								
4a	4 wheels	260	1.34	1,35/1.45	1.80	276	1156	1235
4b	4 wheels	232	0.88	1.12	1.47	224	1024	1327
4c	4 wheels	316	1.34	1.4/1.18/1.4	1.98	441	1393	1709
6a	6 wheels	239	1.53	1.40	1.45	291	1161	1612
6b	6 wheels	260	1.34	1.45	1.80	*	1055	1423
6c	6 wheels	286	1.48	1.35/1.45/1.35	1.70	475	1094	1714
Structure D								
4a	4 wheels	260	1.34	1,35/1.45	1.80	279	1029	795
4b	4 wheels	232	0.88	1.12	1.47	320	868	844
4c	4 wheels	316	1.34	1.4/1.18/1.4	1.98	240	1117	976
6a	6 wheels	239	1.53	1.40	1.45	329	836	1061
6b	6 wheels	260	1.34	1.35 or 1.45	1.80	328	900	925
6c	6 wheels	286	1.48	1.35/1.45/1.35	1.70	285	1132	1263

(*) Non retain measure, negative trust test.

Table 7: Measures synthesis – Max. Values of measured distortions on Asphalt Gravel base (GB), on top Humidified Reconstituted Crushed Gravel (GRH) and on top subgrade, by bogie type of constant characteristic.

n° du bogie	structure B : GB, GRH, subgrade structure C : GB, GRH structure D : GB, GRH	structure C : subgrade structure D : subgrade
4a	C5H-C7-C8	C1-C5H-C7-C8
4b	CB1	CB1
4c	C17	C17
6a	CB2	CB2-C22
6b	C1	C1-C5H-C7-C8
6c	C22	C22

Table 8: Measures synthesis – in account configurations for synthesis realization by different bogie.

II-2-4-6-2 Analyze and comments

Strains at the asphalt concrete GB base

The maximum strains measured at the base of the bituminous base GB are oriented according to the transverse direction, without exception. The relationship between the maximum values measured in the longitudinal and transverse directions is consigned in **Pict.12**; it varies between 1.09 (structure B, configuration C17) and 2.15 (structure C, configuration C22 - bogie A380). The average value is 1.44.

Compared effects of the bogies on the strains in materials

Table 9 draws up the comparison between the effects on the internal strains, of the geometrical and weight characteristics specific to the various bogies.

Distortions on GB base			Distortions on top GRH			Distortions on top subgrade		
str. B	str. C	str. D	str. B	str. C	str. D	str. B	str. C	str. D
comparison between : 4 wheels large bogie (4a) and 6 wheels large bogie (6b) reference for comparison : bogie 4a								
20%	*	18%	5%	-9%	-13%	8%	15%	16%
comparison between : 4 wheels short bogie (4b) and 6 wheels short bogie (6a) reference for comparison : bogie 4b								
35%	30%	*	23%	13%	-4%	*	21%	26%
comparison between : 4 wheels large bogie (4a) and 4 wheels short bogie (4b) reference for comparison : bogie 4a								
14%	-19%	15%	0%	-11%	-16%	6%	7%	6%
comparison between : 6 wheels large bogie (6b) and 6 wheels short bogie (6a) reference for comparison : bogie 6b								
28%	*	0%	17%	10%	-7%	-5%	13%	15%

comparison between : 4 wheels large bogie-260 kN/wheel (4a) and 4 wheels large bogie-316 kN/wheel (4c) reference for comparison : bogie 4a								
36%	60%	-14%	38%	21%	9%	33%	38%	23%
comparison between : 6 wheels large bogie-260 kN/wheel (6b) and 6 wheels large bogie-286 kN/wheel (6c) reference for comparison : bogie 6b								
13%	*	-13%	15%	4%	26%	19%	20%	37%

Table 9: Comparisons on interns' stress effect and geometric characteristic effect

This synthesis suggests the following observations:

- The comparisons between bogies expressed by **table 9** relate exclusively to the maximum values of strain measured in the various layers of materials. One will have to keep in mind that these maximum strains do not express directly the damage created by a given bogie in a given structure. The results of **table 9** should not thus be interpreted in terms of aggressiveness.

- Like that was already underlined, the whole of the data exploited in this study leads to general tendencies on the effects of the great families of parameters characterizing the different configurations tested. On the other hand, the actual precision of the experimental and instrumental system implemented is not able to directly provide precise information on the influence of weak variations of these parameters. The contribution of the results of **tables 7 and 9** is finally at two levels:

    - on the level of the total tendencies which emerge under an angle more qualitative than quantitative for some of them. One appreciates in particular the effects of the 6 wheels bogie compared with the 4 wheels bogie, the effect of the broad bogie compared with the short bogie, finally the effect of the overloaded bogie compared to the normally loaded bogie.

    - On the level of the possibilities offered by these results, with respect to the evaluation and of the calibration of the numerical models.

- Comparison between bogies 4 wheels and bogies 6 wheels ("broad" bogies and "short bogie "): The 6-wheel bogie exerts on the strains in GB and the subgrade an increasing effect. It varies:
    - For the broad bogie (260 kN/wheel), between + 8% and +16% concerning the subgrade, and from approximately +20% concerning the GB.

    - For the short bogie (230 kN/wheel), between + 21% and +26% concerning the subgrade, and between +30% and 35% concerning the GB.

- The effect in GRH is more complex to analyze the highest strain not being always those corresponding to the bogie 6 wheels. The ratio 6 wheels/4 wheel is variable at the same time according to the nature of the bogie (broad or short) and according to the structure. It varies between -13% (broad bogie structure D) and +13% (short bogie structure B).

- Comparison between broad bogies (260 kN/wheel) and short bogies (230 kN/wheel): the short bogie (4 wheels as 6 wheels) exerts on the strains in GB and the subgrade an increasing effect, variable between +6% (subgrade structure B) and +28% (GB structure B). The effect in the GRH is again variable at the same time according to the type of bogie (4 wheels or 6 wheels) and according to the structure. It varies between -16% (4-wheel bogie structure D) and +17% (6-wheel bogie structure B).

- Comparison between broad bogies with 260 kN/wheel and broad bogies with 316 (4 wheels) and 286 kN/wheel (6 wheels): The increase in the load per wheel increases, at top of subgrade, the vertical strains between +19% (bogie 6 wheels with 286 kN/wheel, structure B) and +38% (bogie 4 wheels with 316 kN/wheel, structure C). On the GRH, increase is between 4% (bogie 6 wheels with 286 kN/wheel, structure C) and +38% (bogie 4 wheels with 316 kN/wheel, structure B). On GB, increase varies between +13% (bogie 6 wheels with 286 kN/wheel, structure B) and +60% (bogie 4 wheels with 316 kN/wheel, structure C).

II-2-4-7 SOFTWARE Alizé calibration

II-2-4-7-1 Hypothesis

The aim of this part of the study is to evaluate the possibilities of simulating by numerical way, the maximum strains measured in the PEP structures during static tests on flexible structures. This is done by mean of the classical linear elastic multi-layers model (l.e.m model) of road mechanics. We used Alizé software of LCPC, which is an application of the solutions proposed by Burmister to this problem.

The hypothesis of the simulation are those of Burmister s' model:

Geometrical data

The materials composing the structures are represented by layers of semi-infinite extension in the horizontal plane, and constant thickness equal to the nominal thickness of the project.

Material behavior

The model of Burmister imposes linear and isotropic elastic behavior for all materials. This model of behavior is very convenient in practice because of the low number of parameters of mechanical behavior which it requires (Young modulus E and Poisson's ν). It allows a fast and simple a resolution of the problem to be solved. On the other hand, it is appropriate badly:

- With the untreated granular materials (GRH and subgrades), which in general present in the roadways a non-linear elastic behavior more or less anisotropic. The subdivision of a layer untreated of material in several underlayers is an artifice making it possible to reproduce in an approximate way the isotropic non-linear elastic behavior by the linear elastic model. With each underlayer is allotted a modulus, variable with the underlayer in order to reproduce the variations of module resulting from the non-linearity of behavior of material. One will notice that this technique of subdivision in underlayers was employed

here for the subgrade of the structure C, reproduced by two layers thickness 1 meter each, and for the GRH of the structure D reproduced by 2 layers thickness 0,70 meter each.

- With bituminous materials, which exhibit a viscoelastic or visco-élasto-plastic behavior all the more accentuated since the temperature in material is high, and that the displacement speed of the load is slow. There is no simple modeling artifice, making it possible to take into account, in the linear elastic model, the viscoelastic behavior of bituminous materials.

Representation of the loads

Theoretical simulations exclusively aim the maximum deformations generated by the various configurations in the pavement structures, and the comparison between these values with the measured maximum values. The loads taken into account for modeling are thus the six bogies resulting from the synthesis of measurements done before and not the complete configurations. The exploitation of static measurements indeed showed the not-interaction between the various bogies composing a given configuration, with respect to the maximum strain created by this configuration.

Each load (pneumatic) is considered in calculations as a uniform and static vertical pressure, applied to a circular disc to the road surface. The real prints of the tires on the road surface rather appeared as pseudo-rectangles with cut angles and length-width ratio from 1.05 to 1.25. It was also considered that the contact pressure is equal to the inflation pressure of the tire.

II-2-4-7-2 Step of adjustment of the model

The rules adopted to proceed in the searches of optimized adjustments are as follows:

Variables and criteria of adjustment

The adjustment of the Alizé model is done, for the three structures, with the values of the modulus of rigidity of the various layers of materials and the subgrades. The criterion of appreciation of the adjustments is the agreement between the maximum measured strains and strains calculated by the model.

A given structure is the subject of a single set of modulus, common to the six bogies exploited for the optimum search for adjustment. It was thus admitted in particular that the untreated materials (GRH and subgrades) preserve unchanged modulus values when the applied load varies, which seems to be not very compatible with the more or less accentuated non-linear behavior, which characterizes these materials.

The totality of the successive adjustments carried out showed the incapacity of the linear elastic model to reproduce in a satisfactory way the values of the maximum deformations measured at the base of the sand-gravel mix bitumen. One observes indeed:

- measured maximum values very badly restored by calculations if one admits to preserve constant the modules of the BB and GB of a given structure ;
- and especially, total and systematic contradiction between measurements and calculations, with regard to the direction of the maximum tensile strains as whose announced higher, the measured maximum tensile strains are always directed according to the transverse direction with the axis of motion of the loading. On the contrary, the maximum strains

obtained by the model are directed without exception according to the longitudinal direction of displacement of the load.

This last observation resulted in the fact that tensile strains at the base of the bituminous layer have finally not been taken into account in researching the best structure adjustments. The only criteria considered are thus the vertical strains at top of the GRH and at top of the subgrade.

Modulus of bituminous materials

The modulus of bituminous materials BB and GB are selected identical for the structures B and C, because for these two structures, the average temperature in the bituminous layer during the test of configuration C1 (reference for the temporal harmonization) is about constant, that is to say 16°C. The modulus of bituminous materials for the structure D seems to be higher, because the average temperature in the bituminous mix during the test of the configuration C1 is only 12°C.

E indicating the Young modulus of materials, the relation: Egb = Ebb + 2 000 MPa was fixed for all structures.

Initial structures for the iterative process of adjustment

Research of adjustment is carried out by successive iterations on the modulus of materials. The structures used to initiate the adjustment iterations are the structures which result from the preliminary study of September 1999 (A380 Experimental Pavement Program, PEP static campaign, Size effects of bogies one the resilient strains). Only the results of measurements for the configuration C7, without temporal harmonization, were taken into account to establish this initial calibration of the model.

II-2-4-7-3 Results of the adjustments with the L.E.M model

Adjusted structures

Table 10 shows the structures obtained after adjustment according to the steps presented before.

Structure B *CBR 10*		*Structure C* *CBR 6*		*Structure D* *CBR 4*	
material and thickness	Young modulus (MPa)	material and thickness	Young modulus (MPa)	material and thickness	Young modulus (MPa)
BB 8 cm	3 000	BB 8 cm	3 000	BB 8 cm	6 000
GB 24 cm	5 000	GB 24 cm	5 000	GB 24 cm	8 000
GRH 20 cm	80	GRH 60 cm	110	GRH 70 cm	100
Subgrade 1 m	80	Subgrade 1 m	50	GRH 70 cm	70
substratum	15 000	Subgrade 1 m	150	Subgrade 2 m	60
		substratum	15 000	substratum	15 000

Poisson coefficient: ν = 0,35 (all materials)

Table 10: Simulation of the structures B, C and D for the six bogies resulting from the analysis of the static tests. Structures adjusted with Alizé software.

Table 11 recalls the strains measured at the top of the GRH and at the top of subgrade for the six bogies, after space and temporal harmonization. It provides the strains calculated by Alizé model in the structures after calibration, as well as the relative differences between measurements and calculations.

	Distortions on top GRH			Distortions On top Subgrade		
	measure	calculus	Gap	measure	calculus	gap
			Structure B			
bogie 4a	1306	1338	2%	1131	1124	-1%
bogie 4b	1301	1304	0%	1202	1188	-1%
bogie 4c	1799	1569	-13%	1509	1331	-12%
bogie 6a	1596	1447	-9%	1162	1278	10%
bogie 6b	1365	1378	1%	1217	1180	-3%
bogie 6c	1565	1556	-1%	1444	1348	-7%
			Structure C			
bogie 4a	1156	1088	-6%	1235	1289	4%
bogie 4b	1024	1025	0%	1327	1536	16%
bogie 4c	1393	1272	-9%	1709	1430	-16%
bogie 6a	1161	1155	-1%	1612	1632	1%
bogie 6b	1055	1121	6%	1423	1459	3%
bogie 6c	1094	1258	15%	1714	1698	-1%
			Structure D			
bogie 4a	1029	882	-14%	795	816	3%
bogie 4b	868	882	2%	844	842	0%
bogie 4c	1117	1034	-7%	976	868	-11%
bogie 6a	836	983	18%	1061	1016	-4%
bogie 6b	900	938	4%	925	948	2%
bogie 6c	1132	1060	-6%	1263	1095	-13%

Table 11: Simulation of B, C and D structures for six bogies types, resulting static's tests exploitation. Structures adjusted with Alizé.

Comments on the adjustments obtained

- Quality of simulation : the differences between measurements and calculations show an adjustment very close to the theoretical model (see **Figure 15**):

  - for the GRH, the differences vary between -14% and +18%. 78% of the calculated deformations present a lower deviation less than 10% of measurements;
  - for the subgrade, the differences vary between -16% and +16%. 72% of the calculated deformations present a lower deviation less than 10% of measurements.

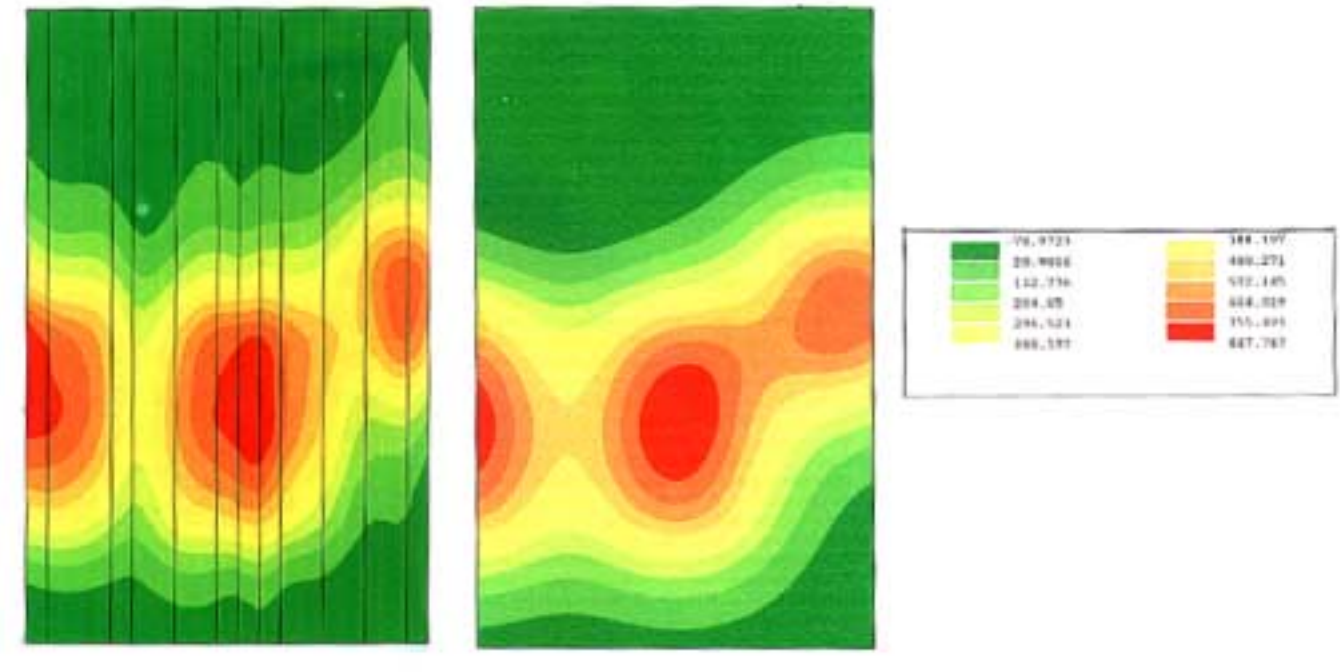

Figure 15: Real A/C – Alizé vertical strain comparison for CBR3.

The values, which precede, characterize from our point of view a very correct adjustment of the model. By way of comparison, adjustments of this quality are rarely obtained with the experiments carried out on the LCPC's fatigue test track. Experimental difficulties encountered on PEP flexible campaign, in particular the precision of spatial and temporal harmonization, come to reinforce this opinion on the quality of the corrections obtained.

- Modules of bituminous materials: the corrections lead for the structures B and C with the values of modules 3 000 MPa for the BB and 5 000 MPa for GB. These values appear in agreement with the conditions of temperature (16°C approximately) and the speed of the simulator (approximately 2 km/h). The values obtained for the structure D, 6 000 MPa and 8 000 MPa respectively, appear also coherent, taking into account the reference temperature which is 12°C approximately for this structure.

- Modules of the GRH: the module obtained on the higher part of the GRH (20 cm for the structure B, 60 or 70 cm for the structures C and D) varies between 80 MPa and 110 MPa. These values relatively low are explained by the significant thickness of the bituminous layers (32 cm) which may attenuate the average constraints supported by the untreated low register, by thus attenuating the nonlinear character of its behavior. In depth (underlayer in GRH of 70 cm of the structure D), the value of modulus of 70 MPa is to be connected in fact to the module of the subgrade support of 60 MPa. Our experiment in road structures leads in general to observe a low discontinuity of modulus in this part of the structure near the interface between the subgrade and the untreated granular sub-base.

- Modules of the subgrade: the values of modules obtained for the subgrades of the three structures seems to be enough surprising, because they badly reflect the values of the respective CBR presented by these three materials at construction. It is difficult however

to stop an opinion on these results, as long as the laboratory tests on the three subgrades will not have identified their law of behavior, different moreover according to the subgrade. The average pressures at the top of the subgrade of the structure B are normally higher than at the top of the subgrade of the structure D, because the thickness of very different GRH. The traditional model of Boyce, who establishes a strengthener of material with the average pressure, would lead to values of module appreciably higher for the subgrade of the structure B than for that of structure D. We have to observe however than this nonlinear model is especially validated for the untreated graded aggregates. The laws of behavior for the subgrades are very varied. One should not exclude that another form of dependence between the average pressure, the shear stress and rigidity can justify the values of modules obtained for the three subgrades, in spite of their initial values of CBR.

II-2-4-7-3 Conclusions on the capacities of the elastic model multi-layer

- The data available made it possible to carry out a realistic calibration of the elastic linear multi-layer model for the structures B, C and D, consisting in the adjustment of the modulus of rigidity of the materials and the subgrade, and the subdivision into underlayers of the thick layers of untreated materials in order to reproduce their nonlinear behavior.

- For the three structures B, C and D resulting from this adjustment, the classical multi-layer linear model elastic (Alizé-LCPC software) allows a rather precise determination of the maximum deformations generated at the top of the subgrade and the top of the GRH by six isolated standard bogies (three bogies 4 wheels and three bogies 6 wheels).

- The questions concerning the influence on the strains in pavements, of the geometrical and weight characteristics of the bogies have partly justified the static tests of the flexible PEP. The experimental results alone do not bring the awaited complete quantitative answers, because of the obligatory complexity of the experimental process, and the low precision of the operations of spatial and temporal harmonization which it was essential to apply. One will find in the multi-layer linear elastic model the sufficiently precise quantitative answers to these questions, only as regards the maximum strains the untreated material and in the subgrade. For the relative comparisons between bogies in a context of flexible pavement other that the flexible PEP, one will find normally in the elastic model reliable answers, not requiring a too constraining preliminary adjustment.

- The classical model appears on the other hand unsuited, to obtain a realistic description of the strains measured at the base of the bituminous layer, in particular the bending strains under the tires which control the possible fatigue damage of this material.
  This limitation applies to:

  - The absolute values of the maximum strains.
  - The ranking of the maximum strains created by the six bogies.
  - And the orientation of the maximum bending tensile strains, longitudinal according to the model and transversals according to measurements.

- This restriction of the linear elastic model is certainly to put on the account of the viscosity of the bituminous material, not taken into account by the elastic model. Its effect is strongly felt on the results of the PEP because the low speed of circulation of the loads. It may be thought that the quality of simulations would improve for an appreciably higher speed of the simulator.

II-2-4-7-4 First elementary visco-elastic simulation of PEP test

We tried to improve the simulation by Alizé software of the maximum strain measured, in particular as regards the direction of the maximum tensile strain, by two approaches:

- By modifying the distribution of contact pressures between the tires and the pavement surface. On the basis of data resulting from the bibliography, various complementary modeling were carried out, by taking into account a non uniform contact pressure, presenting the shape of convex dome (pressure in the center of the print up to 2 higher than the peripheral pressure), or on the contrary concave (up to 2 times lower). These attempts appeared unable to improve to a significant degree the quality of simulations. It is observed that the deformations at the base of the bituminous base are in fact rather not very sensitive to the form of the distribution of the pressures under the tire, because of the strong thickness of the bituminous cover.

- By taking account the viscoelastic behavior of bituminous materials. A simplified and exploratory study was undertaken in this direction, with the use this time of the finite element code of calculation César-LCPC, module CVCR. The module CVCR makes it possible to simulate the behavior of a multi-layer pavement loaded by a moving load, and comprising one or more layers of materials with viscoelastic behavior. The assumptions of this modeling were as follows:

    - modeled structure: structure C
    - Single law of behavior for the BB and GB: model of Huet and Sayegh consisting in two parallel branches. The first branch has a parabolic spring and two absorbers corresponding to instantaneous and delayed elasticity of the material. The second branch has a single spring corresponding to the static or long-term behavior of material. In the absence of test results for the determination in laboratory of the numerical values of the parameters of the law of Huet and Sayegh for bituminous materials of the flexible PEP, we retained the values characteristic of standard asphalt concrete tested by LCPC.
    - Loading of the model: bogie 6b moving at the speed 2.0 km/h, surface of contact with the pavement consisting in a rectangular form (side 0,44 m, uniform pressure applied 1,34MPa).

Figure 16 compares the strains at the base of the bituminous base, obtained by model CVCR, and with those obtained measured on the flexible PEP structure C.

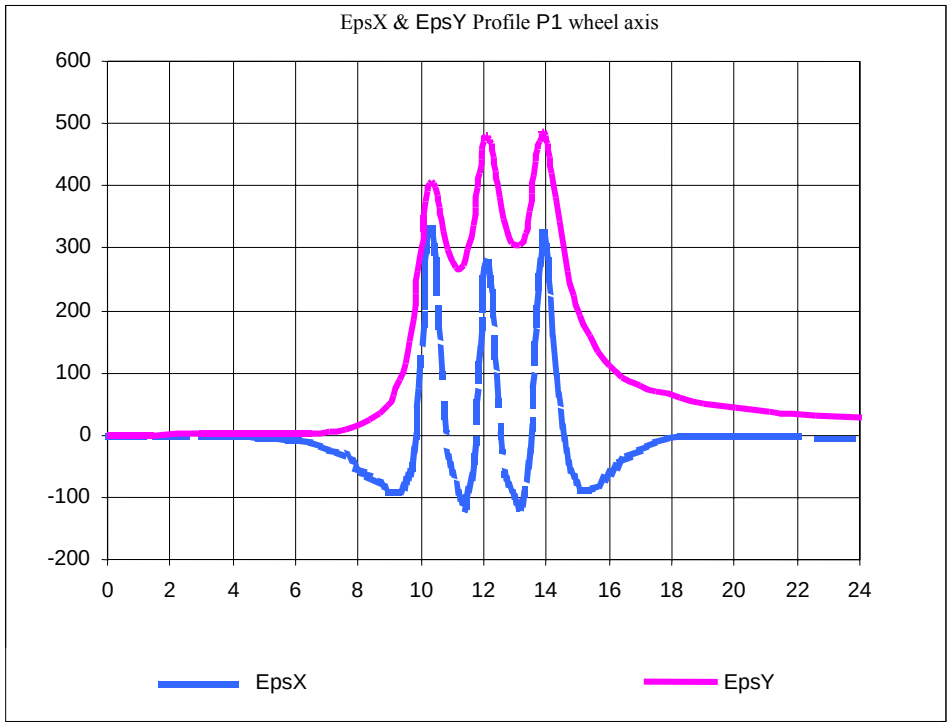

First modelisation CVCR - Configuration C7, structure C

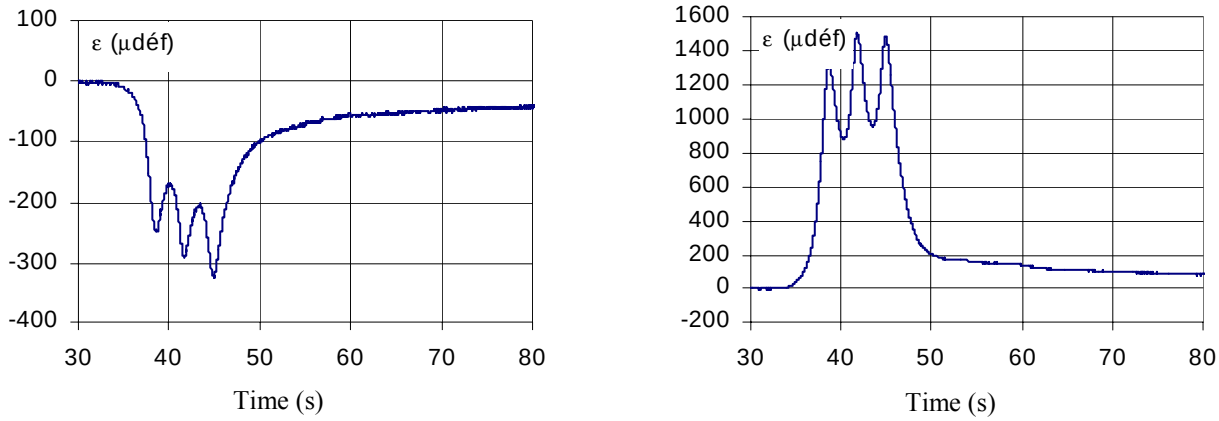

Measures

Figure 16: First visco-elastic modelisations with CESAR-LCPC, module CVCR

It must be underlined that this first modeling have to be consider from a strictly qualitatively angle, in absence any laboratory test which should permit a precise description of the visco-elastic law of bituminous PEP materials.

These first attempt with CVCR is very encouraging, and it clearly indicates that the taking into account of the visco-elasticity of the bituminous material is likely to contribute to a simulation much more realistic of the deformations generated by the slow aeronautical loads in flexible pavement.

The thermo-visco elastic Huet and Sayegh's model

Regarding the interpretation of complex modulus laboratory tests, Huet and Sayegh have introduced in the 60ies a constitutive law for asphalt material which, since then, has always been confirmed.

The representation of experimental data of complex modulus in classical Cole & Cole and Black planes laid Huet and Sayegh to propose the following dependence of E* with ω and θ :

$$E^*(\omega,\tau(\theta)) = E_0 + \frac{E_\infty - E_0}{1+\delta(i\omega\tau(\theta))^{-k} + (i\omega\tau(\theta))^{-h}}$$

With:

- E_0, E_∞ = limits of complex modulus for ω = 0 or ω = +∞
- h, k : exponents such that 1 > h > k >0, related respectively to the ratio E_{imag}/E_{real} when tends to 0 (respectively to infinity)
- δ = dimensionless constant
- τ(θ) is a function of temperature, which accounts for the classical equivalence principle between frequency and temperature. Huet and Sayegh suggest to approximate it by an Arrhenius or Eyring type law : τ(θ) = A exp(-B/T) with T=273°+θ. In fact, as regard to the limited range of temperature observed in pavements, the following convenient exponential-parabolic law can also be used :

$$\tau(\theta) = \exp(A_0 + A_1\theta + A_2\theta^2)$$

See Below other visco-elasticity modeling.

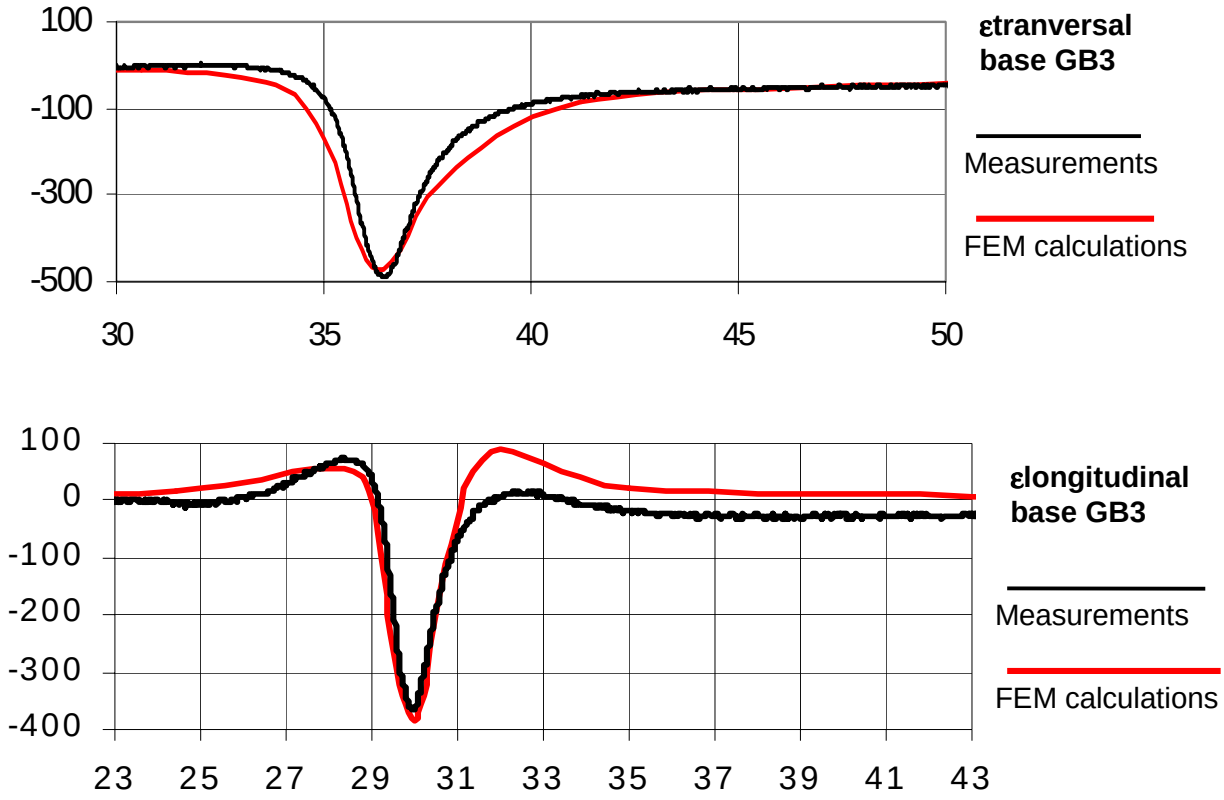

Figure 17: Modeling with the thermo-visco-elastic Huet & Sayegh's Model (FEM César-Lcpc software): comparison between measurements and theoretical results for the 2 wheels bogie of the reference load, structure C

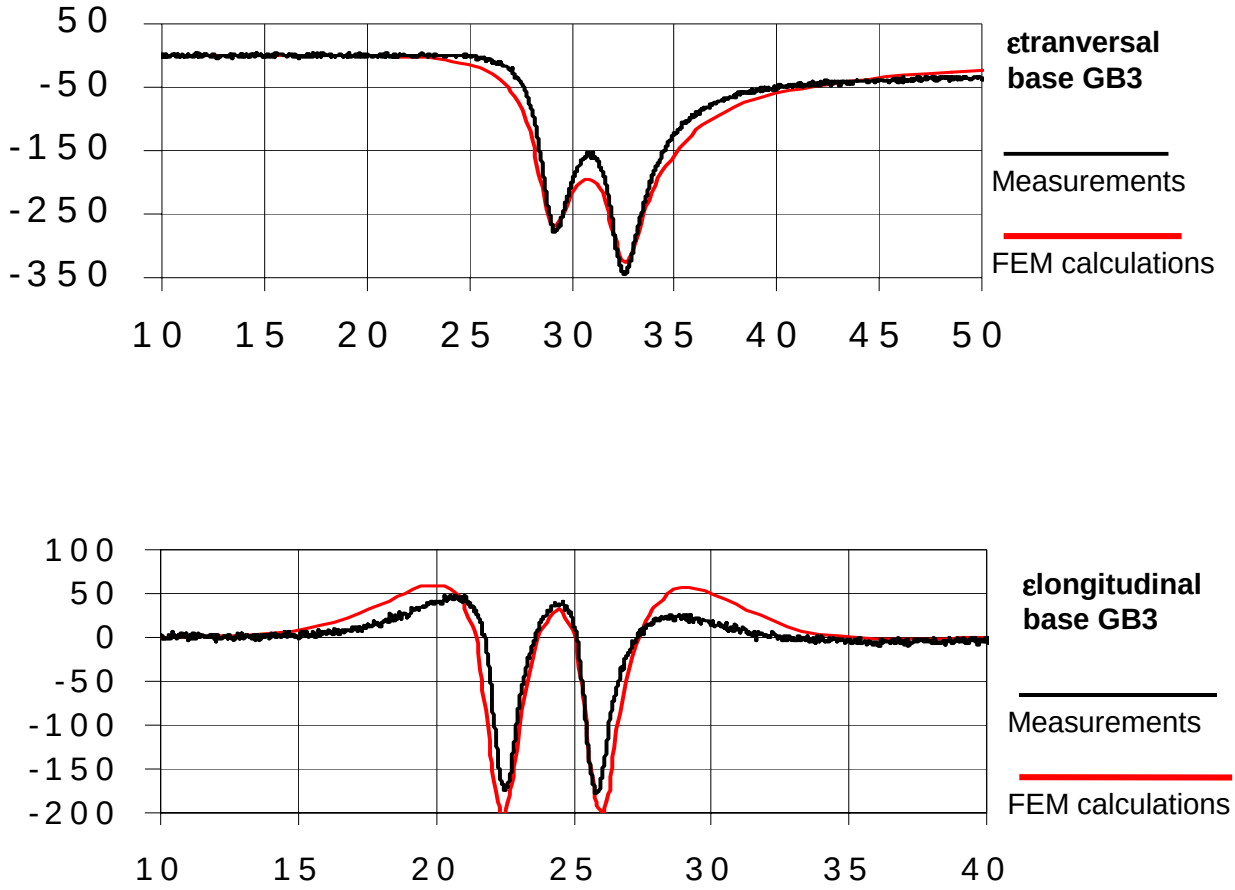

Figure 18: Modeling with the thermo-visco-elastic Huet & Sayegh's Model (FEM César-Lcpc software): comparison between measurements and theoretical results for the 4 wheels bogie of C17 configuration, structure C

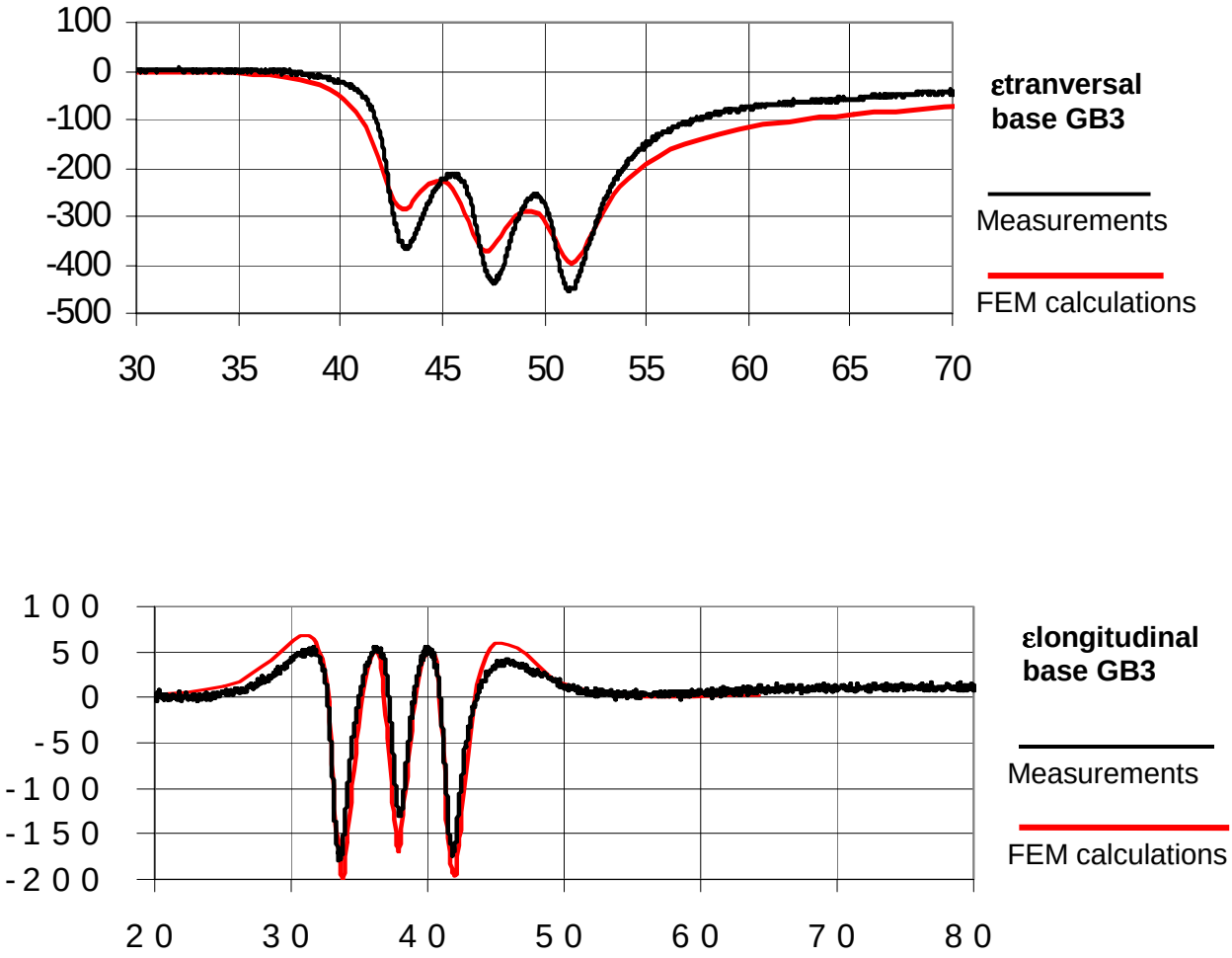

Figure 19: Modeling with the thermo-visco-elastic Huet & Sayegh's Model (FEM César-Lcpc software): comparison between measurements and theoretical results for the 6 wheels bogie of C22 configuration, structure C

II-3 The fatigue tests

II-3-1 Objectives

The two objectives of the fatigue phase were:

i) To determine the real process of damage of PEP structures under traffic in the long term, and therefore to decide which are the most critical material layers and criteria to be considered for the design of airport pavements from that point of view;

ii) To compare the incidence of the number of wheels by bogie and the weight by wheel upon the damage process of PEP structures.

II-3-2 Preliminary

II-3-2-1 Repair of transition areas and section A

The transition areas between the different structures of PEP site had already shown some important deformation, such as differential settlements and ruts, at the end of the fatigue campaign. Therefore it was decided to repair and reinforce them before starting the fatigue phase.

- As shown below, the damage problems on these transition sections were caused by their location over two different Subgrade, with sharp thickness discontinuities.

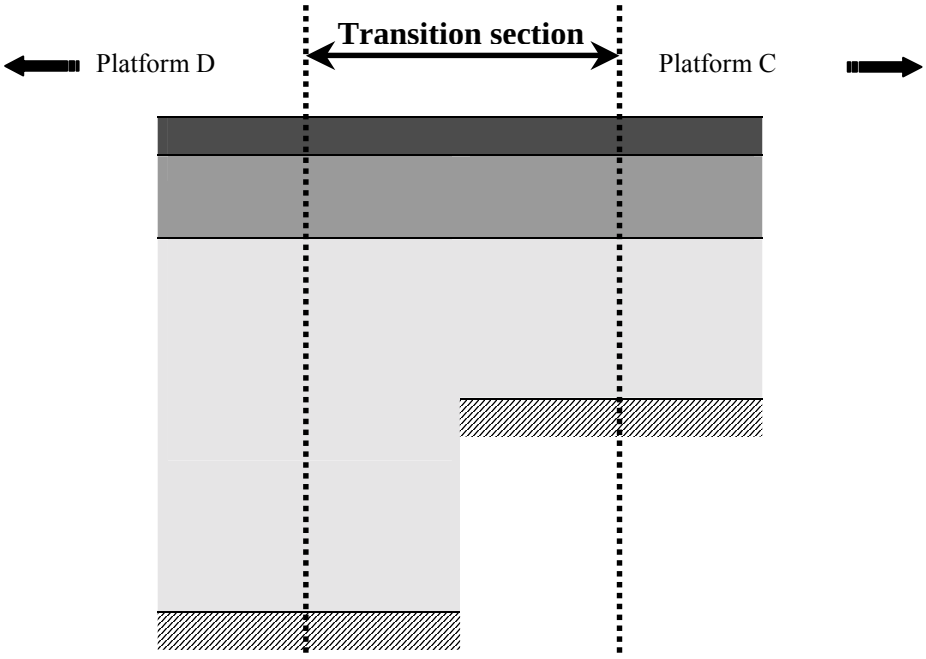

Also because of the building process (platform by platform), it is probable that the compaction of the Subgrade could not be achieved properly at these places.

To cope specifically with this problem of differential settlement, an inverted structure was used as a repairing mean.

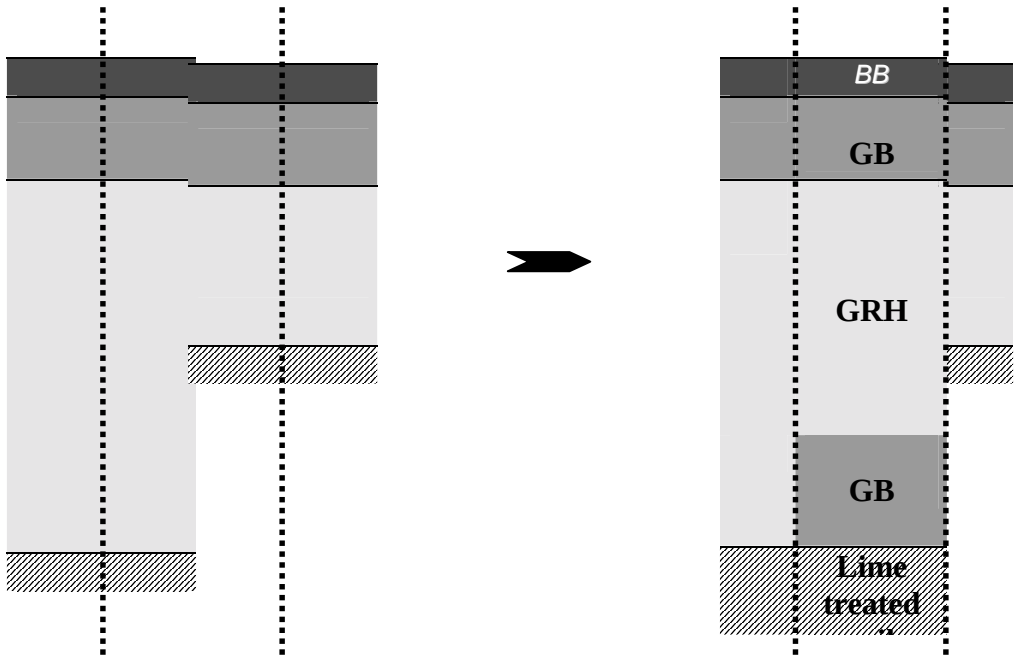

No more problems were encountered later on for these transition sections.

- As already mentioned, platform A, which was designed for stiff Subgrade conditions, encountered some abnormal deformation problems since its origin due to unexpected water trapped in the Subgrade, after a rain storm.

Before starting the fatigue campaign, it was decided to rebuild the bituminous layers of the most damaged part of the platform.

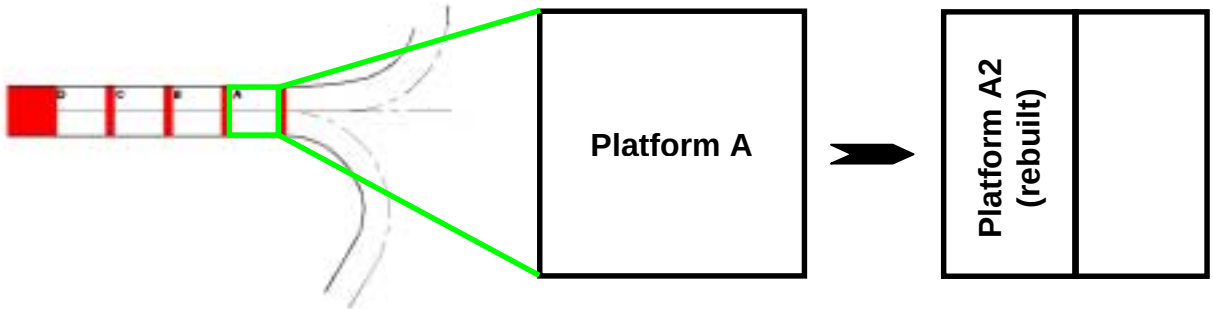

However the Subgrade was left unchanged, with its poorer than expected bearing capacity due to too high moisture content.

Finally the repair was shown to be not efficient enough, and after some coverage, it was decided to stop experimentation and analyses on platform A.
However the area still continued to be trafficked to adjust the simulator trajectory. Two more depressions were required to be repaired during that period (a lean concrete layer as base course, overlaid with a 6-cm thick layer of asphalt concrete, was used as the solution).

II-3-2-2 Simulator configuration for the fatigue campaign

The fatigue phase was conceived as a small factorial 2 x 2 experimental test, with 2 factors (wheels/bogie and weight/wheel) and 2 levels for each. The number of wheels by bogie was taken equal to 4 or 6, whereas the weight by wheel was taken equal to either 230kN or 280 KN.

As shown in table 12, this choice has the advantage to be closely related to the 4 and 6 wheel bogies of A380 aircraft, as well as the bogies of B777 and B747 aircraft.

	4 wheels	**6 wheels**
230 kN/wheel	**B747**	**B777**
280 kN/wheel	**A380**	**A380**

Table 12: the 4 tested bogies during the fatigue phase

These 4 bogies were set up together on the BOGEST simulator, to be run simultaneously, with the same climatic and wandering conditions as during the fatigue phase period.

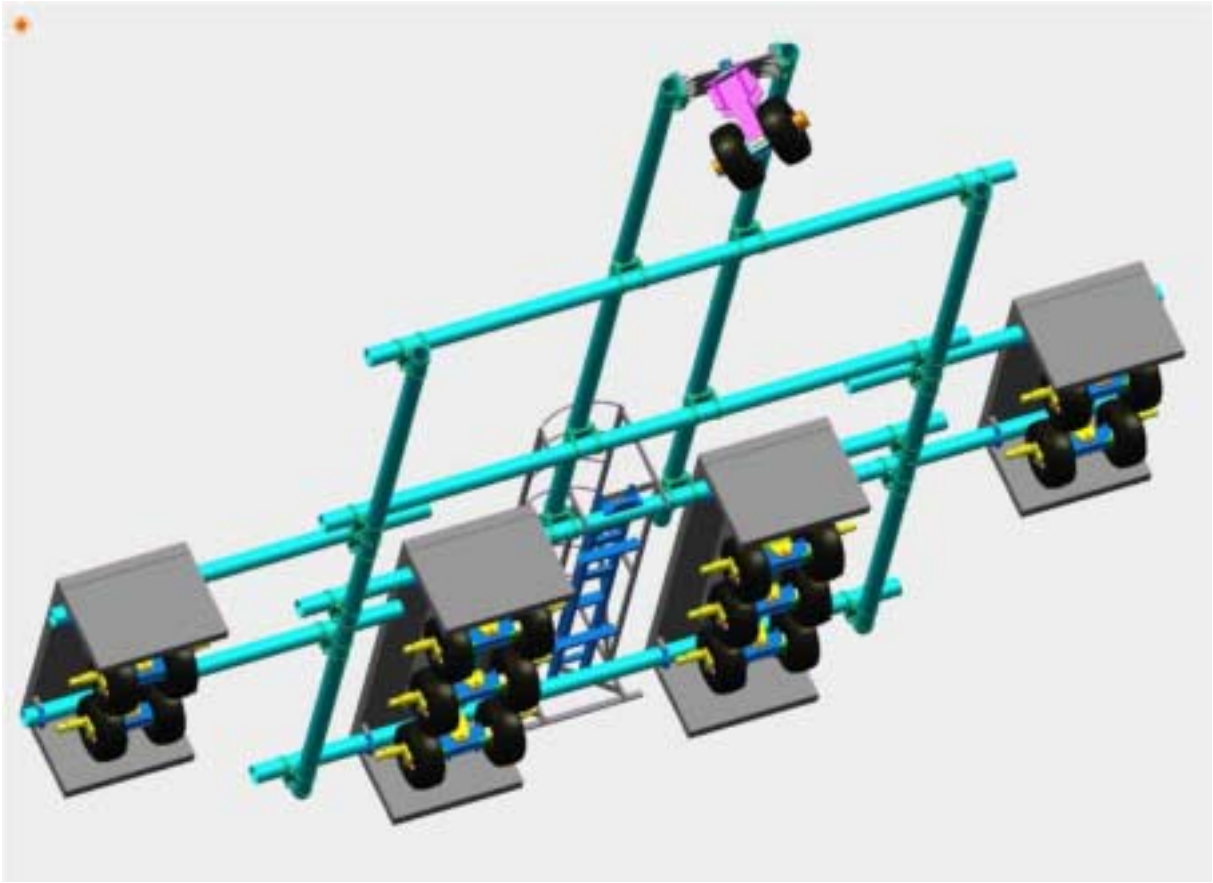

The important assumption during the experimental phase was that the interaction of the 4 bogies could be neglected for most of it, even despite the wandering condition. This assumption is based on the results from PEP static phase, which showed that the resilient strains induced within the bandwidth of a bogie was unaffected by the neighbouring bogies. It is believed therefore that the same conclusion is correct for the damage, which will be induced in the different bandwidth.
Also at places where the coupling between bogies could no longer be any more neglected, such as at mid distance of bandwidths, the damage is expected to be small compared to that induced in the bandwidth, and finally not significant for the analysis.

The figure below shows the configuration, which was used for the test (A380-4W, B777-6W, A380-6W, and B747-4W) as well as the bandwidth for each bogie, including the ± 1m wandering condition, which was adopted during the fatigue campaign.

In addition it was tempted to tow a 5th bogie of B747 type, behind a lorry, along a single lane without wandering for further evaluation of the impact of wandering. However because of the too heavy weight of the bogie compared to that of the lorry, the trial had to be stopped after a few passes.

Fatigue campaign:
Traffic strips & location of permanent deformation sensors

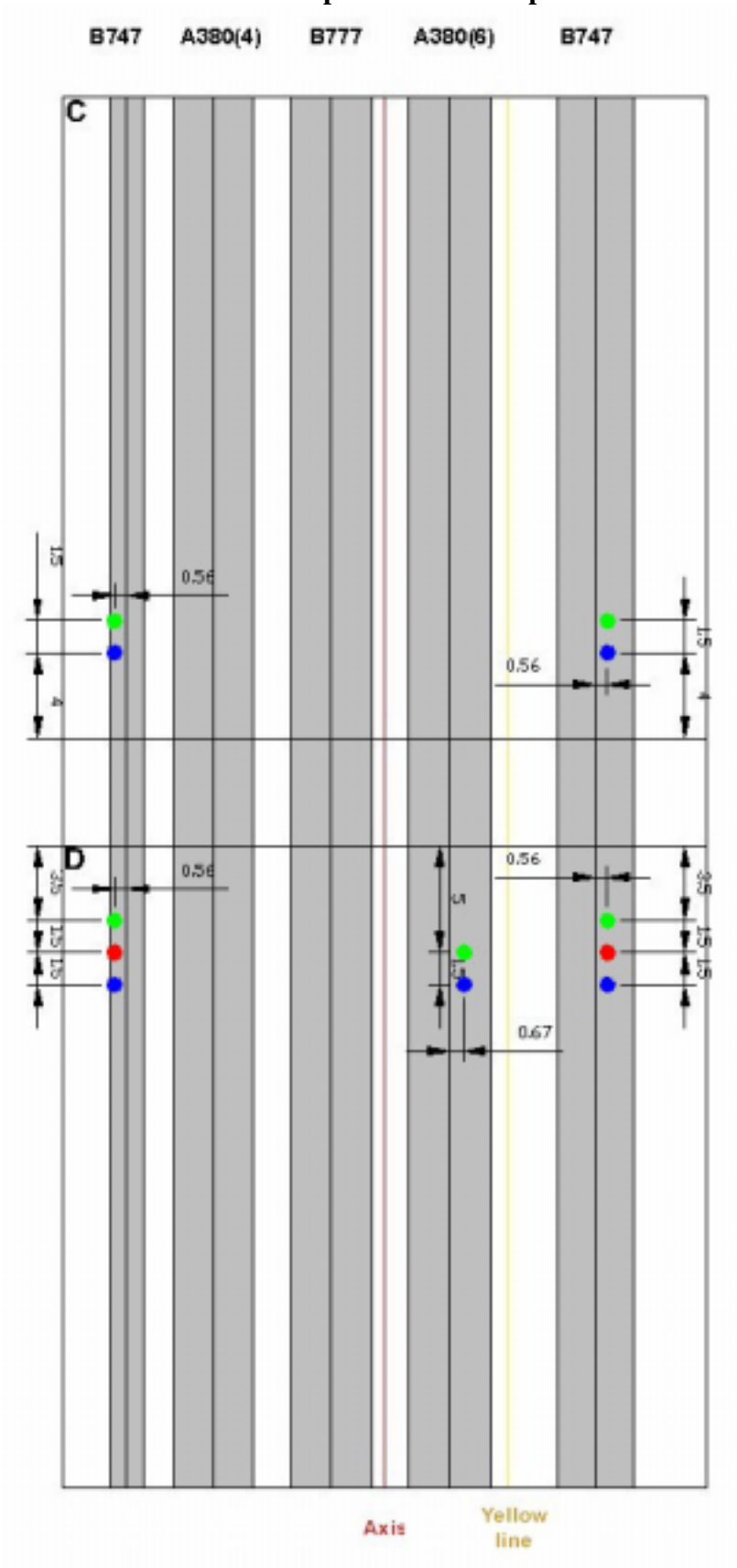

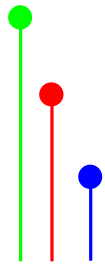

Interface
Base / Subbase

II-3-2-3 Pavement status before the fatigue campaign

A “zero point status” relative to the geometry of the pavement surface (see later) was done before the kick-off of the fatigue campaign, in order to eliminate the effect of deformation induced during the static phase.
A further difficulty should be noted. That was the difficulty to characterise in detail the mechanical state of the pavement at the end of the static phase, which is expected to be transversally heterogeneous, since the coverage was unevenly distributed during that phase. In particular, the area along the yellow reference line of static tests was more trafficked than any other part of the pavement.
However due to the limited passes during that phase, compared to the 5000 passes of the fatigue campaign, it was considered that the static phase would only have a small impact on the damage process of the fatigue campaign.

II-3-2-4 Additional sensors

The instrumentation set which was used during the static campaign was mainly focused on the measurement of the resilient strains in the different material layers.

Then before starting the fatigue campaign, it was decided to add some sensors which would measure the permanent strains, if any, in the different materials.

12 new sensors, developed by the LRPC-T for the measurement of the vertical permanent displacement, were installed on structures D and C. Their transversal location was chosen such as to compare the B747 and A380 b4 wheels bogies. It is shown on the previous picture.

Their bottom part was anchored 6 m below the pavement surface, where settlements are supposed to be negligible (fixed reference). Their upper part was set up either in the bituminous mix, or the subbase, or still the Subgrade depending on the sensor. The aim of such different location is to identify the origin and distribution of permanent deformation along z, if any during the fatigue phase.

The gauges are based on inductive sensors without vertical stiffness and are linked to their base by a sliding PVC tube. The sensor was set after core drilling. Their accuracy also permitted measurement of resilient strains during the passing of a bogie as shown on figure 20 & 21 here after.

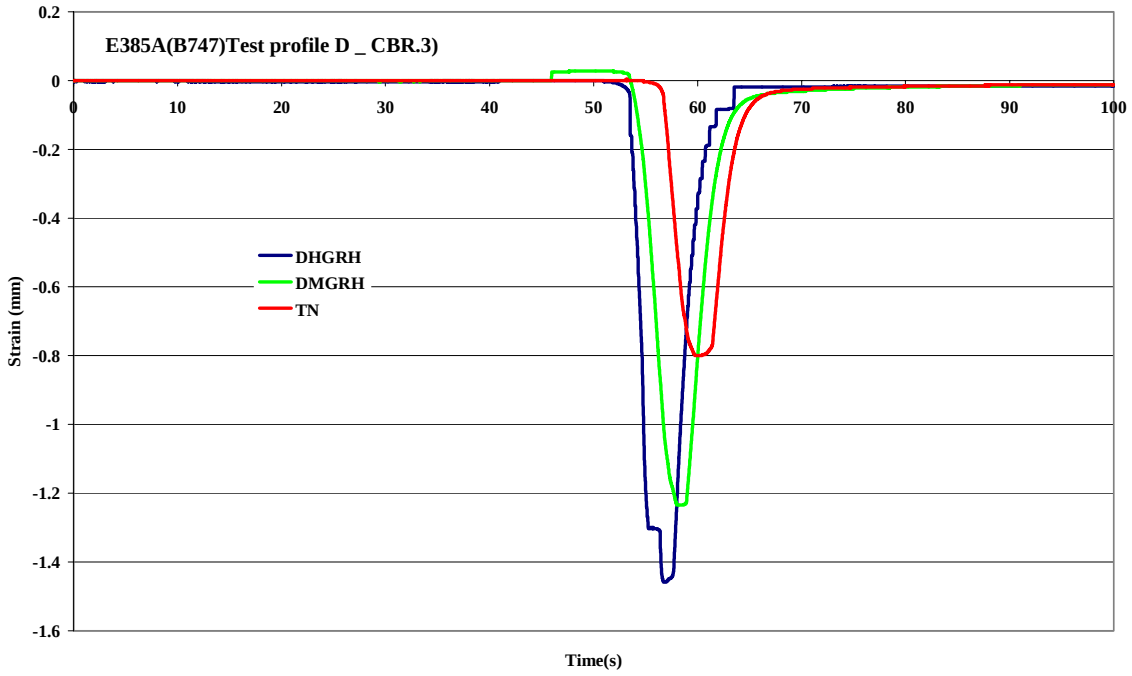

Figure 20: CBR.3 / B747-400 passe

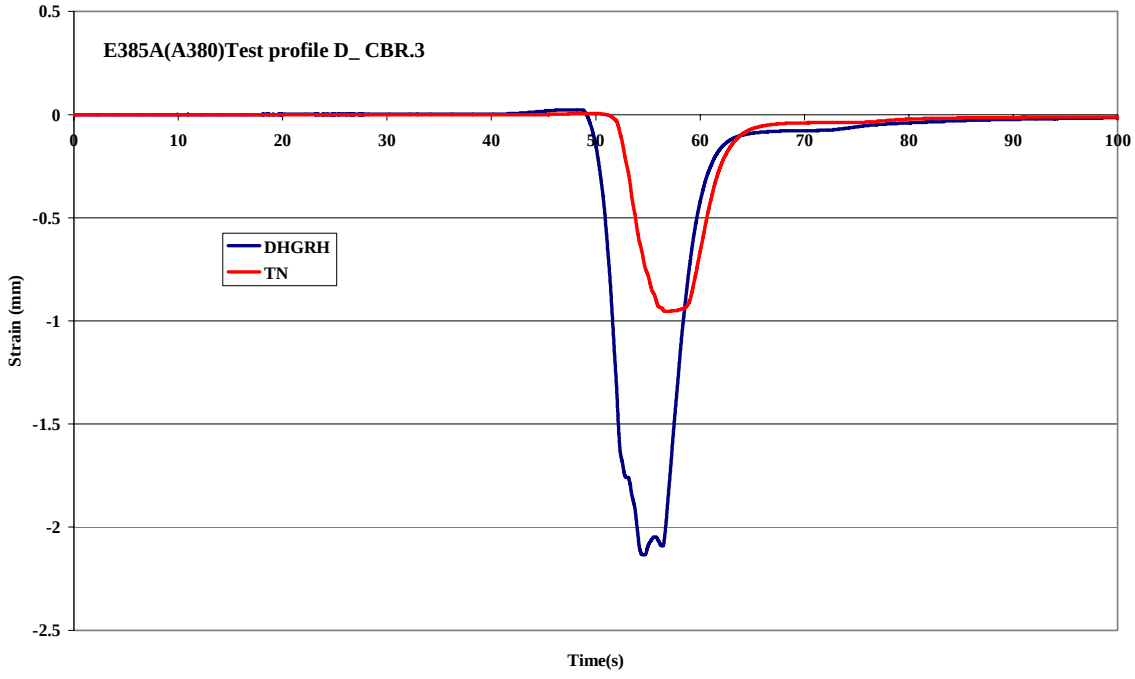

Figure 21: CBR.3 / A380 passe

II-3-3 Tests procedures

The campaign started in October 1999 and ended in July 2000 and was composed of 2 phases.

II-3-3-1 Phase 1 of the fatigue campaign

The first one consisted in running the simulator 2500 times forwards and backwards (5 000 passes) with wandering of ± 1m about a central position. To achieve this goal 9 longitudinal lanes (named A to I), 22 cm width, were painted side by side along the pavement and used as a guide.

The number of passes over the different strips was chosen as below, with lane E as the mean position.

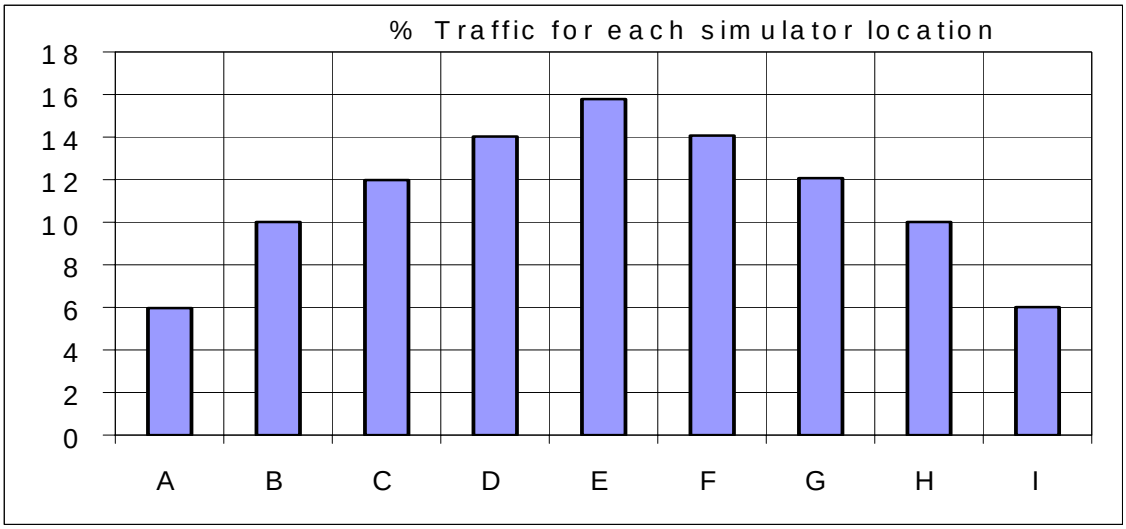

Figure 22: Percentage of traffic on each lane

The average number of forwards and backward movements (F/B) done each day was about 50. Each morning, the simulator commenced the wandering sequence where it stopped it the day before. The difference between the numbers of passes defined in the wandering sequence and that performed each day introduced a natural randomising process, which helped to homogenise the load/temperature histograms between the different lanes. Such a procedure avoided repetitive coverage of the pavement when its temperature was at a maximum or minimum.
The diagram below which illustrates the average and standard deviation (stdd) of temperature/traffic histograms for each lane and shows that the goal was globally achieved.

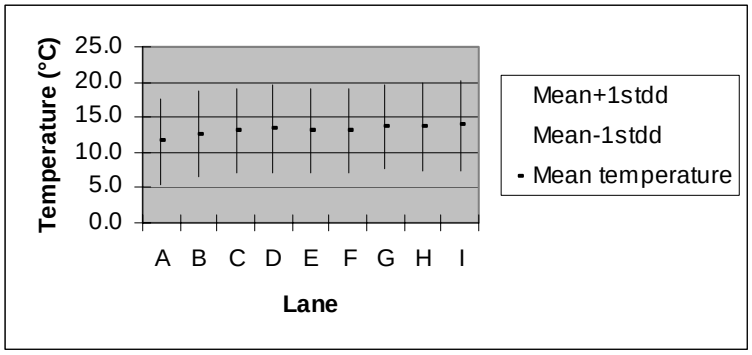

Figure 23: Average and standard deviation of temperature/traffic histograms for the different location of the simulator

Incidentally, it shows that the mean temperature during the fatigue campaign was around 12,5°C, whereas the standard deviation was about 7,5°C. Here note that the temperature value T(t) used for this diagram is itself derived from the mean value $(T_1+T_2+T_3)/3$, where $T_1(t)$, $T_2(t)$ and $T_3(t)$ are the temperatures measured with time at z=-1, -8 and –20 cm .

As an example the diagram below gives more details on the coverage/temperature histogram for lane E.

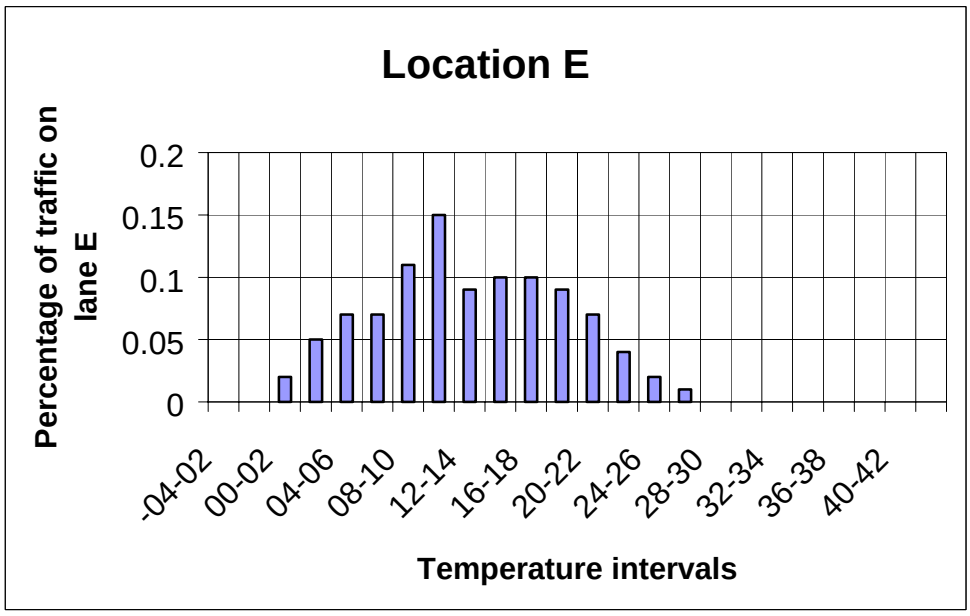

Figure 24: Temperature vs. traffic histogram for lane E
T=(T1+T2+T3)/3

II-3-3-2 Phase 2 of the fatigue campaign

It was decided in the second phase to run 1000 more F/B movements without wandering and to wait for the periods of the day when the pavement temperature was at its maximum.
The objective of that phase was to try accelerate both the rutting of the bituminous layer and the possible the rutting of the GRH and reconstituted soil layers. This last effect was expected from the coupling effect between bound and unbound layers, which predicted that a decrease of stiffness of the bituminous layer (due to temperature increase) would increase the stresses within the unbound layers, and therefore accelerate their plastic deformation.

In order to keep the main deformation pattern obtained around position E unchanged, it was decided for this second phase to run the simulator in position I.

II-3-3-3 Pavement Condition Follow-up

The evolution of PEP pavements during the fatigue campaign was followed through different variables measured with different tools and different modalities. The table below summarizes the auscultation campaign.

Measurement	Tool	Modality
Pavement surface deformation	Topography with external reference	Every 1000 passes
	Straight edge along three predefined transversal profiles for each structure (B,C,D)	Every 100 passes
Calculation of STBA Service Index	Pallas tool = laser measurement over the all pavement surface (see photo below)	Beginning and end of the fatigue campaign
Assessment of the state condition of interlayer interface	ADP radar	Beginning and end of the fatigue campaign
Global assessment of the pavement structural condition	Bearing plate measurements following with STBA procedure	Beginning and end of the fatigue campaign

The photo below shows the French transversal profilograph tool, Pallas, based on the reflection of a laser ray at the pavement surface and fitted in a vehicle. The measurement of the deformation of the whole pavement surface can be obtained in less than one day, by running the car along longitudinal strips with some overlapping between them.

Photography of Pallas tool

II-3-3-4 Materials samplings

Sampling from the soils, as well as from the crushed gravel and bituminous mix were taken out from the structures, B, C and D after the end of the experiment.

The aim is to characterise the evolution of these materials along the whole PEP experimentation, comparing their initial and final states and looking or not at the impact of the traffic, whether the materials were located in the traffic lanes or outside.

Thus some transversal trenches deep to the natural soil and 2,30 m large were realised on structures B, C, D with a circular saw to cut the bituminous mix properly. Their location was chosen close to the transverse profiles, used to measure the evolution of the pavement deformation with the straight rule.

The corresponding prismatic slabs of bituminous mix (about 32 cm thick) were taken carefully to avoid fracture. The unbound materials were put into hermetic bags in order to keep their *in situ* moisture.

The observation of the vertical sides of the trenches could also help analyse the origin of the permanent deformation at the pavement surface (see the photography below).

Example of a trench wall-side located on structure B, in the A380 bogie 6-wheel-path

The trenches also allowed to get *after death* measurement of the soil stiffness (EV2), performing some usual bearing plate tests at their base.

Finally some additional cores, with 32 cm diameter, were taken into the bituminous mix to increase the further set of data (6 from structure D, 6 from B and 21 from C).

The figure below shows the different location of the materials sampling.

All of the sampled materials were sent to LCPC in Nantes for further analysis, except a part of the crushed gravel material, which was left in Toulouse for its evaluation by LRPC-T.

II-3-3-5 Materials testing

II-3-3-5-1 Planned tests for unbound materials

The table below shows the planned lab tests for the unbound materials.

Material	Planned tests
Soil with initial CBR 10 from structure B	Identification Moisture
Soil from CBR 5 from structure C & Soil from CBR 3 from structure D	Characterisation Moisture CBR RLT* with adapted procedure to PEP condition
Crushed gravel	Identification Moisture RLTwith the usual procedure for road condition (LRPC-T) RLT with procedure adapted to the PEP condition

- RTL= Repeated Load Triaxial Test (see appendix 3 for details)

II-3-3-5-2 Planned tests for bituminous materials

The table below shows the planned tests for these materials.

Materials	Binder extraction Grading curve Binder content	Void content*	Complex modulus	Fatigue testing**	Rutting***
Bottom of GB Outside wheel-path	X	X	X	X	
Bottom of GB Under wheel-path		X	X	X	
Top of GB Outside wheel-path		X	X		X
Top of GB Under wheel-path		X	X		
Bituminous wear course Outside wheel-path	X	X	X		X
Bituminous wear course Inside wheel-path		X	X		

* Void content: gamadensimeter + volumetric measurement
** Fatigue and rutting testing will be first performed using the French procedure for roads. Testing conditions more adapted to the aeronautical context will be used latter on.

II-3-4 Data analysis (preliminary)

II-3-4-1 Evolution of the service Index after 5000 movements

II-3-4-1-1 The « Service Index » Method

Overview of the « service index » method

The « Service Index » (S.I) method is now a reference for most of French airport. This method is quick, cheap and compatible with air traffic control. This indicator improves the assessment of the service level of an airfield pavement and its evolution in the course of time; it helps Airport Managers to establish maintenance program.

The « Service Index » is a numerical indicator, which ranges from 0 (failed pavement) to 100 (new pavement).
The value of SI increases with the service level of the pavement.

S.I.	Pavement Condition
0-10	failed
10-25	very poor
25-40	poor
40-55	fair
55-70	good
70-85	very good
85-100	excellent

DISTRESS INSPECTION

The calculation of the Service Index is based on a visual distress inspection on a homogeneous pavement area. For flexible pavement, these area are divided in sample units; their size is generally 500 m2. For rigid pavement, the sample unit is group of about twenty slabs (corresponding to a size of 500 m2, for 5m by 5m slab).
The sample units are inspected, and distress types and their severity levels and densities are recorded, according to requirements of the guide « Distress Identification Manual » published by the STBA. Each distress is characterised by three indicators:

- distress types (twenty two different types for flexible pavement, and ten for concrete pavement),
- the severity level of the distress : low (L), Medium (M), or High (E)
- Density of distress in the sample unit, measured by the surface of the distress into the sample unit.

The « Distress Identification Manual » allows to distinguish distress caused by surface deficiency and those caused by structural deficiency.

	Distress caused by structural deficiency	Distress caused by surface deficiency
Flexible pavement	- Depression - Rutting - Fatigue crack - Alligator cracking - « W » shaped distortion - Swelling - Settlement - Water pumping, Fines pumping	- Ravelling, burning - Pervious bituminous mix - Joint crack, Reflection cracking - Block cracking - Patching - Contamination, Rubber deposit - Punching - Bleeding - Slippage cracking - Pothole - Weathering
Rigid pavement	- Crack, Corner crack - Shattered slab - Pumping - Step	- Spalling - Map cracking scaling - Patching - Joint seal damage, Rubber deposit

HOW DISTRESS SURVEY RESULTS ARE USED

The method is based on the conversion of the three indicators (type of distress, severity level and density) to a numeric value, representative of the impact of this distress on the pavement qualities.
An abacus for each distress type allows to associate for the three indicators, a deduct value.
All deduct values, corresponding to all the distress recorded on the same sample unit, are the summed to obtain a total deduct value.

Figure 25: Flexible pavement deducts values, distress « Depression »

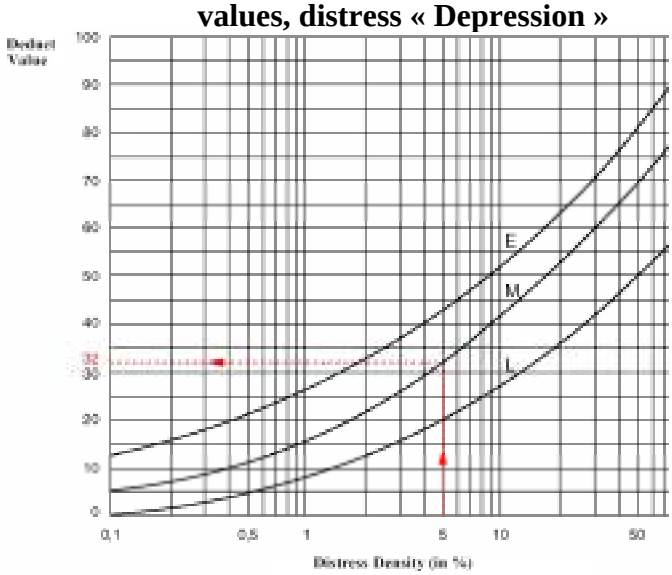

For each sample unit, the total deduct value is corrected with a specific abacus for rigid or flexible pavement (Cf. Fig.25); this correction is function of the number q of significant distress
(Which deduct values are up to 5). The result is a corrected deducts value (CDV). The Service Index of the sample unit is calculated as follows: S.I = 100 - CDV

Finally, the Service Index of the homogeneous area is the average of the Service Index from all sample units inspected.
Either Deduct values abacus or software associated have been established from a very lot of comparison (first by United States of America, and then by STBA) between estimated distress levels and observations on surface pavement.

THE SERVICE INDEX: A MANAGEMENT TOOL FOR AIRFIELD PAVEMENTS

The Service Index calculated from all the distress recorded is called Global Service Index. Two others Indexes exist:

> The Structural Service Index calculated only with distress caused by structural deficiencies.
> The Surface Service Index calculated only with distress caused by surface deficiencies.

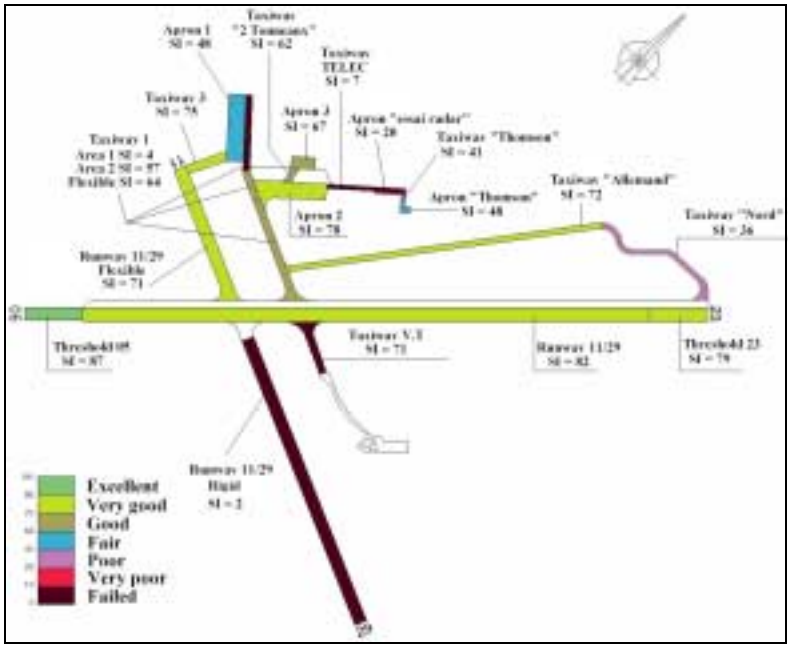

Figure 26 Example of map summing up homogeneous pavement behaviour of an airport

These different Service Indexes allow to:

Figure 27 : Histogram of the Service Index along a runway

- Draw a histogram which illustrates graphically the pavement condition (metric points along the pavement in x-axis, and Service Index in y-axis) (Fig.27).

- Map an area with homogeneous behaviour and identify their service levels (Fig 2)
- Analyse into all the details the homogeneous area and find where structural or surface problems exist to permit corrective actions at an early stage.
- Deduct equivalence coefficient for bituminous layer,
- Verify equivalency between visual aspect of pavement and the bearing strength evaluation
- Define minor maintenance actions,
- Program major pavement repair project, function of the evolution in course of the time of the Service Index.

- **Adaptation of the « SI » method for the A380 PEP**

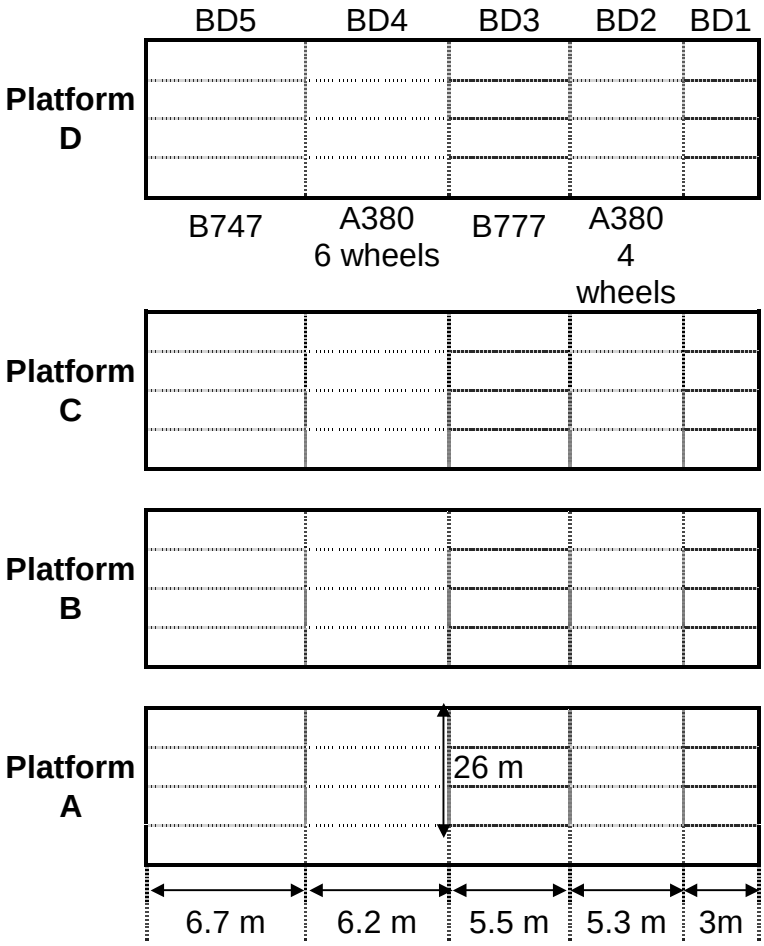

The SI method cannot be used directly in the A380 PEP because the area to be surveyed is very small compare to a classical runway or taxiway.
Each platform is divided into 16 parts (of about 35 to 45 m²) according to the landing gear size.
In order to homogenise, a unique mesh of calculation of 10m long and 6.5m wide was chosen. This operation will modify the raw result of service index but in our case, it doesn't matter because only the relative evolution is important.

- **Evolution of Structural SI**

Generally, there were not many signs of visible distress (except some rutting and some cracks on platform A only). To quantify them precisely, profile surveys were done by a « transversoprofilograph » (a tool which enables measurement of the depressions on the surface) were used.

With this tool, on each platform, the surface and the depth of the depressions and the rutting were measured. Using this «distress assessment », the 3 service indexes are calculated (see the results in annex).

In the following graphs, only the evolution of the structural index is represented because it's the most relevant parameter. Particularly as there was no surface distress, the superficial index and the global index are less important than the structural index.

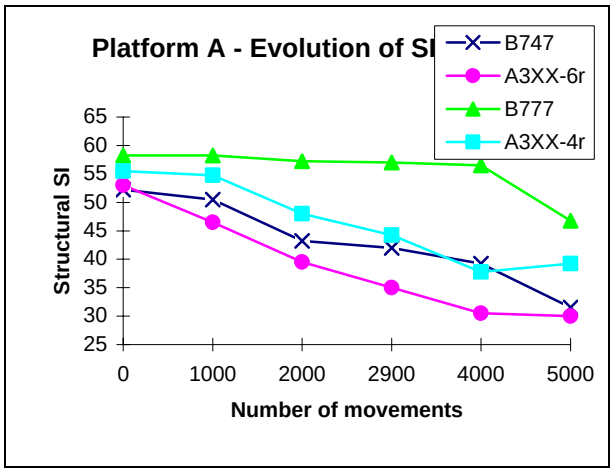

Platform A :

On this platform, there was one first repairing (in December 1999, between 0 and 1000 movements) which included the half of the platform on all the width. And surprisingly, the service index on this area decreased significantly: the distresses were more severe than in the unrepaired area. Is this due to a local problem of the Subgrade in this area or to the difference in the materials used for the reparation?

Then, between 1000 and 4000 movements, the service index drops strongly on the strips of the A380 6 wheels and 4 wheels but also on the B747's strip where as the SI of the B777's strip decreases slightly.

After 4000 movements, other reparations were done on the A380's strips (there were depressions with more than 3cm depth with cracks): that's why the SI increases in some areas between 4000 and 5000 movements. At this stage, we consider that these strips are failed.

Between 4000 et 5000 movements, the SI of both B747 and B777 strips decrease strongly; perhaps the failure is not far for these strips also.

Platform B :

On this platform, it's important to note that the SI decreases strongly on the strips of the B747, the B777 and the A380 4 wheels, where as the SI of the strip of the A380 6 wheels hardly moved.

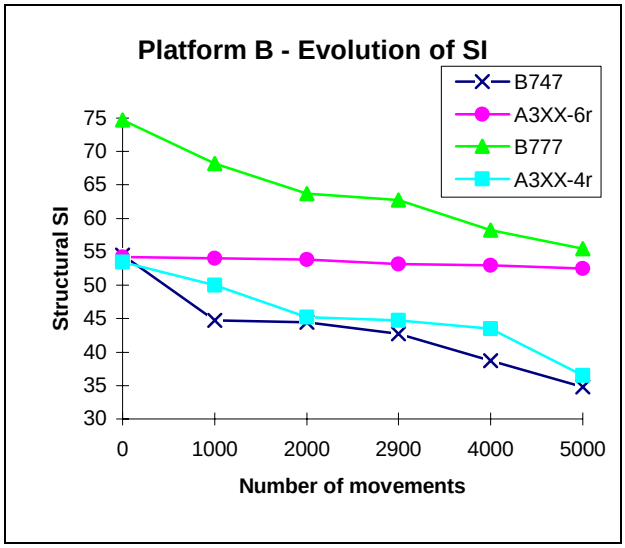

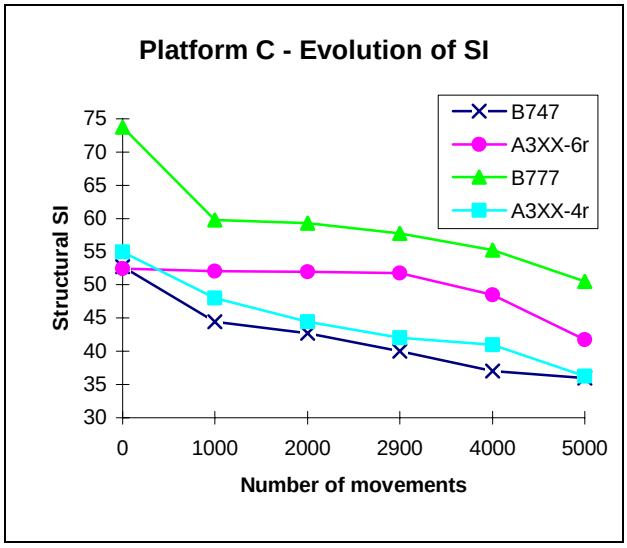

Platform C :

There is a similar evolution of the SI for the B747, B777 and the A380 4 wheels: strips: an important drop of the SI between 0 and 1000 movements and a regular decrease afterwards. The SI of the A380 6 wheels strip stagnates until 2900 movements and then decreases strongly.

Platform D :

The SI of the B747, A380 6 wheels and 4 wheels evolve in a very similar way and as well the value of the SI is also very close.
The SI of the B777 decreases strongly but the initial value of the SI was very high compared to the other strips.

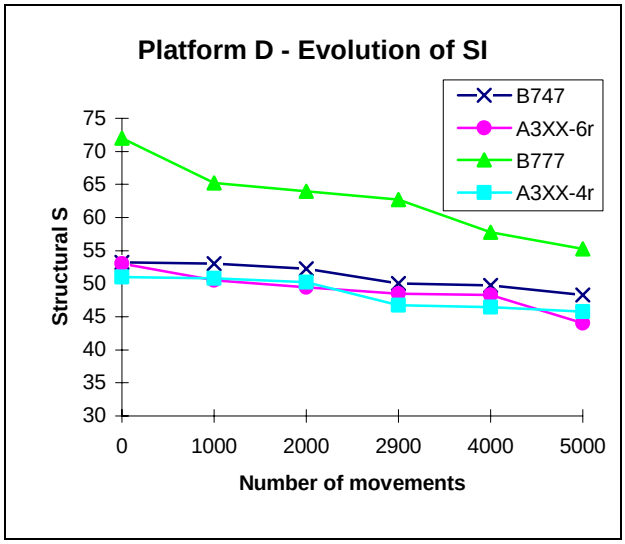

As the failure was not reached on the B, C, D platforms, it was necessary to analyse other parameters such as the maximum depth of the depressions, the evolution of the area of the depressions (with a reference profile)....

II-3-4-1-2 Topographical survey

- **Settlement**

The topographical surveys are done on 3 profiles (profile 1 to 3) on each platform.

After the static test campaign, a « point zero » was realised the 17/05/99 (called R_0). This survey will be used as a reference to follow the evolution on the different profiles in function of the cumulated traffic. The survey of the 1000 and 2000 movements were respectively realised the 20/12/99 (R_{1000}) and the 07/02/00 (R_{2000}). These results are summed in the following table:

		Gap between R_0 et R_{1000} (in mm)			Gap between R_{1000} et R_{2000} (in mm)		
	Gap	Profile 1	Profile 2	Profile 3	Profile 1	Profile 2	Profile 3
Platform A	maximum	16	20,2	35,1	0,9	10,2	4,9
	average	4,3	5,3	17	0,01	1,5	1
Platform B	maximum	11,7	13,9	13,6	0,5	0,8	1,3
	average	3,9	3,6	3,3	0,3	0,03	0,3
Platform C	maximum	36,5	28,5	28,4	1,9	2,9	1,7
	average	19	14,4	13,8	0,8	0,9	0,6
Platform D	maximum	31,1	22,6	19,2	1,4	1,5	1,4
	average	15,8	13,4	10,3	0,03	0,3	0,2

It is interesting to note that there is an important evolution between R_0 and R_{1000} with an average gap of 3 mm until 19 mm according to the platforms where as the average maximum gap between R_{1000} and R_{2000} is only 1.5 mm.

This means that between the « point zero » and the first 1000 movements, there is a significant generalised settlement on all platforms (see profiles in annex). The average settlement on each platform is:

- Platform A: 9 mm,
- Platform B: 4 mm,
- Platform C: 16 mm,
- Platform D: 13 mm.

This shows that the consolidation phase has kept on after the static tests. This conforms to what happens in reality, as it is well known that the consolidation stage takes place one or two years of the pavement life.

The result is that the pavement works completely in the fatigue mode after the first 1000 movements.

- **Other parameters**

These parameters are: the evolution of the maximum of the depression and the evolution of the area of the depression compare to the « point zero » (called respectively ***Max*** and ***Aire***).

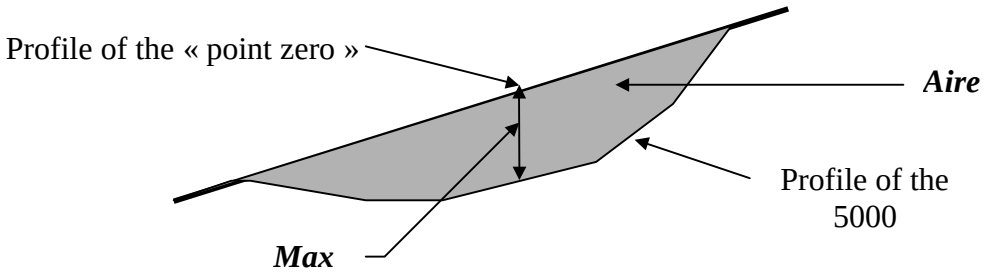

In the following graphs, there are the evolution of the parameters ***Aire*** and ***Max:***

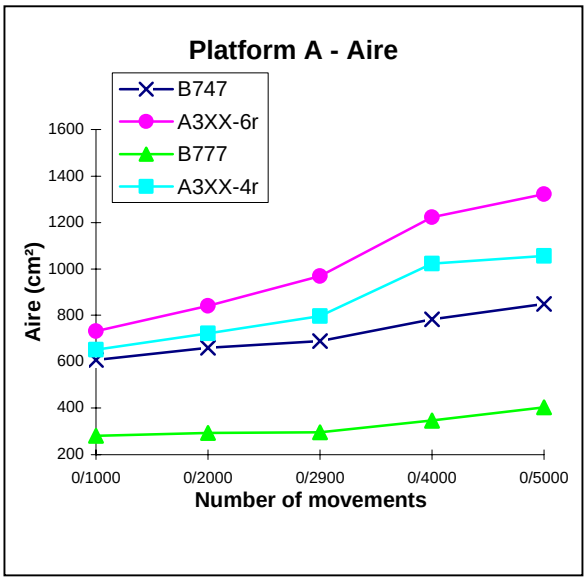

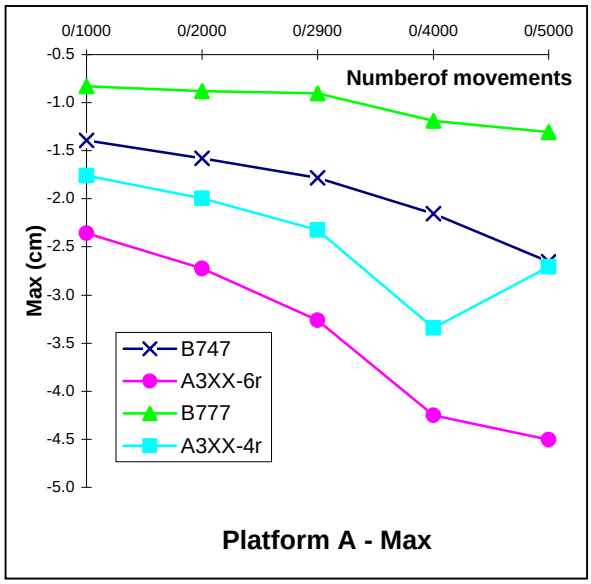

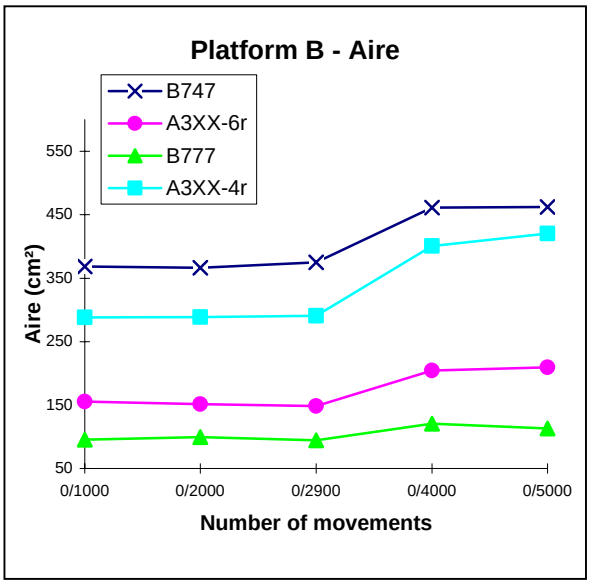

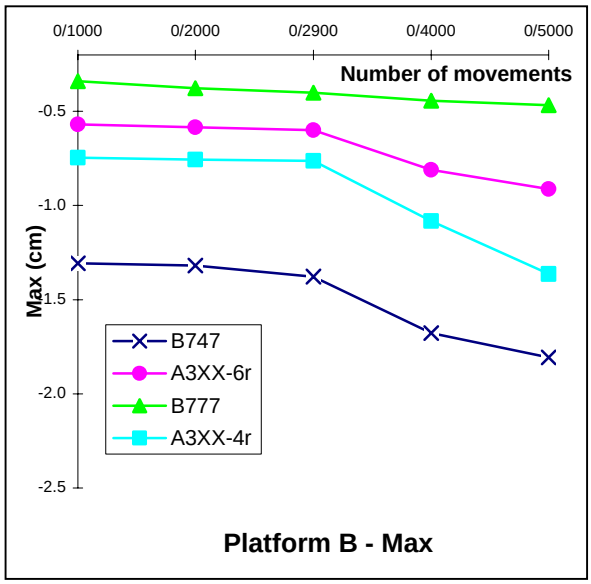

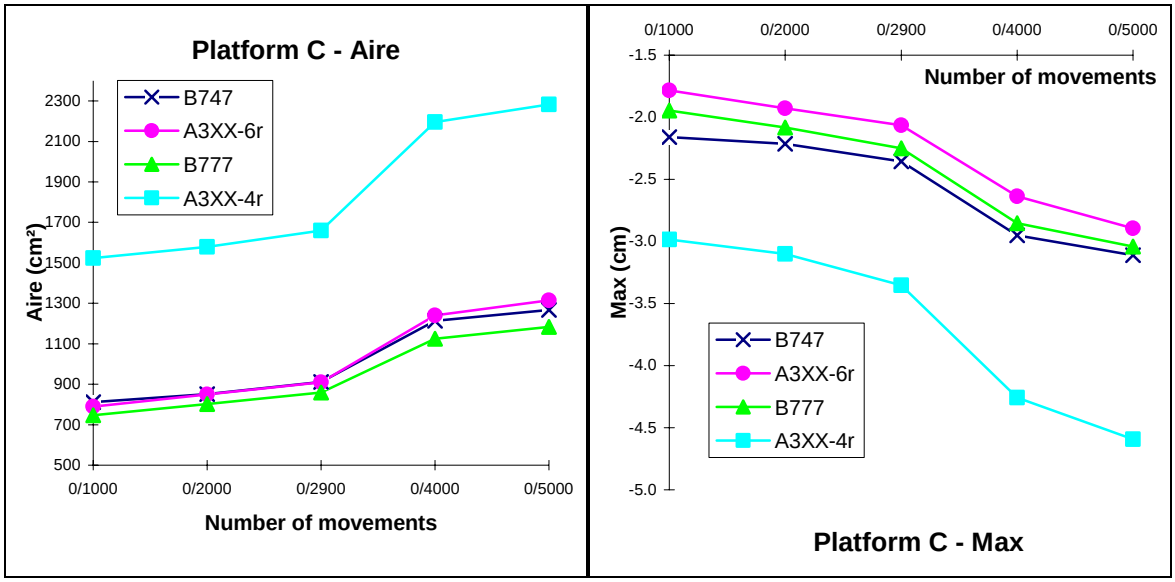

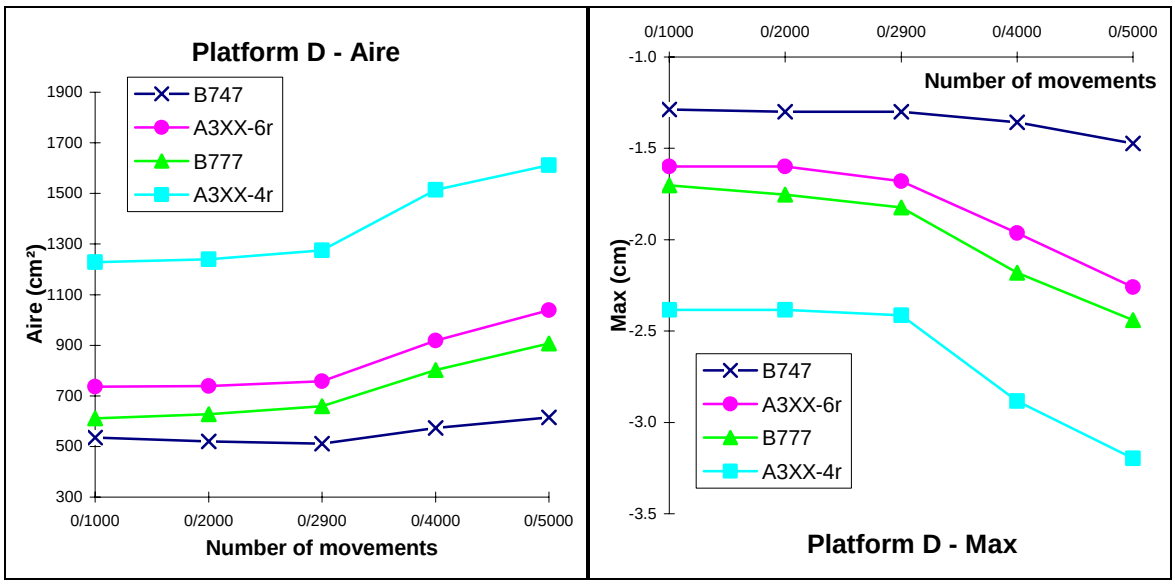

On the platform A, there is the same evolution as for the service index: the distresses are the most severe for the A380 6 wheels and 4 wheels strips followed by the B747 strip. The B777 strip is the less damaged but the distresses tend to increase at the end of the 5000 movements

On the platform B, the strips of both B747 and A380 4 wheels are those who have the most important distresses but the settlement on these strips is also the most important. The strip of the B777 evolves very few for both parameters *Aire* and *Max* where as the service index has decreased a lot: it can be explained by the low gravity distresses encountered on this strip (essentially depressions of less than 1cm depth).

On the platforms C and D, there is a big difference between the strip of the A380 4 wheels and the other strips: this strip has much more collapsed than the others (see profiles in annex).

It is necessary to explain why there is localised settlement (especially for the B747 on platform B and A380 4 wheels on platforms B, C and D): was the quality of the non-treated gravel poor? Or was the Subgrade on this area weak?

II-3-4-1-3 Synthesis of the results

The tables below show the result of the three parameters (*SI*, *Aire* and *Max*) between the « point zero » and the 5000 movements:

		Aire (cm²)	*Max* (cm)	*SI* (%)
Platform A	B747	848	-2.7	-38
	A380-6r	1323	-4.5	-43
	B777	403	-1.3	-19
	A380-4r	1057	-2.7	-30

		Aire (cm²)	*Max* (cm)	*SI* (%)
Platform B	B747	462	-1.8	-36
	A380-6r	210	-0.9	-2
	B777	113	-0.5	-25
	A380-4r	420	-1.4	-31

Platform C	B747	1267	-3.1	-32
	A380-6r	1314	-2.9	-18
	B777	1183	-3.0	-31
	A380-4r	2283	-4.6	-35

Platform D	B747	615	-1.5	-9
	A380-6r	1039	-2.3	-17
	B777	907	-2.4	-24
	A380-4r	1612	-3.2	-10

The graphs below are obtained by dividing the value of each parameter by the maximum of the same parameter on all the strips. For instance, on the platform A, the strip of A380 6 wheels has 100% for 2 parameters and the B747 strip has 100 % for one parameter: it means that it is on A380-6w strip the maximum is reached for the area of the depression (*Aire*) and the maximum of depression (*Max*) and on the B747 strip, there is the most important decrease of the service index (*SI*).

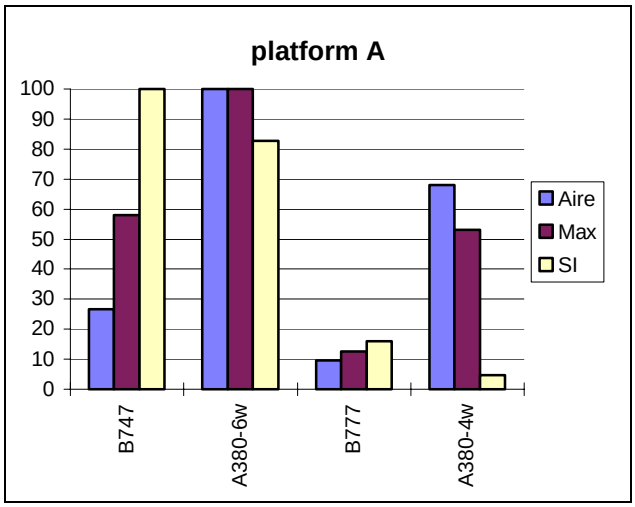

Thanks to these 3 parameters, a relative aggressiveness of each landing gear can be deduced :

A380-6w > A380-4w ≈ B747 > B777

It is hard to decide between B747 and A380-4w.

For this platform, only the non-repaired area has been taken into account; as the second half of the platform has undergone some important work, the interpretation of the results on this area are difficult.

On the platform B :

B747 > A380-4w > B777 ≈ A380-6w

It is hard to decide between B777 and A380-6w.

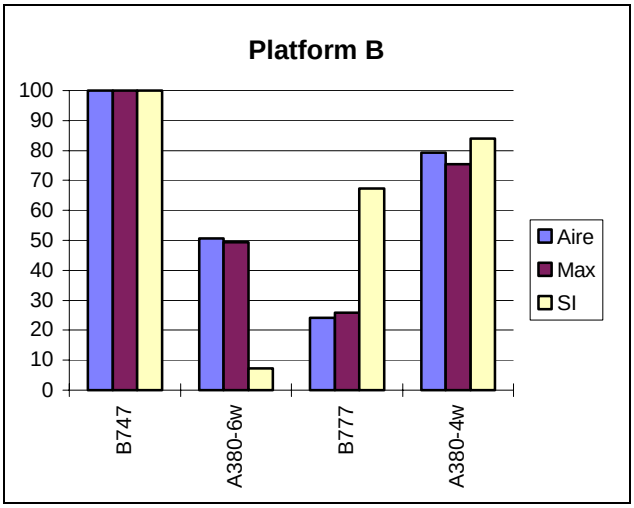

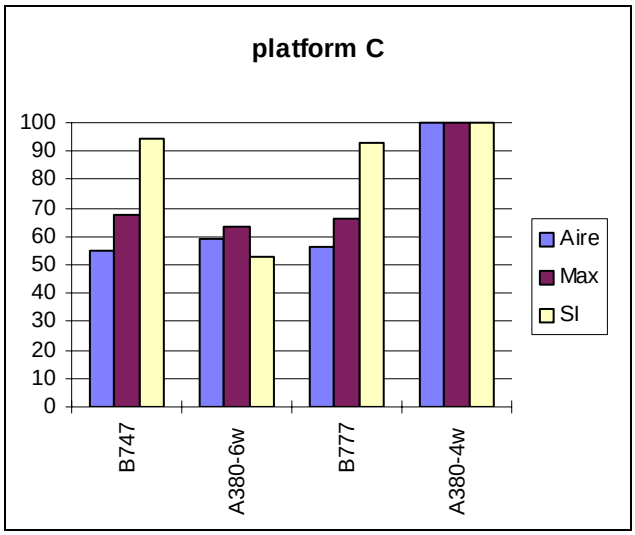

On the platform C :

A380-4w > B777 ≈ B747 ≈ A380-6w

The B777, B747 and A380-6w are quite close for each other (except for the SI of the A380-6w).

On the platform D :

A380-4r ≈ B777 > A380-6r > B747

It is hard to decide between B777 and A380-4w.

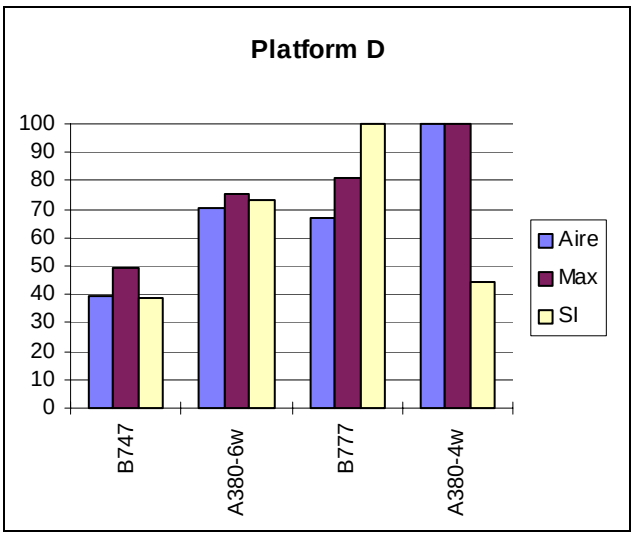

Note:
On the platform B, the two parameters *Aire* and *Max* are not really significant because the profiles evolves very few (hence a more important relative error).

CONCLUSION:

There is not a clear hierarchy for the effect of the landing gear on the 3 parameters: maximum depression, area depression and service index.

By comparing the 6 wheel bogies and the 4 wheel bogies between themselves, the influence of the dynamic overloading on the landing gear (due to the slope) is cancelled. Then, we can outline the following tendency:

- The A380 4 wheel bogie seems to have more impact than the B747 one. (trend observed on platform A,C and D),
- The 6 wheel bogie of the B777 and of the A380 are very close to each other (except on the platform A).

Nevertheless, examining more precisely the parameters of the 6 wheel bogie on the platform C and D, it appears that there are the same results as the simulations done by Alizé: the B777 causes a deep surface deflexion but on a small area where as the A380 6 wheel causes a shallower surface deflexion but on a bigger area.

These results are to be taken with caution as long as the results of the bore drillings and the results of the plate bearing capacity are not well known.

II-3-4-2 Radar auscultation

The road and in a general way, ground auscultation principles, by means of radar techniques are known for more than twenty years. This technique into this domain was introduced in France by the LCPC.

As it has been in use for about ten years by *Aéroports of Paris* (ADP), this technique allows correlation in a qualitative and especially quantitative way, information provided by other sources. For instance, radar technology allows in a considerable reduction the number of samplings while increasing the quality of the information.

The measurement uses the reflection principle of part of the electromagnetic wave emitted through materials, at any electric discontinuity (heterogeneousness, materials chemically different).
Specifically, electromagnetic pulses are transmitted into the road by the antenna along an axis of measure. The signals partially reflected upon discontinuities of in place materials structures are received by this antenna, and given as amplitude vs. time.
The time dependent position of the echo provides the location of dielectric heterogeneousness (mainly interfaces) while the amplitude of the echo is related to the values of materials dielectric constants.
The echo succession is represented as time dependent diagrams, a function of the position along the measured axis of the road.

Time dependent track in the middle of the 4 wheels A380 bogie before Fatigue Campaign

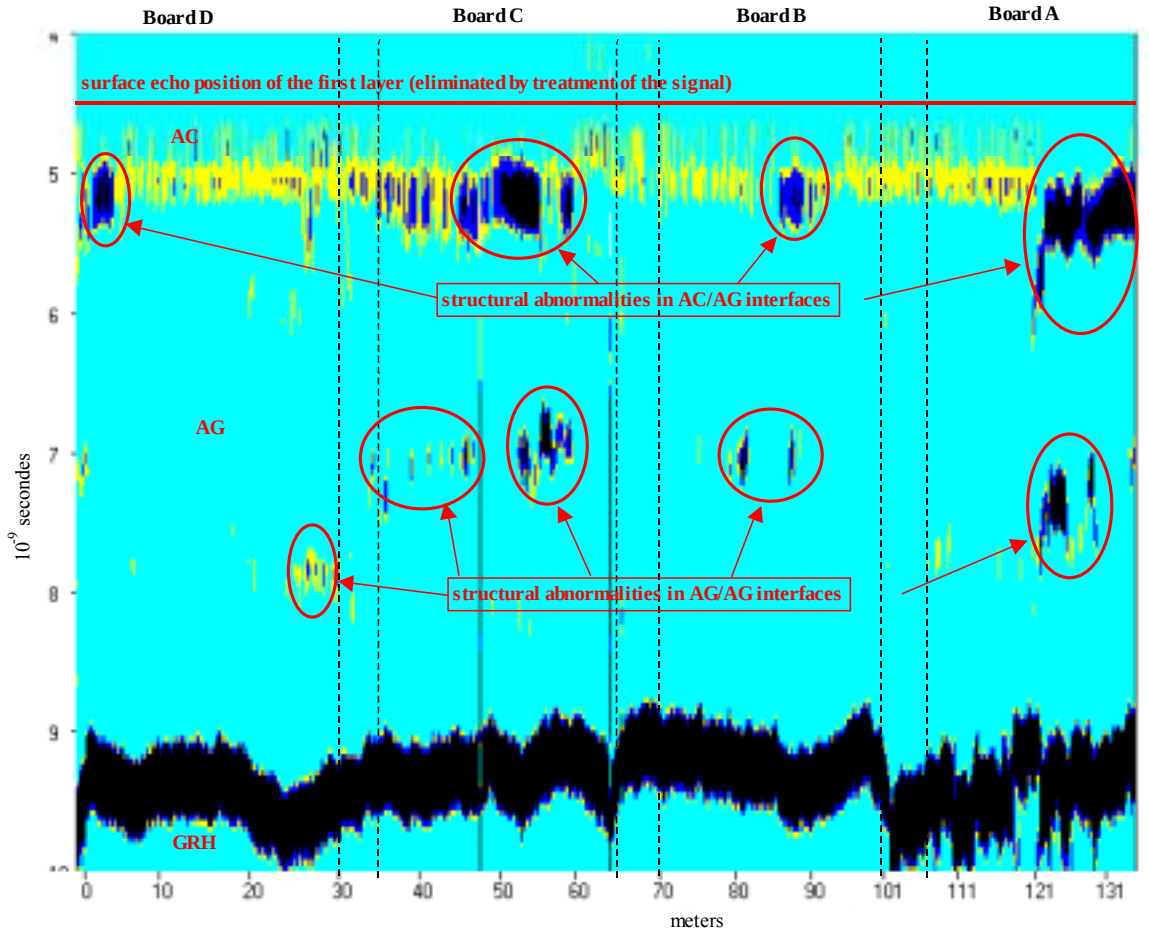

An interface between two identical materials and well-stuck layers has dielectric factors closely related. Therefore, such an interface is invisible by Radar.
Other parameters as capacity of the wave to penetrate into the material and the time dependence resolution of the system limit the capabilities of this technique. Presence of water on surface or in the material reduces or prevents radar signals penetration. Conductive materials cause a total reflection.
After timely localised physical recognition of materials and thickness, by core sampling and by analogy, these diagrams allow to define thickness, quality or absence of visible interface in the right of the axis of measure on the road.

Geographic diagram of the track in the right of the middle of the four wheels bogie A380 before Fatigue Campaign

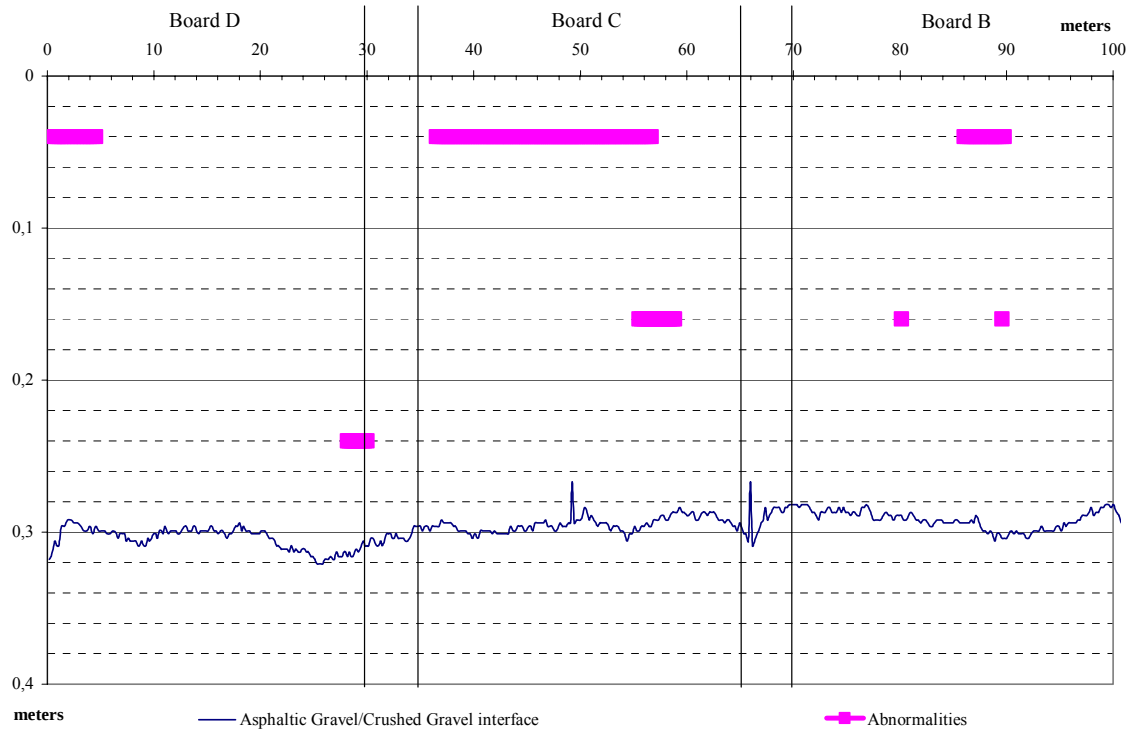

For the wearing course first layer the dielectric factor can be assessed by comparison of reflection on a sheet put on the ground (method of the Radar wave reflection coefficients). Variations of dielectric factor on the same material provide the superficial density evaluation of this material.

The flexible PEP experiment objective was to discover and to localize the structural defects in particular in the layers interfaces, to check the effect of layers thickness and to evaluate a possible result after application of the agreed loads.

A first passage of the Radar was carried out before the Flexible Fatigue Campaign in March 1999 and a second at the end in September 2000. Climatic conditions were good during each measurement. In particular there was no water on the road surface that would have limited radar signal penetration.

Measures were made on axis in the right of the simulator wheels average tracks and transversely, in the middle of each of the platforms.

Measures on the platform A made in 1999 allowed quantification of the structural damage importance of the pavement and which involved its relinquish for the Fatigue Campaign.
Subsequently, only the measurements on platforms B, C and D are exploited.

During the measurement of 1999 and 2000, the Radar has couldn't easily distinguish the interfaces between the asphalt concrete layers (BBA) and asphalt gravel (GB). This is an indication of a good adhesion and was confirmed by core samplings.

Most of the dielectric discontinuities considered as identified but very net structural abnormalities before the fatigue traffic is eased, even disappeared after the fatigue test.

Interfaces BBA / GB qualification before Fatigue Campaign.

Not	**Not interpretable**
Normal	**Normal**
Présomption	**Presemption**
Abnormal	**Abnormal**

Before trafic

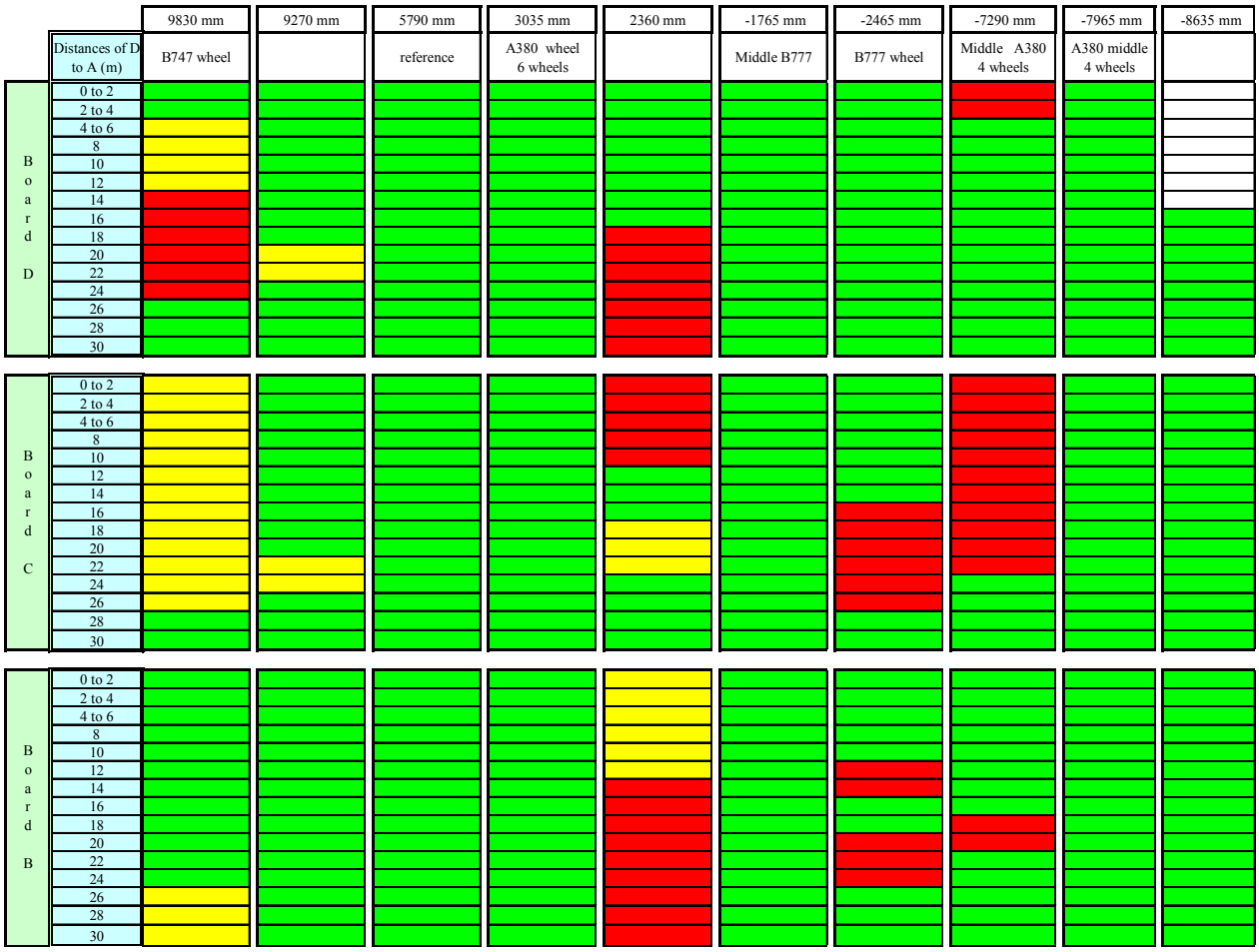

Interfaces BBA / GB qualification after Fatigue Campaign

After trafic

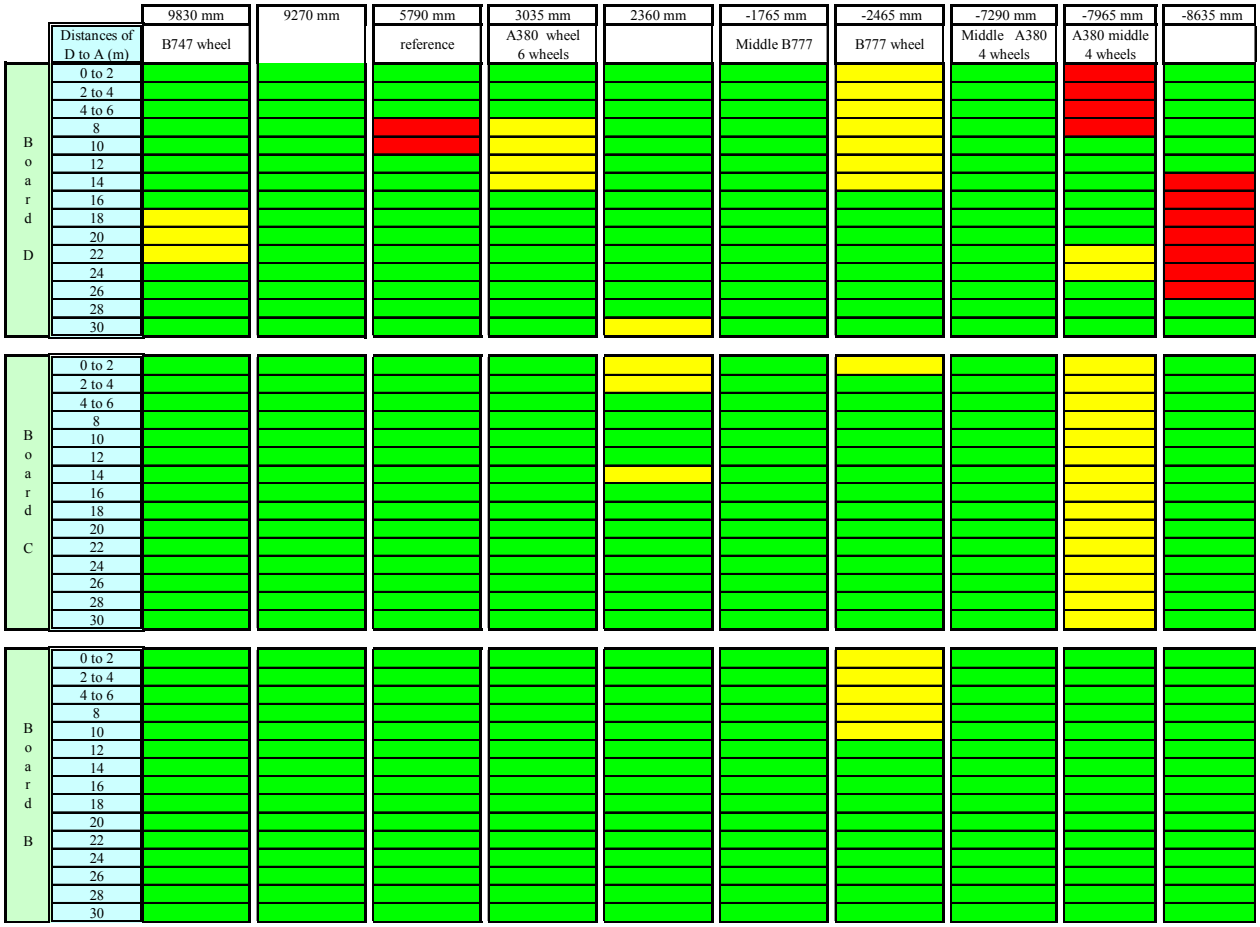

These zones may have undergone a post compaction by traffic, making materials globally more homogeneous in density in BBA and GB's layers, improving interfaces contact and decreasing humidity traces. Only the measurements made in the right of the A380 4 wheels bogie track evolve in the qualification of the interface BBA / GB of the platform D. **Thickness** of each layers BBA and GB shows a good correlation between the measures made in 1999 and 2000. There is not or a little evolution in one or the other of the tracks accounting for to the Radar precision at this depth (variation about the centimeter in a depth from 25 to 30 centimeters).

BBA + GB thickness found with Radar before and after the Fatigue Campaign in the middle of the A380's 4 wheels bogie (Track 8 - 7290 mm)

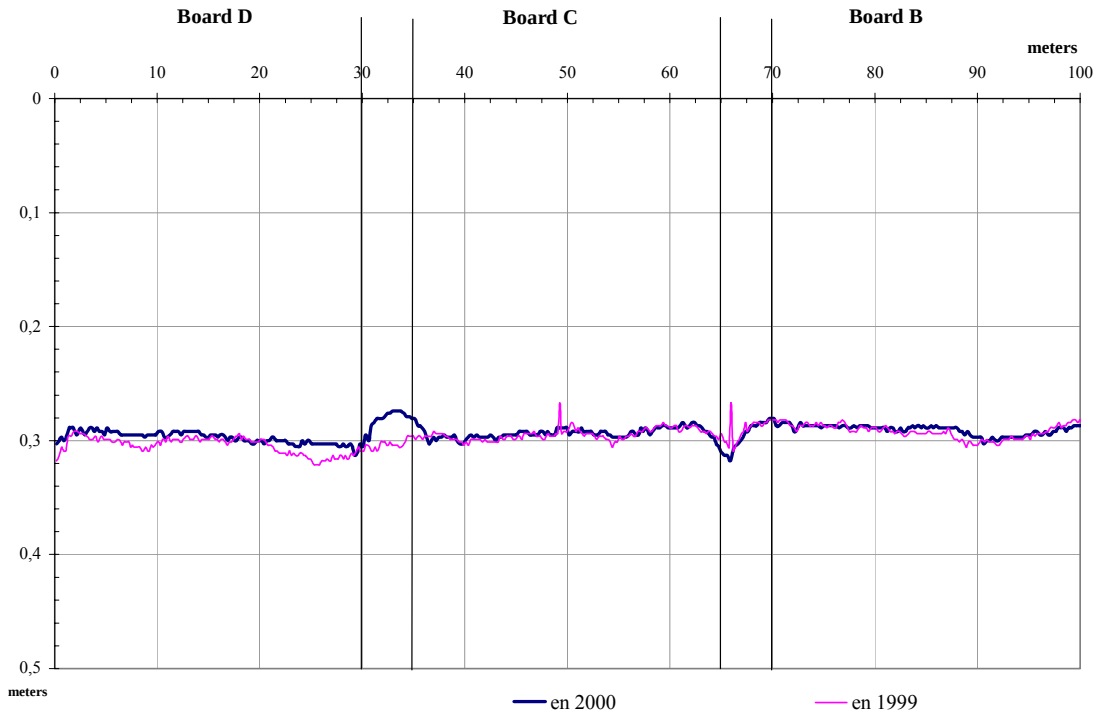

Measurements of **dielectric factor** by the Radar method wave reflection coefficients were not significantly different before and after traffic (6.5 to 6.7). This slight change however may result from a compaction of the wearing course. What is confirmed by the Sand Patch Test made by the LCPC.

APPENDIX

Appendix.1: Wheel-track & Wheel-base effect around C7 configuration
Appendix.2: Ruler measurement all the 1000 passes(Cumulative damage tests)
Appendix.3: Repeated Triaxial testing procedure for road geotechnics

Appendix.1: Wheel-track & Wheel-base effect around C7 configuration

INTRODUCTION / METHODOLOGY

1 ANALYSIS OF EXPERIMENTAL DATA FOR CONFIGURATION C7

2 ALIZE MATCHING
- 2.1 Structure D - CBR 3
- 2.2 Structure C - CBR 6
- 2.3 Structure B - CBR 10
- 2.4 Structure A - CBR 15

3 PARAMETRIC STUDY WITH ALIZE
- 3.1 Structure D - CBR 3
- 3.2 Structure C - CBR 6
- 3.3 Structure B - CBR 10
- 3.4 Structure A – CBR 15
- 3.5 General conclusion of the parametric study

CONCLUSION

INTRODUCTION / METHODOLOGY

Part of the objective of PEP static campaign was to investigate the effects of A3XX bogie dimensions on the maximal strains induced in the different structures and layers of Toulouse-Blagnac experimental pavement. The question is to know how much a change of ±10cm or ±15cm of the wheel-track (WT) or wheel-base (WB) around some given average dimensions of A3XX bogies may affect the static response of airport flexible structures, whereas other parameters are kept constant.

Owing to BOGEST simulator capabilities several 4664-configurations were tested on site for which the only parameters being varied were the wheel-track (WT) and the wheel-base (WB) of both wing and body landing gears (table 1).

WB *WT*	*165*	*170*	*180*	*190*
135	C16	not tested	C5h	C5
145	not tested	C15	C7	not tested

Table 1: Tested configurations for the study of bogie dimensions effect

All these configurations have a total weight of 5,2 MN[1] (260 kN/wheel) with tyre pressure around 1.34 MPa.

In a first attempt we tried to compare between them the experimental data coming from the different configurations of table 1. However due to the experimental uncertainties, compared with the slight variations of signals expected from such relative changes of bogie dimensions, this approach appeared to be inefficient[2]. In particular and despite the use of reference loads for correction, the important variations of temperature which occurred between the testing of the different configurations make it difficult to deduce any clear quantitative, or even qualitative trends on the impact of bogie dimensions[3].

Instead it was decided to use the following methodology: i) select one configuration among those of table 1 as reference, ii) determine the maximal strains measured for this configuration in the different structures and layers of PEP pavement, iii) match ALIZE input data[4] to account for the previous strain values, iv) keeping this set of data constant, perform a

[1] Gravity is taken equal to $10 m^2/s$.

[2] Results presented and discussed in March in Nantes with STBA and Airbus.

[3] The important impact of temperature on the stiffness of bituminous layers and the global response of PEP structures has already been mentioned in our previous reports.

[4] ALIZE is the computer program used in France for the design of roads and pavements. It is based on the famous Burmister's semi-analytical solution for elastic multi-layered media submitted to uniform circular loads. STBA has demonstrated the very good correlation of ALIZE results with that of foreign codes, such as APSDS or CIRCLY. The matching of input data mentioned here above is relative to the elastic characteristics of the layers.

numerical parametric study on WT and WB effects, v) conclude on the relative impact of bogie dimensions on strains.

Configuration C7 (145 x 180) is taken here as the reference configuration. The determination of the experimental maximal strains in step ii) takes into account the 'spatial' corrections, but not the 'time' corrections[5], which are unnecessary for our purpose or even may add some perturbation. Actually it must be clear with this approach that we do not need a very accurate determination of experimental strains, nor a very accurate fitting of experimental data from ALIZE. Indeed the most important issue is to find a 'consistent' set of materials data for ALIZE, with right physical content and right contrast between materials, such as the relative variations given by the parametric study can be assumed to be closed to real ones.

Airbus also asked for including the simulation of different configurations (CB1, CB2, δ, C18, and A330) in the parametrical study of part 3. These results are given for each structure, after the discussion on size bogie effects. Nevertheless, following our present methodology, these figures must be taken with care, since some of these configurations are relatively 'far' from the configuration C7, considering either the weight by wheel or the bogie dimensions[6]. In particular due to the variation of stiffness of untreated materials with stress, it is not sure that the matching found for the configuration C7 is totally valid for all the contemplated aircrafts.

It must also be clear that this report is limited to the study of resilient strains, but does not intend to conclude at this stage on pavement damage and aircraft 'agressivity' at long run. Indeed the passing from strains to damage is still a difficult and challenging task in pavement mechanics. It necessitates to possess relevant cumulative laws of damage for each material[7] and take into account the variability of loading (e.g., wandering) and climatic conditions along a pavement life, which discussion is far beyond the scope of this report. In any case it should be wise to wait for the end of PEP fatigue campaign scheduled in the second part of 1999 to address this question.

1 ANALYSIS OF EXPERIMENTAL DATA FOR CONFIGURATION C7

This configuration was tested on week 48 (23/11 and 24/11) of 1998. At that time the temperature ranged around 6 to 10°C from the base to the top of the bituminous layers.

The analysis of the raw data is performed as mentioned in previous reports with the help of programs *cama.f, sima.f* for sensors in position A and *cambl.f, simb.f* for sensors in position

[5] See our previous reports on the treatment of raw data with the help of the reference loads. 'Spatial' corrections allow to harmonise the response of the different sensors in each layer. 'Time' corrections allow to harmonise the response of the materials despite their change with temperature (bituminous mixes) or moisture content (subbase, subgrade, substratum).

[6] Recall : CB1 (WT x WB) = 112 x 147, weight/wheel = 232 kN ; CB2= 140 x 145, weight/wheel = 239 kN, δ_{MLG}= 198 x 140, weight/wheel = 286 kN, δ_{CLG}= 198 x 118, weight/wheel = 272 kN ,
C18 (MLG) = 163 x 137, weight/wheel = 276 kN, A330 = 198 x 140, weight/wheel = 250 kN.

[7] Mainly fatigue or crack propagation laws for bituminous materials and permament strain laws for untreated materials.

B[8]. However as explained before the 'time' correction procedure included in these programs is neutralised for the present purpose.

The experimental strain maps obtained for the configuration C7 and in untreated layers of structures D, B and A are joined in appendix 1. As usual they show the whole consistency of the acquisition and restitution procedures. Depending on the depth of strain sensors, they allow to visualise either both the 6 wheels BLG and the 4 wheels WLG, or the 4 wheels WLG only.

From these maps as well as from the straightful reading of strain signals in bituminous layers, we can now define some 'typical' figures for the maximal strains induced in PEP pavement by A3XX-C7 configuration (see the tables below); those are used later on as 'target' values to back-fit ALIZE input data.

Of course these tables are also completed with deflection data[9], which account for the global deformation of PEP structures.

Structure D - CBR3

Layer	Maximal strains under the 4 wheels WLG (10^{-6})	Maximal strains under the 6 wheels BLG (10^{-6})
Base of bituminous gravel	220*	not measured
Top of subbase	1000**	not measured
Bottom of subbase	720***	850***
Top of subgrade	750***	850***
Surface deflection	2,2 mm	2,6 mm

Location of maxima: * = transversal strain under the wheel, ** = under the wheel, ***= LG geometric centre

Table 2 : Target strains and deflections extracted from C7 experimental data for structure D

[8] Sensors in position A are those placed with large spacing at the top of subgrade and bottom of subbase of structures D and C. All other sensors close to the pavement surface and placed with small spacing are said to be in position B. Owing to their transversal repartition, the first ones allow to capture the strains both under the wing and body landing gears. The second ones are only sensitive to the WLG. The program *cama.f* is used for the spatial harmonisation of sensors in position A. The program *sima.f* is used to build experimental strain maps of sensors A, after correction of raw signals with *cama.f*. Programs *cambl.f* and *simb.f* do the same but for sensors B.

[9] These are provided by STBA, which was in charge of deflection measurement. The raw data are issued from inclinometers placed at the surface of the pavement along transversal axes of structures A, B, C, D. Then the signals are integrated along the simulator path to provide deflection figures and maps under the different bogies. The process has recently been proved to be highly accurate by comparison with straightful measurement of the vertical displacement of the pavement surface from deeply (6 m) anchored gauges.

Structure C - CBR6		
Layer	Maximal strains under the 4 wheels WLG (10^{-6})	Maximal strains under the 6 wheels BLG (10^{-6})
Base of bituminous gravel	170*	not measured
Top of subbase	950**	not measured
Bottom of subbase	1000** &***	
Top of subgrade	940***	1060***
Surface deflection	1,9 mm	2,4 mm

Location of maxima: * = transversal strain under the wheel, ** = under the wheel, ***= LG geometric centre (visco-elastic effects generally lead the experimental maxima to be under or close to the rear wheels)

Table 3: Target strains and deflections extracted from C7 experimental data for structure C

Structure B - CBR 10	
Layer	Maximal strains under the 4 wheels WLG (10^{-6})
Base of bituminous gravel	230 *
Mid-depth of subbase	1300 **
Top of subgrade	1150 ** & ***
Surface deflection	1,2 mm

Table 4: Target strains and deflection extracted from C7 experimental data for structure B

Structure A - CBR 15	
Layer	Maximal strains under the 4 wheels WLG (10^{-6})
Base of bituminous gravel	165 *
Top of subgrade	700 **
Surface deflection	1,2 mm

Table 5: Target strains and deflection extracted from C7 experimental data for structure A

2 ALIZE MATCHING

The input data for ALIZE include the geometrical description of the pavement structure (number of layers, thickness), the load description (number of circular loads, radii, pressures) and the mechanical characteristics of materials (Young modulus, Poisson's ratio) and interfaces (perfectly sticking or perfectly gliding).

In the present case the geometry of PEP structures as well as loading conditions are perfectly mastered[10]. Besides Poisson's ratio is taken equal to 0.35 in all materials and all interfaces are supposed perfectly sticking.

Therefore the remaining unknowns, used to fit ALIZE simulations, are the Young modulii of the different materials, which of course have to remain in their usual range of magnitude.

Actually because of the non-linear behaviour of untreated materials, it may also be decided to subdivide the subbase or subgrade layer into several layers, with decreasing or increasing modulus downwards. This possibility is used hereafter to fit the results of structures D and C.

Among material properties, it must be noticed that the least constraint is the Young's modulus of the semi-infinite homogeneous substratum which accounts in ALIZE for the natural soil under the subbgrade layer. The fitting process shows that the best criterion to adjust this parameter is the deflection.

The tables below give the sets of properties which we finally propose to retain for the structures D, C, B and A, in order to fit the values of tables 2 to 5. These were obtained after a few hand-guided iterations. Of course these sets are not unique and the match not perfect, only reasonably good, but as previously explained there is no need in our methodology for such high accuracy.

2.1 Structure D - CBR 3

Material	Thickness (cm)	Young modulus (MPa)	Poisson's ratio
BB	8	9000	0.35
GB	24	9000	0.35
GRh1	70	80	0.35
GRh2	70	70	0.35
Subgrade (CBR3)	200	65	0.35
Substratum	∞	15000	0.35

Table 6: ALIZE matching for structure D

[10] It has been shown in our first report and from experimental data that the interaction between bogies were neglectable when looking at the maximal strains. Therefore the simulations performed in this report only deal with a single landing gear, either the 4 wheels WLG or the 6 wheels BLG, depending upon the case.

Layer	Targeted strains 4 wheels WLG	ALIZE strains 4 wheels WLG	Targeted strains 6 wheels BLG	ALIZE strains 6 wheels BLG
Base of bituminous gravel	220	232	none	235
Top of subbase	1000	963	none	1046
Bottom of subbase	720	715	850	833
Top of subgrade	750	752	850	880
Surface deflection (mm)	2,2	2,1	2,6	2,5

Table 7: Structure D - Comparison between targeted and computed values for C7 configuration

Comments:

i) The match of material properties was performed with the data of the 4 wheels WLG only. The 6 wheels BLG was simulated afterwards. It can be observed that the 'predicted' values for this bogie compare relatively well with the experimental data.
Besides ALIZE simulations show the same location of maximal strains than those observed on the experimental strain maps.

ii) The 9000 MPa figure found in the bituminous layers fits well with expected values for temperatures around 8°C and low speed sollicitation (2 Km/h).

iii) Because of the important thickness of the subbase and because of the classical non-linear elastic behaviour of crushed gravel, it was decided to subdivide this layer in 2 parts. But it can be observed that such a refinement is probably unnecessary since at the end the 2 layers almost behave with the same modulus. Actually this finding is in accordance with other observations on flexible pavements: when the thickness of bituminous layers is relatively important and the load widespread (which is the case here), then the stress diffusion within the subbase layer is limited and therefore the secant modulus of the material quasi-constant.

Moreover the 70, 80 MPa figure which could seem low is not unexpected regarding the mean value *p* derived from ALIZE simulation in the subbase layer, which is only around 60 kPa [11].

iv) The 65 MPa figure obtained for the subbase is somehow more surprising, since its originate CBR is only 3. But decreasing this value too much increases the vertical strain at the top of the subbase and increases the global deflection, which makes it difficult to match the experimental data of table 2.

v) In these simulations the substratum has been rendered rigid (15000 MPa), in order to account for the right magnitude of deflection.

[11] The secant modulus of untreated materials is generally found to be an increasing function of the mean pressure *p* (e.g., k-θ model, and Boyce's model). This has 2 consequences: i) where this value is uniform, no much change of the material stiffness is expected; ii) the lower *p*, the lower the secant modulus.

2.2 Structure C - CBR 6

Material	Thickness (cm)	Young modulus (MPa)	Poisson's ratio
BB	8	16000	0.35
GB	24	16000	0.35
GRh	60	60	0.35
Subgrade 1(CBR6)	100	45	0.35
Subgrade 2(CBR6)	100	150	0.35
Substratum	∝	15000	0.35

Table 8: ALIZE matching for structure C

Layer	Targeted strains 4 wheels WLG	ALIZE strains 4 wheels WLG	Targeted strains 6 wheels BLG	ALIZE strains 6 wheels BLG
Base of bituminous gravel	170	165	none	173
Top of subbase	..980	890	none	1003
Bottom of subbase	1000	1019	none	1169
Top of subgrade	940	960	1060	1160
Surface deflection (mm)	1,9	1,9	2,4	2,3

Table 9: Structure C - Comparison between targeted and computed values for C7 configuration

Comments:

i) The Young modulus found for the bituminous layers is rather high (16000 MPa). But the mean temperature in these layers at the time of testing was also particularly cold (≈3°C).

ii) in order to fit the measured deflection as well as the strain data at the top of the subgrade, it looks necessary to share the subgrade into 2 sublayers, with increasing modulus downwards. Of course this subdivision - 2 x 1m, here - is somewhat arbitrary since there is no strain measurement in the subgrade at other depth.

iii) as for structure D, the matching was done only considering the 4 wheels WLG. The simulation of the 6 wheels WLG performed afterwards shows a reasonable agreement with measured data, especially with the deflection.

2.3 Structure B - CBR 10

Material	Thickness (cm)	Young modulus (MPa)	Poisson's ratio
BB	8	8000	0.35
GB	24	8000	0.35
GRh	20	50	0.35
Subgrade (CBR 10)	100	60	0.35
Substratum	∝	15000	0.35

Table 10 : ALIZE matching for structure B

Layer	Targeted strains 4 wheels WLG	ALIZE computed strains 4 wheels WLG
Base of bituminous gravel	230	235
Mid-depth of subbase	1300	1335
Top of subgrade	1150	1080
Surface deflection	1,2 mm	1,3 mm

Table 11: Structure B - Comparison between target and computed values for configuration C7

Comment:

The data set matching ALIZE on structure B is globally close to the data set found for structure D, which is rather satisfying. The most questionable point is relative to the subgrade modulus, which is found to be similar to that of structure D, despite the difference in CBR.

2.4 Structure A - CBR 15

Material	Thickness (cm)	Young modulus (MPa)	Poisson's ratio
BB	8	10000	0.35
GB	24	10000	0.35
Subgrade (CBR 15)	100	100	0.35
Substratum	∞	1000	0.35

Table 12 : ALIZE matching for structure A

Layer	Targeted strains 4 wheels WLG	ALIZE computed strains 4 wheels WLG
Base of bituminous gravel	165	187
Top of subgrade	700	688
Surface deflection	1,2 mm	1,1 mm

Table 13: Structure A - Comparison between target and computed values for Configuration C7

Comments:

Here the substratum has to be given a lower value (1000 MPa) than in previous structures (15000 MPa) in order to account for the right magnitude of deflection. Besides the subgrade stiffness is found to be larger than in previous structures, which is not in contradiction with the higher CBR this structure is supposed to have.

3 PARAMETRIC STUDY WITH ALIZE

This study is done considering a single 6-wheels BLG.

The materials data are derived from the previous tables for each structure (D, B, A) and kept constant, as well as the basic wheel load (circular load, 260kN, pressure 1,34MPa). Then the only parameters which are varied are the WT and WB of the BLG.

The tables below summarise the incidence of bogie dimensions on the maximal strains

computed with ALIZE.

For structure D, the 8 combinations crossing the conditions WT ∈ [135, 145] x WB ∈ [165, 170, 180, 190] are considered.

For structures B and A, we only calculate the 'partial derivative' of strains versus WT and WB around the C7 configuration (3 calculations instead of 8).

3.1 Structure D - CBR 3

	Wheel-base : 135				**Wheel-base : 145**			
Config. WT x WB	**C16 135x165**	**α 135x170**	**C5h 135x180**	**C5 135x190**	**β 145x165**	**C15 145x170**	**C7 145x180**	**χ 145x190**
Deflection (mm)	2,6	2,6	2,6	2,6	2,6	2,6	2,6	2,6
Base GB	247	244	239	235	243	240	235	231
Top subbase	1115	1099	1069	1043	1090	1075	1045	1021
Bottom subbase	903	885	851	817	885	867	833	801
Top subgrade	951	932	896	861	932	913	877	844

Table 14: Structure D - Parametric study of WB and WT Computed maximal strains under the 6 wheels BLG of A3XX

As expected, results of table 14 predict decreasing strains with increasing dimensions of WB or WT. Actually in terms of algebraic relative variations, the table below can be summarised as follows. For structure D:

i) a positive change of 10cm of the WB around 170 cm creates a negative change Δε/ε about :

i1) 2,0 % at the base of the bituminous gravel
i2) 2,7 % at the top of subbase
i3) 4,0 % at the bottom of subbase
i4) 4,0 % at the top of subgrade

ii) a positive change of 10cm of the WT around 140cm creates a negative change Δε/ε about :

i1) 1,7 % at the base of the bituminous gravel
i2) 2,3 % at the top of subbase

i3) 2,0 % at the bottom of subbase
i4) 2,0 % at the top of subgrade

Invert the conclusions in case of negative variations of WB or WT.

Structure D - Additional calculations for extended comparison between aircrafts

Config. WT x WB Weight/wheel(kN)	C7 145x180 260	CB1 112x147 232	CB2 140x145 239	δMLG 140x198 286	δCLG 118x198 272	$C18_{MLG}$ 137x163 276	A330 140x198 250
Deflection(mm)	2,6	2,3	2,7	2,2	2,1	2,4	2,0
Base GB	235	231	239	252	249	254	221
Top subbase	1045	980	1100	1043	1043	1064	912
Bottom subbase	833	737	908	757	750	806	662
Top subgrade	877	775	956	796	789	847	696

Table 14(bis): Structure D - Parametric study Computed maximal strains for different aircrafts

3.2 Structure C - CBR 6

Config. WT x WB	C5h 135x180	C7 145x180	C15 145x170
Deflection(mm)	2,3	2,3	2,3
Base GB	178	173	177
Top subbase	1024	1003	1033
Bottom subbase	1205	1169	1221
Top subgrade	1180	1160	1202

Table 15: Structure C - Parametric study of WB and WT Computed maximal strains under the 6 wheels BLG of A3XX

Again this table below can be summarised as follows. For structure C:

i) A positive change of 10cm of the WB around 170 cm creates a negative change Δε/ε about:

i1) 2,2 % at the base of the bituminous gravel
i2) 3,0 % at the top of the subbase
i3) 4,3 % at the bottom of the subbase

i4) 3,6 % at the top of subgrade

ii) a positive change of 10cm of the WT around 140cm creates a negative change Δε/ε about :

i1) 2,8 % at the base of the bituminous gravel
i2) 2,1 % at the top of the subbase
i3) 3,1 % at the bottom of the subbase
i4) 1,7% at the top of subgrade

Structure C - Additional calculations for extended comparison between aircrafts

Config. WT x WB Weight/wheel(kN)	C7 145x180 260	CB1 112x147 232	CB2 140x145 239	δMLG 140x198 286	δCLG 118x198 272	$C18_{MLG}$ 137x163 276	A330 140x198 250
Deflection(mm)	2,3	2,0	2,5	2,1	2,0	2,2	1,8
Base GB	173	168	178	178	176	182	155
Top subbase	1003	862	1057	909	907	1021	795
Bottom subbase	1169	1110	1305	1065	1070	1173	930
Top subgrade	1160	966	1235	1021	1005	1069	893

Table 15(bis): ***Structure C - Parametric study Computed maximal strains for different aircrafts***

3.3 Structure B - CBR 10

Config. WT x WB	C5h 135x180	C7 145x180	C15 145x170
Deflection (mm)	1,4	1,4	1,4
Base GB	235	232	234
Mid-depth of subbase	1526	1483	1541
Top subgrade	1246	1207	1260

Table 16: Structure B - Parametric study of WB and WT Computed maximal strains under the 6 wheels BLG of A3XX

Thus we find that for structure B:

i) a positive change of 10cm of the WB around 170 cm creates a negative change Δε/ε about :

i1) 1,0 % at the base of the bituminous gravel
i2) 3,9 % in the subbase
i3) 4,3 % at the top of subgrade

ii) A positive change of 10cm of the WT around 140cm creates a negative change Δε/ε about:

i1) 1,5 % at the base of the bituminous gravel
i2) 2,9 % in the subbase
i3) 3,2% at the top of subgrade

Structure B - Additional calculations for extended comparison between aircrafts

Config. **WT x WB** **Weight/wheel(kN)**	**C7** **145x180** **260**	**CB1** **112x147** **232**	**CB2** **140x145** **239**	**δMLG** **140x198** **286**	**δCLG** **118x198** **272**	**C18$_{MLG}$** **137x163** **276**	**A330** **140x198** **250**
Deflection(mm)	1,4	1,5	1,6	1,3	1,4	1,5	1,2
Base GB	232	233	233	258	255	257	225
Mid-depth of subbase	1483	1422	1637	1438	1459	1503	1257
Top subgrade	1207	1248	1363	1162	1192	1246	1016

Table 16(bis): Structure B - Parametric study Computed maximal strains for different aircrafts

3.4 Structure A – CBR 15

Config. **WT x WB**	**C5h** **135x180**	**C7** **145x180**	**C15** **145x170**	**CB1** **112x147**	**CB2** **140x145**

Deflection (mm)	1,3	1,3	1,3	1,3	1,4
Base GB	187	185	186	184	184
Top of subgrade	819	796	829	773	887
Base of subgrade	996	955	1005	1031	1114

Table 17: Structure A - Parametric study of WB and WT Computed maximal strains under the 6 wheels BLG of A3XX

For structure A:

i) a positive change of 10cm of the WB around 170 cm creates a negative change $\Delta\varepsilon/\varepsilon$ about :

i1) 1,0 % at the base of the bituminous gravel
i2) 4,1 % at the top of subgrade

ii) a positive change of 10cm of the WT around 140cm creates a negative change $\Delta\varepsilon/\varepsilon$ about :

i1) 2,0 % at the base of the bituminous gravel
i2) 2,9 % at the top of subgrade

Structure A - Additional calculation for extended comparison between aircrafts

Config. WT x WB Weight/wheel(kN)	**C7 145x180 260**	**CB1 112x147 232**	**CB2 140x145 239**	**δMLG 140x198 286**	**δCLG 118x198 272**	**$C18_{MLG}$ 137x163 276**	**A330 140x198 250**
Deflection(mm)	1,3	1,3	1,4	1,1	1,2	1,3	1,0
Base GB	185	184	184	205	203	203	180
Top of subgrade	796	773	887	728	738	801	636
Base of subgrade	955	1031	1114	902	927	1046	789

Table 17(bis): Structure A - Parametric study Computed maximal strains for different aircrafts

3.5 General conclusions of the parametric study

i) Increasing bogie dimensions, either the WB, or the WT has a decreasing effect on static strains.

ii) For the same (total) variation of WB or WT, the relative impact of WB is higher than that of WT.

iii) As expected the effect of WB and WT is generally increasing with depth. (A slight exception exists for the impact of the WT on the subbase of structure D).

iv) Nevertheless the relative impact of variations of WB or WT remain small. In any case, it does not exceed 4,5% for a change of 10cm. This explains the difficulty to extract any clear trend from experimental data even comparing the most extreme configurations such as C7 and C16 or C5 and C16.

CONCLUSION

This study aims to appreciate the impact of A3XX bogies size on the resilient strains induced in the experimental pavement of Toulouse-Blagnac airport.

The approach is based on a combination of raw data issued from the static PEP campaign and numerical results issued from ALIZE calculations.

The experimental data used in this report come principally from the testing of the configuration C7. They are first checked to make a consistent set of data, using the numerical tools, which were developed for the analysis of PEP static campaign. This phase allows to extract some typical maximal values of deflection and strains induced by the different bogies of the configuration C7, for the different instrumented levels of PEP structures.

Then these values are taken as target values to backcalcultate from ALIZE simulations consistent sets of stiffness moduli for the different layers of PEP structures.

Finally the size effect of A3XX bogies is appreciated through a parametric study, based on ALIZE calculations, keeping the previous matching of materials data constant.

The same materials data are also used with ALIZE to compare the static impact of different aircrafts on PEP structures.

The main result relative to the size effect of A3XX bogies is to show that variations of ±10cm of A3XX wheel-track or wheel-base around the C7 tested configuration (WT x WB = 145 cm x 180 cm) induce less than ± 4,5% relative changes of strain in the flexible pavement structures of Toulouse-Blagnac.

It is difficult to know at this stage whether such variations are significant or not in terms of pavement life. This question should probably have to be addressed after the PEP fatigue campaign scheduled end of 1999, when we get a better knowledge about the most significant phenomena and criteria at stake during fatigue.

One should also be careful about the fact that the present study does not take into account the effect of temperature variations on flexible pavements behaviour. In fact the results obtained here are only valid in the case of asphalt layers at rather low temperature, since this one varied approximately between 7 and 10°C at the time of C7 testing.

In the case of high temperatures (> 35°C) the conclusions could change quite significantly since the stiffness of asphalt layers would be at least 10 times smaller than those considered here (typically, 1000 MPa instead of 10000 MPa). This question will have to be investigated in a future report.

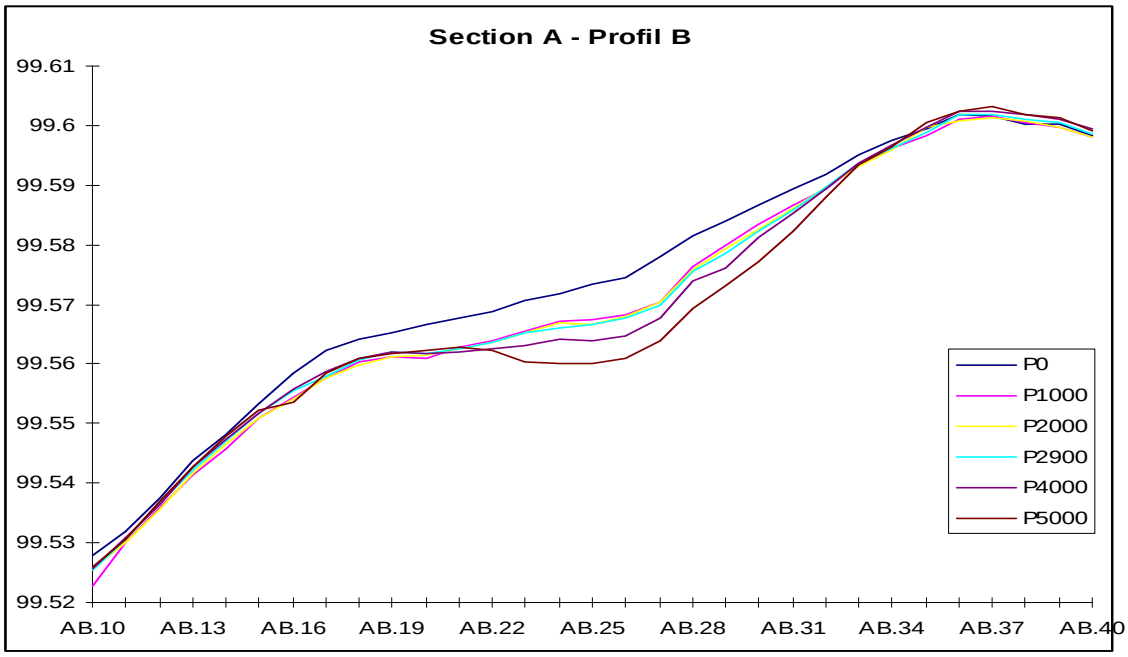
Section A - Profil B
99.61
99.6
99.59
99.58
99.57
99.56
99.55
99.54
99.53
99.52
AB.10
AB.13
AB.16
AB.19
AB.22
AB.25
AB.28
AB.31
AB.34
AB.37
AB.40
P0
P1000
P2000
P2900
P4000
P5000

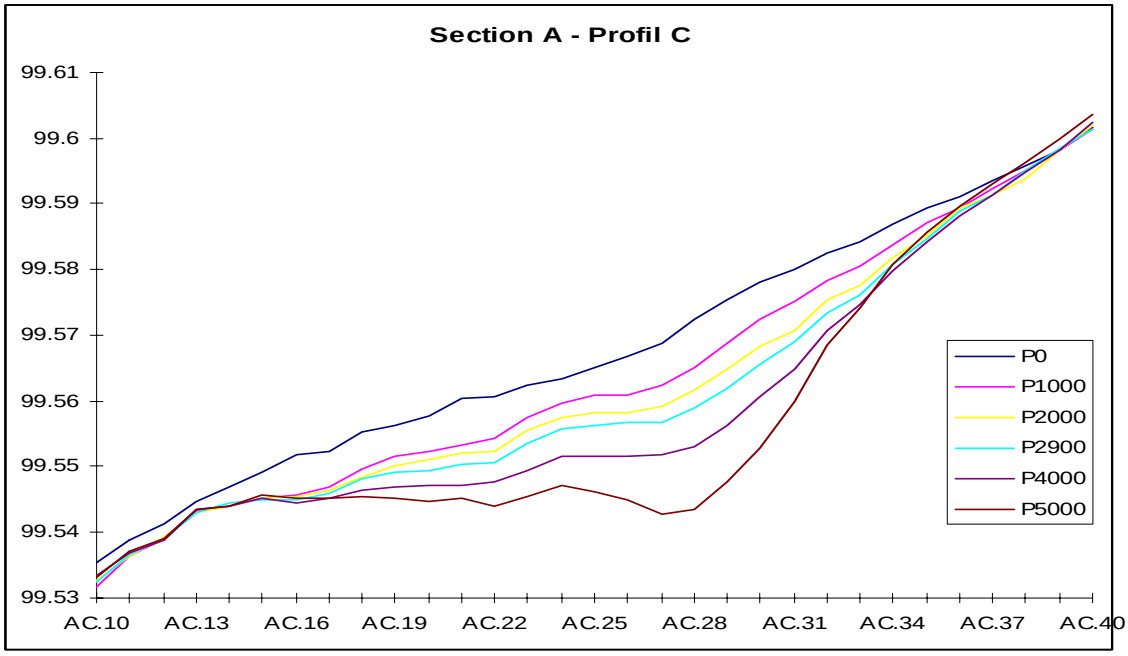
Section A - Profil C
99.61
99.6
99.59
99.58
99.57
99.56
99.55
99.54
99.53
AC.10
AC.13
AC.16
AC.19
AC.22
AC.25
AC.28
AC.31
AC.34
AC.37
AC.40
P0
P1000
P2000
P2900
P4000
P5000

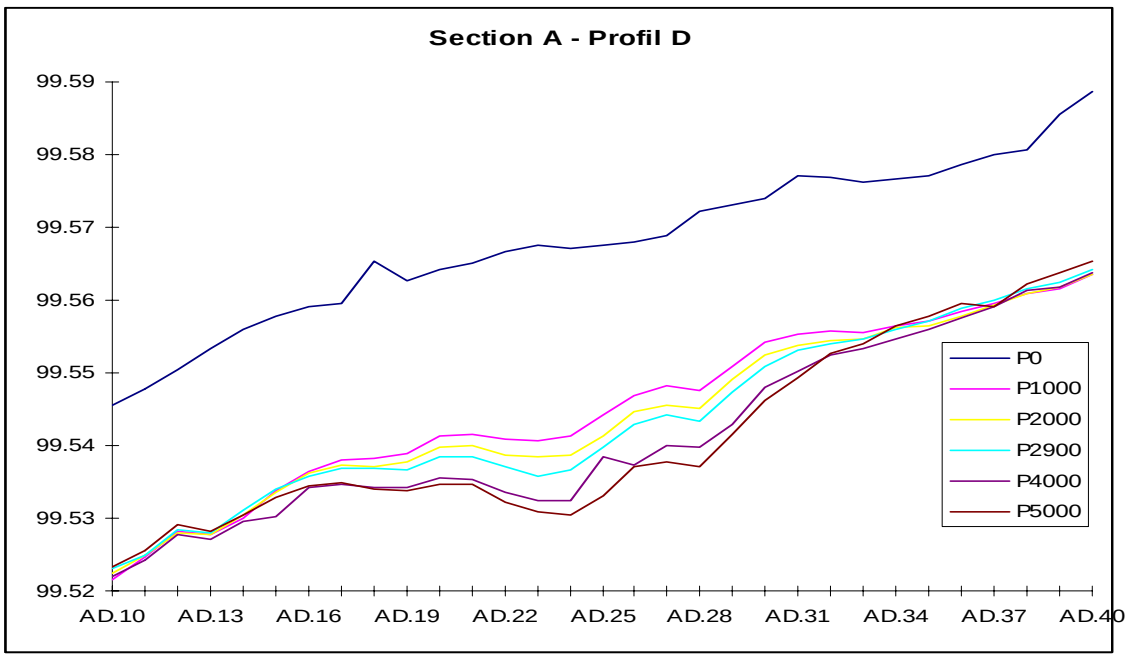
Section A - Profil D
99.59
99.58
99.57
99.56
99.55
99.54
99.53
99.52
AD.10
AD.13
AD.16
AD.19
AD.22
AD.25
AD.28
AD.31
AD.34
AD.37
AD.40
P0
P1000
P2000
P2900
P4000
P5000

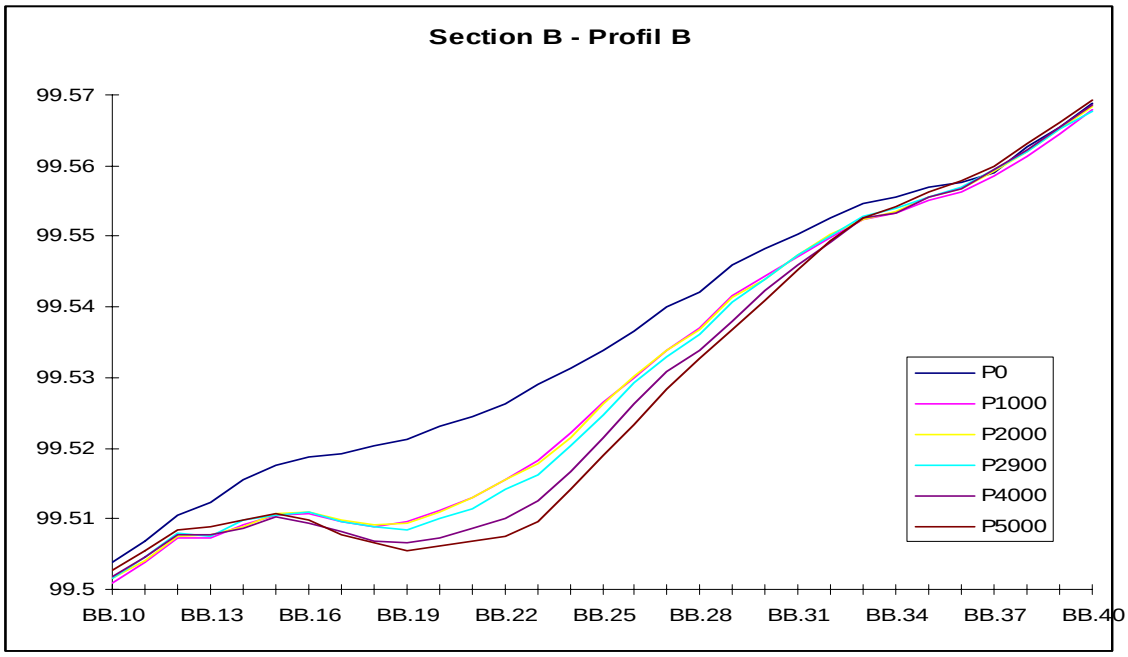
Section B - Profil B
99.57
99.56
99.55
99.54
99.53
99.52
99.51
99.5
BB.10
BB.13
BB.16
BB.19
BB.22
BB.25
BB.28
BB.31
BB.34
BB.37
BB.40
P0
P1000
P2000
P2900
P4000
P5000

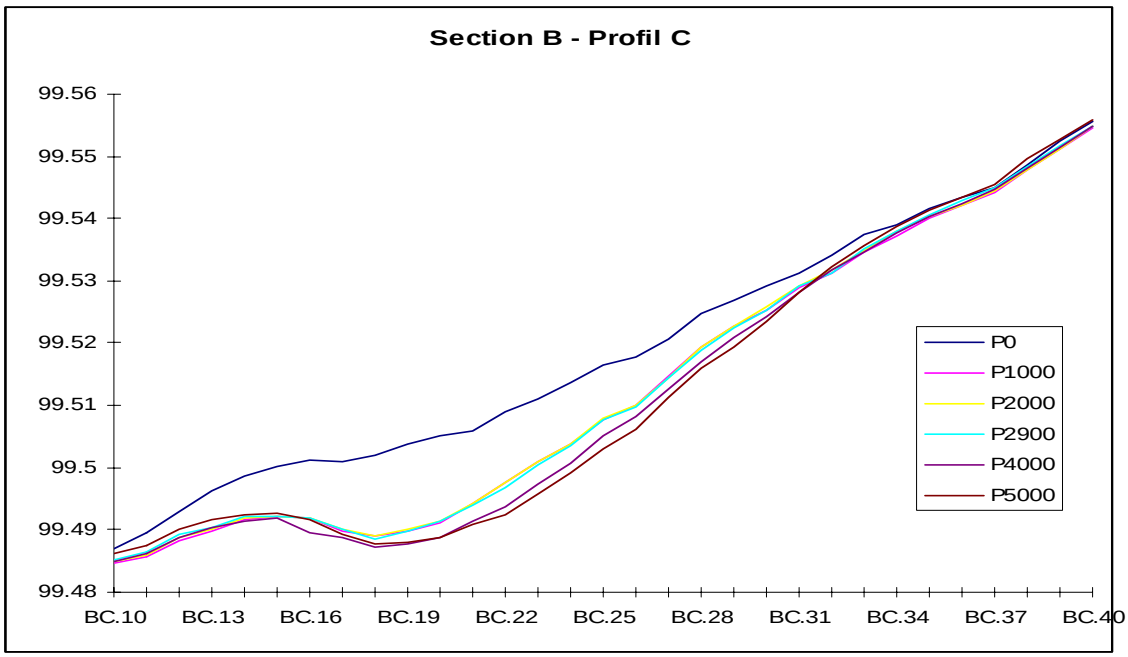
Section B - Profil C
99.56
99.55
99.54
99.53
99.52
99.51
99.5
99.49
99.48
BC.10
BC.13
BC.16
BC.19
BC.22
BC.25
BC.28
BC.31
BC.34
BC.37
BC.40
P0
P1000
P2000
P2900
P4000
P5000

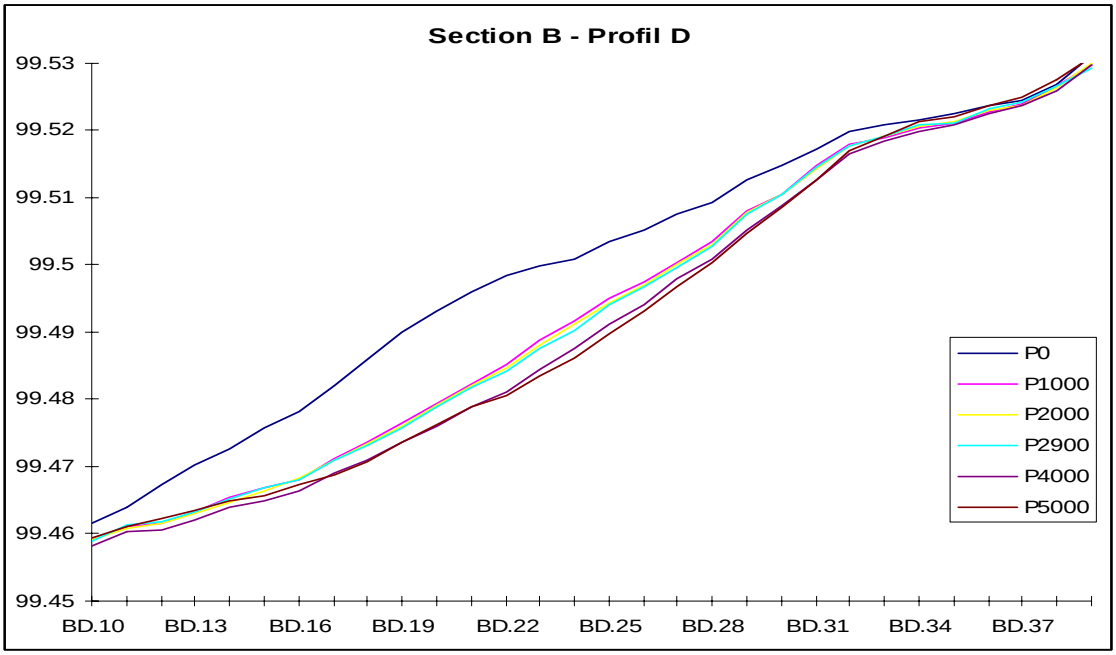
Section B - Profil D
99.53
99.52
99.51
99.5
99.49
99.48
99.47
99.46
99.45
BD.10
BD.13
BD.16
BD.19
BD.22
BD.25
BD.28
BD.31
BD.34
BD.37
P0
P1000
P2000
P2900
P4000
P5000

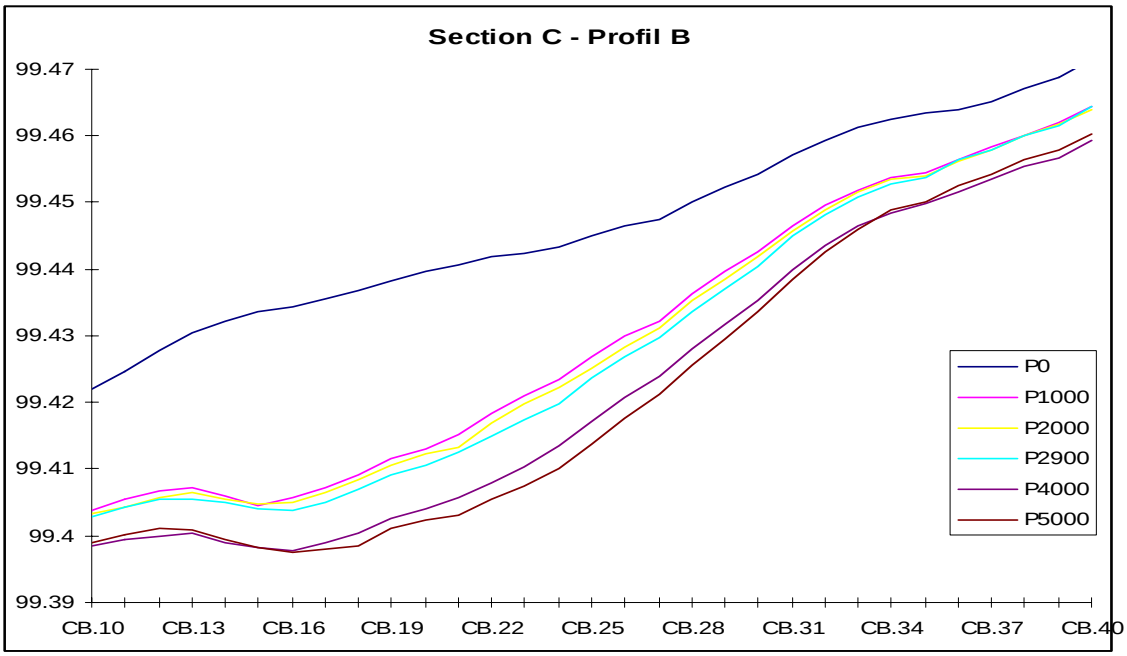
Section C - Profil B
99.47
99.46
99.45
99.44
99.43
99.42
99.41
99.4
99.39
CB.10
CB.13
CB.16
CB.19
CB.22
CB.25
CB.28
CB.31
CB.34
CB.37
CB.40
P0
P1000
P2000
P2900
P4000
P5000

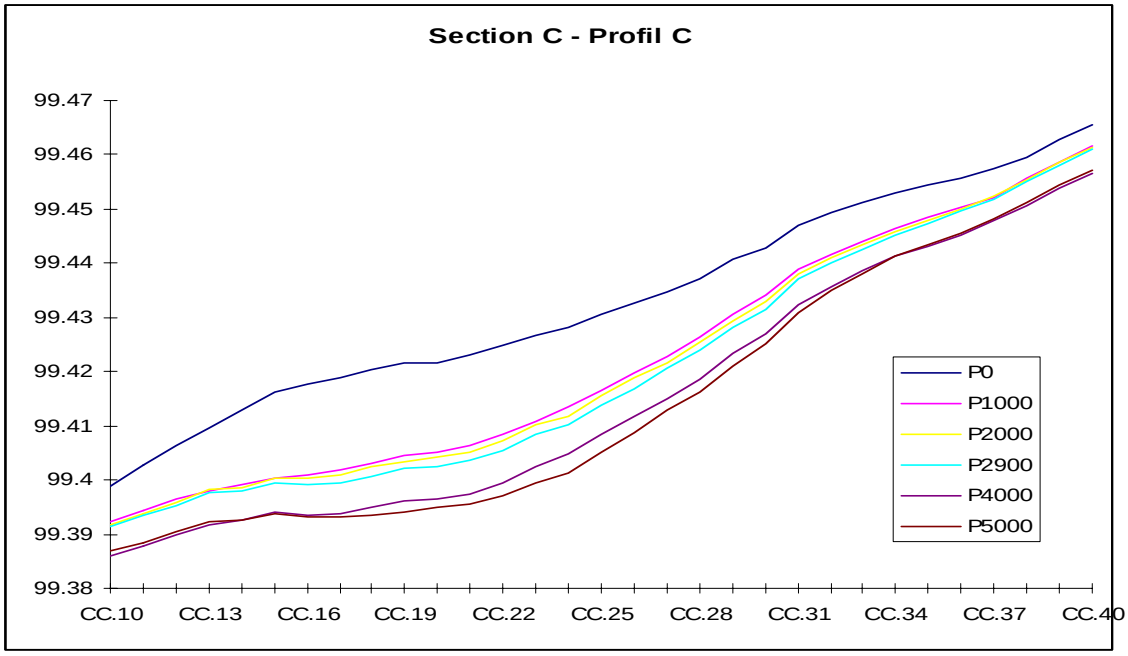
Section C - Profil C
99.47
99.46
99.45
99.44
99.43
99.42
99.41
99.4
99.39
99.38
CC.10
CC.13
CC.16
CC.19
CC.22
CC.25
CC.28
CC.31
CC.34
CC.37
CC.40
P0
P1000
P2000
P2900
P4000
P5000

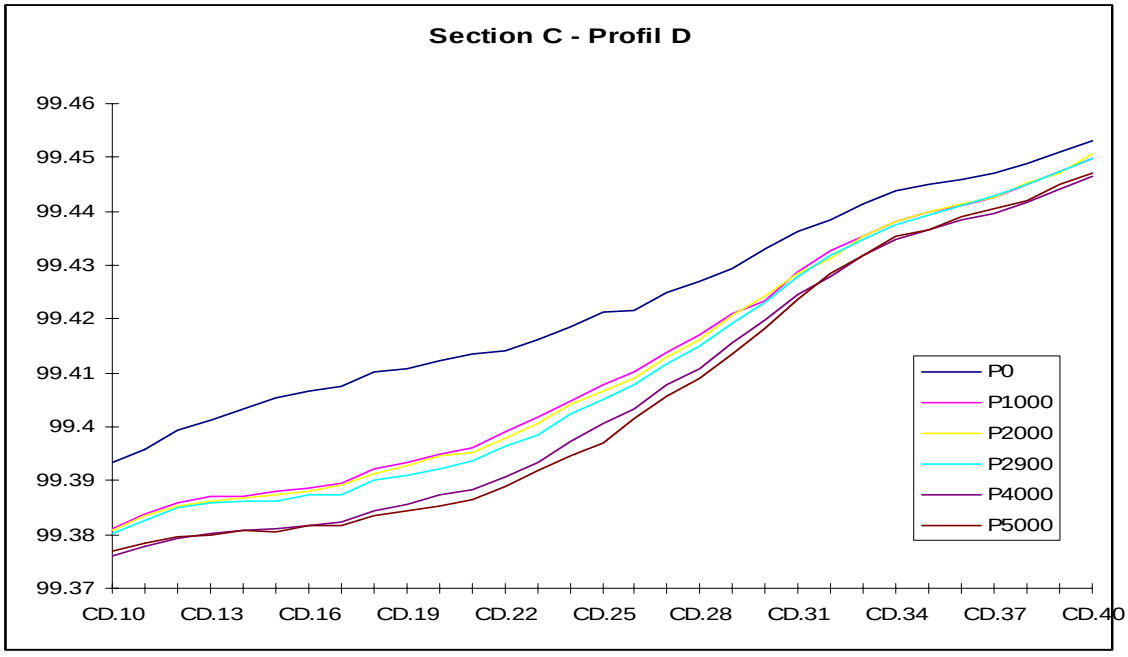
Section C - Profil D
99.46
99.45
99.44
99.43
99.42
99.41
99.4
99.39
99.38
99.37
CD.10
CD.13
CD.16
CD.19
CD.22
CD.25
CD.28
CD.31
CD.34
CD.37
CD.40
P0
P1000
P2000
P2900
P4000
P5000

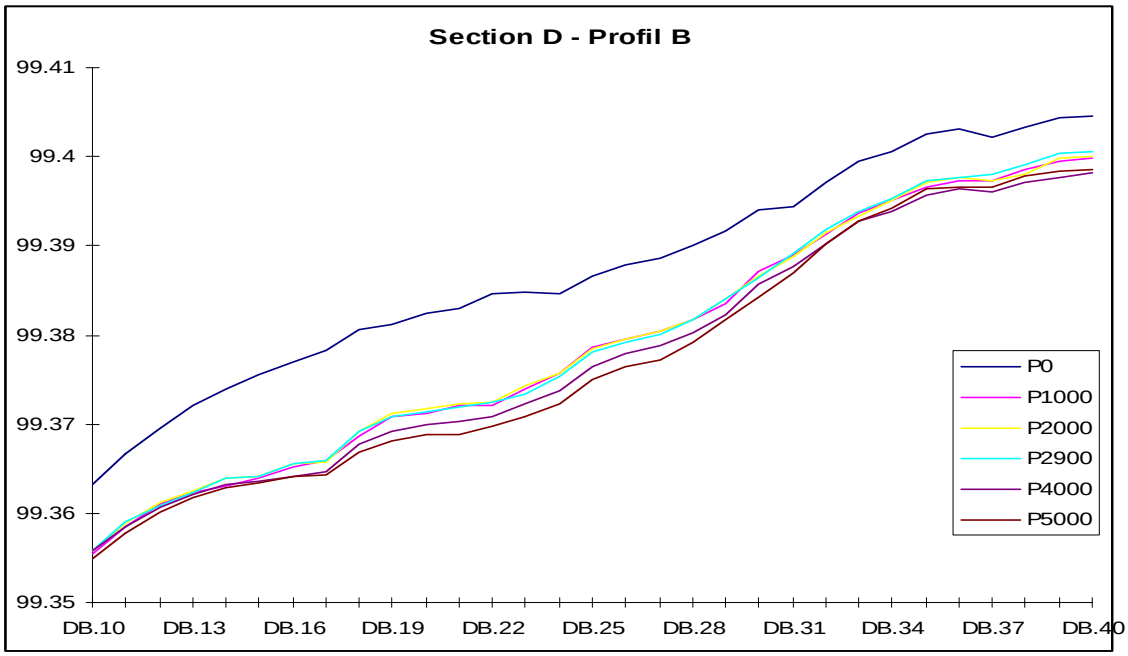
Section D - Profil B
99.41
99.4
99.39
99.38
99.37
99.36
99.35
DB.10
DB.13
DB.16
DB.19
DB.22
DB.25
DB.28
DB.31
DB.34
DB.37
DB.40
P0
P1000
P2000
P2900
P4000
P5000

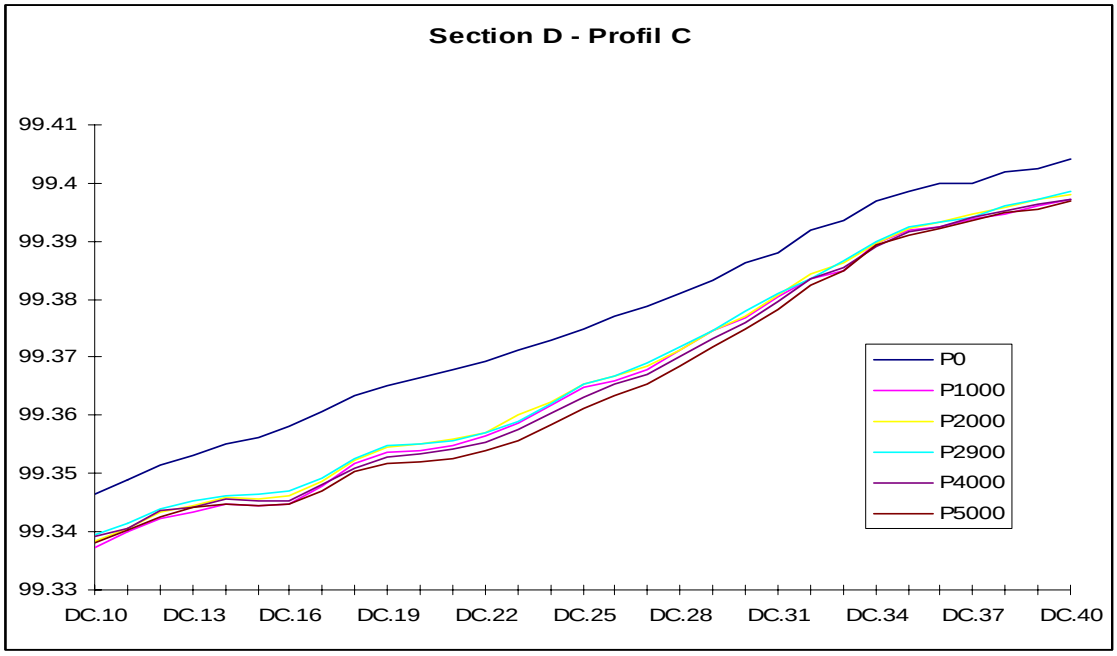
Section D - Profil C
99.41
99.4
99.39
99.38
99.37
99.36
99.35
99.34
99.33
DC.10
DC.13
DC.16
DC.19
DC.22
DC.25
DC.28
DC.31
DC.34
DC.37
DC.40
P0
P1000
P2000
P2900
P4000
P5000

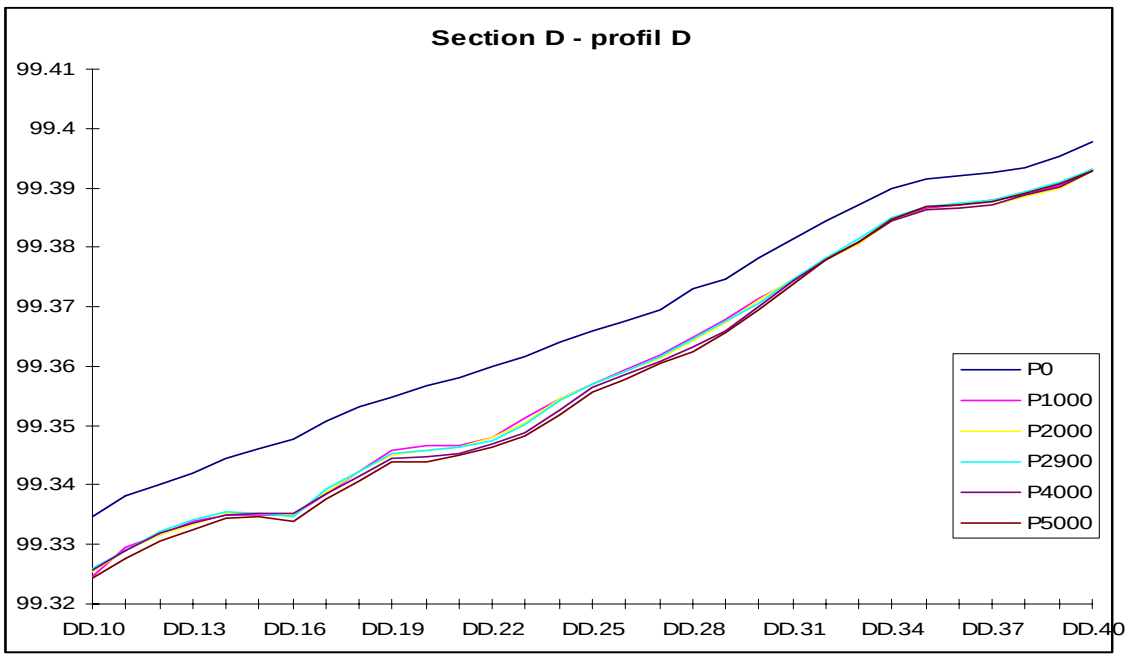
Section D - profil D
99.41
99.4
99.39
99.38
99.37
99.36
99.35
99.34
99.33
99.32
DD.10
DD.13
DD.16
DD.19
DD.22
DD.25
DD.28
DD.31
DD.34
DD.37
DD.40
P0
P1000
P2000
P2900
P4000
P5000

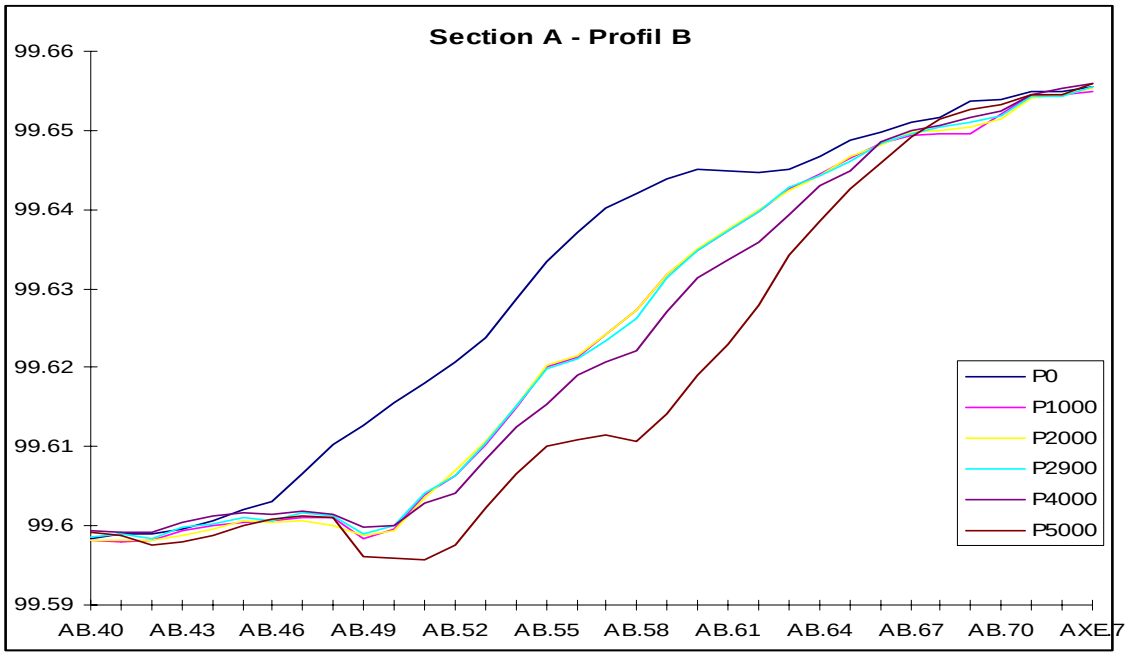
Section A - Profil B
99.66
99.65
99.64
99.63
99.62
99.61
99.6
99.59
AB.40
AB.43
AB.46
AB.49
AB.52
AB.55
AB.58
AB.61
AB.64
AB.67
AB.70
AXE.7
P0
P1000
P2000
P2900
P4000
P5000

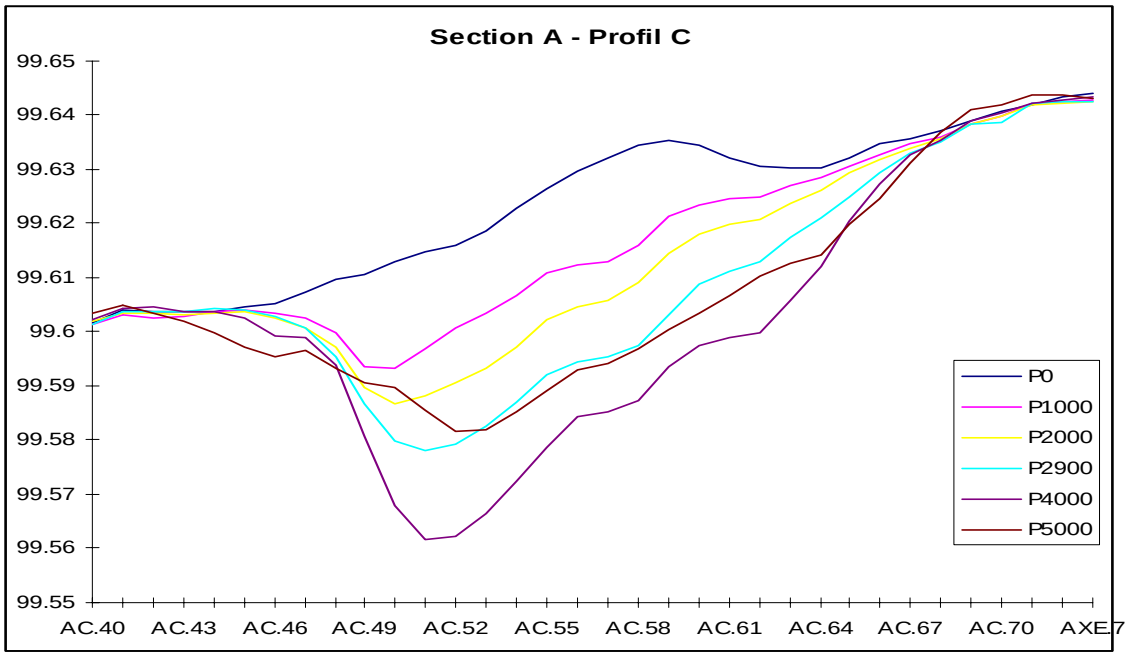
Section A - Profil C
99.65
99.64
99.63
99.62
99.61
99.6
99.59
99.58
99.57
99.56
99.55
AC.40
AC.43
AC.46
AC.49
AC.52
AC.55
AC.58
AC.61
AC.64
AC.67
AC.70
AXE.7
P0
P1000
P2000
P2900
P4000
P5000

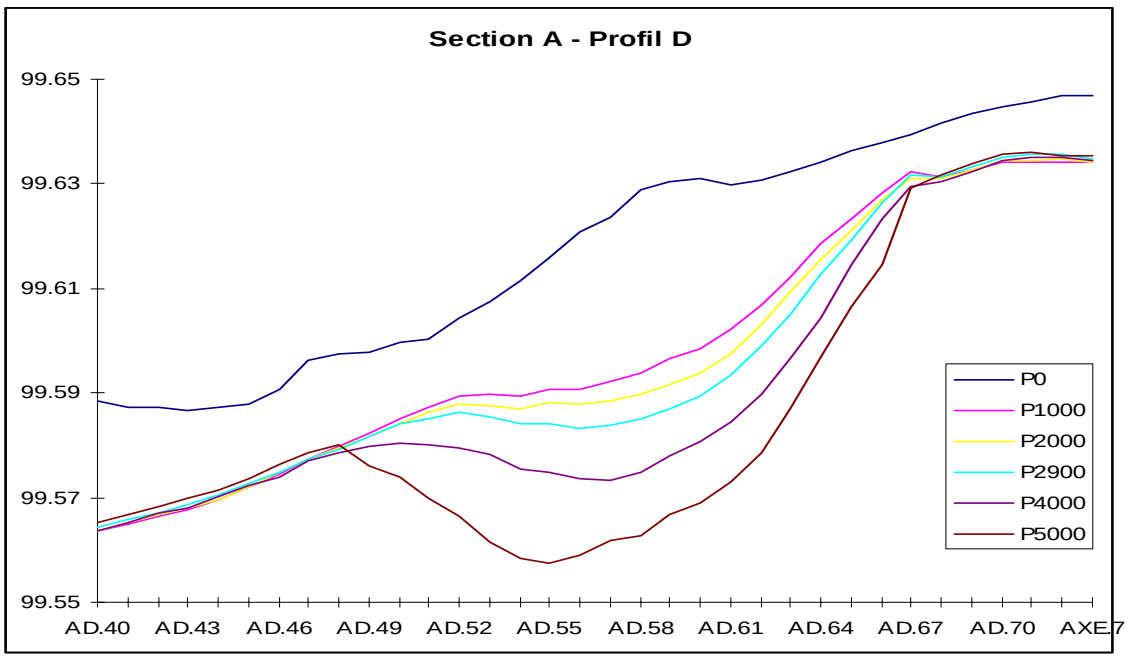
Section A - Profil D
99.65
99.63
99.61
99.59
99.57
99.55
AD.40
AD.43
AD.46
AD.49
AD.52
AD.55
AD.58
AD.61
AD.64
AD.67
AD.70
AXE.7
P0
P1000
P2000
P2900
P4000
P5000

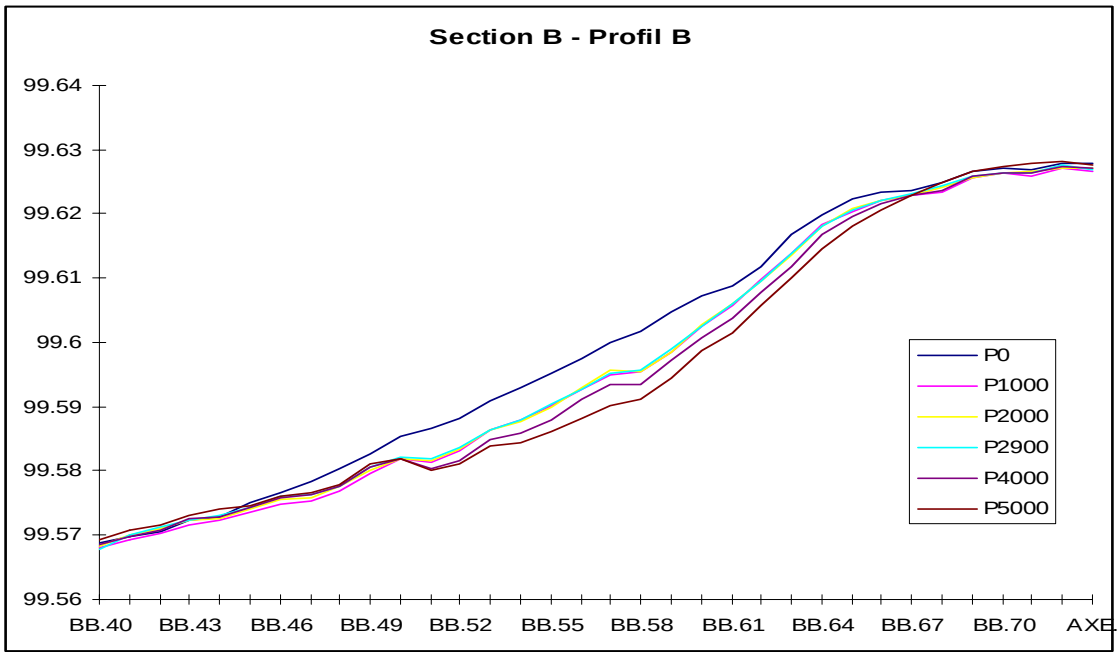
Section B - Profil B
99.64
99.63
99.62
99.61
99.6
99.59
99.58
99.57
99.56
BB.40 BB.43 BB.46 BB.49 BB.52 BB.55 BB.58 BB.61 BB.64 BB.67 BB.70 AXE
P0
P1000
P2000
P2900
P4000
P5000

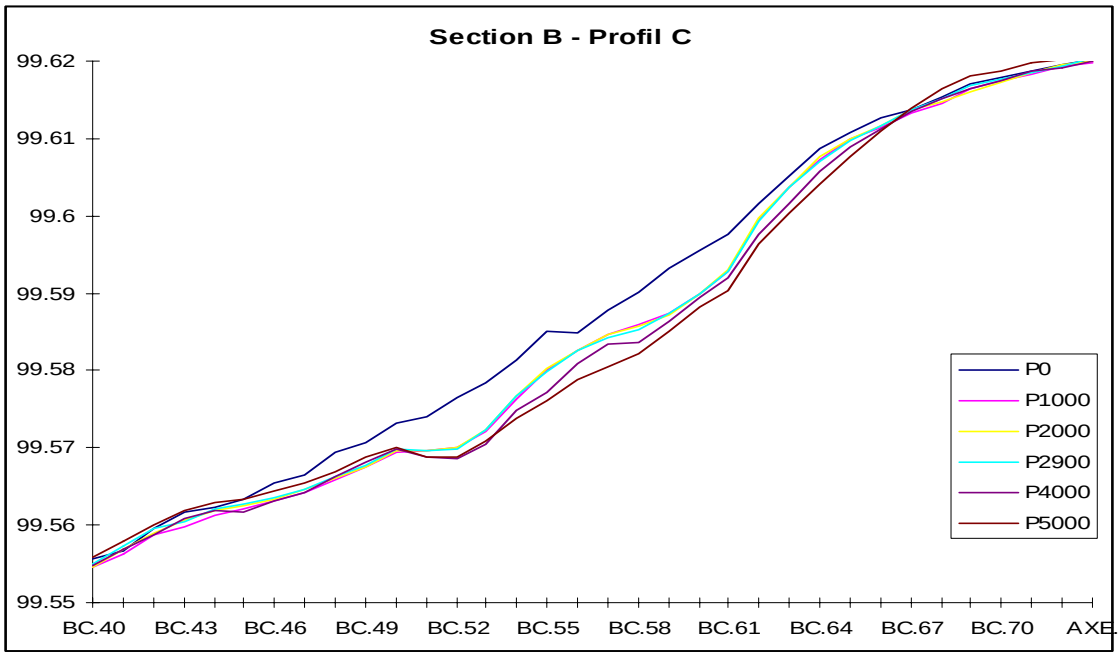
Section B - Profil C
99.62
99.61
99.6
99.59
99.58
99.57
99.56
99.55
BC.40 BC.43 BC.46 BC.49 BC.52 BC.55 BC.58 BC.61 BC.64 BC.67 BC.70 AXE
P0
P1000
P2000
P2900
P4000
P5000

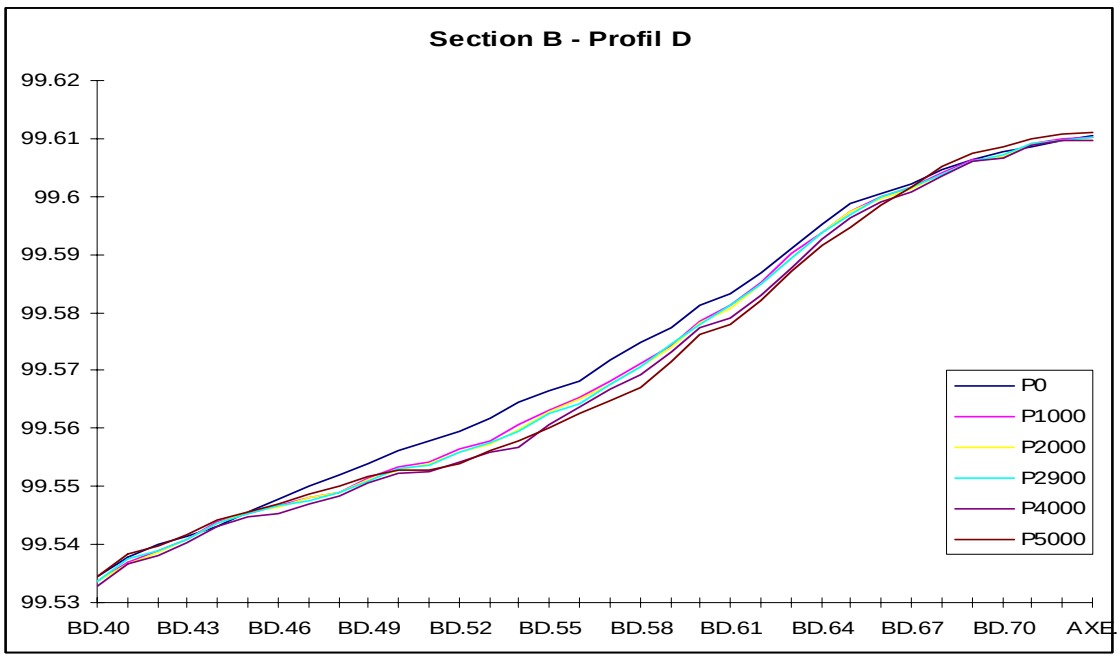
Section B - Profil D
99.62
99.61
99.6
99.59
99.58
99.57
99.56
99.55
99.54
99.53
BD.40 BD.43 BD.46 BD.49 BD.52 BD.55 BD.58 BD.61 BD.64 BD.67 BD.70 AXE
P0
P1000
P2000
P2900
P4000
P5000

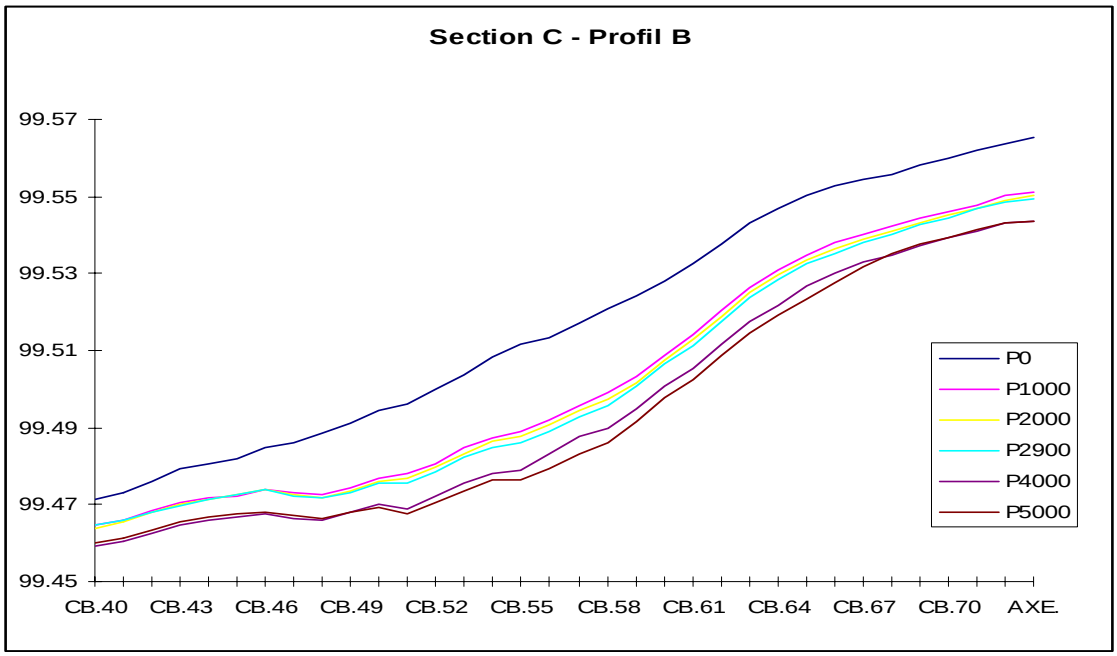
Section C - Profil B
99.57
99.55
99.53
99.51
99.49
99.47
99.45
CB.40 CB.43 CB.46 CB.49 CB.52 CB.55 CB.58 CB.61 CB.64 CB.67 CB.70 AXE
P0
P1000
P2000
P2900
P4000
P5000

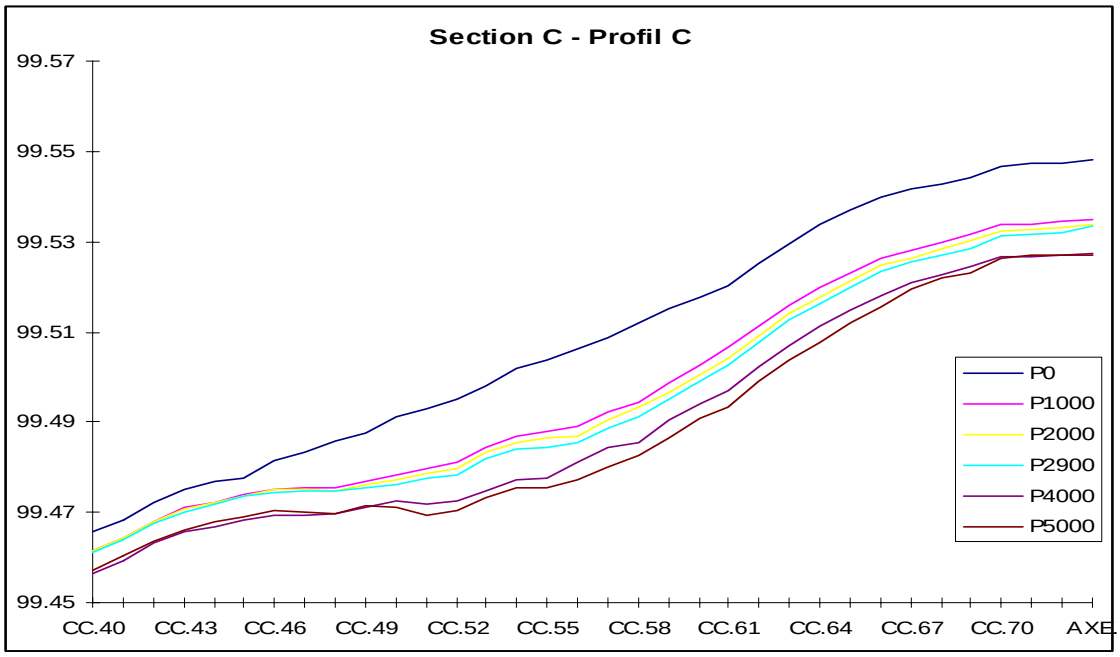
Section C - Profil C
99.57
99.55
99.53
99.51
99.49
99.47
99.45
CC.40 CC.43 CC.46 CC.49 CC.52 CC.55 CC.58 CC.61 CC.64 CC.67 CC.70 AXE
P0
P1000
P2000
P2900
P4000
P5000

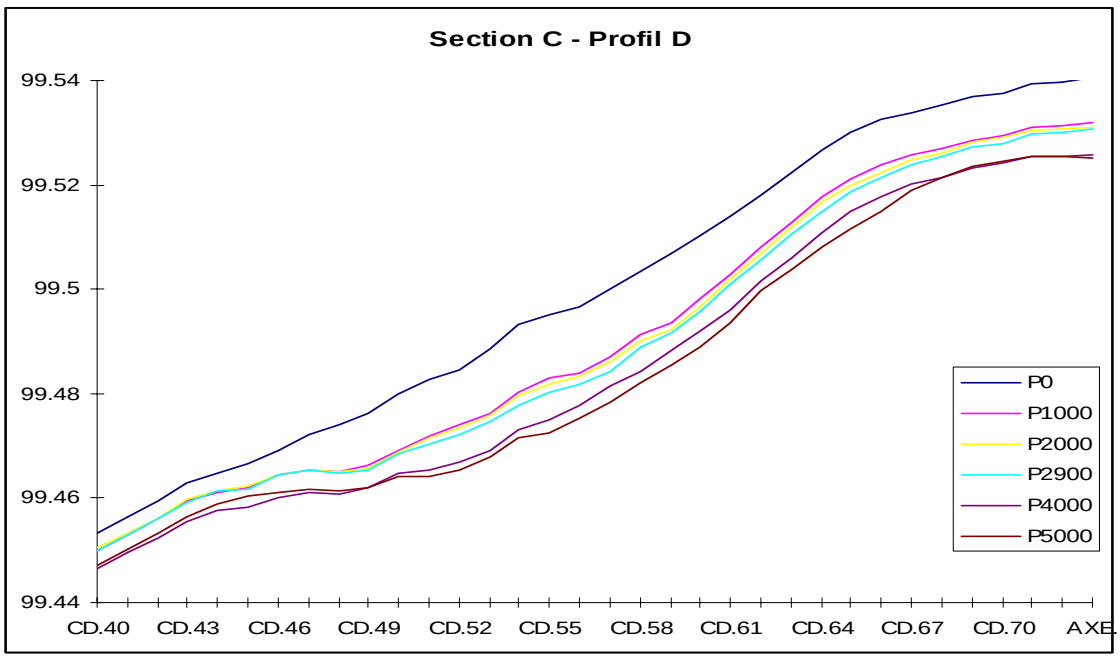
Section C - Profil D
99.54
99.52
99.5
99.48
99.46
99.44
CD.40 CD.43 CD.46 CD.49 CD.52 CD.55 CD.58 CD.61 CD.64 CD.67 CD.70 AXE
P0
P1000
P2000
P2900
P4000
P5000

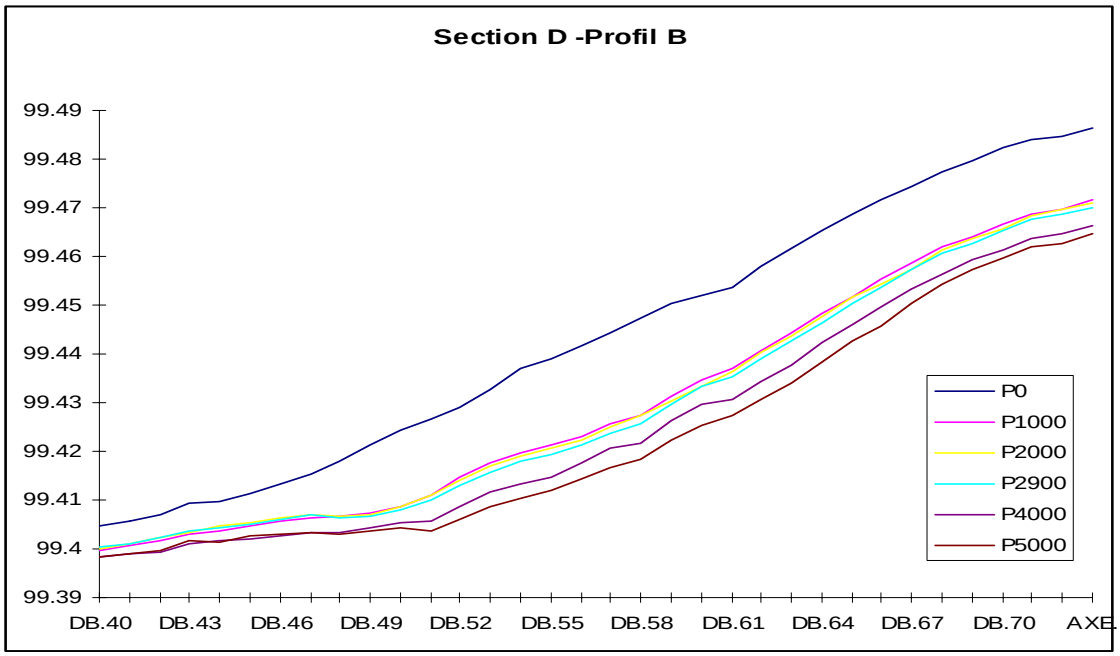
Section D -Profil B
99.49
99.48
99.47
99.46
99.45
99.44
99.43
99.42
99.41
99.4
99.39
DB.40
DB.43
DB.46
DB.49
DB.52
DB.55
DB.58
DB.61
DB.64
DB.67
DB.70
AXE
P0
P1000
P2000
P2900
P4000
P5000

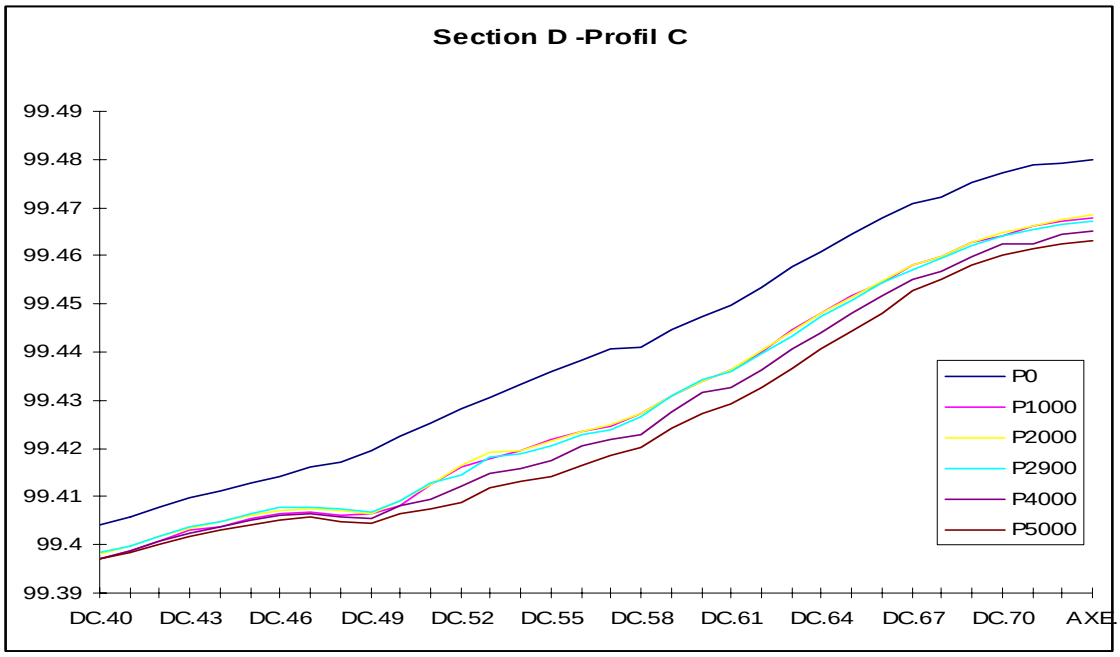
Section D -Profil C
99.49
99.48
99.47
99.46
99.45
99.44
99.43
99.42
99.41
99.4
99.39
DC.40
DC.43
DC.46
DC.49
DC.52
DC.55
DC.58
DC.61
DC.64
DC.67
DC.70
AXE
P0
P1000
P2000
P2900
P4000
P5000

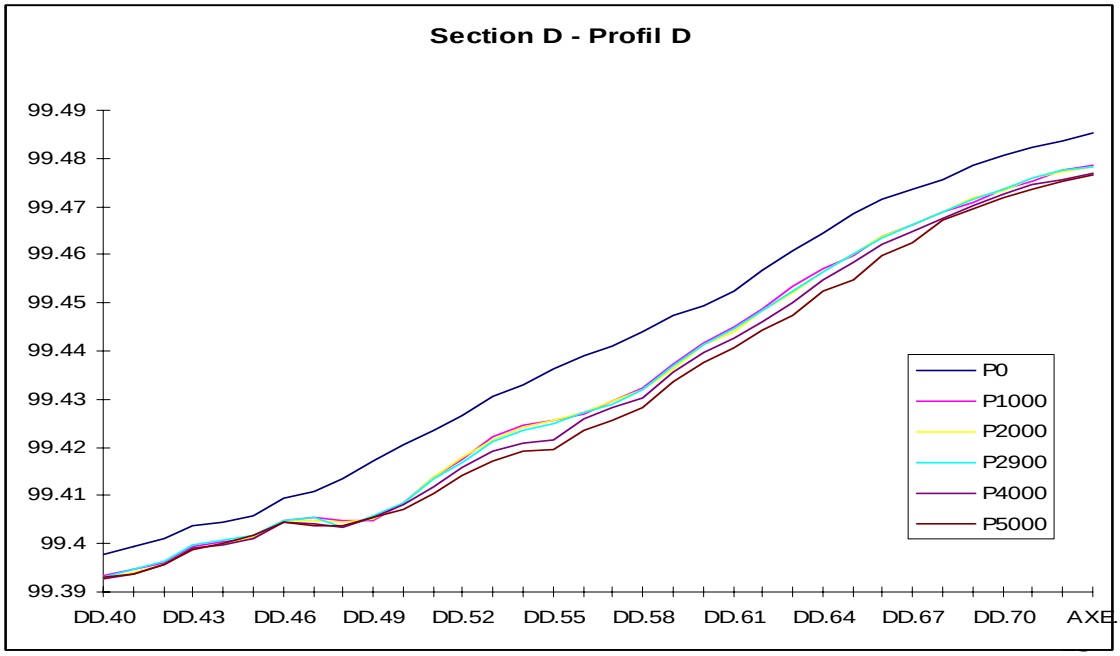
Section D - Profil D
99.49
99.48
99.47
99.46
99.45
99.44
99.43
99.42
99.41
99.4
99.39
DD.40
DD.43
DD.46
DD.49
DD.52
DD.55
DD.58
DD.61
DD.64
DD.67
DD.70
AXE
P0
P1000
P2000
P2900
P4000
P5000

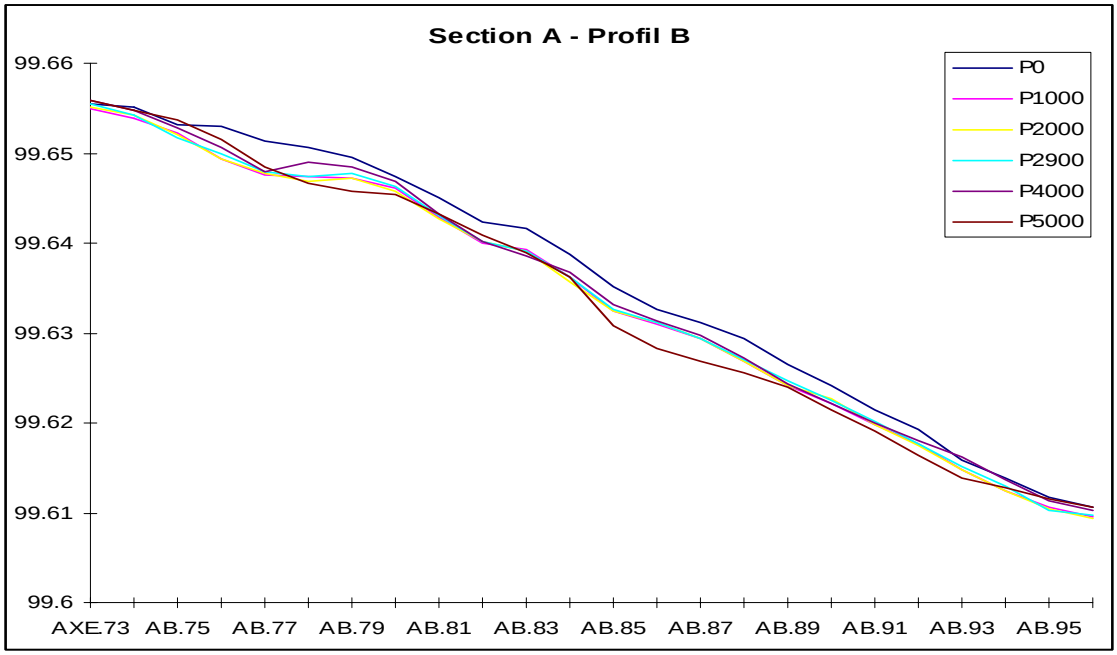
Section A - Profil B
99.66
99.65
99.64
99.63
99.62
99.61
99.6
AXE.73 AB.75 AB.77 AB.79 AB.81 AB.83 AB.85 AB.87 AB.89 AB.91 AB.93 AB.95
P0
P1000
P2000
P2900
P4000
P5000

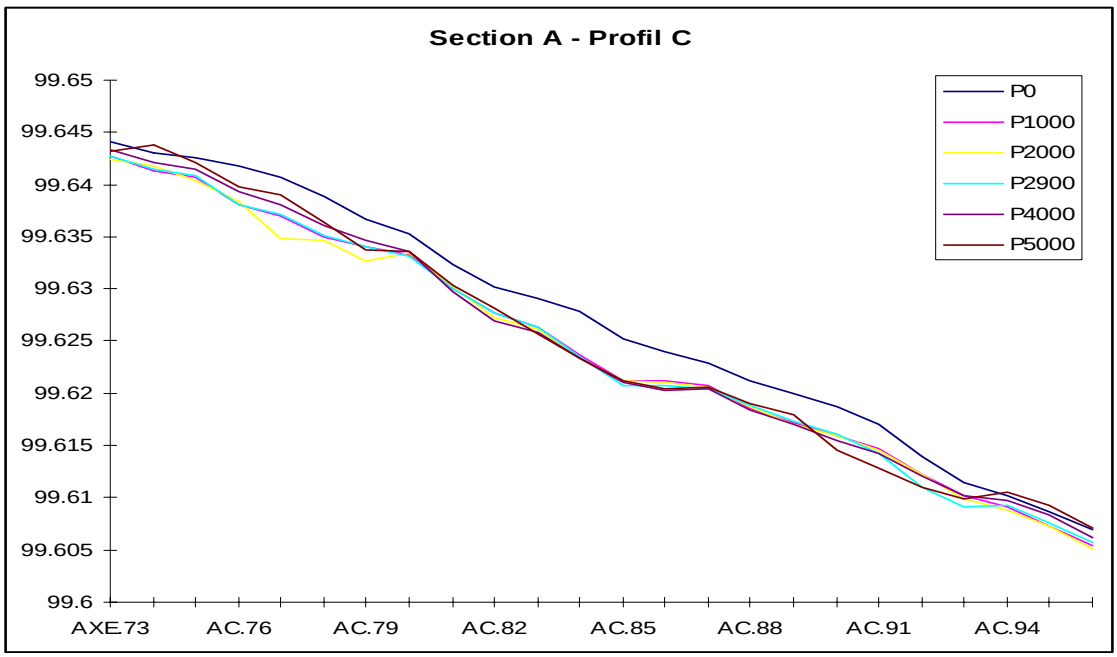
Section A - Profil C
99.65
99.645
99.64
99.635
99.63
99.625
99.62
99.615
99.61
99.605
99.6
AXE.73 AC.76 AC.79 AC.82 AC.85 AC.88 AC.91 AC.94
P0
P1000
P2000
P2900
P4000
P5000

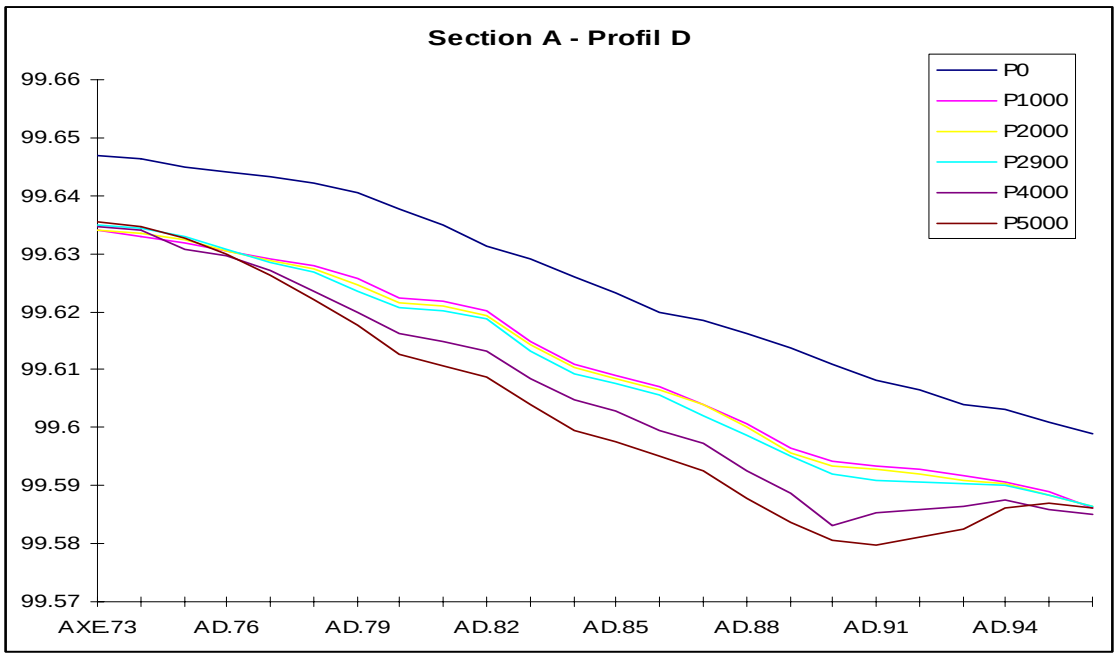
Section A - Profil D
99.66
99.65
99.64
99.63
99.62
99.61
99.6
99.59
99.58
99.57
AXE.73 AD.76 AD.79 AD.82 AD.85 AD.88 AD.91 AD.94
P0
P1000
P2000
P2900
P4000
P5000

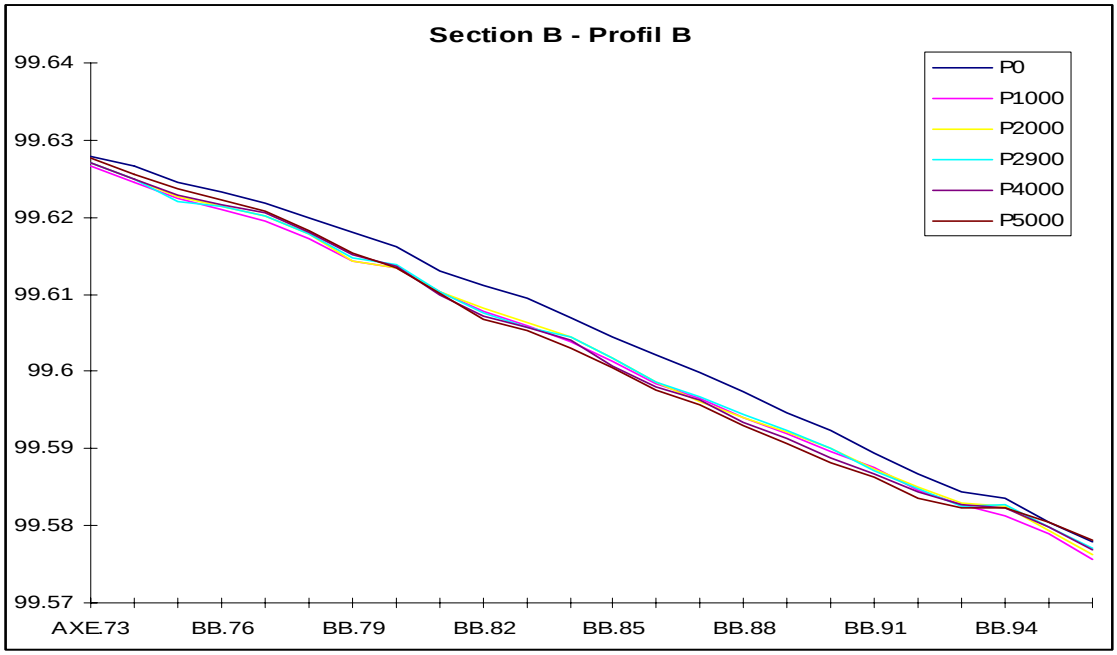
Section B - Profil B
99.64
99.63
99.62
99.61
99.6
99.59
99.58
99.57
AXE.73
BB.76
BB.79
BB.82
BB.85
BB.88
BB.91
BB.94
P0
P1000
P2000
P2900
P4000
P5000

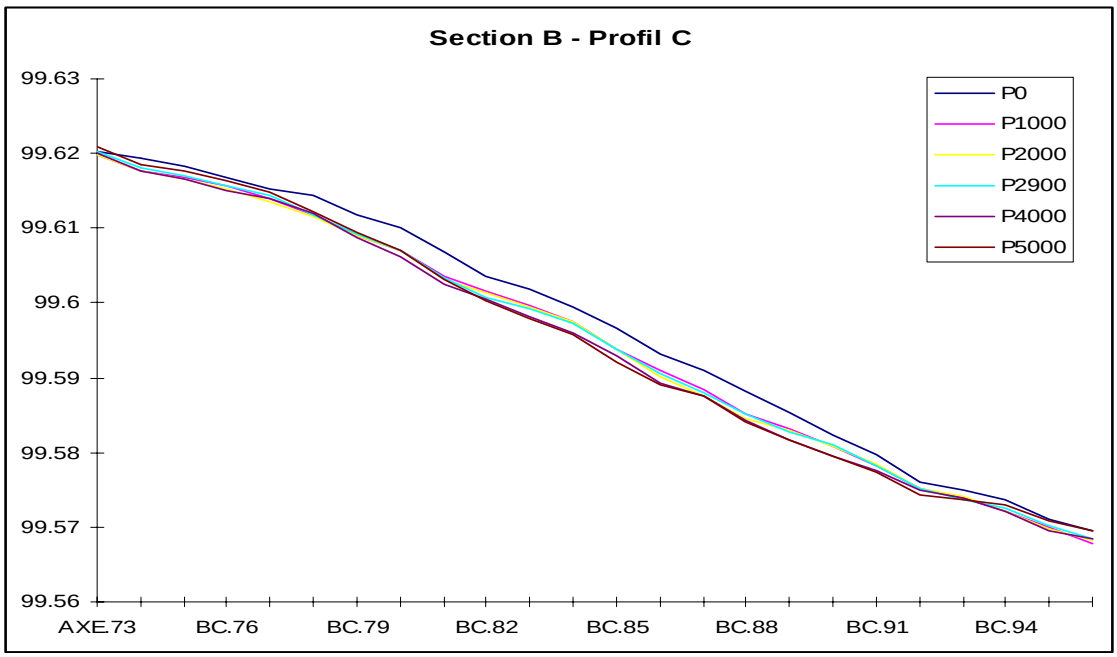
Section B - Profil C
99.63
99.62
99.61
99.6
99.59
99.58
99.57
99.56
AXE.73
BC.76
BC.79
BC.82
BC.85
BC.88
BC.91
BC.94
P0
P1000
P2000
P2900
P4000
P5000

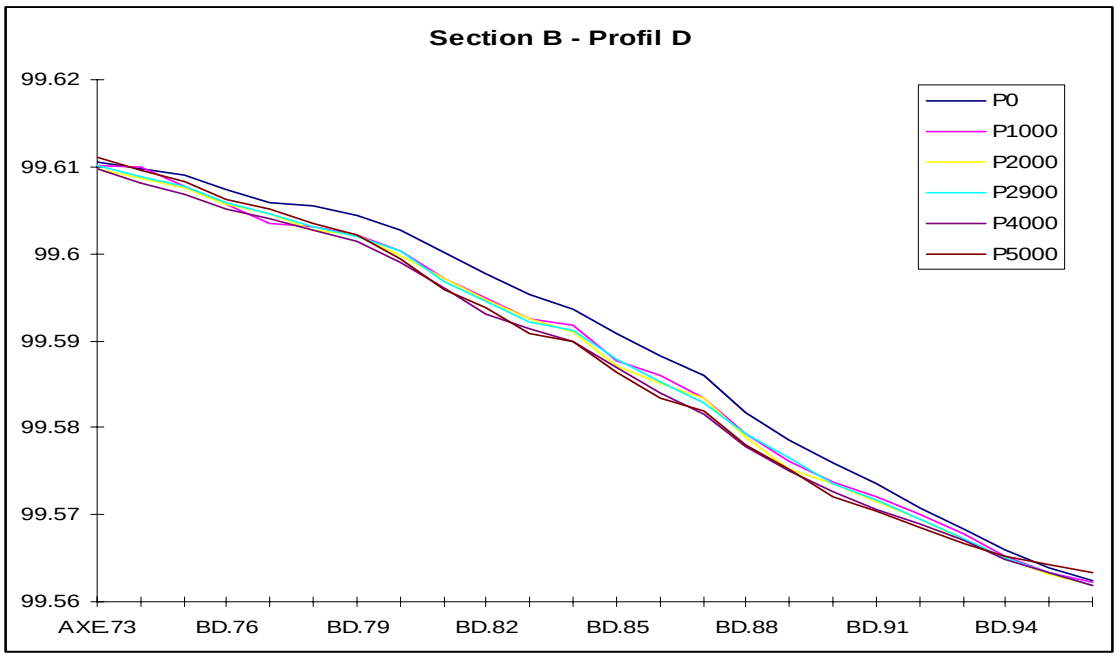
Section B - Profil D
99.62
99.61
99.6
99.59
99.58
99.57
99.56
AXE.73
BD.76
BD.79
BD.82
BD.85
BD.88
BD.91
BD.94
P0
P1000
P2000
P2900
P4000
P5000

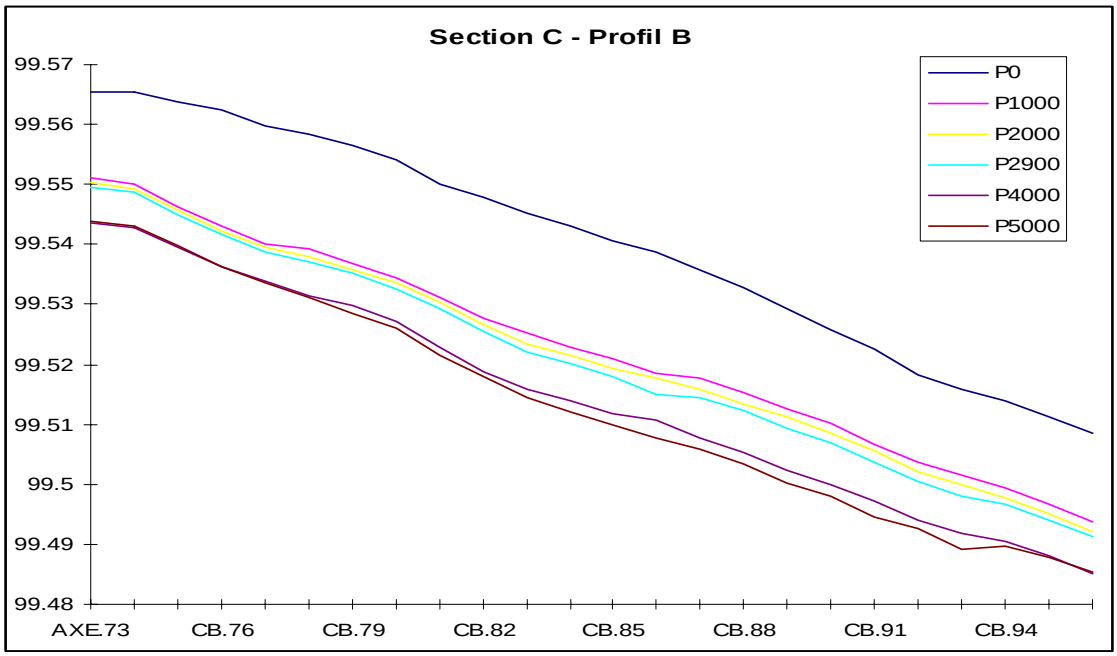
Section C - Profil B
99.57
99.56
99.55
99.54
99.53
99.52
99.51
99.5
99.49
99.48
AXE.73
CB.76
CB.79
CB.82
CB.85
CB.88
CB.91
CB.94
P0
P1000
P2000
P2900
P4000
P5000

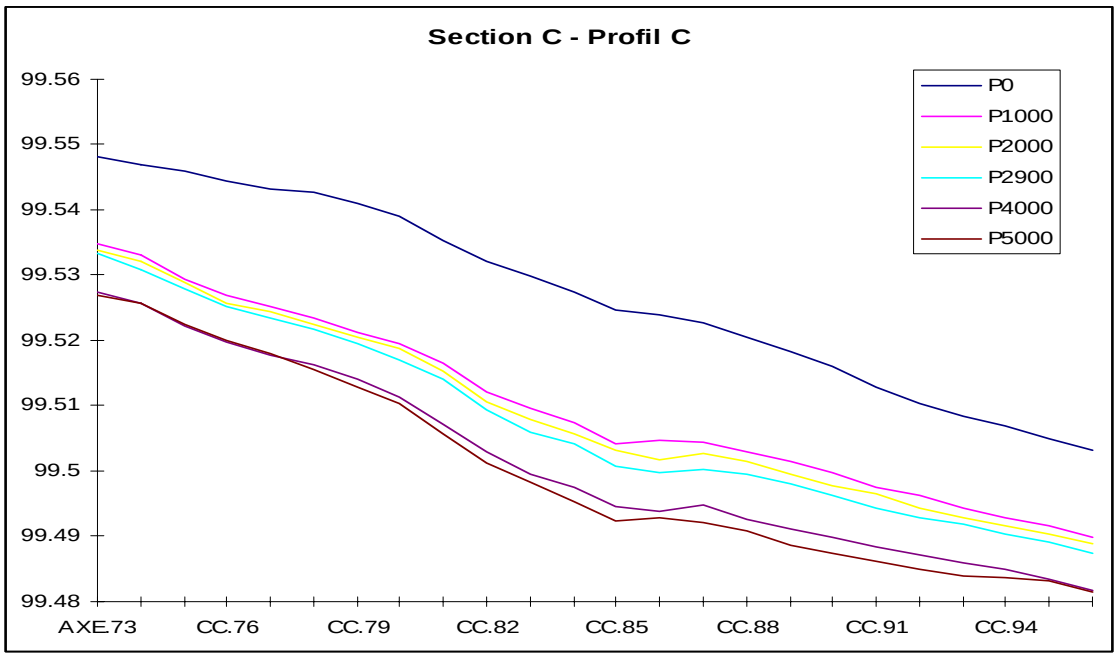
Section C - Profil C
99.56
99.55
99.54
99.53
99.52
99.51
99.5
99.49
99.48
AXE.73
CC.76
CC.79
CC.82
CC.85
CC.88
CC.91
CC.94
P0
P1000
P2000
P2900
P4000
P5000

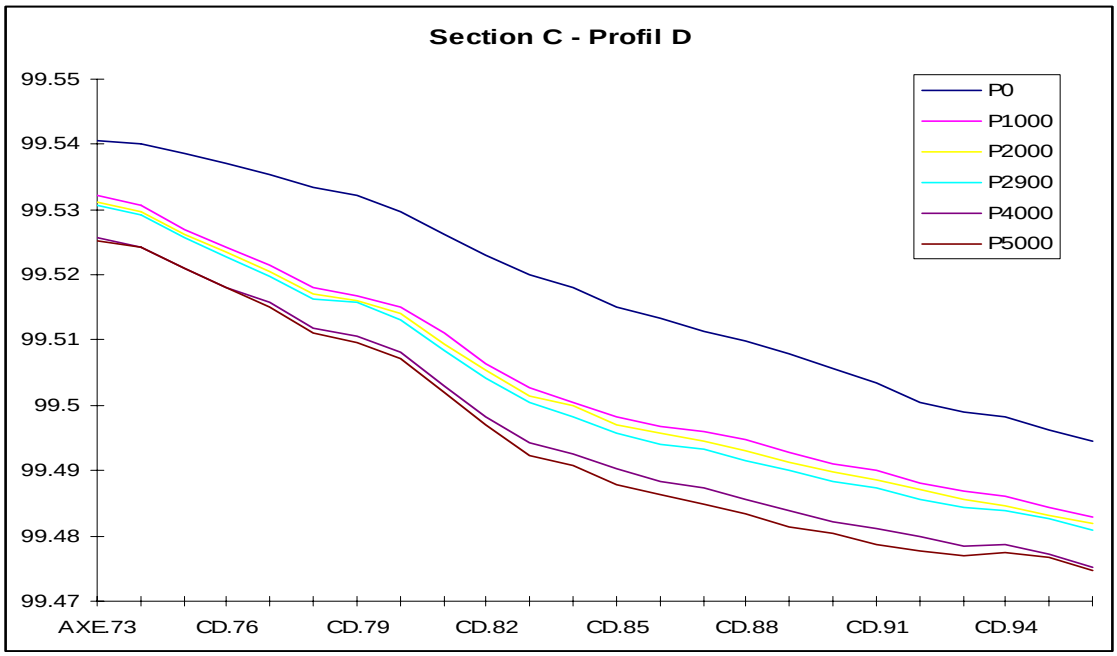
Section C - Profil D
99.55
99.54
99.53
99.52
99.51
99.5
99.49
99.48
99.47
AXE.73
CD.76
CD.79
CD.82
CD.85
CD.88
CD.91
CD.94
P0
P1000
P2000
P2900
P4000
P5000

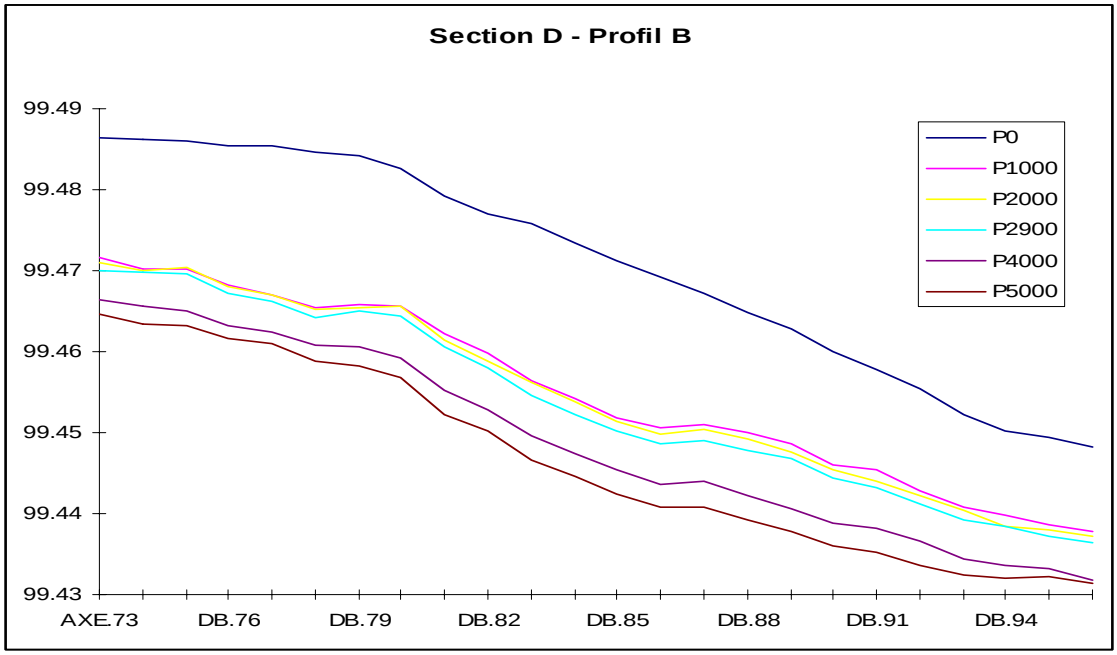
Section D - Profil B
99.49
99.48
99.47
99.46
99.45
99.44
99.43
AXE.73
DB.76
DB.79
DB.82
DB.85
DB.88
DB.91
DB.94
P0
P1000
P2000
P2900
P4000
P5000

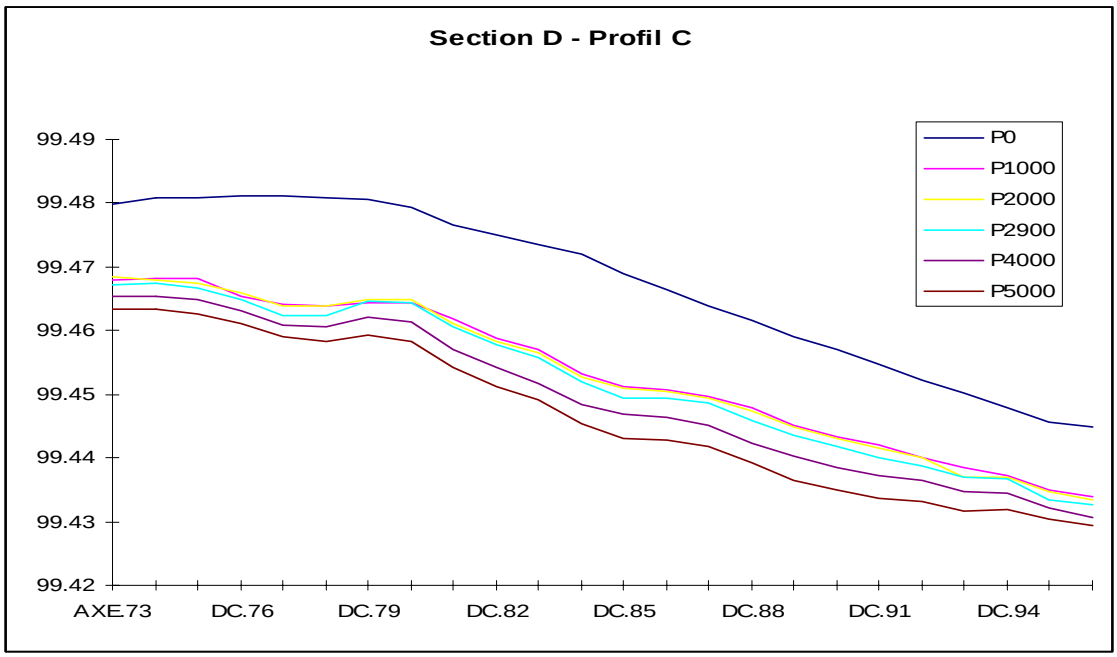
Section D - Profil C
99.49
99.48
99.47
99.46
99.45
99.44
99.43
99.42
AXE.73
DC.76
DC.79
DC.82
DC.85
DC.88
DC.91
DC.94
P0
P1000
P2000
P2900
P4000
P5000

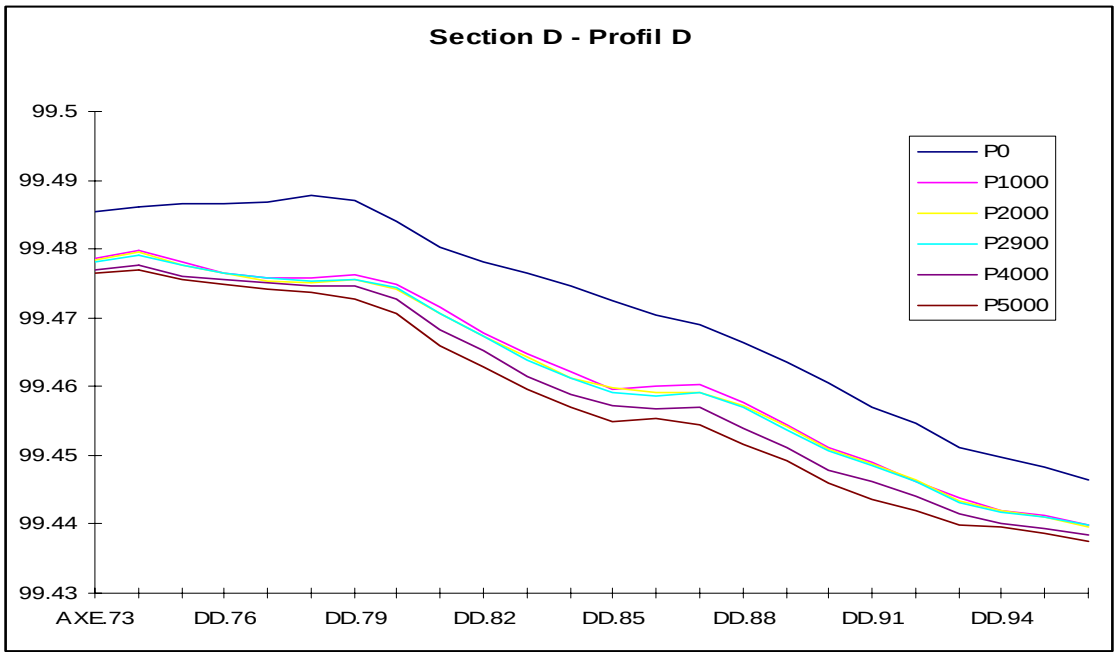
Section D - Profil D
99.5
99.49
99.48
99.47
99.46
99.45
99.44
99.43
AXE.73
DD.76
DD.79
DD.82
DD.85
DD.88
DD.91
DD.94
P0
P1000
P2000
P2900
P4000
P5000

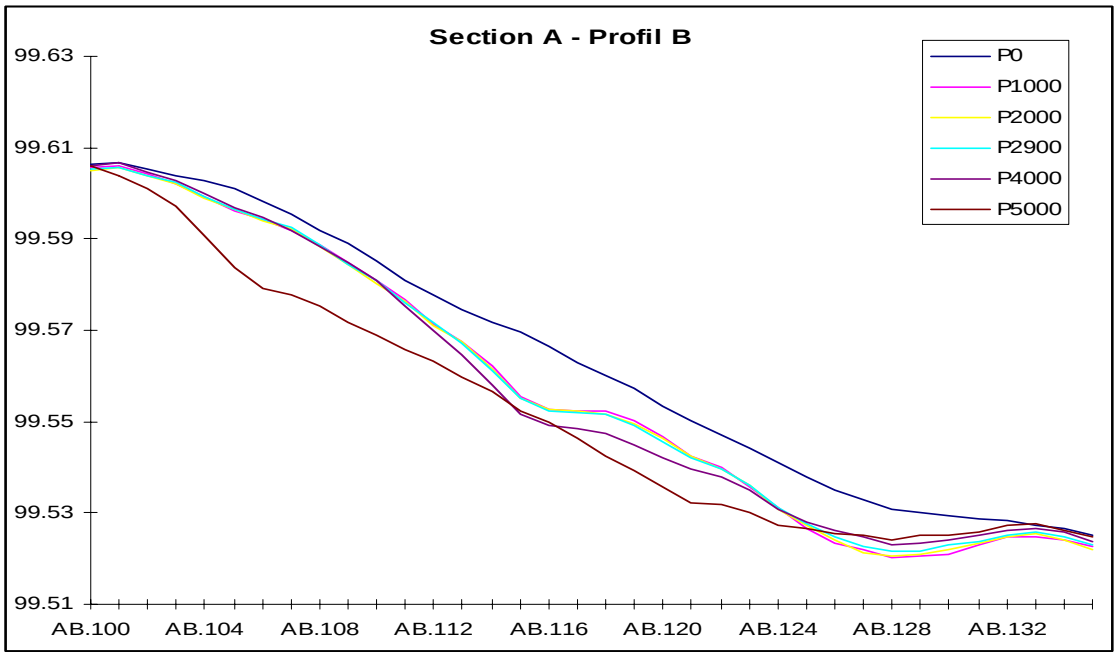
Section A - Profil B
99.63
99.61
99.59
99.57
99.55
99.53
99.51
AB.100
AB.104
AB.108
AB.112
AB.116
AB.120
AB.124
AB.128
AB.132
P0
P1000
P2000
P2900
P4000
P5000

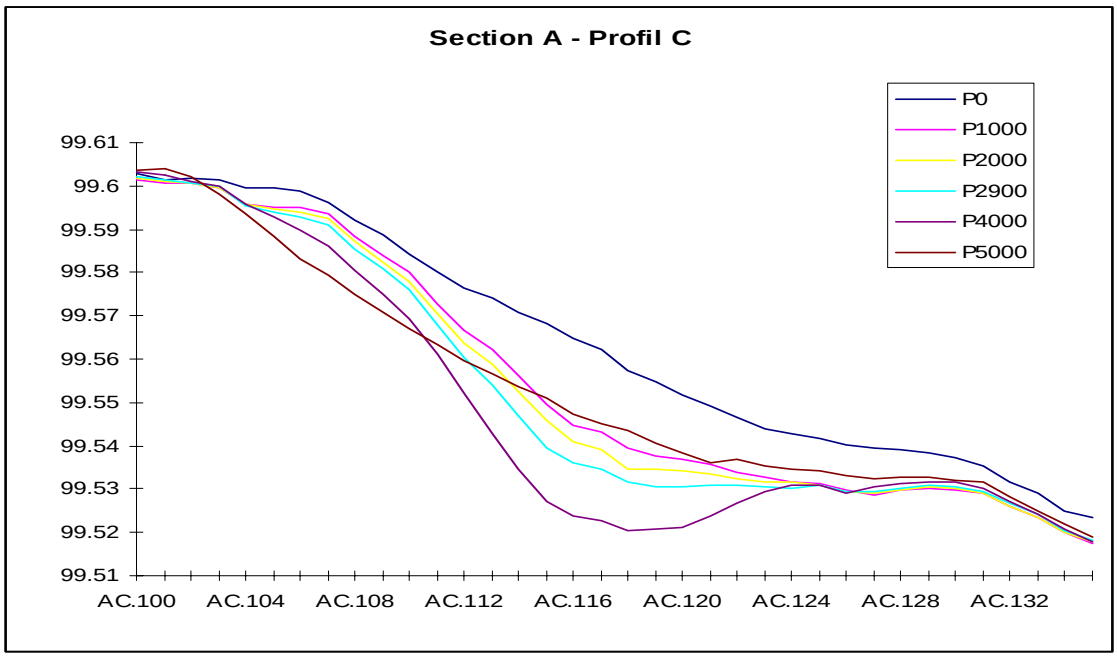
Section A - Profil C
99.61
99.6
99.59
99.58
99.57
99.56
99.55
99.54
99.53
99.52
99.51
AC.100
AC.104
AC.108
AC.112
AC.116
AC.120
AC.124
AC.128
AC.132
P0
P1000
P2000
P2900
P4000
P5000

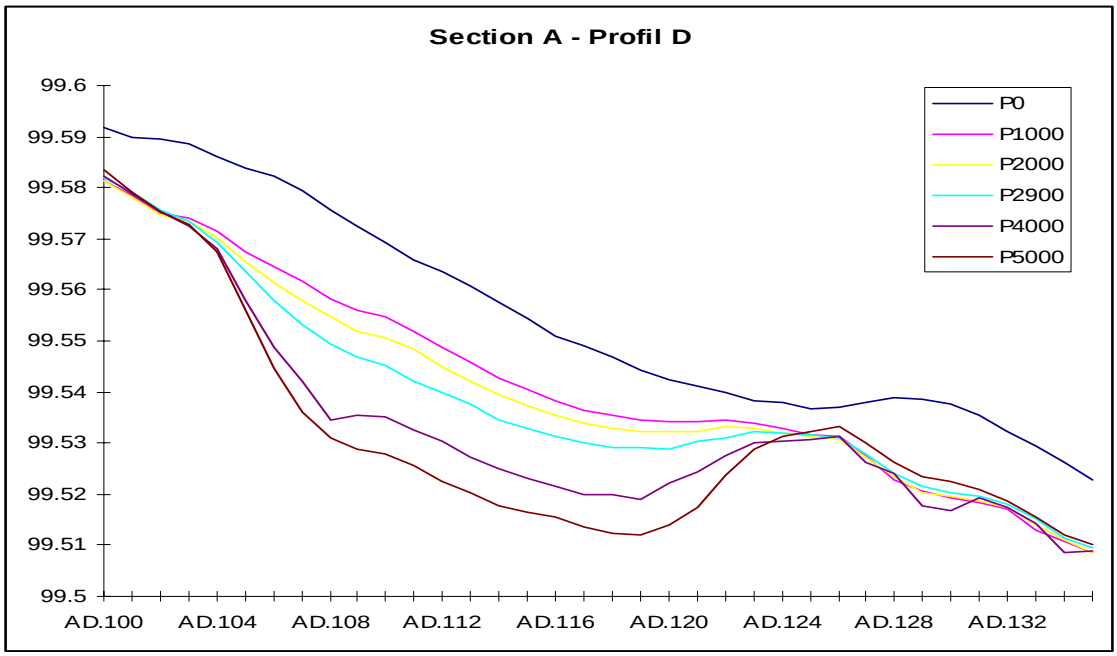
Section A - Profil D
99.6
99.59
99.58
99.57
99.56
99.55
99.54
99.53
99.52
99.51
99.5
AD.100
AD.104
AD.108
AD.112
AD.116
AD.120
AD.124
AD.128
AD.132
P0
P1000
P2000
P2900
P4000
P5000

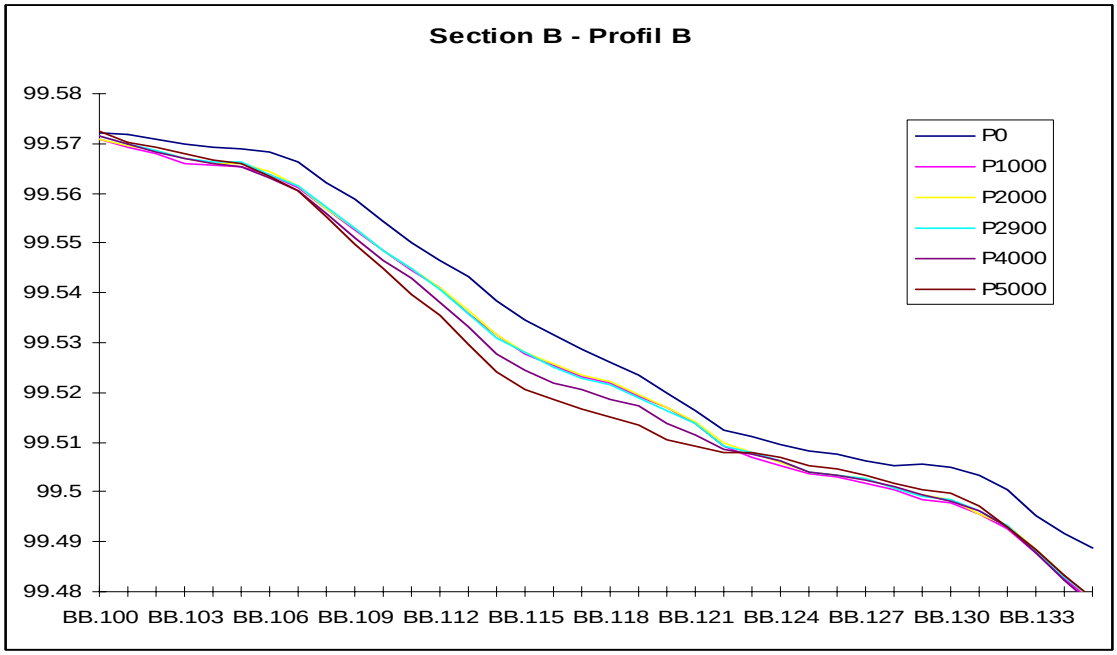
Section B - Profil B
99.58
99.57
99.56
99.55
99.54
99.53
99.52
99.51
99.5
99.49
99.48
BB.100 BB.103 BB.106 BB.109 BB.112 BB.115 BB.118 BB.121 BB.124 BB.127 BB.130 BB.133
P0
P1000
P2000
P2900
P4000
P5000

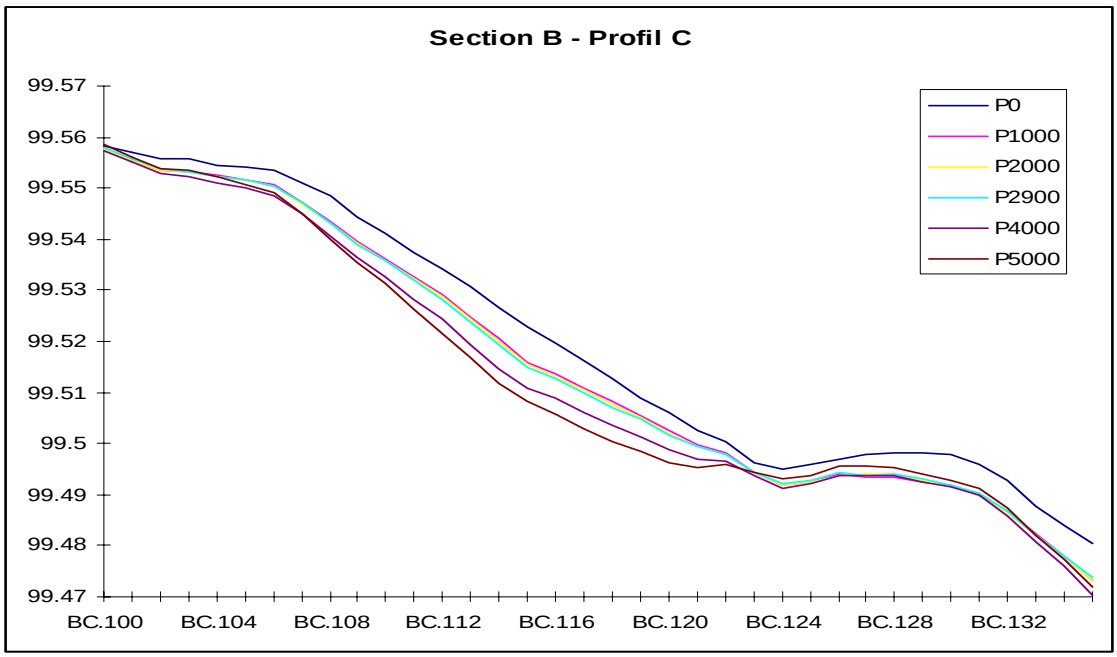
Section B - Profil C
99.57
99.56
99.55
99.54
99.53
99.52
99.51
99.5
99.49
99.48
99.47
BC.100 BC.104 BC.108 BC.112 BC.116 BC.120 BC.124 BC.128 BC.132
P0
P1000
P2000
P2900
P4000
P5000

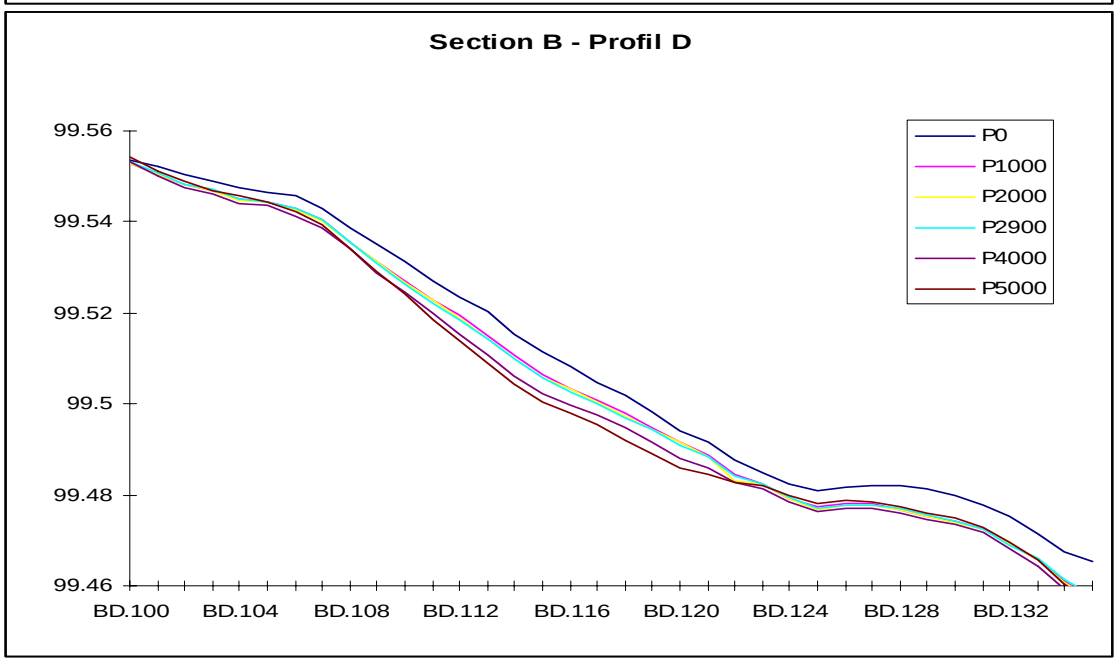
Section B - Profil D
99.56
99.54
99.52
99.5
99.48
99.46
BD.100 BD.104 BD.108 BD.112 BD.116 BD.120 BD.124 BD.128 BD.132
P0
P1000
P2000
P2900
P4000
P5000

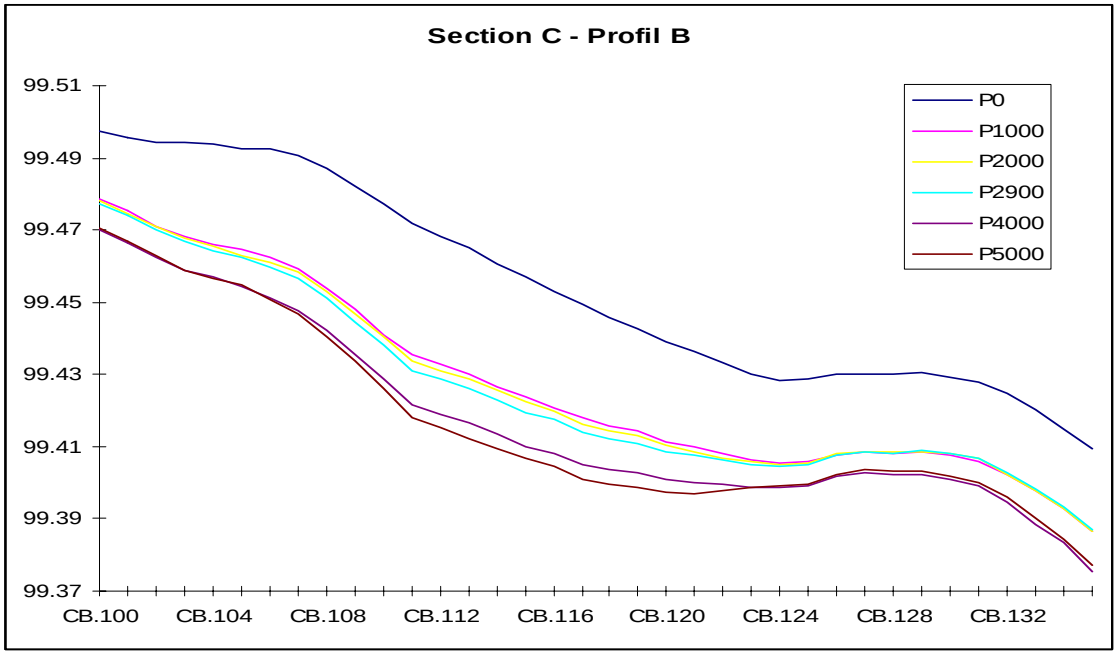
Section C - Profil B
99.51
99.49
99.47
99.45
99.43
99.41
99.39
99.37
CB.100
CB.104
CB.108
CB.112
CB.116
CB.120
CB.124
CB.128
CB.132
P0
P1000
P2000
P2900
P4000
P5000

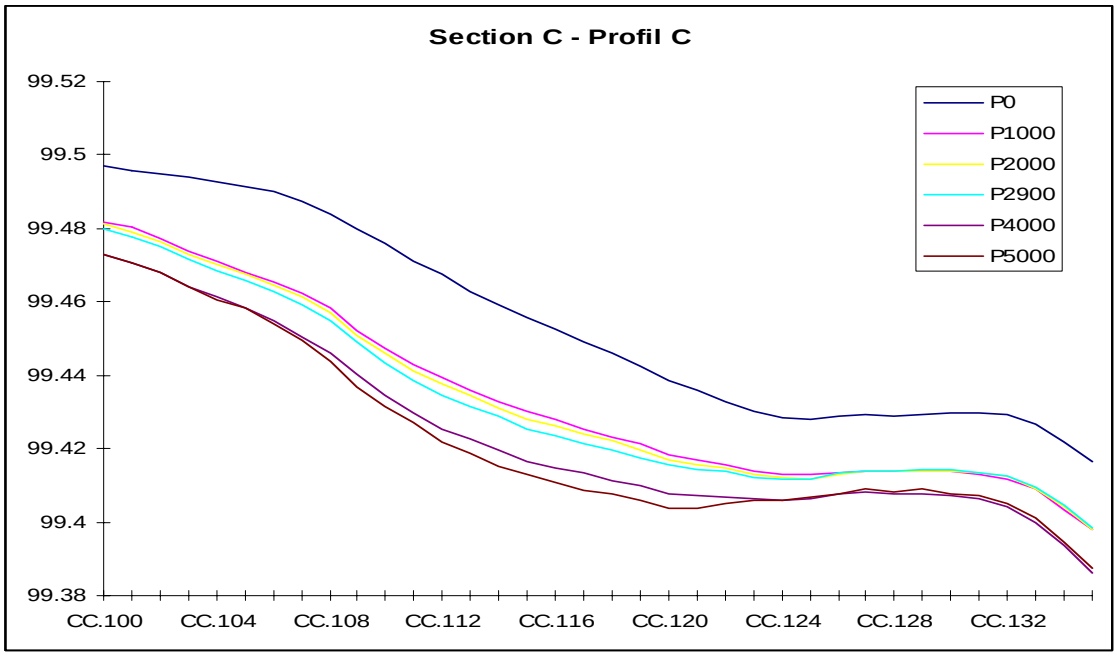
Section C - Profil C
99.52
99.5
99.48
99.46
99.44
99.42
99.4
99.38
CC.100
CC.104
CC.108
CC.112
CC.116
CC.120
CC.124
CC.128
CC.132
P0
P1000
P2000
P2900
P4000
P5000

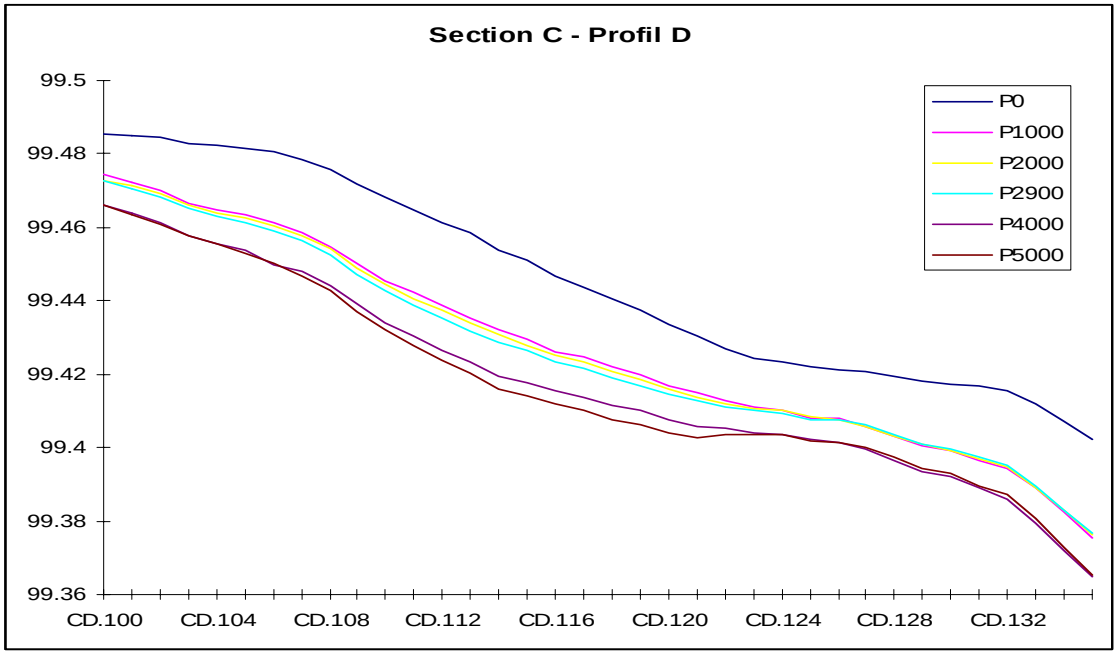
Section C - Profil D
99.5
99.48
99.46
99.44
99.42
99.4
99.38
99.36
CD.100
CD.104
CD.108
CD.112
CD.116
CD.120
CD.124
CD.128
CD.132
P0
P1000
P2000
P2900
P4000
P5000

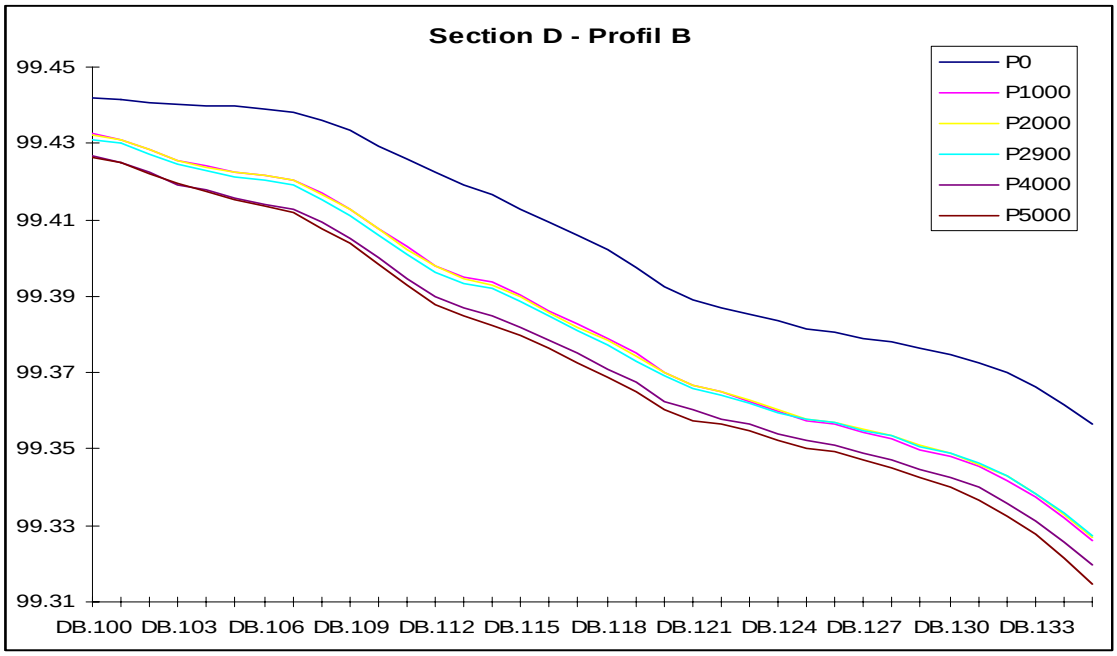
Section D - Profil B
99.45
99.43
99.41
99.39
99.37
99.35
99.33
99.31
DB.100 DB.103 DB.106 DB.109 DB.112 DB.115 DB.118 DB.121 DB.124 DB.127 DB.130 DB.133
P0
P1000
P2000
P2900
P4000
P5000

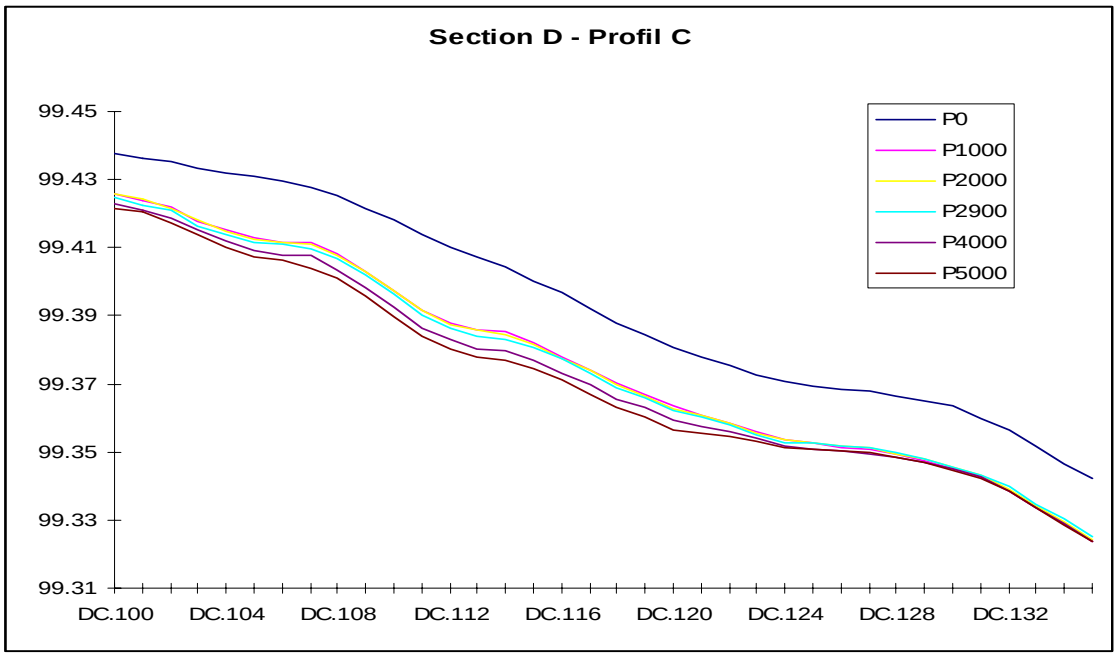
Section D - Profil C
99.45
99.43
99.41
99.39
99.37
99.35
99.33
99.31
DC.100 DC.104 DC.108 DC.112 DC.116 DC.120 DC.124 DC.128 DC.132
P0
P1000
P2000
P2900
P4000
P5000

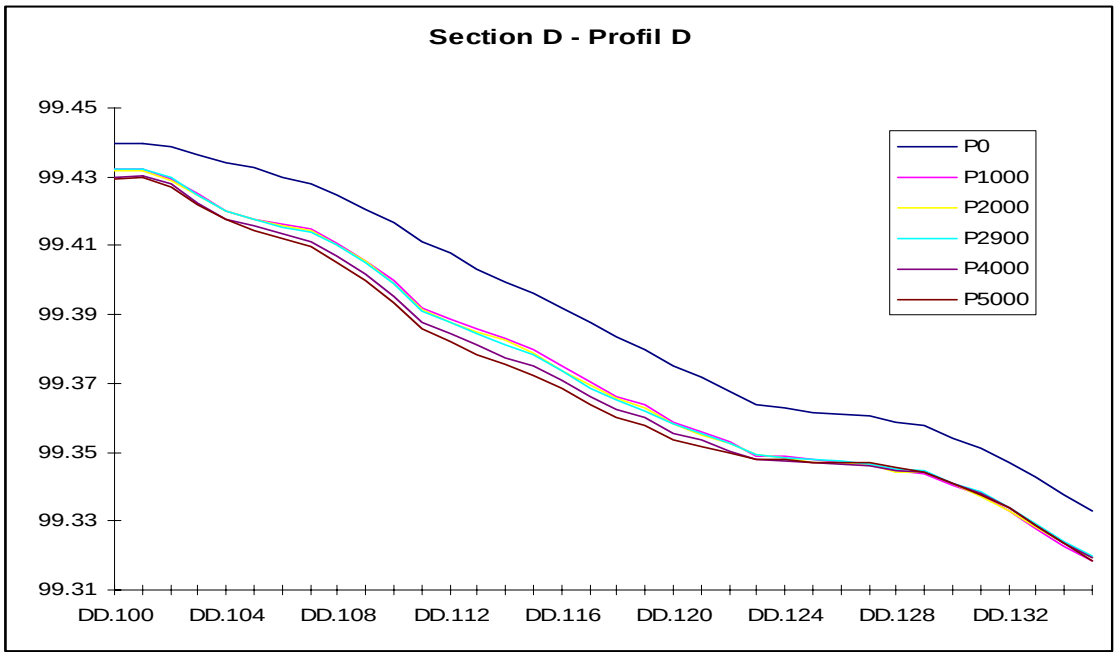
Section D - Profil D
99.45
99.43
99.41
99.39
99.37
99.35
99.33
99.31
DD.100 DD.104 DD.108 DD.112 DD.116 DD.120 DD.124 DD.128 DD.132
P0
P1000
P2000
P2900
P4000
P5000

Appendix.3

The repeated Triaxial testing procedure for road geotechnics

REPEATED LOAD TRIAXIAL APPARATUS

A diagrammatic representation of the test equipment used for performing the repeated load Triaxial test is shown in Figure 1, as well as the type of cyclic loading applied to the sample (Figure 2).

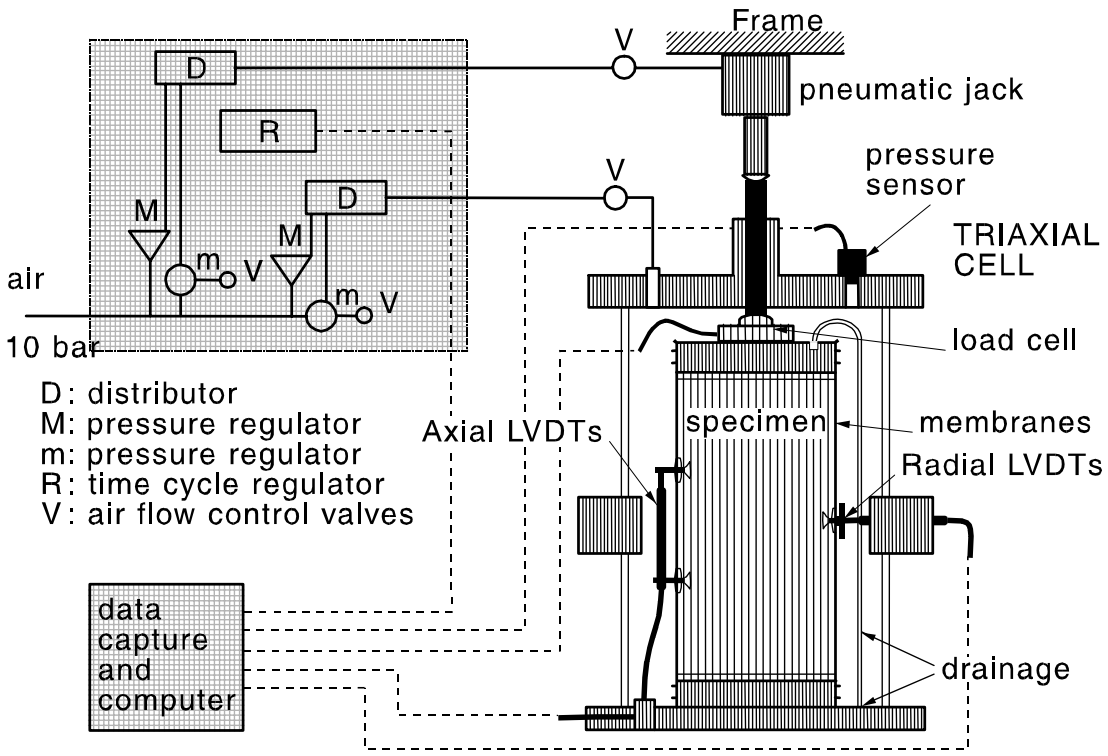

FIGURE 1: VARIABLE CONFINING PRESSURE TRIAXIAL APPARATUS (VCP)

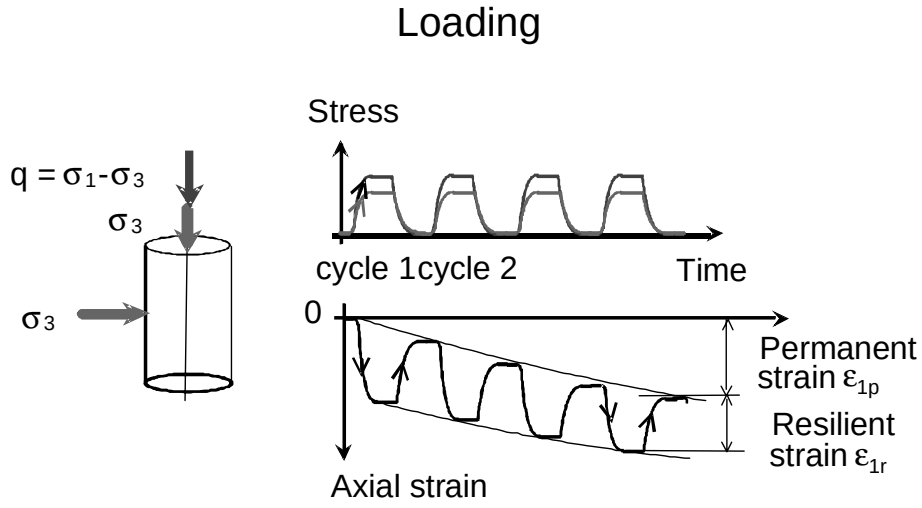

Figure 2: Cyclic load applied by the VCP apparatus and
typical strain response of the material

TEST PROCEDURE FOR UNBOUND GRANULAR MATERIALS

In general, test specimens are manufactured to the desired density and moisture content conditions required.

PRECONDITIONING TEST:

Test specimens are subjected to a preconditioning test of 20,000 cycles involving an applied loading of p_{max} = 300kPa and q_{max} = 600kPa (or σ_{1max} = 700kPa and σ_{3max} = 100kPa).

RESILIENT MODULUS STRESS STAGE TEST:

Following the preconditioning test, the material specimens are subjected to stress stage resilient modulus test of 100 cycles per stage, with a range of applied loading sequenced according to the CEN procedure with stress ratio loading paths of q/p = 0, 0.5, 1.0, 1.5, 2.0 and 2.5 performed in sequence.

A plot of the stress paths used for the resilient modulus tests is illustrated below in Figure 3.

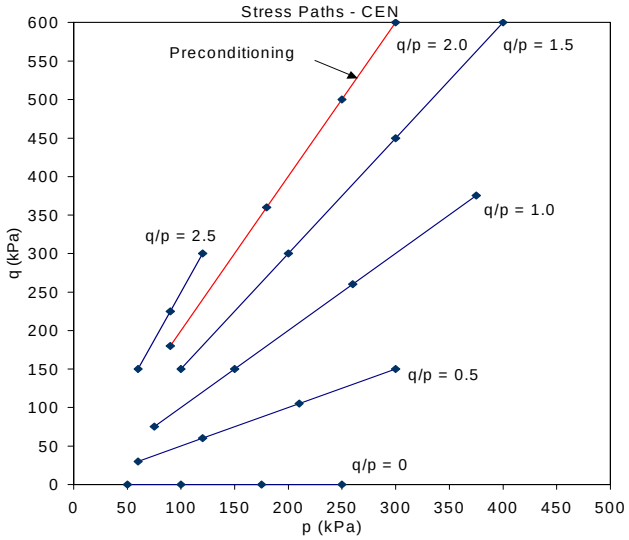

FIGURE 3: CEN RLT STRESS PATHS FOR RESILIENT MODULS TESTING

TEST PROCEDURE FOR SOILS

The same procedure with two steps (preconditioning and loading) was applied to the soils, but with p_{max} and q_{max} levels adapted to their expected values on PEP site, from numerical modeling of the pavement.